uOttawa

L'Université canadienne
Canada's university

FACULTÉ DES ÉTUDES SUPÉRIEURES ET POSTOCTORALES

uOttawa

L'Université canadienne
Canada's university

FACULTY OF GRADUATE AND POSDOCTORAL STUDIES

Clement Poon

AUTEUR DE LA THÈSE / AUTHOR OF THESIS

Ph.D. (Chemistry)

GRADE / DEGREE

Department of Chemistry

FACULTÉ, ÉCOLE, DÉPARTEMENT / FACULTY, SCHOOL, DEPARTMENT

Unimolecular and Collision Dynamics of Gas-Phase Ions

TITRE DE LA THÈSE / TITLE OF THESIS

Paul Mayer

DIRECTEUR (DIRECTRICE) DE LA THÈSE / THESIS SUPERVISOR

CO-DIRECTEUR (CO-DIRECTRICE) DE LA THÈSE / THESIS CO-SUPERVISOR

EXAMINATEURS (EXAMINATRICES) DE LA THÈSE / THESIS EXAMINERS

Travis Fridgen

David Bryce

Ed Lai

Javier Giorgi

Gary W. Slater

Le Doyen de la Faculté des études supérieures et postdoctorales / Dean of the Faculty of Graduate and Postdoctoral Studies

UNIMOLECULAR AND COLLISION DYNAMICS OF GAS-PHASE IONS

Clement Poon

Thesis submitted to the
Faculty of Graduate and Postdoctoral Studies

In partial fulfillment of the requirements for
the degree of Doctor of Philosophy

In the Ottawa-Carleton Chemistry Institute
Department of Chemistry, University of Ottawa
Ottawa, Ontario, Canada

December 2007

Candidate	Supervisor
Clement Poon	Dr. Paul M. Mayer

© Clement Poon, Ottawa, Ontario, Canada, 2008

Library and Archives Canada

Published Heritage Branch

395 Wellington Street
Ottawa ON K1A 0N4
Canada

Bibliothèque et Archives Canada

Direction du Patrimoine de l'édition

395, rue Wellington
Ottawa ON K1A 0N4
Canada

Your file Votre référence
ISBN: 978-0-494-50752-0
Our file Notre référence
ISBN: 978-0-494-50752-0

NOTICE:
The author has granted a non-exclusive license allowing Library and Archives Canada to reproduce, publish, archive, preserve, conserve, communicate to the public by telecommunication or on the Internet, loan, distribute and sell theses worldwide, for commercial or non-commercial purposes, in microform, paper, electronic and/or any other formats.

The author retains copyright ownership and moral rights in this thesis. Neither the thesis nor substantial extracts from it may be printed or otherwise reproduced without the author's permission.

AVIS:
L'auteur a accordé une licence non exclusive permettant à la Bibliothèque et Archives Canada de reproduire, publier, archiver, sauvegarder, conserver, transmettre au public par télécommunication ou par l'Internet, prêter, distribuer et vendre des thèses partout dans le monde, à des fins commerciales ou autres, sur support microforme, papier, électronique et/ou autres formats.

L'auteur conserve la propriété du droit d'auteur et des droits moraux qui protège cette thèse. Ni la thèse ni des extraits substantiels de celle-ci ne doivent être imprimés ou autrement reproduits sans son autorisation.

In compliance with the Canadian Privacy Act some supporting forms may have been removed from this thesis.

While these forms may be included in the document page count, their removal does not represent any loss of content from the thesis.

Conformément à la loi canadienne sur la protection de la vie privée, quelques formulaires secondaires ont été enlevés de cette thèse.

Bien que ces formulaires aient inclus dans la pagination, il n'y aura aucun contenu manquant.

Canada

Abstract

This thesis describes the research work on two aspects of gas-phase ion reactions. In the first project, the unimolecular chemistry of a series of nitroalkane proton-bound pairs was investigated by mass spectrometry and theoretical calculations. In addition to a simple dissociation reaction in which the hydrogen bond is cleaved to form protonated and neutral nitroalkanes, the nitroalkane proton-bound pairs can also lose nitrous acid via an internal S_N2 rearrangement and t-butanol via a nitro-nitrite isomerization. The dissociations of $(CH_3NO_2)((CH_3)_3CNO_2)H^+$ and $(CH_3CH_2NO_2)((CH_3)_3CNO_2)H^+$ proton-bound pairs were studied by variational transition state theory. $\Delta(\Delta S^{\ddagger})$ and $\Delta(\Delta S)$ of the two dissociation channels are similar for the dissociations of $(CH_3NO_2)((CH_3)_3CNO_2)H^+$ but deviation becomes larger in the case of $(CH_3CH_2NO_2)((CH_3)_3CNO_2)H^+$. One should therefore be cautious when assuming $\Delta(\Delta S^{\ddagger}) = \Delta(\Delta S)$ in competitive dissociation reactions of proton-bound pairs.

In the second part of the research work, keV $N_2^{+\cdot}$/He, $N_2^{+\cdot}$/Ar and $CO_2^{+\cdot}$/He collisions were investigated by emission spectroscopy. The results provide two pieces of evidence that support the curve-crossing mechanism for collisional activation. Firstly, the relative emission intensities of the molecular ions and the fragments are independent of the ion translational energy within the studied energy range and secondly, the difference in the $N_2^{+\cdot}$ $B\ ^2\Sigma_u^+ \rightarrow X\ ^2\Sigma_g^+$ emission intensities from $N_2^{+\cdot}$/He and $N_2^{+\cdot}$/Ar collisions can be accounted for by the slope difference at the crossing points based on the

Landau-Zener curve-crossing model. Although the investigation of the relative intensities within the A $^2\Pi_u \rightarrow$ X $^2\Pi_g$ emission of $CO_2^{+\cdot}$ resembles the Franck-Condon picture at high collision energy, the Franck-Condon principle can also be applied to the curve-crossing model as it is purely based on the grounds of short transition time. Therefore, linking this principle immediately to vertical transitions for collisional excitation could be misleading.

Acknowledgements

I would like to express my sincere gratitude to my supervisor, Dr. Paul Mayer, for his guidance, encouragement, and for the confidence he has always shown in me. My PhD study would not have been possible without his endless enthusiasm and patience. I am indebted to him for introducing me to mass spectrometry and giving me the experience of working on various research projects in mass spectrometry since my undergraduate study.

Special thanks go out to Dr. John Holmes and Dr. Emma Rennie for their helpful comments and discussion on my work, Dr. Sander Mommers for making all the filaments and for always being there when the instrument is not working, and Dr. Clement Kazakoff for discussions on analytical instruments. Over the past eight years in the Mass Spectrometry lab (starting from my undergraduate study), I have worked with a number of colleagues who have been incredibly supportive and encouraging. I would like to take this opportunity to thank all of them for making the lab an enjoyable place to work: (in no particular order) Dr. Julie Grabowy, Dr. Xian Wang, Dr. Annick St-Amand, Dr. Richard Ochran, Dr. Jie Cao, Anne-Marie Boulanger, Abdulrahman Alhazmi, Yawei Lin, Madlena Rabaev, Marie-Soleil Giguère, Danielle Dubien, Lisa Walrond, Wei Wei Yong and all other past colleagues.

Last but not least, I would like to thank my family for being supportive and understanding throughout the course of my studies. I would also like to thank the Natural Sciences and Engineering Research Council of Canada, the Province of Ontario, the University of Ottawa and my supervisor Paul Mayer for financially supporting me with scholarships and research assistantship. My studies would have been difficult without these generous financial supports.

Table of Contents

List of Figures

List of Schemes

List of Tables

Abbreviations

B3-LYP	Becke 3-Parameter Lee-Yang-Parr Method
CCD	Charge-Coupled Device
CID	Collision-Induced Dissociation
CIE	Collision-Induced Emission
CISD	Configuration Interaction with Single and Double Excitations
Da	Dalton (= Atomic Mass Unit)
DFT	Density Functional Theory
E	Internal Energy
E_0	Activation Energy
ECR	Electron Cyclotron Resonance
EI	Electron Ionization
ESA	Electrostatic Analyzer
FFR	Field-Free Region
FWHM	Full Width at Half Maximum
G3	Gaussian-3 Theory
IE	Ionization Energy
INT	Intermediate
IRC	Intrinsic Reaction Coordinate
IVR	Intramolecular Vibrational Energy Redistribution
m/z	Mass-to-Charge Ratio

MI	Metastable Ion
MIKES	Mass-Analyzed Ion Kinetic Energy Spectrometry
MO	Molecular Orbital
MP2	Second-Order Møller-Plesset Perturbation Theory
MP4	Fourth-Order Møller-Plesset Perturbation Theory
MS/MS	Tandem Mass Spectrometry
$N^{\ddagger}$	Sum of States of Transition State
NR	Neutralization-Reionization
NRMS	Neutralization-Reionization Mass Spectrometry
PBD	Proton-Bound Dimer
PES	Potential Energy Surface **OR** Photoelectron Spectroscopy
QCISD	Quadratic Configuration Interaction with Single and Double Excitations
QET	Quasi-equilibrium Theory
RRKM	Rice-Ramsperger-Kassel-Marcus Theory
S_N2	Bimolecular Nucleophilic Substitution
TES	Translational Energy Spectroscopy
TS	Transition State
VTST	Variational Transition State Theory
ΔS	Thermodynamic Reaction Entropy
$\Delta S^{\ddagger}$	Entropy of Activation
$\rho(E)$	Density of States

Preface

This thesis explores two different aspects of gas-phase reactions, namely unimolecular dynamics and collision dynamics of gas-phase ions. Cluster ions have been of interest to many atmospheric chemists for decades due to their common occurrence in the atmosphere. In this respect, I investigated by both experiments and theory competing dissociations and rearrangements in nitroalkane proton-bound pairs. These results will be presented and discussed in the first part (Part A) of the thesis. In the second part (Part B), I will address a more fundamental question as to the mechanism of collisional excitation. Upon collisions, molecules and ions are excited and photons can be emitted (such as those in the atmosphere resulting in aurora). Therefore, keV bimolecular collisions of a few atmospheric species were studied by emission spectroscopy as a function of ion translational energy to obtain information as to how ions are excited by collisions.

Each of the two parts is composed of four chapters: a chapter of introduction, covering fundamental theories and past works relevant to the project; a chapter on the methods of study, including a brief description of the instrument and techniques used and any modifications made to the mass spectrometer for the study; a chapter on the results and discussion and finally a concluding chapter. Each part is ended with a section of references and two appendices are also included at the end of the thesis as supporting information.

Part A

Unimolecular Dynamics of Nitroalkane Proton-Bound Pairs

1 Introduction

1.1 Gas-Phase Ion Chemistry

Mass spectrometry is one of the most versatile analytical techniques. It is the method of choice by many scientists for the qualitative and quantitative analyses of environmental, pharmaceutical and biological samples. To ion chemists, mass spectrometers are not just a powerful analytical tool but they also serve as a "laboratory" in which the chemistry of ions can be studied. Because of the ability of mass spectrometers to direct ions and a near-vacuum condition inside the instrument, mass spectrometers are often used to study ion reactions related to our atmosphere and interstellar space.[1,2] Recent spatial explorations of the dense atmosphere of Titan, Saturn's largest satellite, have also stimulated many studies in this area.[3,4]

Ions often have much richer chemistries than their neutral counterparts. The presence of the charge permits the existence of a great number of stable isomers and results in a number of so-called non-classical ion structures (i.e. ion structures whose neutral counterpart is unstable). For example, if we look at the molecular formula C_2H_6O, only two neutral compounds (ethanol and dimethyl ether) are known but for its ionized form, $C_2H_6O^{+\cdot}$, at least six stable isomers have been found by theoretical

calculations,[5,6] five of which have been characterized experimentally.[7,8] Figure 1.1 shows these $C_2H_6O^{+\cdot}$ isomers (structures **1-6**) and their relative energy in kJ mol^{-1}.

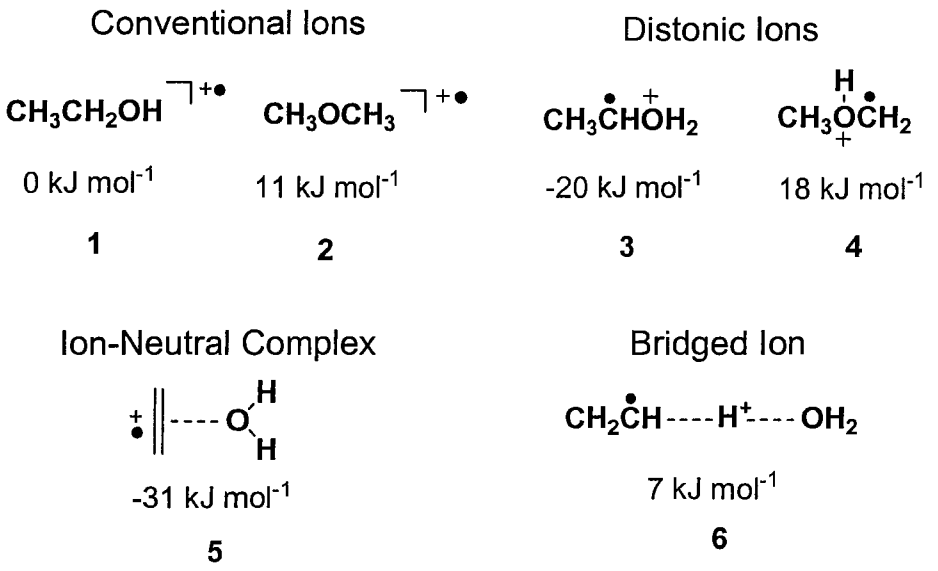

Figure 1.1 Different structures of $C_2H_6O^{+\cdot}$ that have been studied experimentally and/or theoretically.

Structures **1** and **2** are ionized ethanol and dimethyl ether. They are known as the conventional ions as they retain the same connectivity as their neutral form. An example of non-classical ions is distonic ions (Structures **3** and **4**). Unlike typical radical cations, distonic ions refer to covalently-bound ions in which the charge site and the radical site are not at the same atom. As a result of a change in connectivity, isomer **3**, for example, has the charge site on the oxygen atom while the radical site is on the carbon atom. This isomer can be viewed as a protonated $CH_3C^{\cdot}HOH$ radical in which the proton is not at the radical site on carbon but at the adjacent hetero-atom. Distonic ions have been found to be more thermodynamically stable for many ionized alcohols, thiols and haloalkanes and are often found as important intermediates in ion isomerization mechanisms.[9,10] Other

common types of non-classical ions include ion-neutral complexes (**5**) and bridged ions (such as proton-bound species) (**6**). These ions can be viewed as electrostatically-bound complex ions.

Due to the increased number of isomeric structures of ions, a central feature to the chemistry of gaseous ions is their propensity for rearrangement. An example of gas-phase rearrangement processes can be illustrated by the dissociation of ionized methylacetate (Figure 1.2). Early work assumed the products were CH_3CO^+ and $CH_3O^{\cdot}$. However, collisional ionization and dissociation of the neutral product showed that the neutral product was actually a mixture of $CH_3O^{\cdot}$ and $^{\cdot}CH_2OH$.[11-13] Investigation of this rearrangement process found both distonic and bridged ions as intermediates (Figure 1.2).[9] Due to the complex rearrangement that can be involved in ions, gas-phase ion structures cannot be guessed or assumed from neutral chemistry. Holmes and co-workers, for example, have recently published a book on assigning structures to ions in mass spectrometry.[14]

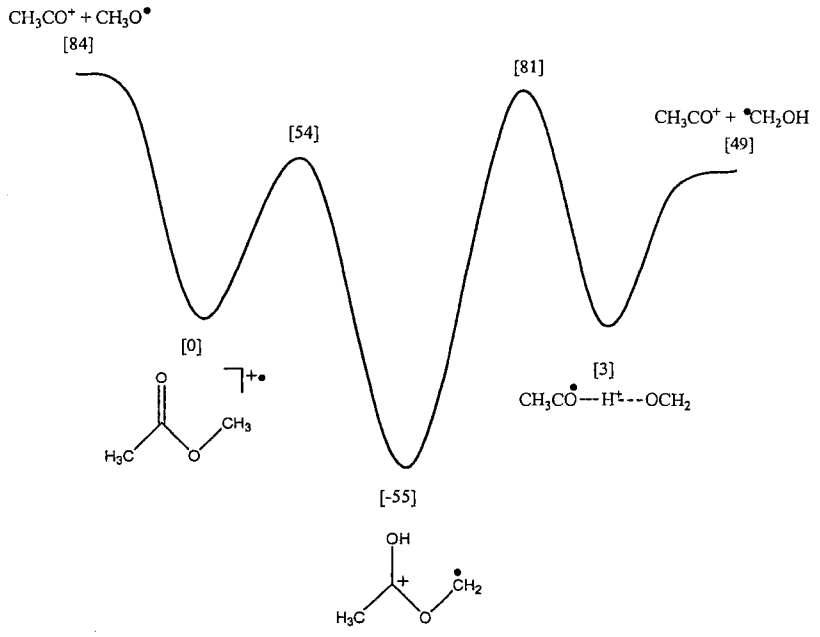

Figure 1.2 Potential energy surface of ionized methylacetate showing how CH_3CO^+ (with different accompanying neutral species) is produced from two different reaction channels. Relative energy (in kJ mol^{-1}) calculated at MP2/6-31G(d) is shown in square brackets.

1.2 Unravelling Rearrangement Mechanisms

Isotopic labelling is an important technique used in mass spectrometry for unraveling ion fragmentation mechanisms as well as revealing any hidden and unexpected rearrangement processes. Isotopic labels such as D, ^{13}C and ^{15}N are used for tracking the atoms involved in the dissociation or rearrangement process. An interesting example is the metastable ionized benzoic acid, C_6H_5COOD, which loses both OD and OH, in a ratio of 1:2, indicating that the deuterium atom on the carboxyl group has undergone unexpected H/D exchange with the hydrogens from the benzene ring.[15] Further experiments with deuterium labels on the meta, ortho and para positions show that H/D exchange occurs only with the ortho-hydrogen atoms.[16]

An extreme and unfortunate case would have exchange of atoms occurring between all labelled and unlabelled atoms, leading to the complete loss of positional identity. This phenomenon is known as atom scrambling and is common for many hydrocarbon cations. In this case, it provides no mechanistic information other than to show that many isomeric ion structures are accessible below the ion's first dissociation limit.

With the advance of computational chemistry, theoretical calculations have become an important tool for exploring reaction mechanisms. Calculations can provide information on the geometry and relative energy of different possible isomers, including their transition states; thus, allowing the complete potential energy surface of an ion's

dissociation or rearrangement pathway to be probed. It is now very common to see experimental results being supported by calculations in research publications. *Ab initio*[17] and density functional theory[17,18] are by far the most popular for studies of small molecules and ions. While *ab initio* methods use molecular orbitals to describe electrons and wavefunctions, density functional theory expresses the total energy in terms of the total electron density. Composite methods such as Gaussian theory have also been developed to improve accuracy without much increase in computational cost by combining single-point energy calculations at various levels of theory. Gaussian-3 (G3) theory will be described in more detail in Chapter 2.

1.3 Gas-Phase vs. Solution-Phase S_N2 Reaction

The major difference between gas-phase and solution-phase chemistry is the lack of solvation effect in the former. It is these solvent effects that often cause the large difference between the rates and the mechanisms of gas-phase and solution-phase reactions.

All chemists will undoubtedly be familiar with the bimolecular nucleophilic substitution reaction in the solution phase as it is taught in virtually all introductory organic chemistry courses.[19]

$$X^- + RY \rightarrow Y^- + RX \qquad (1.1)$$

where X^- is the nucleophile, RY is the substrate and Y^- is the leaving group. The role of steric and solvent effects has been extensively studied for this reaction. In the S_N2

mechanism, the reaction proceeds in one single step in which the attack on the substrate by the nucleophile and the displacement of the leaving group occurs concertedly, resulting in one single large energy barrier as shown in the potential energy profile in Figure 1.3b.

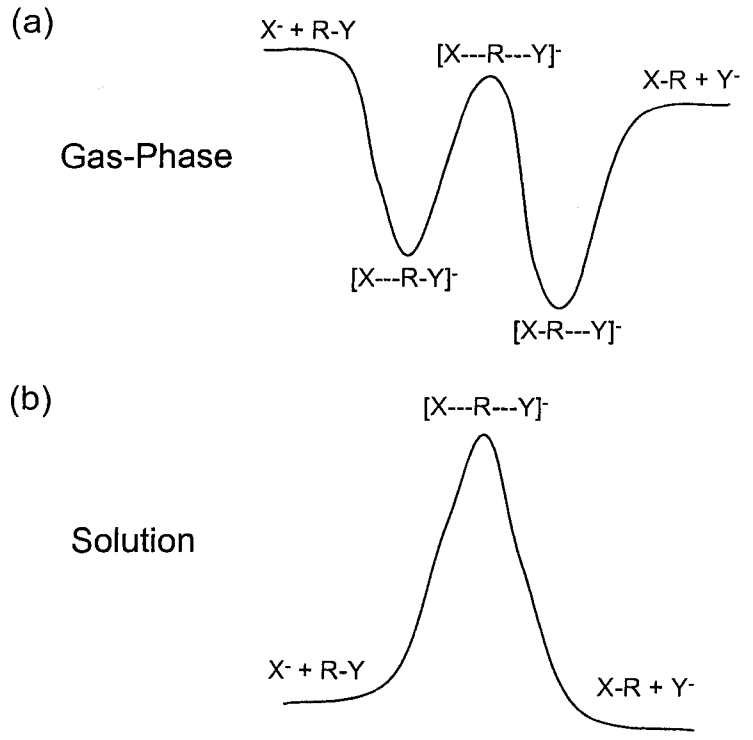

Figure 1.3 General potential energy surface for (a) gas phase and (b) solution phase S_N2 reactions.

However, the gas-phase S_N2 reaction has proven to be significantly more complicated and the potential energy profile shown in Figure 1.3b is not sufficient to describe it. This type of reaction was first investigated experimentally by Bohme[20,21] using the flowing afterglow technique and by Brauman[22,23] with pulsed ion cyclotron resonance (ICR) spectrometry. Olmstead and Brauman examined many different S_N2 reactions and found that the rates of reaction ranged from almost collision rate to being too slow for the reaction to be observed. This observation does not agree with the

solution-phase potential energy surface as the barrier would prevent the reaction from occurring at the collision rate. Dougherty et al.[24-26] observed stable intermediates corresponding to complexes between various halides and alkyl halide substrates. But if the potential energy surface consists of only a single well, all exothermic reactions should occur at near the collision rate. This was not the case, however. As a result, a potential energy surface consisting of a double well with a central barrier was postulated (Figure 1.3a). The double well model can no longer be described as a one-step process. Rather, it can be thought of as occurring in a series of three individual steps. In the first step, the nucleophile and the substrate form an intermediate, $[X^{-}\cdots RY]$. This is followed by an alkyl cation transfer, resulting in the formation of a second intermediate $[XR\cdots Y^{-}]$. Finally, this second intermediate dissociates into RX and Y^{-}. Later work by McMahon and co-workers contributed to the knowledge of these reactions by using a combination of mass spectrometry and theory to probe the characteristics of the gas-phase S_N2 potential energy surface.[27-29]

The difference between the gas-phase and the solution-phase potential energy profile can be accounted for by considering the solvation effect. When the nucleophile or the product ion is surrounded by solvent molecules, the localized charge on the ion enters a favourable interaction with the solvent molecules, resulting in much lower energy in solution than in the gas phase. In comparison, stabilization of the transition state by solvent molecules is not as significant due to charge delocalization over the transition state complex. The greater stabilization of the nucleophilic and product ions by the

solvent over that for the complexes therefore results in the disappearance of the double well in the solution-phase potential energy profile.

In solution, the reaction rates are usually orders of magnitude lower. This is largely due to the need for solvent reorganization in the activation step which results in unfavorable entropies of activation.

1.4 Unimolecular S_N2 Reaction

Cluster ions are of interest to many atmospheric ion chemists as electrostatically-bound ions such as hydrated hydronium ions, $H_3O^+(H_2O)_n$, have been found to be a dominant positive ion species in the mesosphere.[30,31] Proton-bound pairs such as $(ROH)(R'OH)H^+$ exhibit an almost universal tendency to lose H_2O.[32-36] Calculations[28,37-40] and experiments[41-45] on the methanol proton-bound dimer indicated that isomerization proceeds via an internal S_N2-type reaction. Work from our laboratory and that of other labs also showed that the family of methyl-substituted nitrile-alcohol proton-bound pairs[38,46-49] and dimethyl ether proton-bound dimer[50] loses water and methanol in a similar fashion. The potential energy surface (PES) for the $(CH_3CN)(CH_3OH)H^+$ proton-bound pair is shown in Figure 1.4. Its PES is similar to the two-well PES originally proposed by Brauman (as shown in Figure 1.3a) except that there is an intermediate complex between the two transition states, TS1 and TS2.

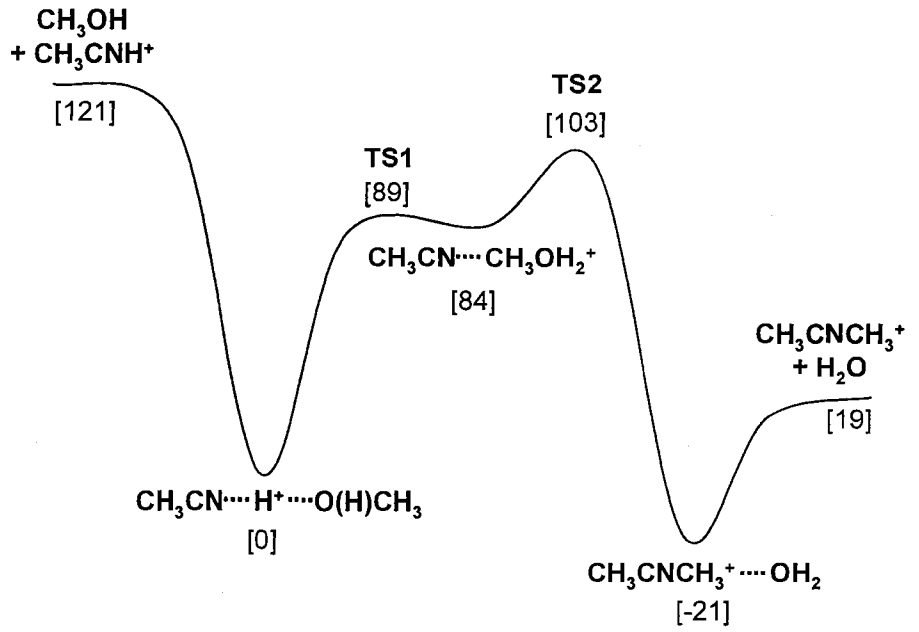

Figure 1.4 Potential energy surface of the acetonitrile-methanol proton-bound pair calculated at the MP2/6-31+G(d) level of theory. Relative energy in kJ mol^{-1} are shown in brackets.[48]

The reaction proceeds by first forming the proton-bound pair in the ion source of the mass spectrometer which subsequently isomerizes to an intermediate ion ($CH_3CN\cdots CH_3OH_2^+$) via a transition state (TS1). The C-O bond in this intermediate ion is then stretched (through a higher energy transition state TS2) to form a thermodynamically stable isomer $(H_2O)(CH_3CNCH_3)^+$, which then dissociates into $CH_3CNCH_3^+$ and H_2O. As the proton-bound pair can also dissociate into CH_3CNH^+ and CH_3OH, the competition between this dissociation process and the rearrangement can be observed.

1.5 Role of Internal Energy and Reaction Barriers

The chemistry that an ion undergoes depends on its internal energy. In terms of fragmentation reactions, each fragmentation product will require a particular minimum internal energy. This is illustrated in Figure 1.5. An ion $M^{+\cdot}$ having an energy X can only access reaction channels A, B and C since the ion does not have sufficient internal energy to access the higher energy channels, D and E. The relative importance of A to C will change with internal energy since the rate of each process varies with energy in a unique fashion.

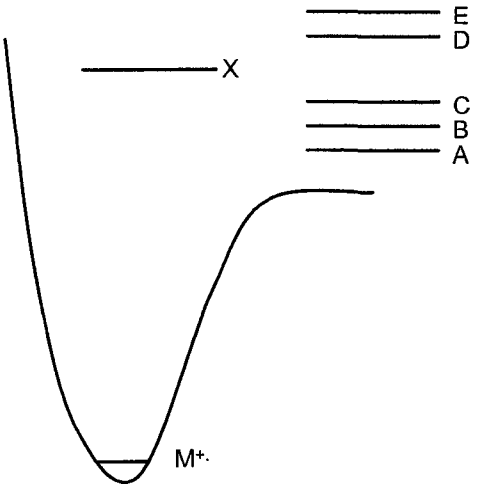

Figure 1.5 Reaction channel accessibility of ions as a function of ion internal energy. An ion with internal energy X can only access reaction channels requiring a lower critical energy than X (i.e. channel A, B and C in the diagram).

Let us now consider several cases in which the competition of two processes may occur. When an isomerization can occur in addition to dissociation, it may greatly complicate the interpretation of mass spectra. The relative energy barriers for dissociation (E_{diss}) and isomerization (E_{iso}) are important parameters as to whether and to what extent an ion A^+ will rearrange to an isomeric ion B^+ at a given internal energy E.

In Figure 1.6a, the barrier for isomerization is much larger than that for the dissociation (i.e. $E_{iso}>>E_{diss}$). Due to the large barrier for isomerization, ion isomerization is not feasible. As a result, the fragment ions will reflect the original structure of the precursor ion, either A^+ or B^+.

In Figure 1.6b, isomerization can occur at internal energies lower than the dissociation threshold (i.e. $E_{iso}<<E_{diss}$). In this case, there will be a mixture of rapidly interconverting structures, A^+ and B^+ at internal energy above E_{iso}. At higher internal energy, dissociations are possible but since dissociations are preceded by a number of interconversions, the fragment ions observed will no longer be characteristic of the initial structure of the precursor ion. Therefore, even if we started with a pure sample of A^+ or B^+, fragmentations from both A^+ and B^+ will be observed.

In Figure 1.6c, A^+ must isomerize to B^+ prior to dissociation. Both A^+ and B^+ will also generate similar mass spectral results but in this case, E_{iso} is the predominant factor in governing the reaction process.

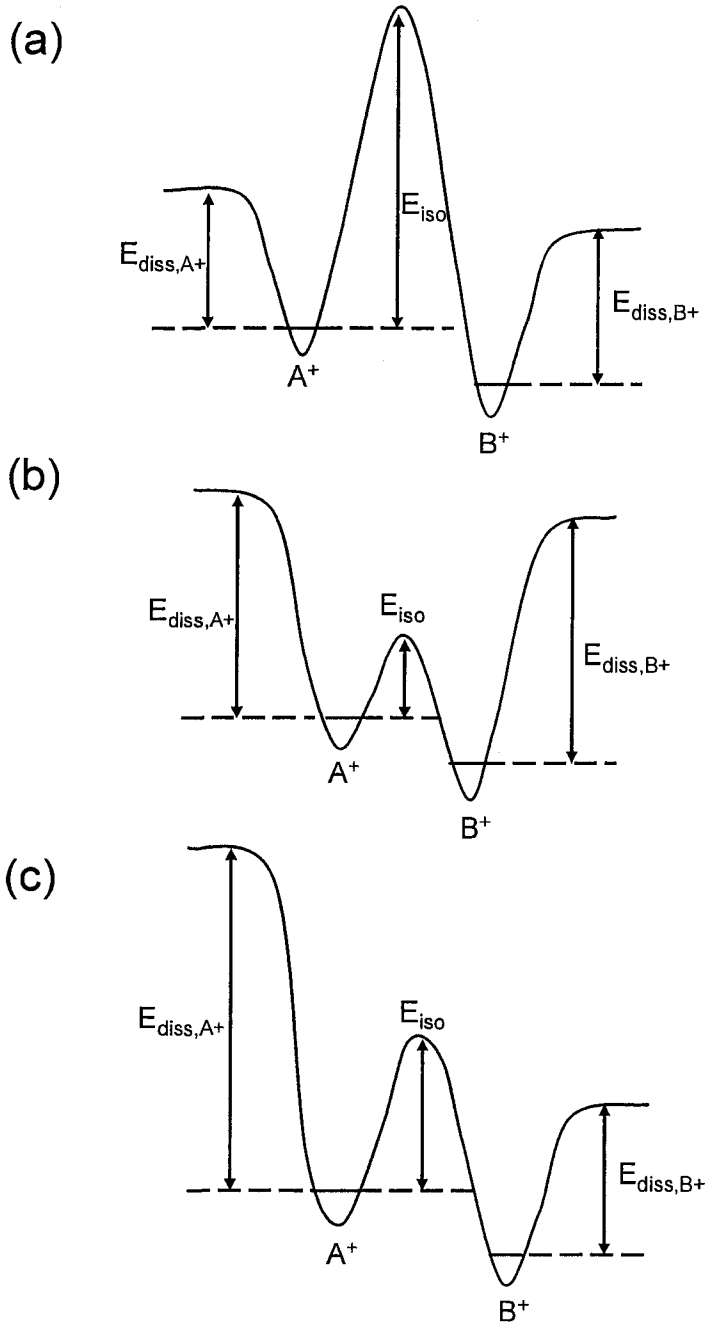

Figure 1.6 Potential energy diagrams showing the effects of ion isomerization in relation to dissociations.

1.6 RRKM and VTST Theory

The kinetic theory taught in most undergraduate courses is based on the Arrhenius equation.[51]

$$k(T) = Ae^{\frac{-E_a}{RT}} \qquad (1.2)$$

The Arrhenius equation refers an ensemble of reactants to a particular temperature. However, the low pressure (~ 10^{-6} Torr) in the ion source of a mass spectrometer means that the newly-formed molecular ion is not in equilibrium with its surroundings and therefore cannot be referred to as having a particular temperature. Instead, it is usually more convenient to think of it as a group of ions with a particular internal energy. This relationship is given by the Rice-Rampsberger-Kassel-Marcus (RRKM)[52,53] or the quasi-equilibrium (QET)[54] theory. These two theories were independently developed by two groups of scientists at about the same time and are now accepted to be different formulations of the same theory.[55-57]

As in all statistical models, the basic assumption underlying the theory is that intramolecular vibrational energy redistribution (IVR) occurs much faster than the rate of the reaction. As a result, the total internal energy is rapidly fully randomized (i.e. statistically redistributed over the active degrees of freedom) before any chemical reaction takes place.

The reaction rate constant (k) at an internal energy E can be expressed in terms of the density of states of the reactant and the transition state as shown below. The density of states, $\rho(E)$, is defined as the number of quantum states at energy E per unit energy.

$$k(E) = \frac{\rho^{\ddagger}(E - E_0)}{h\rho(E)} + \frac{\rho^{\ddagger}(E - E_0 - \varepsilon_1)}{h\rho(E)} + \frac{\rho^{\ddagger}(E - E_0 - \varepsilon_2)}{h\rho(E)} + \ldots\ldots = \frac{\int_0^{E-E_0} \rho^{\ddagger}(E - E_0 - \varepsilon)d\varepsilon}{h\rho(E)} \qquad (1.3)$$

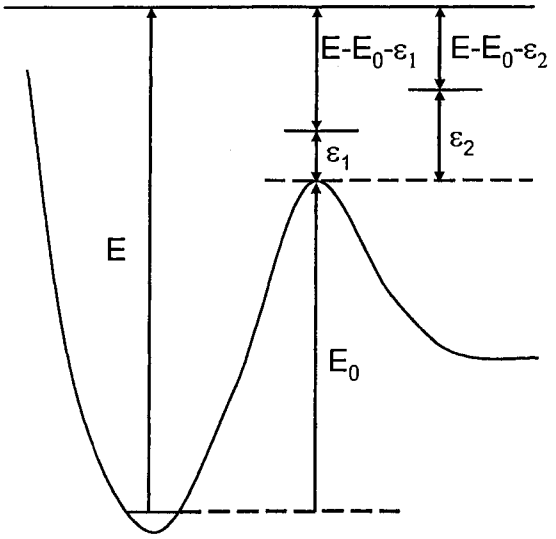

Figure 1.7 Reaction coordinate for a dissociation with a real barrier, E_0. The amount of energy available to be statistically distributed among the vibrational modes of the transition state is E-E_0-ε, where ε represents the amount of inactive energy that remains in the same quantum state during the course of reaction.

Figure 1.7 shows a reaction coordinate involving a reaction barrier with activation energy E_0. The total energy of the transition state E-E_0 can be classified as either active or inactive. The inactive energy, ε, is the energy that remains in the same quantum state during the course of reaction. It therefore cannot contribute to the breaking of bonds. As the reaction coordinate at the transition state consists of translational energy of the departing fragments, this energy can also be thought of as the translational energy of the fragments. Therefore, the total energy of the transition state E-E_0 is partitioned between the inactive energy ε and the remaining internal energy E-E_0-ε.

By summing all the possible ways of partitioning, the transition-state sum of states, $N^{\ddagger}(E-E_0)$ is obtained. The RRKM expression can therefore be expressed as

$$k(E) = \frac{\sigma}{h}\frac{N^{\ddagger}(E-E_0)}{\rho(E)} \qquad (1.4)$$

where $N^{\ddagger}(E-E_0)$ is the transition state sum of states from 0 to $E-E_0$, h is Planck's constant and $\rho(E)$ is the reactant density of states at energy E. Finally, σ is added to the expression to take into account reaction degeneracy. Reaction degeneracy refers to the number of equivalent paths that can lead to the transition state from the reactants. For the H atom loss from CH_4, for example, $\sigma = 4$.

In a more qualitative sense, the transition state sum of states $N^{\ddagger}(E-E_0)$ can be regarded as the number of ways the reacting ion can cross the dividing surface to products (i.e. the probability that a reaction will proceed to products), whereas the reactant density of states $\rho(E)$ reflects the probability that the energy in the ion will "get lost" among the various rotational-vibrational modes and not get into the mode responsible for taking the reaction to the transition state. As a result, k increases with increasing sum of states of the transition state and decreasing density of states of the reactant.

For reactions that contain a substantial activation barrier, the transition state is well defined. In this case, the reaction barrier can be located by searching for the saddle point along the reaction coordinate as energy is such a dominating factor in determining the transition-state sum of states. However, if no obvious barrier exists along the reaction

coordinate (such as that for a dissociation reaction), both activation energy and activation entropy play an important role in defining the transition state. In this case, RRKM theory can be used to calculate the reaction rates at small intervals along the reaction coordinate to locate a point at which the rate constant is smallest. This point can be viewed as the bottleneck for the reactive event and from the RRKM expression, it corresponds to the minimum sum of states of the transition state. This method of locating the transition state is known as the variational transition state theory (VTST).[55]

Figure 1.8 shows a typical picture of how the transition-state sum of states varies with the reaction coordinate for a simple bond cleavage reaction. The existence of the minimum sum of states is due to an interplay between increasing potential energy and decreasing vibrational frequencies for the transitional modes. The increase in potential energy leads to a reduction in the available energy and the sum of states while the decrease in vibrational frequencies for the transitional modes (which are evolving into product rotations and translations) leads to an increase in the sum of states. The two opposing trends result in a minimum in the sum of states at a value of $R^{\ddagger}$.

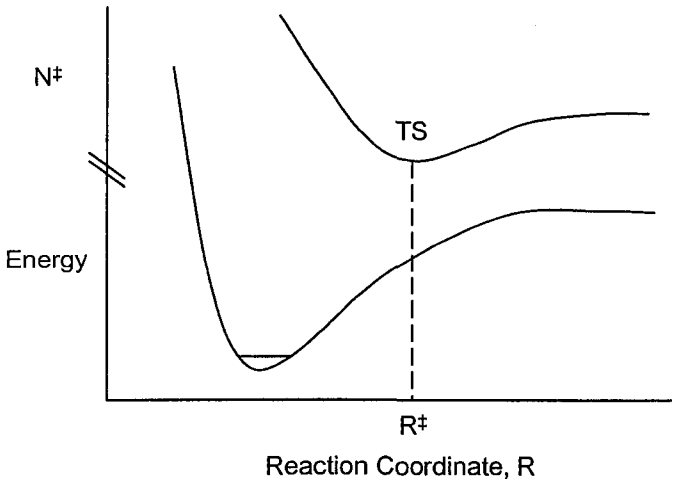

Figure 1.8 (Below) Potential energy surface of an ion leading to a dissociation. (Above) The variation of the sum of states as a function of the reaction coordinate.

1.7 Metastable Ion Window

Ions generated in the ion source have a distribution of internal energy. Only those that decompose inside the field-free region of the mass spectrometer will be observed. For the VG ZAB sector mass spectrometer, this corresponds to ions that decompose with rate constants between 10^4 and 10^6 s^{-1}. These ions are referred to as the metastable ions. Ions that have higher internal energy will decompose before they arrive in the field-free region while those having lower internal energy will decompose after they have been detected. In both cases, dissociation products will not be detected.

Two reaction processes can compete metastably. This is best illustrated with a log k vs. E plot. These plots illustrate how rates vary with increasing internal energy. The variation of the rates is governed by the activation energy E_0 and the activation entropy $\Delta S^{\ddagger}$ of the reaction process. E_0 can be regarded as a parameter indicating at what internal energy reaction starts to proceed while $\Delta S^{\ddagger}$ determines how fast the rate increases with respect to internal energy. If the transition state is more ordered than the reactant ion ($\Delta S^{\ddagger} < 0$), the transition state is said to be tight. This is typical for an isomerization reaction. On the other hand, if the transition state is less ordered than the reactant ion ($\Delta S^{\ddagger} > 0$), the transition state is said to be loose, which is typical for a simple bond cleavage process.

Figure 1.9 illustrates how two processes differing in activation energy and activation entropy can compete with each other. Process 1 refers to a simple bond

cleavage reaction with higher E_0 and $\Delta S^{\ddagger}$ whereas Process 2 is an ion rearrangement with lower E_0 and $\Delta S^{\ddagger}$. At lower internal energy, Process 2 is more favourable because of its lower activation barrier but as we go to higher internal energy, Process 1 starts to dominate, due to its more favourable entropic effect. An overall outcome is a competition within the metastable window on the microsecond timescale.

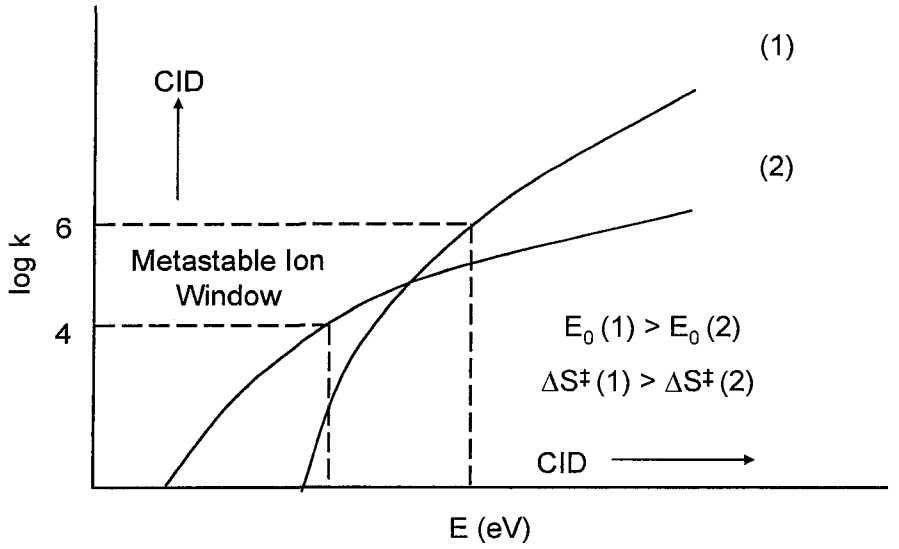

Figure 1.9 Plot of log k vs E revealing a competition of two reaction channels within the metastable ion window.

2 Methods of Study

2.1 The Modified VG-ZAB Mass Spectrometer

The mass spectrometer used for the experiments in this thesis is a modified VG-ZAB triple-focusing mass spectrometer.[58] Figure 2.1 shows the schematic diagram of this instrument. It consists of an ion source, a magnetic mass analyzer (B) and two electrostatic analyzers (ESA). Ions are generated from neutrals in the ion source by electron ionization. The magnetic analyzer and the electrostatic analyzer acts as mass analyzers where ions of different mass-to-charge (m/z) ratio can be separated. It is followed by a detector to measure the intensity of these ions. Between the magnetic and the electrostatic sectors are the second (2FFR) and the third field-free region (3FFR), where ion reactions are studied. Each of these field-free regions is equipped with two collision cells and a deflector to perform various mass spectrometric experiments such as collision-induced dissociations (CID), charge stripping (CS) and neutralization-reionization mass spectrometry (NRMS).

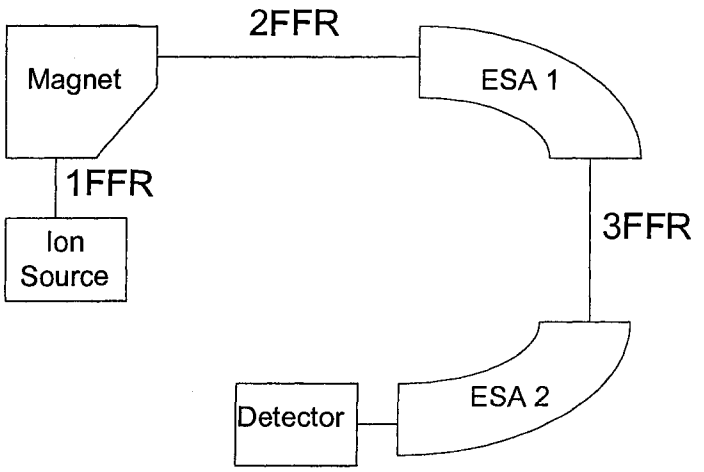

Figure 2.1 Schematic diagram of the modified VG-ZAB mass spectrometer used in this research work.

2.1.1 Ion Source

A number of ionization methods have been developed for mass spectrometry. The method used in my experiments is electron ionization (EI).[59] A schematic diagram of the ion source is shown in Figure 2.2. It consists of a small source block, a filament, a trap electrode, a repeller electrode and an acceleration region. There are four ways to introduce samples to the ion source. There is a liquid septum for volatile liquid, two variable leak valves (one for gas sample and one for liquid vapour) and a solid probe for solid sample. An electron beam (of about 80 eV) is created from a heated helical filament, accelerated towards the block by a potential gradient and collected at the trap electrode. This electron beam interacts with the sample molecules along its path and the newly formed ions are subsequently forced out of the source through an exit slit by the ion repeller and are accelerated to the operating kinetic energy of the instrument

(typically at 8 kV). The kinetic energy of an ion is therefore 8 keV for singly-charged ions (or more generally, zV_{acc} electronvolts where z is the ion charge and V_{acc} is the accelerating voltage).

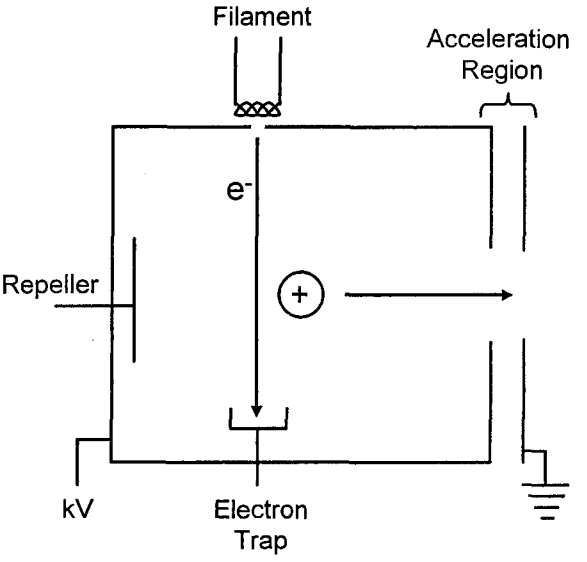

Figure 2.2 A typical electron ionization (EI) ion source used in mass spectrometers.

In order to produce proton-bound pairs or other cluster ions, a relatively high pressure is required in the ion source to ensure sufficient encounters between ions and molecules. Therefore, a modified high-pressure (HP) ion source was used.[60] An HP source was made by sealing the GC inlets and mounting an in-house manufactured gas inlet in the solids-probe inlet. The liquid inlet was untouched. In addition, the exit slit has been narrowed to 0.015 ± 0.005 mm wide by spot welding two stainless steel plates on the source block. These modifications result in an actual pressure that is three orders of magnitude higher than that read on the ionization gauge. The measured pressure in the ion source chamber, read from the gauge, is typically at 10^{-7} Torr and with sample, between 10^{-5} and 10^{-4} Torr.

All chemicals were commercially obtained and used without further purification. Isotopically-labelled compounds (C/D/N Isotopes Ltd, Montreal, QC, Canada) were of over 99% purity. To produce pairs bound by D^+ instead of H^+, the ion source was flushed with several injections of D_2O to the source and a small amount of D_2O was injected to give a D^+ medium in the ion source.

2.1.2 *Magnetic Analyzer*

The magnetic analyzer consists of two parallel electromagnets surrounding an iron core. Under a magnetic field strength B, an ion of mass m will travel through with a curvature radius of r. This is given by the mathematical relationship[61]

$$mv = rBze \qquad (2.1)$$

v is the ion velocity, z is the ion charge and e is the unit of elementary charge. This formula indicates that the magnetic sector is really a momentum analyzer rather than an actual mass analyzer.

As the ions are accelerated by a certain potential (e.g. 8 kV), the velocity of the ion can be determined. Therefore, the above equation can be converted into one that involves the accelerating voltage, V_{acc}. Using the relationship,

$$zeV_{acc} = \frac{1}{2}mv^2 \qquad (2.2)$$

we obtain

$$\frac{m}{z} = \frac{B^2r^2e}{2V_{acc}} \qquad (2.3)$$

Since r is fixed for most instruments and V_{acc} can be held constant, ions of different mass-to-charge ratio (m/z) can be selected by varying B.

2.1.3 Electrostatic Analyzer (ESA)

The electrostatic analyzer consists of two curved parallel plates between which a potential difference is applied to produce an electric field of strength E. Transmission of ions is given by the following relationship:[61]

$$V = \frac{rE}{2} \qquad (2.4)$$

where V is the ion translational energy in electronvolts and r is the radius of curvature. The ESA may seem useless for mass detection as all ions were accelerated by the same accelerating voltage at the ion source. However, as will be discussed later in Section 2.2.1, dissociation products will have translational energy that is proportional to their mass and therefore, energy can be used to identify the mass of these product ions.

2.1.4 Detector

The detectors installed on the VG-ZAB mass spectrometer are off-axis photomultipliers. They consist of a conversion dynode, a CaF_2 scintillator and a photomultiplier (Figure 2.3). When detecting positive-charged ions, a high negative potential of -20 kV is applied to the conversion dynode to attract ions coming from the mass analyzer. The positive ions hit the central portion of the conversion dynode and secondary electrons are emitted. These electrons are then accelerated towards the

scintillator. The scintillations produced are detected by an optically coupled photomultiplier and the signal is amplified. All spectra were recorded with the ZAB-CAT program[62] written by Mommers Technologies.

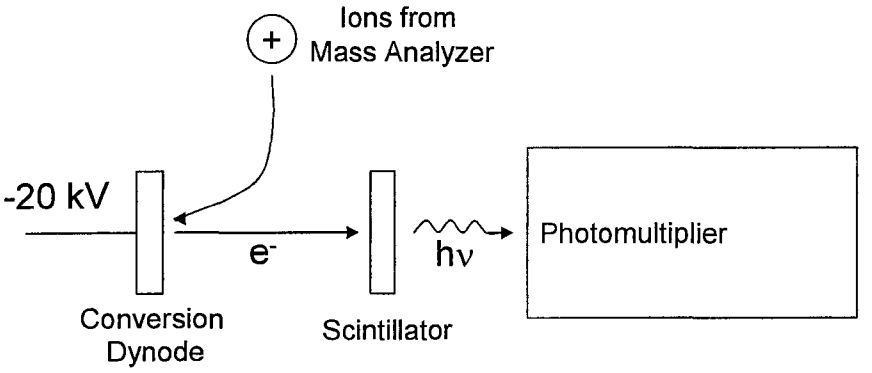

Figure 2.3 Schematic diagram of the ion detector used in the mass spectrometer.

2.2 Experiments Performed in the VG ZAB Mass Spectrometer

The areas between the magnetic and the electrostatic analyzers are the second and third field-free regions. These are the regions where ion reactions are studied. In each of the field-free regions, there are two collision cells and an ion deflector (Figure 2.4). The collision cells consist of 2-3 cm long steel blocks with a 2 mm wide groove cut through it to allow the ion beam to pass through. They are connected to gas lines so that collision gas can be introduced to the cell for ion-target collisions. The pressure in the cells is monitored by ionization gauges placed in close proximity. When it is desired to remove ions out of the beam path, a voltage (e.g. 500 V) can be applied to the deflector.

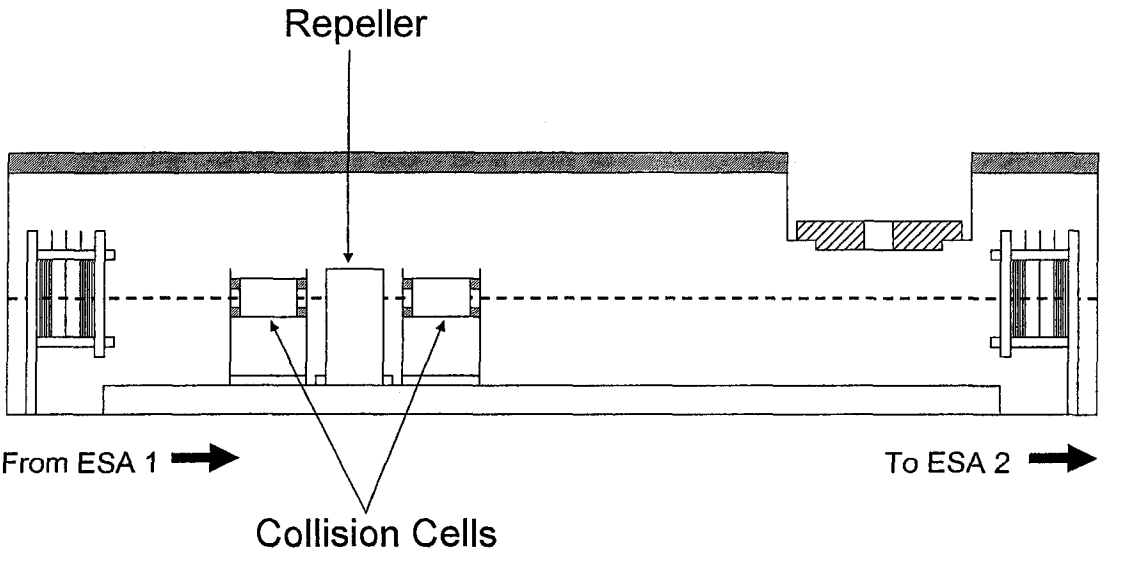

Figure 2.4 Diagram of the inside of the third field-free region of the modified VG-ZAB mass spectrometer used in this work.

2.2.1 Mass-Analyzed Ion Kinetic Energy Spectrometry (MIKES)

Ions accelerated out of the ion source with keV kinetic energies will arrive to the second and third field-free regions within microseconds. Ions that dissociate within this timescale are referred to as metastable ions. When the precursor ion M_1^+ falls apart into M_2^+ and M_3 without any conversion of internal energy to translational energy, the fragments will continue to move along the ion beam at the same velocity as the precursor ion and therefore, fragments that have a smaller mass will have a lower kinetic energy ($1/2mv^2$). An outcome is that the ratio of the kinetic energy of M_1^+ and M_2^+ is proportional to the ratio of their mass.[59]

$$\frac{V_2}{V_1} = \frac{m_2}{m_1} \qquad (2.5)$$

This allows kinetic energies to be correlated back to the mass of the dissociation products.

$$\frac{1}{2}m_1v^2 = \frac{1}{2}m_2v^2 + \frac{1}{2}m_3v^2 \qquad (2.6)$$

A mass spectrum obtained in this manner is known as a MIKE or a metastable ion (MI) mass spectrum. The latter term is used as the observed fragments arise from metastable ions.

2.2.2 Collision-Induced Dissociation (CID) Mass Spectrometry

Collision-induced dissociation is an important tool in mass spectrometry for elucidating ion structures.[14] A CID mass spectrum is obtained in a similar way as an MI mass spectrum except that a target gas is introduced to a collision cell to induce fragmentations. Collision energy can vary significantly between mass spectrometers depending on the translational energy of the ions. It ranges from 10 keV for sector mass spectrometers to 100 eV for quadrupole or ion trap mass spectrometers. Collisions occurring in the VG-ZAB mass spectrometer are at high energy as the ion accelerating potential is typically set at 8 kV.

CID process occurs in two steps. Upon collisions with the target gas, some of the ion's translational energy is converted into internal energy, resulting in ion activation. Subsequently, these activated ions dissociate unimolecularly into fragment ions. The timescale of a CID process is quite different from that of metastable ions. It ranges from the time of the collision event ($t = 10^{-15}$ s) to the time the ions leave the field-free region.

As explained in Section 1.7, at high internal energy, dissociations usually dominate over rearrangements due to their more favourable entropic factor. As a result, CID mass spectra are often characteristic of ion connectivity, allowing isomeric ions to be distinguished.

In my CID experiments, helium was introduced to the collision cell until the ion flux is reduced by 10% (i.e. single collision conditions).[63] Helium was chosen because it is chemically inert. It can be quickly pumped away after a CID experiment and its ionization energy is high, therefore charge transfer process between the ions and the target gas is minimized.

2.2.3 Neutralization-Reionization Mass Spectrometry (NRMS)

Mass spectrometers are most often used to study ions as charged species can easily be manipulated using magnetic or electric field. One way to study neutral molecules with mass spectrometers is by neutralization-reionization mass spectrometry (NRMS).[64-67] In this technique, a fast ion beam is first neutralized by collisions to a target gas, permitting study of the neutral molecules. These molecules are then reionized before they enter the mass analyzer. The most basic requirement for carrying out neutralization-reionization experiments is being equipped with two collision cells separated by a deflector electrode in the field-free region of a tandem mass spectrometer. The purpose of the deflector electrode is to deflect all the ions out of the beam path; thus,

allowing only the neutrals to enter and be reionized in the second collision cell. The process is shown schematically in Scheme 2.1.

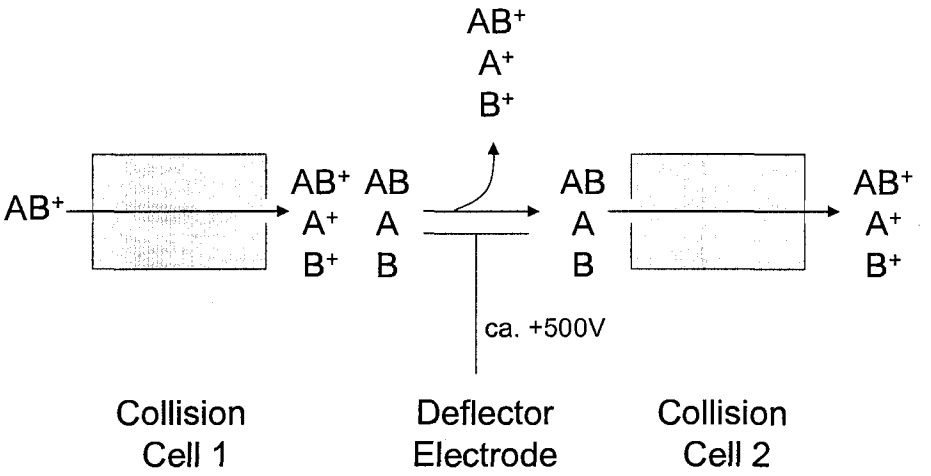

Scheme 2.1 Neutralization-reionization mass spectrometry

Upon collisions with a target gas in the first collision cell, some of the precursor ions are neutralized by charge transfer. Dissociations may also occur. By applying a voltage (e.g. +500 V) to the deflector electrode, all the ions are deflected from the trajectory and only the neutrals will enter the second collision cell for reionization. If it is desired to study the neutral counterpart of the precursor ions, a target with low ionization energy (e.g. O_2 or Xe) is usually preferred, as opposed to He for CID mass spectrometry. This is to facilitate charge transfer between the target and the precursor ions while minimizing ion dissociations. Reionization efficiencies depend on both the projectile and the target. A study by Danis et al. finds that O_2 is generally the optimum target.[68] Therefore, in my NRMS experiments, O_2 was introduced to both collision cells for neutralization and reionization such that each cell achieves a 10% reduction in the ion flux. Due to the short flight time between the first and the second collision cell (~ 0.1

μs), if a precursor ion can survive both neutralization and reionization, it indicates that the neutral species has a lifetime of at least a tenth of a microsecond.

2.3 Theoretical Procedures

2.3.1 Geometry Optimizations and Frequency Calculations

Ab initio molecular orbital and density function theory (DFT) calculations were carried out using the Gaussian 98[69] or Gaussian 03[70] suite of programs. Optimized geometries and the energies of all minima and transition states were calculated at the B3-LYP/6-31+G(d) level of theory. Geometry optimizations converge an initial structure on the potential energy surface into one where the forces on the system are essentially zero. Harmonic vibrational frequencies were then calculated on this optimized geometry. If the structure being sought is a (local) minimum, all vibrational frequencies should turn out to be positive. In contrast, a transition state corresponds to a saddle point at which it is a minimum in all directions except along the reaction coordinate. In this respect, all vibrational frequencies should be positive except the one corresponding to the transitional mode which should have a negative eigenvalue (i.e. an imaginary frequency).

Transition states are further confirmed by the intrinsic reaction coordinate (IRC) procedure in the Gaussian programs. An IRC calculation starts at the saddle point, steps along the reaction path in both directions from the transition state in several small steps (e.g. 6) while optimizing the geometry of the molecular system at each point along the

path. As a transition state is a maximum along the reaction coordinate, IRC calculations should result in lowering the energy. A subsequent geometry optimization on the IRC structure should result in a local minimum. This procedure confirms that the saddle point found is the true transition state connecting the two minima on a potential energy surface.

All computed energies were corrected by the zero-point energy scaled by a factor of 0.9806 (for B3-LYP/6-31+G(d)) as recommended by Scott and Radom.[71] Relative energies were converted from Hartrees into kJ mol^{-1} (1 Hartree = 2625.461 kJ mol^{-1}).

2.3.2 Gaussian-3 (G3) Theory

G3 theory[72] is a composite method in which results from several calculations are combined for higher accuracy. A high level of theory and a large basis set will generally give a more accurate result. However, for larger molecules, this is computationally very expensive. The idea behind composite methods is to combine methods with a high level of theory and a small basis set with methods that employ lower levels of theory and larger basis sets. It is assumed that the various energy changes are additive and so, results from different calculations can be manipulated mathematically to extrapolate the energy to a value equivalent to that from a high level of theory with a large basis set.

In the G3//B3LYP variation,[73] the B3-LYP geometry is used. Therefore, optimized geometry at the B3-LYP/6-31+G(d) level of theory was used to carry out single-point energy calculations at the following levels of theory:

MP4(FC)/6-31G(d)

MP4(FC)/6-31+G(d)

MP4(FC)/6-31G(2df,p)

QCISD(T,FC)/6-31G(d)

MP2(FU)/G3large

The mathematical manipulation of the results from these calculations are as given in the original publication by Baboul et al.[73] and will not be reproduced here. In addition, several final corrections are made to the energy. Zero-point vibrational energy is scaled by 0.96 according to the G3 procedure. A higher level correction (an empirical correction) is made to take into account factors that are not considered in the mathematical manipulation. The correction formulae are as follows:

$$-6.760\, n_\beta - 3.233\, (n_\alpha - n_\beta) \quad \text{(for molecules)} \qquad (2.7)$$

$$-6.786\, n_\beta - 1.269\, (n_\alpha - n_\beta) \quad \text{(for atoms)} \qquad (2.8)$$

where n_α and n_β are the number of α and β valence electrons. The constants (in mhartrees) are obtained by calibrating theoretical results against experimental results for a set of molecules. For molecules containing heavy atoms, a further term is added to account for spin-orbit coupling. Based on the test set of molecules, G3//B3-LYP gives an accuracy to within 1 kcal mol^{-1} of the experimental values.[73]

2.3.3 An Assessment of Computational Methods

An assessment of computational methods is often made to compare results between different levels of theory. In my study, the potential energy surface for the

rearrangement of the nitromethane proton-bound dimer was obtained at the MP2/6-31+G(d) and G3//B3-LYP levels of theory for comparison to the B3-LYP/6-31+G(d) results. All three theories give results that are in agreement with each other (see Chapter 3).

In addition, the nitrite form of the proton-bound dimer of 2-methyl-2-nitropropane, $(CH_3)_3CO(H)(NO)^+((CH_3)_3CNO_2)$, can dissociate into t-butanol and $((CH_3)_3CNO_2)(NO)^+$ with a dissociation energy of 90 kJ mol^{-1} (calculated at B3-LYP/6-31+G(d)). It has previously been shown that B3-LYP gives an erroneous energy for NO^+.[74] So, G3 calculations were performed on both these dissociation products and the products $(CH_3)_3CNO_2H^+ + (CH_3)_3CNO_2$ for comparison. The G3 calculations result in a relative dissociation energy for the two sets of products that is 9 kJ mol^{-1} lower than the B3-LYP results, indicating that B3-LYP is treating $((CH_3)_3CNO_2)(NO)^+$ in a reasonable fashion.

2.3.4 RRKM Theory

To determine the rate constants based on the RRKM expression, information regarding the activation energy and the harmonic vibrational frequencies of the precursor ion and the transition state is required. In the study, this information was obtained from theoretical calculations performed at the B3-LYP/6-31+G(d) level of theory. All frequencies were scaled by 0.9614 as recommended by Scott and Radom.[71] The computing algorithm known as the direct count method[75] was used to determine the

density and sum of states. A copy of this algorithm (in FORTRAN) can be found in Appendix A of this thesis. According to this algorithm, the computer carries out a direct count of the harmonic vibrational energy levels starting from the zero-point energy, counting each of them until it reaches the specified maximum energy of interest. A similar algorithm exists for the sum of states at which the number of states is being added up during the counting process.

The hindered rotor is a hybrid between a free rotor and a vibration. Whether this mode is treated as an oscillator, or as a free rotor depends upon the energy range of interest and the molecule. While at low energy, this motion resembles a vibration; at energy above the barrier height, the motion turns into a free rotation. Therefore, in the study, the intracluster torsion mode was treated as a free rotor in the RRKM calculations.

2.3.5 Variational Transition State Theory (VTST)

VTST was used to locate the transition state of the dissociations of nitroalkane proton-bound pairs. In cases of $(R_1NO_2)(R_2NO_2)H^+$ where $R_1 \neq R_2$, there are two dissociation processes, resulting in $R_1NO_2H^+$ or $R_2NO_2H^+$. For each of the dissociation processes, the N-N bond distance in the proton-bound pair is stretched from about 6 Å to about 25 Å at intervals of 1 Å. The optimized geometry and the harmonic vibrational frequencies at each of these bond distances were calculated at the B3-LYP/6-31+G(d) level of theory and the density and the sum-of-states were calculated by the direct count

method.[75] The optimized geometry resulting in the smallest sum of states is designated as the transition state.

2.3.6 *Thermodynamic Reaction Entropy and Entropy of Activation*

Thermodynamic reaction entropy (ΔS) and the entropy of activation ($\Delta S^{\ddagger}$) were calculated based on the expression for statistical entropy:

$$S = \frac{U}{T} + Nk_B lnQ \qquad (2.9)$$

where k_B is Boltzmann's constant, N is Avogadro's number, T is the temperature, U is the internal energy and Q is the partition function. Translational, rotational and vibrational components to entropy were calculated for the reactants, the transition states and the dissociation products to derive ΔS and $\Delta S^{\ddagger}$. All entropy values were calculated at 600 K.

3 Results & Discussion

3.1 Mass Spectrometric Studies of $(R_1NO_2)_2H^+$

Metastable ion (MI) mass spectrometry probes the accessible reaction channels that occur spontaneously without the aid of collisions. MI experiments on a series of $(RNO_2)_2H^+$ where R = CH_3, CH_2CH_3, $(CH_3)_2CH$ and $(CH_3)_3C$ therefore reflect how the methyl groups on the nitroalkane affect the competition of the reaction channels on the microsecond timescale. The MI mass spectra of these four methyl-substituted proton-bound dimers are presented in Figure 3.1. They all exhibit a peak nominally due to the protonated nitroalkane, at m/z 62, 76, 90 and 104 respectively, as a result of the breaking of the electrostatic interaction between the bridging proton and a neutral nitroalkane molecule. In the cases of $(CH_3NO_2)_2H^+$ and $(CH_3CH_2NO_2)_2H^+$ (Figure 3.1 a, b), this reaction is the only reaction channel observed on the microsecond timescale. The MI mass spectra of $((CH_3)_2CHNO_2)_2H^+$ and $((CH_3)_3CNO_2)_2H^+$ (Figure 3.1 c, d) exhibit a second channel at m/z 132 and 160 (i.e. a loss of 47 Da) that can only be attributed to the loss of nitrous acid (HONO). The similarity between these proton-bound dimers and those previously studied (for example, the water loss from the alcohol-alcohol and alcohol-nitrile proton-bound pairs)[47,48,76] suggests that the loss of nitrous acid is likely to be the result of an S_N2-type of rearrangement (Scheme 3.1). The MI results also indicate that methyl substituents favour this rearrangement process, similar to that observed for

$(ROH)(R'OH)H^+$ and $(RCN)(R'OH)H^+$.[48] Supporting computational results on this rearrangement will be given in Section 3.4.

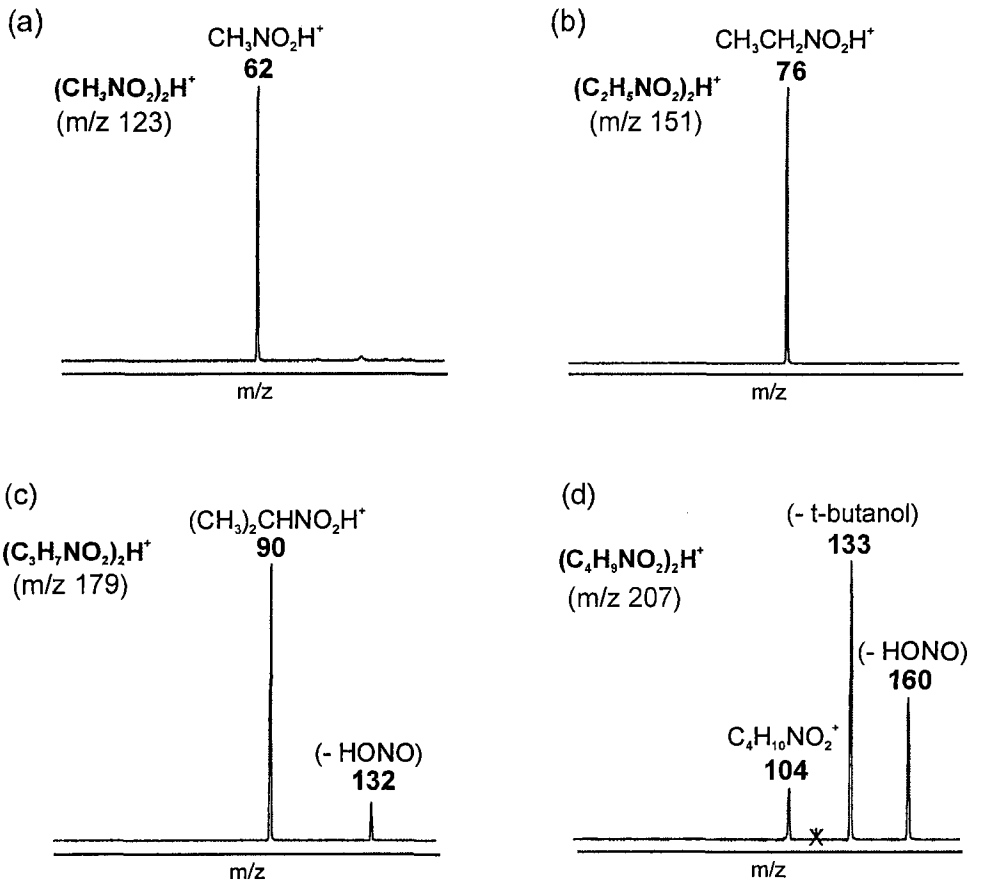

Figure 3.1 MI mass spectra of the proton-bound dimers $(CH_3NO_2)_2H^+$, $(CH_3CH_2NO_2)_2H^+$, $((CH_3)_2CHNO_2)_2H^+$ and $((CH_3)_3CNO_2)_2H^+$.

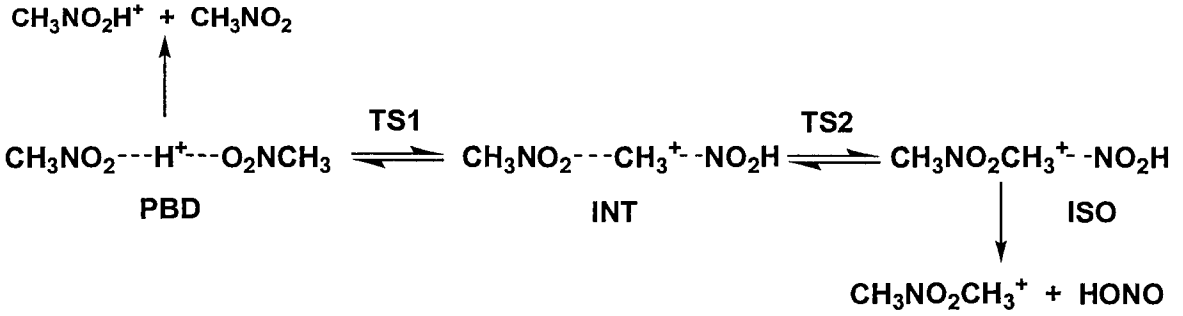

Scheme 3.1 Reaction scheme for the loss of nitrous acid from nitromethane proton-bound dimers via an internal S_N2 process.

The MI mass spectrum of $((CH_3)_3CNO_2)H^+$ (Figure 3.1d) exhibits a third channel, the loss of 74 Da. This was identified as the loss of t-butanol. Its identity is supported by isotopic-labelling experiments as well as characterization of the resulting ion which suggests the formation of a complex between NO^+ and a neutral nitroalkane molecule. This ion (m/z 133) was transmitted to the third field-free region where it was analyzed by collision-induced dissociations (CID) and neutralization-reionization mass spectrometry (NRMS). The identity of this ion is discussed in Section 3.3. Based on these results, it was proposed that t-butanol may have been lost via a nitro-nitrite rearrangement (Scheme 3.2). Supporting computational results for this rearrangement will be given in Section 3.5 and 3.6.

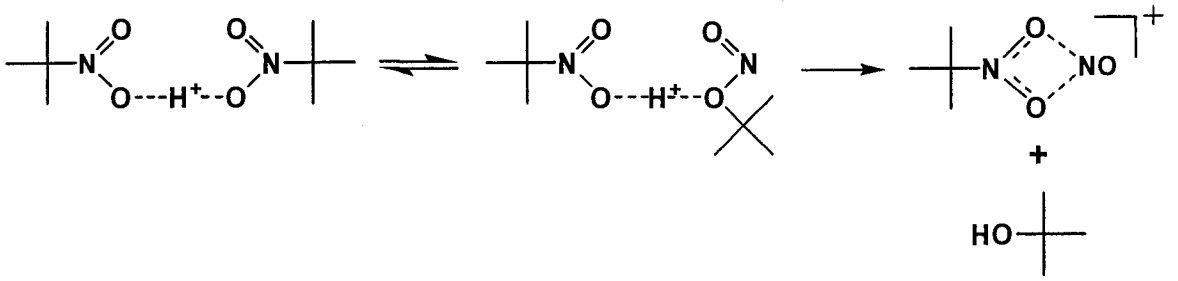

Scheme 3.2 Reaction scheme for a possible loss of t-butanol from the proton-bound dimer via a nitro-nitrite rearrangement.

The MI mass spectrum of $((CH_3)_3CNO_2)_2D^+$ was also obtained. It exhibits three main peaks at m/z 105, 133 and 160. These masses are consistent with the assignment of the peaks. It also confirms that the nitrous acid and the t-butanol loss involve the bridging proton and that there is no hydrogen exchange between this proton and the alkyl hydrogens.

3.2 Mass Spectrometric Studies of $(R_1NO_2)(R_2NO_2)H^+$

Unsymmetric proton-bound pairs have also been investigated. The MI mass spectra of six different proton-bound pairs are presented in Figure 3.2. All cases exhibit the formation of only one protonated nitroalkane. Upon dissociation, the proton remains on the more substituted nitroalkane. This is consistent with their proton affinity. Methyl substituents are known to increase the proton affinity of organic ions. For nitroalkanes, each methyl substituent increases the proton affinity by about 15 kJ mol^{-1}, a difference that is large enough to cause dissociation to occur preferentially between the bridging proton and the less methyl-substituted species.

Nitrous acid loss was observed from $(CH_3CH_2NO_2)((CH_3)_2CHNO_2)H^+$, $(CH_3NO_2)((CH_3)_3CNO_2)H^+$, $(CH_3CH_2NO_2)((CH_3)_3CNO_2)H^+$ and $((CH_3)_2CHNO_2)((CH_3)_3CNO_2)H^+$ (Figure 3.2 c-f), emphasizing the importance of highly methyl-substituted species in the proton-bound pair in favouring this rearrangement process. Together with the observation from the proton-bound dimers $(R_1NO_2)_2H^+$, this indicates that for these proton-bound pairs, the reaction proceeds exclusively through isopropyl or t-butyl transfer as methyl and ethyl transfer do not occur.

The t-butanol loss channel (i.e. M - 74) is observed for the proton-bound pair $((CH_3)_2CHNO_2)((CH_3)_3CNO_2)H^+$ only (Figure 3.2f), indicating not only the important role the t-butyl substituent plays in this process but also the importance of the methyl substituents in the other species of the proton-bound pair as well. The MI spectra of

deuterium-labelled species $((CD_3)_2CHNO_2)((CH_3)_3CNO_2)H^+$ exhibits a peak due to the loss of 74 Da whereas for $((CD_3)_2CHNO_2)((CH_3)_3CNO_2)D^+$, a peak was observed as a result of a loss of 75 Da. These results indicate that the bridging proton is included in the neutral product that is lost but exclude the involvement of the $(CH_3)_2CH$ moiety in the neutral product. The nature of this m/z 119 ion will be discussed in Section 3.3.

Therefore, from the MI study of the nitroalkane proton-bound pairs, there are three different reaction channels that can compete on the microsecond timescale. One occurs by a simple bond cleavage process, resulting in protonated nitroalkane, and the other two processes are results of a rearrangement process leading to either a loss of nitrous acid (M - 47) or a loss of t-butanol (M - 74).

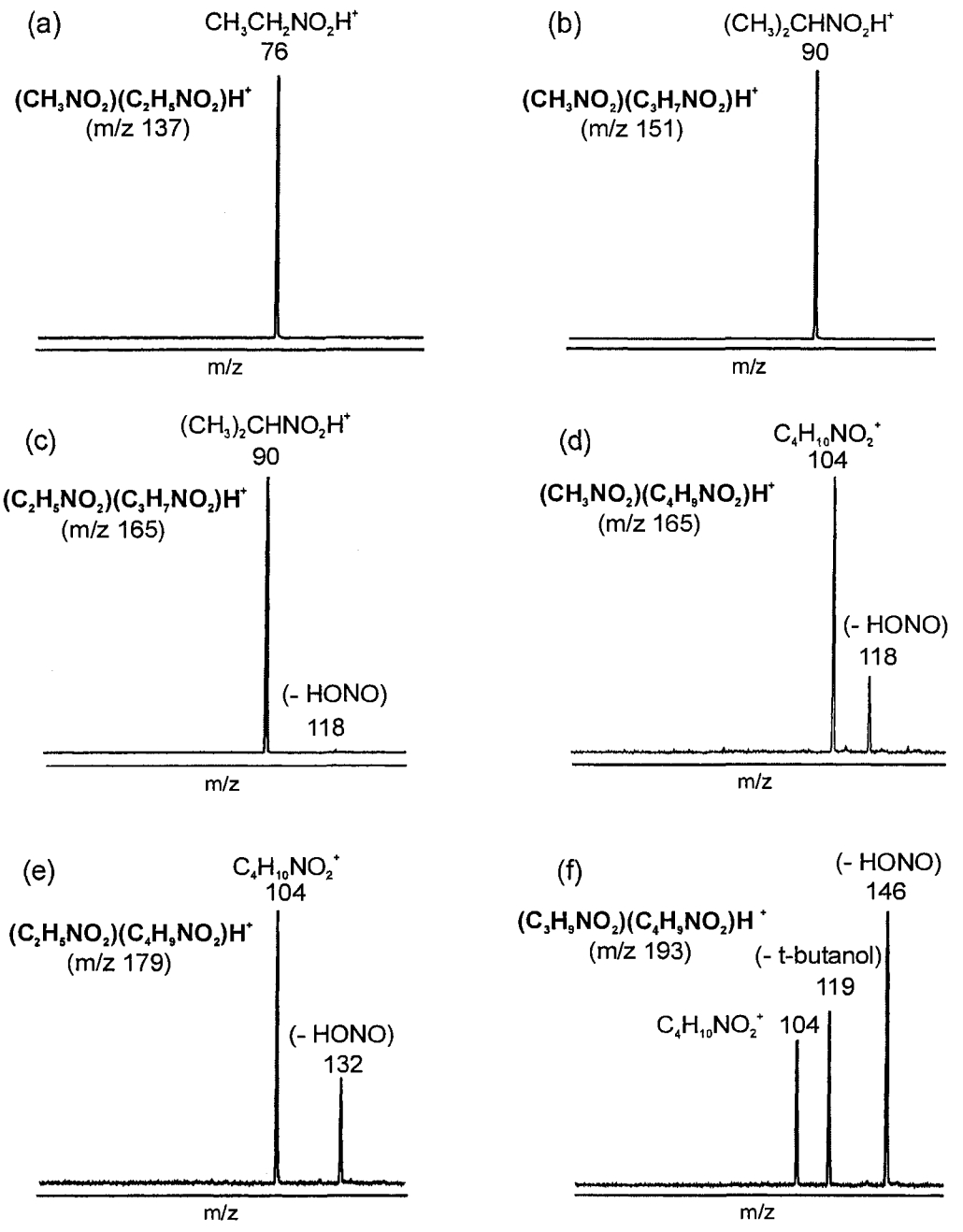

Figure 3.2 MI mass spectra of the unsymmetric proton-bound pairs.

3.3 The Identity of m/z 119 and 133

The metastably-generated m/z 119 ion (in Figure 3.2f) was transmitted to the third field-free region where it was analyzed by CID. The CID mass spectrum shows intense peaks at m/z 30 (NO^+) and 43 ($(CH_3)_2CH^+$) as well as several smaller peaks (see Figure 3.3a). To test that this ion was due to the interaction of NO^+ and $(CH_3)_2CHNO_2$, NO and $(CH_3)_2CHNO_2$ were co-introduced into the ion source and the resulting ion at m/z 119 (having 5 keV translational energy) was transmitted to the second field-free region. The CID mass spectrum (Figure 3.3b) of this ion is similar to Figure 3.3a, confirming that the product ion (m/z 119) derived from $((CH_3)_2CHNO_2)((CH_3)_3CNO_2)H^+$ to be a complex between NO^+ and $(CH_3)_2CHNO_2$. There are some variations in the relative intensities of the peaks, especially those of the weaker ones. This is subject to reproducibility of the spectrum due to the weak signal that was being transmitted to the third field-free region. Further supporting the nature of this structure is the MI mass spectrum of the source-generated complex (Figure 3.3c) which shows a predominant peak at m/z 30. The observation of NO^+ instead of $(CH_3)_2CHNO_2^+$ agrees with the relative ionization energies of NO and 2-nitropropane (9.26 and 10.74 eV respectively).[77]

The NR mass spectrum of the source-generated complex (Figure 3.3d) exhibits three main peaks, m/z 30, 43 and 46. The precursor ion (m/z 119) can be neutralized upon collision in the first collision cell (Scheme 3.3a). The resulting neutral NO and $(CH_3)_2CHNO_2$ can then be reionized to form NO^+ and $(CH_3)_2CHNO_2^+$. The latter

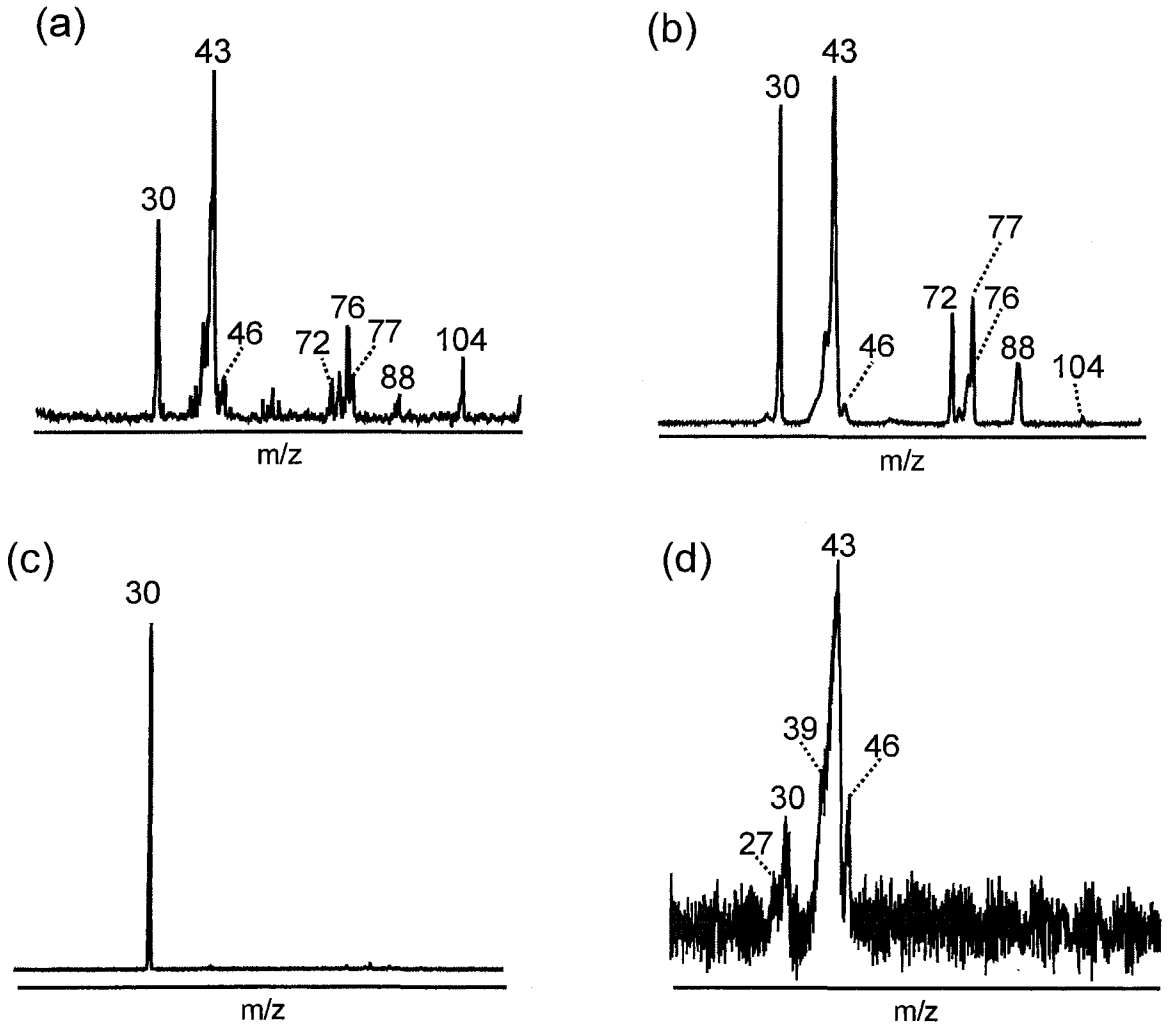

Figure 3.3 CID mass spectra of (a) metastably-generated m/z 119 from the proton-bound pair $((CH_3)_2CHNO_2)((CH_3)_3CNO_2)H^+$. (b) CID, (c) MI and (d) NR mass spectrum of source-generated m/z 119 $((CH_3)_2CHNO_2)(NO)^+$ at 5 keV.

subsequently falls apart into the isopropyl cation (m/z 43) and NO_2 due to the low stability of the ion (for example, the molecular ion is barely observed in the EI mass spectrum of 2-nitropropane).[77] As the ionization energy for O_2 (12.06 eV) is higher than that of NO (9.26 eV), some collisions likely result in only dissociation into NO^+ + $(CH_3)_2CHNO_2$ (Scheme 3.3b). NO^+ is deflected away from the ion beam by a voltage on the deflector between the two collision cells. Therefore, only $(CH_3)_2CHNO_2$ is transmitted for reionization, which falls apart into the isopropyl cation (m/z 43) and NO_2. A similar argument can be made for the formation of $(CH_3)_2CHNO_2^+$ which dissociates into the isopropyl cation and neutral NO_2 and NO (which could be a complex) which is then reionized into NO_2^+ and NO^+ (Scheme 3.3c). Therefore, both CID and NRMS experiments suggest a structure for the m/z 119 ion in which NO^+ is electrostatically bound to $(CH_3)_2CHNO_2$.

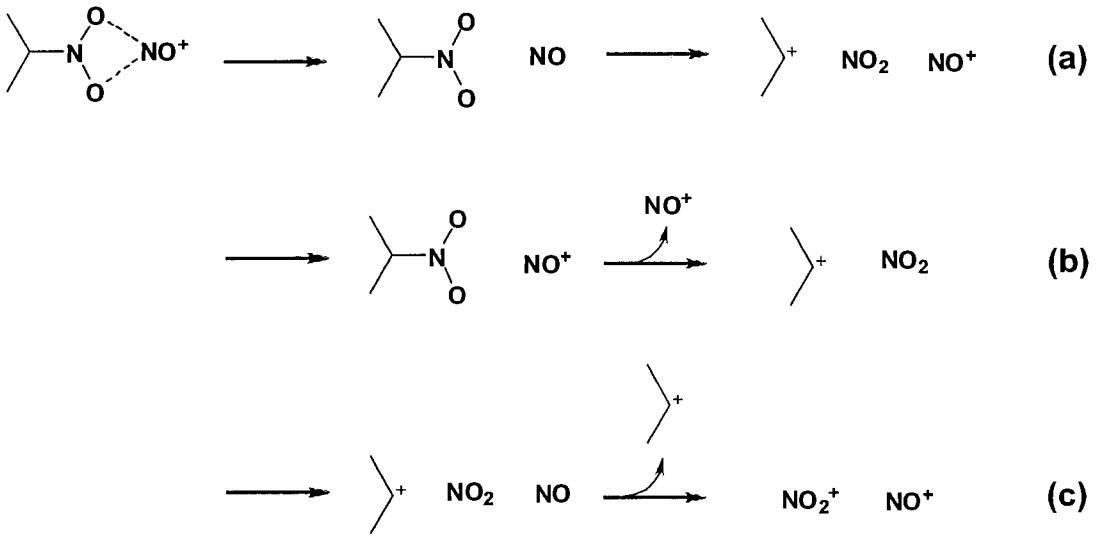

Scheme 3.3 Reaction schemes for the production of isopropyl cation, NO^+ and NO_2^+ from the proton-bound pair $((CH_3)_2CHNO_2)((CH_3)_3CNO_2)H^+$ in the neutralization-reionization mass spectrometry experiment.

The fragment ion having m/z 133 from $((CH_3)_3CNO_2)_2H^+$ (as in Figure 3.1d) was transmitted to the third field-free region where it was analyzed by CID. The CID mass spectrum shows intense peaks at m/z 57 ($(CH_3)_3C^+$) and 86 ($C_4H_8NO^+$) (see Figure 3.4a). This spectrum is the same as the CID mass spectrum of the ion generated from the association reaction of NO^+ and $(CH_3)_3CNO_2$ in the ion source (Figure 3.4b). These two peaks are also observed in the MI mass spectrum except that the peak at m/z 86 (due to loss of HONO, obviously resulting from a rearrangement) is more intense than m/z 57 (Figure 3.4c). Strikingly, no NO^+ was observed in any of these spectra. Based on the ionization energies of NO and 2-methyl-2-nitropropane (9.26[77] and 10.47 eV respectively, the latter being calculated at the G3 level of theory), formation of NO^+ might be expected to be the favoured product. G3 calculations based on B3-LYP geometries found the lowest energy dissociation products to be $(CH_3)_3C^+ + N_2O_3$, which lie 8 kJ mol^{-1} lower than $(CH_3)_3CNO_2 + NO^+$. Therefore, the stability of the t-butyl ion has favoured the dissociation forming the t-butyl cation over that which makes NO^+. As NO^+ was not observed in the MI mass spectrum, the nature of how NO^+ is bound to the molecule cannot be determined.

The NR mass spectrum of the source-generated complex (Figure 3.4d) exhibits several main peaks, m/z 30, 46 and 57. Similar schemes as for m/z 119 can be drawn to explain for these peaks. The m/z 133 ions neutralized in the first collision cell would likely fall apart into NO and 2-methyl-2-nitropropane. Upon reionization, ionized 2-methyl-2-nitropropane would itself dissociate into the t-butyl cation (m/z 57) and NO_2 due to the low stability of the molecular ion. This is consistent with the fact that the

molecular ion is not observed in the EI mass spectrum of 2-methyl-2-nitropropane.[77] The peak with m/z 46 can arise from the dissociation in the first collision cell of the m/z 133 ion into the t-butyl cation and N_2O_3 (or NO_2 + NO) which is then reionized to NO_2^+ (m/z 46) and NO^+ (m/z 30). Based on G3 calculations on B3-LYP geometries, N_2O_3 is very weakly bound with respect to NO_2 + NO (N–N bond = 1.9 Å and binding energy = 37 kJ mol^{-1}). $N_2O_3^+$ was not observed in the NR mass spectrum due to the instability of the ion. G3 calculations give an N–N bond length of 2.5 Å and a binding energy of -11 kJ mol^{-1} with respect to NO^+ + NO_2 for $N_2O_3^+$. While it is hard to believe that there is no binding energy when NO^+ interacts with NO_2, the calculations indicate that this binding will be small. All the experimental and theoretical results discussed above are at least consistent with an electrostatically bound complex structure $((CH_3)_3CNO_2)(NO^+)$ for m/z 133.

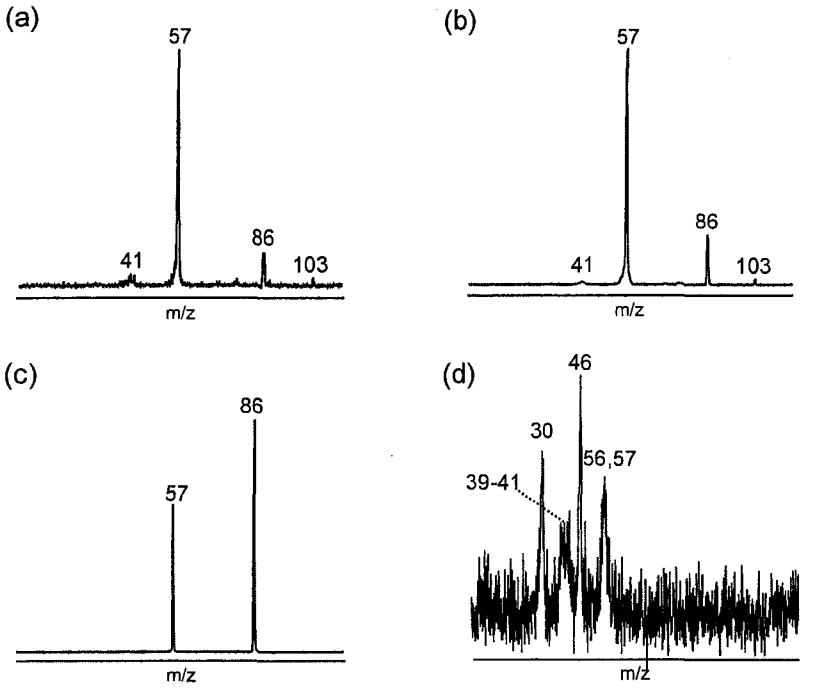

Figure 3.4 CID mass spectra of (a) metastably-generated m/z 133 from the proton-bound dimer $((CH_3)_3CNO_2)_2H^+$. (b) CID, (c) MI and (d) NR mass spectrum of source-generated m/z 133 $((CH_3)_3CNO_2)(NO)^+$ at 5 keV. The labels 39-41 and 56, 57 in (d) indicate relatively broad peaks that cover more than one mass.

3.4 The Nitrous Acid Loss Channel of $(CH_3NO_2)_2H^+$, $(CH_3CH_2NO_2)_2H^+$ and $((CH_3)_3CNO_2)_2H^+$

The theoretical reaction profile for $(CH_3NO_2)_2H^+$ at the B3-LYP/6-31+G(d), MP2/6-31+G(d) and G3 levels of theory are presented in Figure 3.5 (with the corresponding structures from B3-LYP shown below). The isomerization reaction resulting in HONO loss involves an S_N2-type of mechanism. The first step of the process consists of a barrier (**TS(1-2)**, TS1) involving the rotation of one moiety to set up for a backside attack on the protonated species by the neutral nitroalkane. This barrier is small (almost negligible) relative to the intermediate (**2**, INT). The second step (the key barrier in the rearrangement, TS2, see **TS(2-3)** in Figure 3.5) involves an alkyl cation transfer, where the attack of the neutral molecule on the carbon results in the lengthening of the C–N bond in the protonated nitromethane moiety and the shortening of the O–C bond in $[CH_3NO_2\cdots CH_3\cdots NO_2H]^{+\ddagger}$. After some conformational changes, it results in a thermodynamically stable isomer **3**, $(HONO)(CH_3NO_2CH_3)^+$. Simple dissociation from this complex results in the final products of $CH_3NO_2CH_3^+$ and HONO. Another conformer of **2** was found to lie 10 kJ mol^{-1} higher in energy (see **2b** in Figure 3.5) which may be involved in the conversion of **2** to **TS(2-3)**.

Three isomeric structures of nitrous acid were calculated: HNO_2 (**4**), where the hydrogen is bonded to the nitrogen and cis- (**5**) and trans-HONO (**6**). HONO has been a subject of extensive theoretical and experimental investigations.[78] The trans conformer of HONO is the most stable structure lying 1 kJ mol^{-1} lower than the cis conformer and

24 kJ mol^{-1} below HNO_2. The final product of the isomerization process should therefore be a mixture of trans- and cis-HONO.

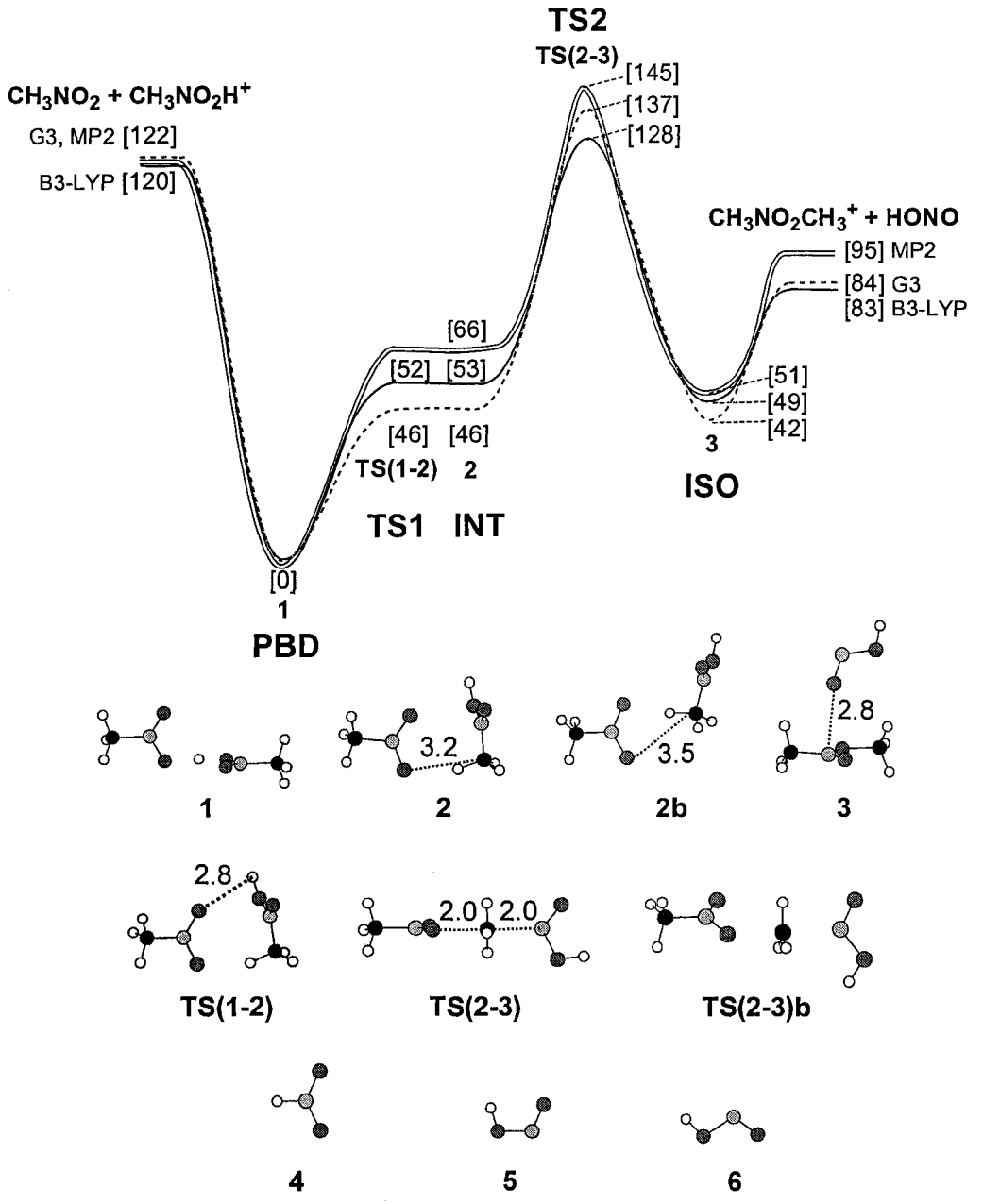

Figure 3.5 Potential energy surface for the isomerization of the nitromethane proton-bound dimer $(CH_3NO_2)_2H^+$ leading to loss of nitrous acid, calculated at the B3-LYP/6-31+G(d) (—), MP2/6-31+G(d) (==) and G3 (---) levels of theory. Relative energy values (kJ mol^{-1}) for MP2, G3 and B3-LYP are in square brackets. Optimized geometries at B3-LYP/6-31+G(d) level of theory are shown below the figure. Selected bond length values are presented in Å.

The effect of the HONO conformation in the transition state was also examined. Calculations show that **TS(2-3)** in which the proton is in the cis conformation lies 19 kJ mol^{-1} below its trans conformer **TS(2-3)b**; the cis-trans conformational change in HONO should thus occur primarily after the alkyl cation transfer step is completed.

The surface for this S_N2-type rearrangement in $(CH_3NO_2)_2H^+$ was also calculated at the MP2/6-31+G(d) and G3 (on B3-LYP geometries) levels of theory (Figure 3.5). The G3 value for TS2 lies between the B3-LYP and MP2 results. In general, there is consistency between the three levels of theory. As a result, B3-LYP was used for all other proton-bound pairs since B3-LYP is less computationally expensive and therefore, more suitable for larger molecules and ions.

The relative energies of the dissociation and S_N2-isomerization process for the nitroalkane proton-bound dimers of $(CH_3NO_2)_2H^+$, $(CH_3CH_2NO_2)_2H^+$ and $((CH_3)_2CHNO_2)_2H^+$ are included in Figure 3.6 for comparison (their optimized geometries in Figure 3.7). The threshold of dissociation to protonated and neutral nitroalkane does not vary significantly with methyl substitution, ranging from 120 to 125 kJ mol^{-1}. This is consistent with the trends observed for other proton-bound dimers.[79] The isomerization barrier is consistently decreased with increased methyl substitution, going from 128 kJ mol^{-1} for $(CH_3NO_2)_2H^+$, to 124 kJ mol^{-1} for $(CH_3CH_2NO_2)_2H^+$ and 98 kJ mol^{-1} for $((CH_3)_2CHNO_2)_2H^+$, a result of charge stabilization in TS2. The fact that the isomerization and dissociation thresholds are similar for $(CH_3NO_2)_2H^+$ and $(CH_3CH_2NO_2)_2H^+$ and yet no nitrous acid loss is observed is a clear indication of the less

favourable entropies for the isomerization process.[55] The tighter transition state associated with the S_N2 rearrangement reduces the rate constant of the process in comparison to the simple H-bond cleavage reaction, resulting in the isomerization being non-competitive with the dissociation process.

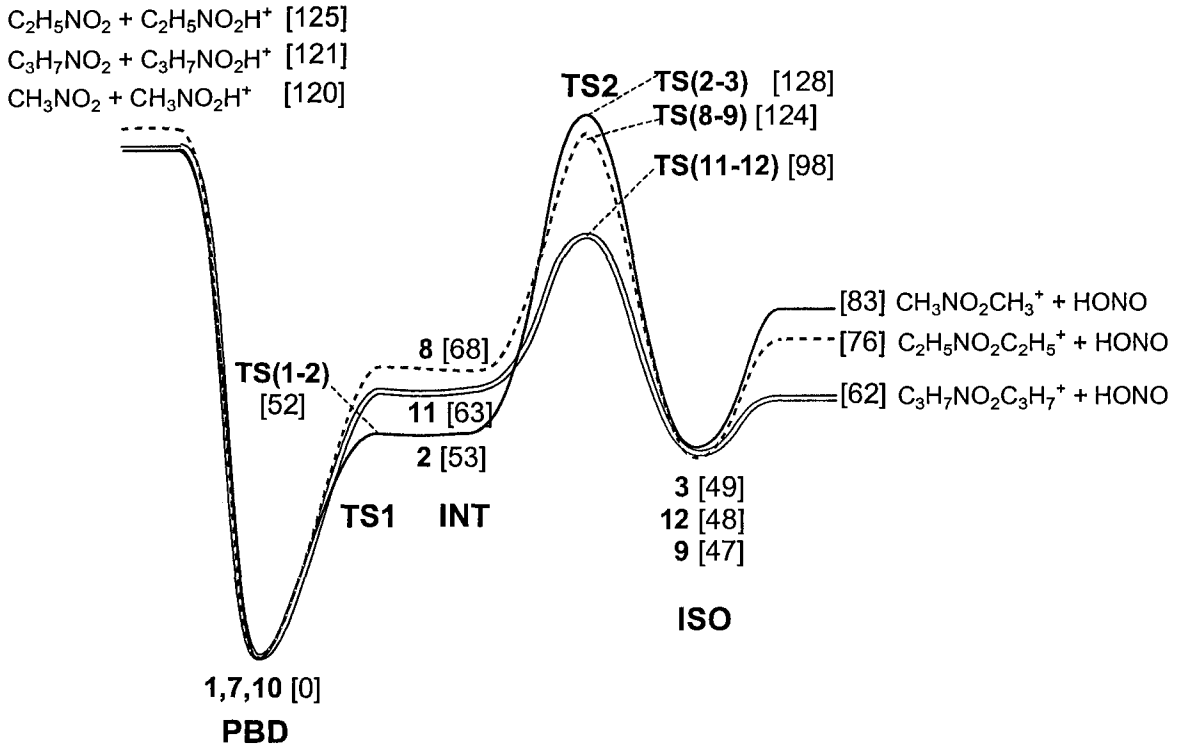

Figure 3.6 Potential energy surface with relative energies (in square brackets, kJ mol^{-1}) for the proton-bound dimer of nitromethane (—), nitroethane (---) and 2-nitropropane (==) to lose nitrous acid at the B3-LYP/6-31+G(d) level of theory. Optimized geometries are presented in Figure 3.7.

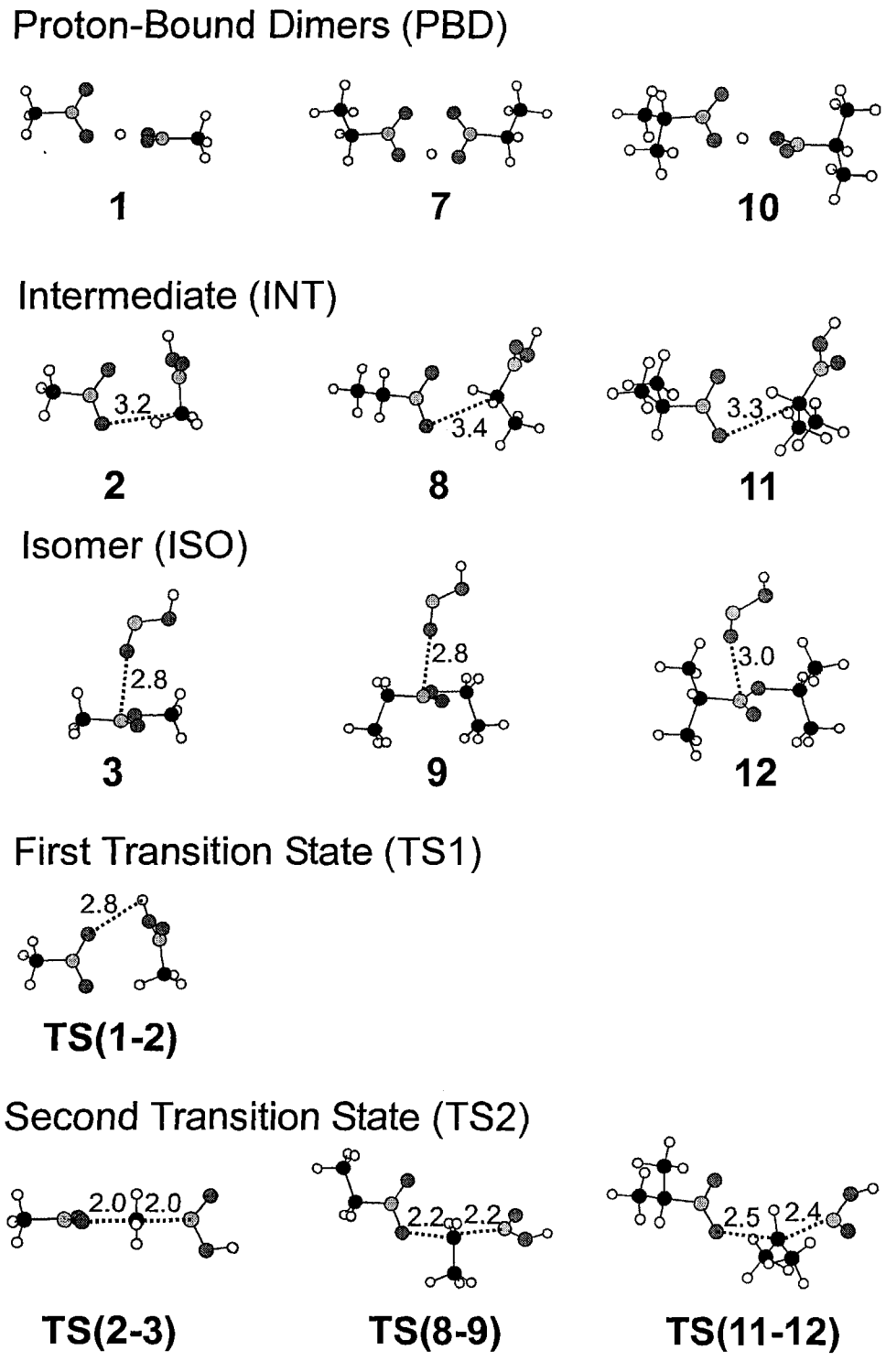

Figure 3.7 Optimized geometries at the B3-LYP/6-31+G(d) level of theory. Selected bond length values are presented in Å.

3.5 Nitro-Nitrite Rearrangement of Protonated Nitroalkanes

The potential energy surface of $((CH_3)_3CNO_2)_2H^+$ would be much more complicated as there are now three reaction channels that compete on the microsecond timescale. It will therefore be discussed separately as an individual case. Nitrous acid is likely lost through an internal S_N2 isomerization similar to the other nitroalkane proton-bound dimers discussed in Section 3.4. But how is t-butanol lost? As shown previously in Scheme 3.2, a proposed mechanism for the formation of neutral t-butanol will have the proton-bound pair isomerized to its nitro-nitrite isomer that can subsequently lose t-butanol (74 Da) by a simple bond cleavage. A similar loss of t-butanol from the associative ion-molecule reactions of t-butyl nitrite with enol ions[80] or protonated aromatics[81] further supports the proposed mechanism. It is worth noting that the rearrangement turns out to be the kinetically most favoured channel on the microsecond timescale for $((CH_3)_3CNO_2)_2H^+$ but no loss of any other alcohol was observed from the other proton-bound dimers, emphasizing the importance of the t-butyl substituents in favouring this rearrangement process.

The observation of a nitro-nitrite rearrangement in $((CH_3)_3CNO_2)_2H^+$ led to an investigation of the effect of protonation on the process in isolated nitroalkanes. Thermal decomposition of nitromethane has been extensively studied in the literature.[82-90] Theoretical studies generally find that the isomerization barrier is high for neutral nitroalkane. In contrast, the barrier is significantly lowered in nitrosilane.[91] A recent study on nitroalkane molecules and their radical cations showed that while the reaction

fails to occur at room temperature with most aliphatic nitroalkanes, the barrier is greatly reduced in the corresponding radical cations.[92] Therefore, a question to be asked is whether protonation has a similar effect in lowering the barrier as was found for radical cations. If so, this rearrangement may be significant in the ion source of the mass spectrometer and hence influence the nature of the proton-bound pairs generated therein.

The nitro-nitrite rearrangement of nitromethane is slightly endothermic (ΔE = 11 kJ mol^{-1}) with a high activation barrier (272 kJ mol^{-1}) (Figure 3.8a). This value is in fairly good agreement with values from QCISD/6-31G(d), MP2/6-31G(d) and MP2/6-311++G(df,p) levels of theory, though the energy can range from 244 to 357 kJ mol^{-1}, depending on the level of theory.[92] IRC calculations clearly show that this reaction path leads to the trans-isomer and confirm the concerted behaviour of the transition state noted by Arenas et al.[89] and Nguyen et al.[90]

The nitro-nitrite rearrangement of protonated nitromethane consists of two distinct pathways (Figure 3.8b). The methyl group can migrate to either oxygen to form both cis- and trans-isomers with respect to the proton. Transfer to the protonated oxygen is more favourable (lower by about 23 kJ mol^{-1}), driven by the exothermicity of the process. The product of this isomerization may also be described as a complex of NO^+ and methanol separated by 2.0 Å. Compared to its neutral form, protonation of nitromethane lowers the nitro-nitrite barrier by over 50 kJ mol^{-1}.

Results for 2-methyl-2-nitropropane and its protonated form are also compared. The mechanism for 2-methyl-2-nitropropane (Figure 3.8c) is very similar to that of nitromethane and also forms a trans-isomer. The process is nearly thermoneutral with a lower barrier (214 kJ mol^{-1}) due to stabilization of the transition state by the methyl groups. The concerted motion of the transition state is also confirmed by IRC calculations. Protonating 2-methyl-2-nitropropane results in a significantly different mechanism (Figure 3.8d). The rearrangement can now be described as a three-step process with "loose" transition states. The process begins by breaking the C–N bond, followed by the migration of the t-butyl moiety towards the oxygen atom, and finally forming a C–O bond to produce a product ion that resembles a complex between NO^+ and t-butanol. This multi-step process results in a nearly barrierless isomerization. So, protonated 2-methyl-2-nitropropane does not really exist as a distinct entity in the gas phase. This raises questions about the nature of the proton-bound pairs involving 2-methyl-2-nitropropane formed in the ion source of our instrument and suggests it be a mixture of nitro-nitro and nitro-nitrite proton-bound pairs.

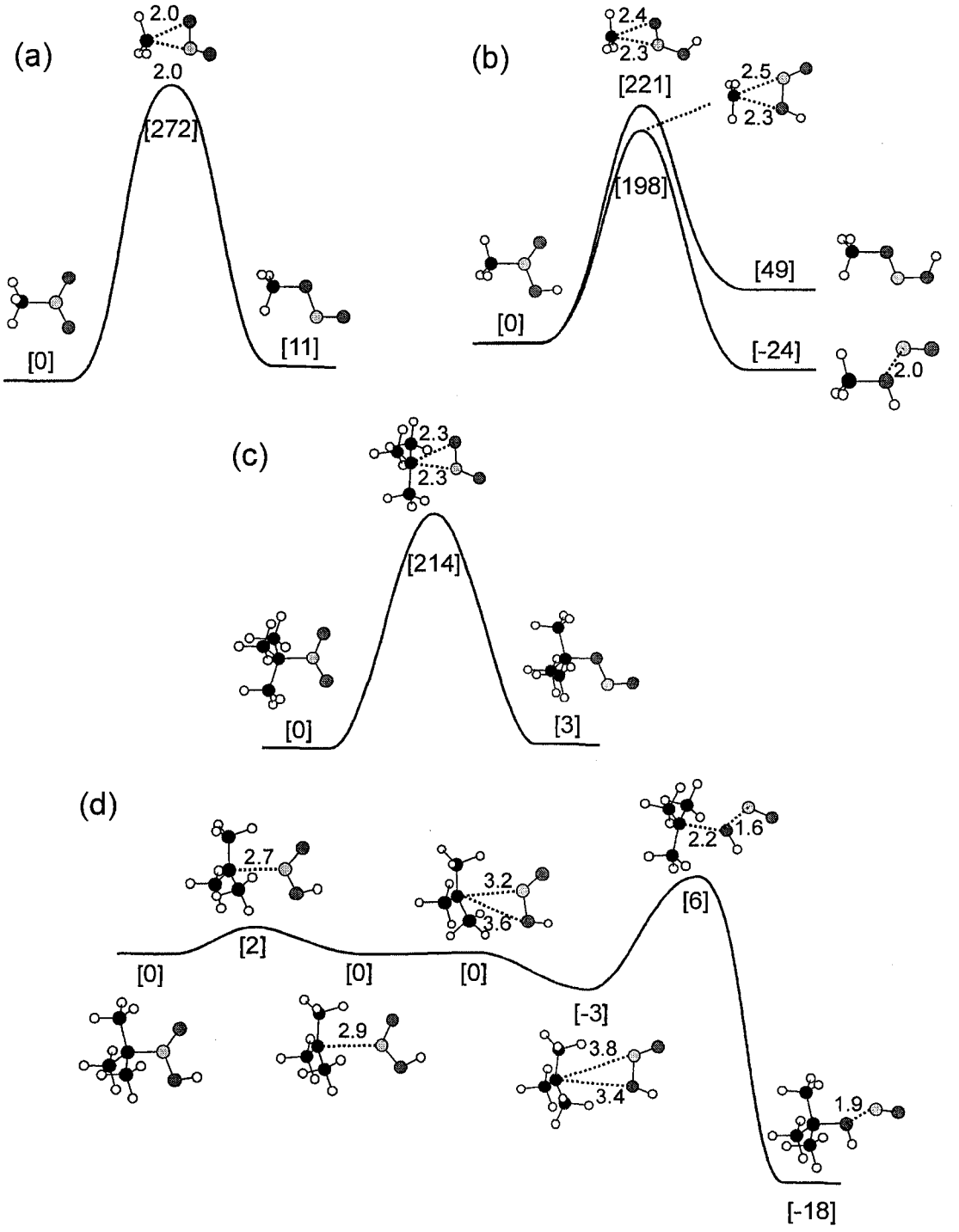

Figure 3.8 Potential energy surface with relative energies (in square brackets, kJ mol^{-1}) and corresponding geometries for the nitro-nitrite rearrangement of (a) CH_3NO_2, (b) $CH_3NO_2H^+$, (c) $(CH_3)_3CNO_2$ and (d) $(CH_3)_3CNO_2H^+$ calculated at the B3-LYP/6-31+G(d) level of theory. Bond length values are in Å. The trans isomer of the protonated nitrite products lie 1-4 kJ mol^{-1} lower in energy.

3.6 The Isomerization and Dissociation Channels of $((CH_3)_3CNO_2)_2H^+$

The potential energy surface for the nitro-nitrite isomerization for the proton-bound dimer of 2-methyl-2-nitropropane, $((CH_3)_3CNO_2)_2H^+$, is shown in Figure 3.9a. The corresponding structures can be found in Figure 3.10. The isomerization in the proton-bound dimer **13** to **15** follows a multi-step mechanism similar to that of isolated protonated 2-methyl-2-nitropropane as in Figure 3.8d. The nitrite form **15** is only 8 kJ mol^{-1} higher in energy than the proton-bound dimer but the intermediate **14** is raised by 57 kJ mol^{-1} compared to that shown in Figure 3.8d. This indicates that the other molecule does not simply behave as a spectator molecule. By electrostatically bonding to the bridging proton, it helps to stabilize the charge on the proton, making the overall isomerization process less favourable. The transition states were not found for this process due to the difficulty in locating the saddle point for such large molecules. However, it is reasonable to believe that these barriers are not very large as optimization jobs of slightly modified geometries of the intermediate (e.g. by a methyl torsion) fall into the two deeper potential energy wells. It can therefore be concluded that the initially formed proton-bound complex can be a mixture of **14** $((CH_3)_3CNO_2)_2H^+$ and **15** $(CH_3)_3CO(H)(NO)^+((CH_3)_3CNO_2)$ which will interconvert below their dissociation limits.

In addition, t-butanol loss could also result from a nitro-nitrite rearrangement in structure **17** in Figure 3.9a. This structure is similar to the intermediate for an S_N2 isomerization in which the neutral moiety has set up for a backside attack. Isomers of **17** that consist of $(CH_3)_3CNO_2\cdots(CH_3)_3C\cdots NO_2H^+$ are calculated to have relative energies of

61, 60 and 63 kJ mol^{-1} for **18**, **19** and **20** respectively. Assuming a small barrier between **17** and these isomers (see Figure 3.8d), **17** could also act as a precursor to m/z 133.

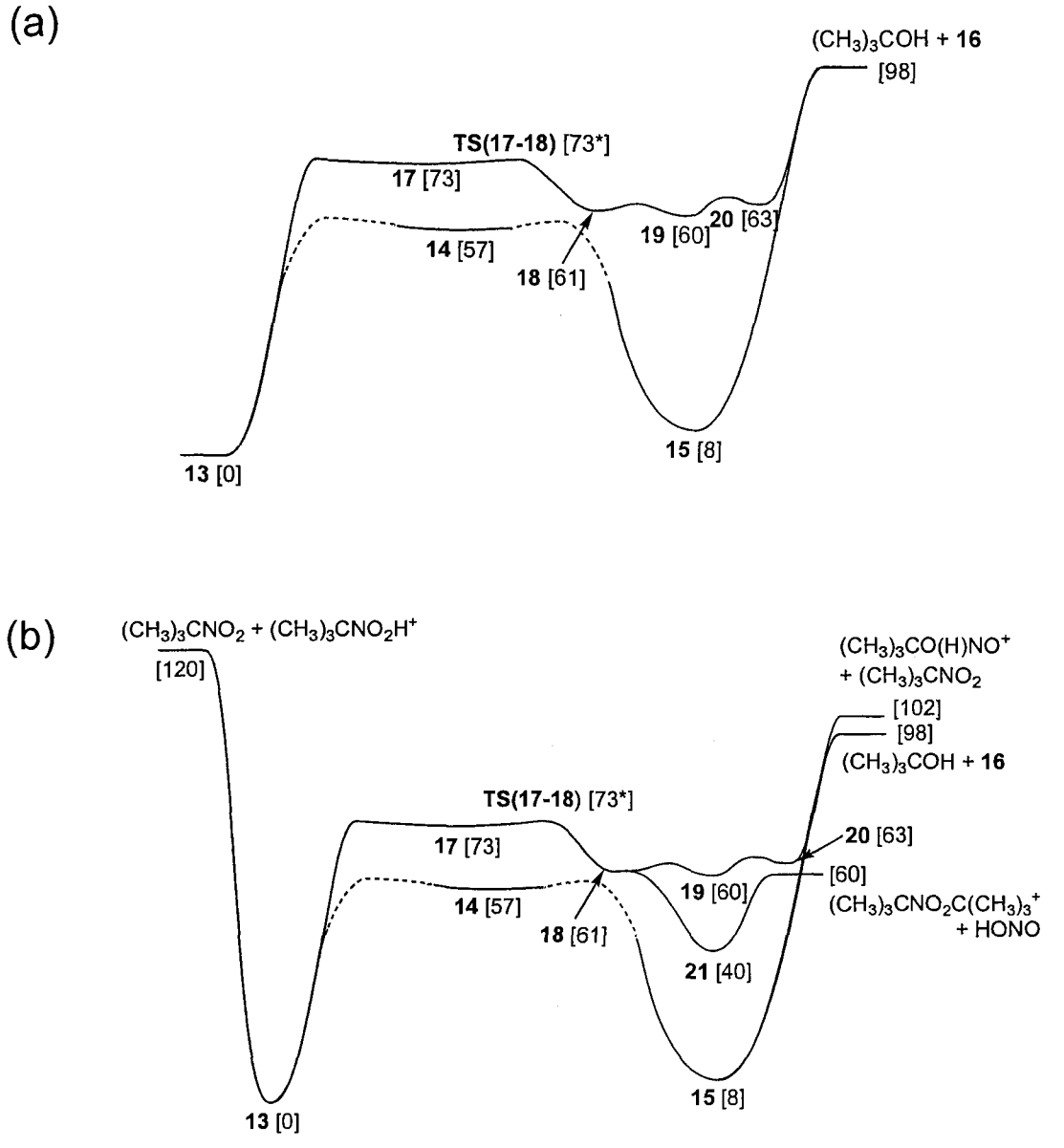

Figure 3.9 (a) Potential energy surface (with relative energies in square brackets, kJ mol^{-1}) for the loss of t-butanol from the proton-bound dimer $[(CH_3)_3CNO_2]_2H^+$, (b) Complete potential energy surface for $[(CH_3)_3CNO_2]_2H^+$. Calculations were performed at B3-LYP/6-31+G(d) level of theory. The value marked with * comes from an opt=qst2 calculation in Gaussian 98. Structures are shown in Figure 3.10.

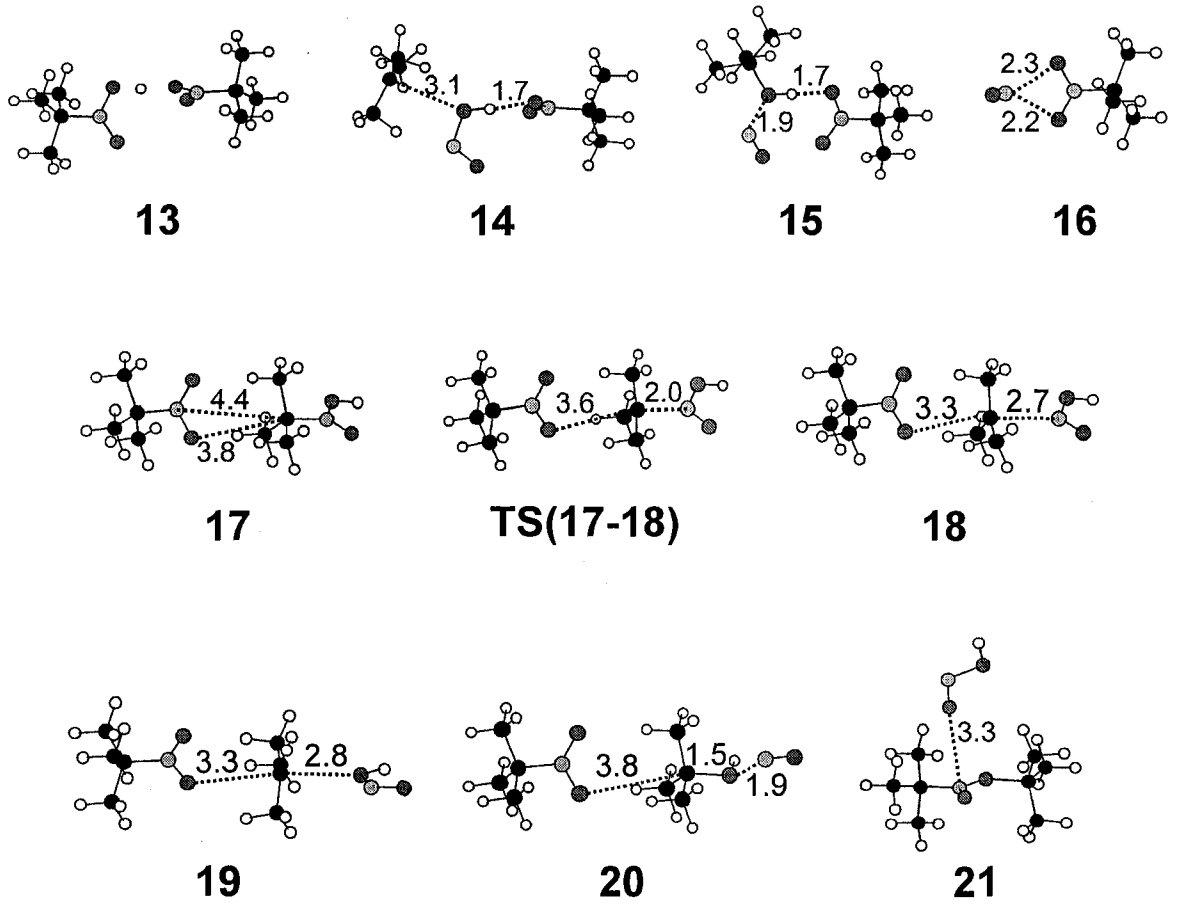

Figure 3.10 Optimized geometries at the B3-LYP/6-31+G(d) level of theory for Figure 3.9. Selected bond length values are presented in Å.

The total potential energy surface for $((CH_3)_3CNO_2)_2H^+$ is presented in Figure 3.9b. The nitrite form of the proton-bound pair **15** can also dissociate into protonated t-butyl nitrite and neutral 2-methyl-2-nitropropane by a simple hydrogen-bond cleavage. This dissociation energy lies about 4 kJ mol^{-1} higher than that leading to the loss of t-butanol at the B3-LYP/6-31+G(d) level of theory. The dissociation channel producing protonated t-butyl nitrite could therefore compete with the loss of t-butanol. In contrast, the dissociation of the proton-bound 2-methyl-2-nitropropane dimer **13** into protonated and neutral 2-methyl-2-nitropropane requires an energy of 120 kJ mol^{-1}. Both

dissociation channels are probably accessible but the m/z 104 observed in MI mass spectrum (Figure 3.1d) is likely to be coming primarily from the nitrite isomer. In addition, since there is only a 6 kJ mol^{-1} barrier between protonated 2-methyl-2-nitropropane and protonated t-butyl nitrite (Figure 3.8d), the fragment ion at m/z 104 will be a mixture of the two species, and it would be impossible to characterize them individually.

The potential energy surface for the nitrous acid loss of $((CH_3)_3CNO_2)_2H^+$ is also included in Figure 3.9b. The rearrangement barrier (**TS(17-18)**, TS2) is decreased substantially compared to that of the other nitroalkane proton-bound pairs, in good agreement with the experimental result. However, the barrier is lowered to an extent that the rearrangement process evolves over a rather flat surface, with the alkyl cation transfer barrier TS2 lying close in energy to the barrier (TS1) for forming the intermediate (**17**, INT) from the original proton-bound dimer **13**. In addition, the alkyl cation transfer (TS2) has also changed from a one-step to a two-step process. A stable minimum structure (**18** in Figure 3.9, 3.10) was found at the mid-way point of the alkyl cation transfer step. This result reflects the greater stability of the t-butyl ion vs. the less methyl-substituted alkyl cations.

It is conceivable that a 1,5-hydrogen shift in the product ion ($RNO_2R'^+$) (Scheme 3.4) could result in the formation of a protonated nitroalkane (RNO_2H^+) and a neutral alkene. Based on their heats of formation[77] the products $(CH_3)_3CNO_2H^+ + CH_2C(CH_3)_2 + HONO$ lie 80 kJ mol^{-1} above $(CH_3)_3CNO_2H^+ + (CH_3)_3CNO_2$ and thus 140 kJ mol^{-1}

above $(CH_3)_3CNO_2C(CH_3)_3^+$ + HONO, and will not be accessible to the metastable ions in this study.

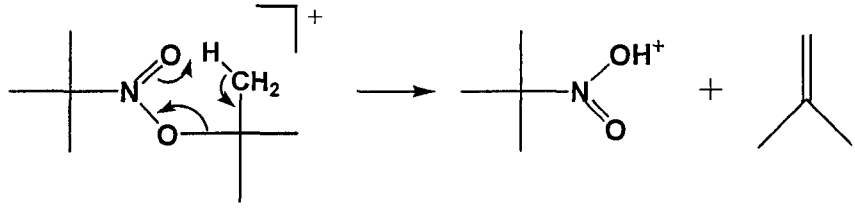

Scheme 3.4 A conceivable reaction scheme for the formation of protonated nitroalkane from product ion ($RNO_2R'^+$).

3.7 Dissociations of $(CH_3NO_2)((CH_3)_3CNO_2)H^+$ & $(CH_3CH_2NO_2)((CH_3)_3CNO_2)H^+$

The competing dissociation of electrostatically-bound molecular pairs ABH^+ (see equation 3.1) is the basis of the kinetic method for obtaining thermochemical information such as relative proton affinities.

$$A + BH^+ \xleftarrow{1} A\text{---}H^+\text{---}B \xrightarrow{2} AH^+ + B \qquad (3.1)$$

This method relates the ratio of the rate constants, k_1/k_2, to the difference in the proton affinities of the two molecular species. The original implementation of the kinetic method assumed that the $\Delta S^{\ddagger}$ values for the two competing channels are the same (i.e. $\Delta(\Delta S^{\ddagger}) = 0$).[93] To take into account the difference in activation entropy of the two competing channels, modifications were made to the original method by assuming $\Delta(\Delta S^{\ddagger})$ (i.e. $\Delta S_1^{\ddagger}$-$\Delta S_2^{\ddagger}$) is equal to $\Delta(\Delta S)$ (i.e. ΔS_1-ΔS_2)).[94] This results in the following expression:

$$ln\left(\frac{k_1}{k_2}\right) = \frac{PA(B) - PA(A)}{RT_{eff}} - \frac{\Delta(\Delta S)}{R} \qquad (3.2)$$

where *PA(B)* and *PA(A)* are the proton affinities of B and A, respectively, *R* is the gas constant, and T_{eff} is the effective temperature. As a verification to this assumption, the effective transition state of the dissociations of $(CH_3NO_2)((CH_3)_3CNO_2)H^+$ and $(CH_3CH_2NO_2)((CH_3)_3CNO_2)H^+$ were located based on variational transition state theory. The thermodynamic reaction entropy (ΔS) and the entropy of activation ($\Delta S^{\ddagger}$) of both dissociations were subsequently calculated.

Figure 3.11 presents the variation of the transition-state sum of states as a function of N-N bond distance in the dissociation of $(CH_3NO_2)((CH_3)_3CNO_2)H^+$ into CH_3NO_2 and $((CH_3)_3CNO_2)H^+$. In all cases, the transition-state sum of states consistently decrease with bond distance until it nearly reaches a plateau. The location of the minimum sum of states is marked by arrows. These labels however are arbitrary. As differences with adjacent points are small, designation of any adjacent points as the transition state will yield similar entropy. This indicates that the effective transition states are located near products. As the variation of the transition-state sum of states is an interplay between increasing potential energy and decreasing vibrational frequencies for the transitional modes, these plots indicate that the increasing energy is playing a dominant role in these dissociations and that the frequencies are not decreasing fast enough to cause an increase in the sum-of-states.

A comparison study is made on the entropy (ΔS and $\Delta S^{\ddagger}$) for the dissociation processes (Table 3.1). In contrast to the previous study[95] of the acetonitrile-alcohol proton-bound pairs $(CH_3CN)(ROH)H^+$, $\Delta(\Delta S^{\ddagger})$ remains constant with respect to methyl

substitutions. $\Delta(\Delta S)$, on the other hand, increases. While $\Delta(\Delta S^{\ddagger}) \sim \Delta(\Delta S)$ for the dissociations of $(CH_3NO_2)((CH_3)_3CNO_2)H^+$, difference becomes more significant for $(CH_3CH_2NO_2)((CH_3)_3CNO_2)H^+$. By assuming $\Delta(\Delta S^{\ddagger}) = \Delta(\Delta S)$, it results in a ΔPA of 47 kJ/mol (an error of only 2 kJ/mol) for $(CH_3NO_2)((CH_3)_3CNO_2)H^+$ compared to an error of 8 kJ/mol if $\Delta(\Delta S^{\ddagger})$ is assumed to be zero. However, for the proton-bound pair $(CH_3CH_2NO_2)((CH_3)_3CNO_2)H^+$, using $\Delta(\Delta S)$ for $\Delta(\Delta S^{\ddagger})$ results in an error of 7 kJ/mol, an error that is almost the same as that without the entropy correction. These results therefore reaffirm that one should be cautious when using the assumption $\Delta(\Delta S^{\ddagger}) = \Delta(\Delta S)$ in the entropy correction.

Table 3.1 $\Delta S^{\ddagger}$ and ΔS for the dissociations of $(CH_3NO_2)((CH_3)_3CNO_2)H^+$ and $(CH_3CH_2NO_2)((CH_3)_3CNO_2)H^+$.[a,b]

	$\Delta S^{\ddagger}$	$\Delta S^{\ddagger}$	ΔS	ΔS	$\Delta(\Delta S^{\ddagger})$	$\Delta(\Delta S)$
	$C_4H_9NO_2H^+ + RNO_2$	$C_4H_9NO_2 + RNO_2H^+$	$C_4H_9NO_2H^+ + RNO_2$	$C_4H_9NO_2 + RNO_2H^+$		
$R = CH_3$	57	43	129	118	14	11
$R = CH_3CH_2$	60	46	151	125	14	26

[a] in J K^{-1} mol^{-1} at 600 K.
[b] Estimated uncertainty, ± 3 J K^{-1} mol^{-1}.

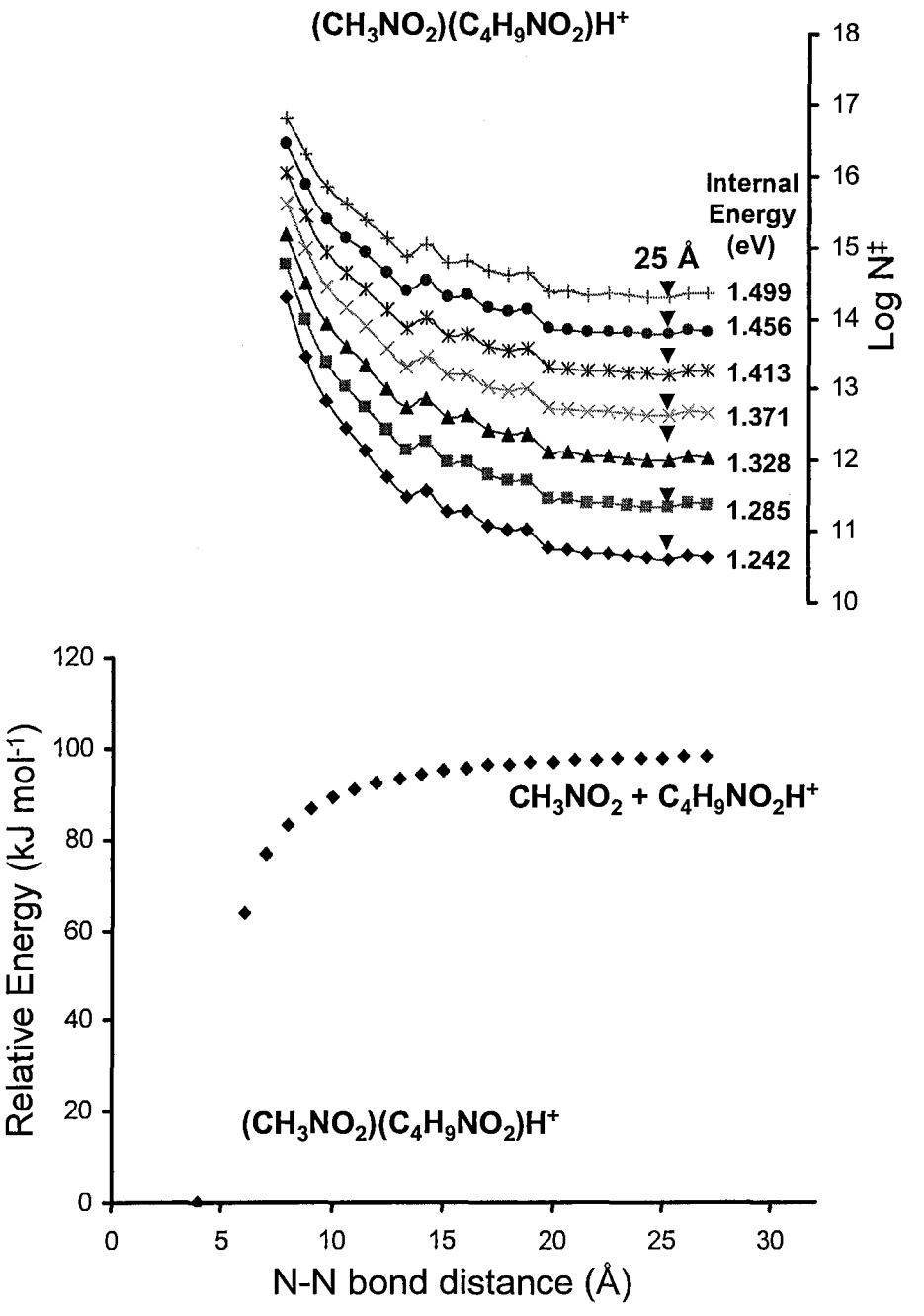

Figure 3.11 (Below) Potential energy surface of the dissociation of $(CH_3NO_2)((CH_3)_3CNO_2)H^+$ into CH_3NO_2 and $((CH_3)_3CNO_2)H^+$. (Above) The variation of the sum of states as a function of the N-N bond distance in the proton-bound pair.

4 Conclusions

The unimolecular chemistry of a series of nitroalkane proton-bound pairs was investigated by both mass spectrometry and theoretical calculations. This chemistry can involve hydrogen bond cleavage reactions, an internal S_N2-type reaction that leads to loss of HONO and, for the pairs involving 2-methyl-2-nitropropane, a nitro-nitrite rearrangement that leads to the loss of t-butanol. The loss of nitrous acid is the result of an internal S_N2 rearrangement that involves the formation of intermediate complexes ($RNO_2\cdots R'NO_2H^+$ and $RNO_2R'^+\cdots HONO$) prior to the loss of HONO. This rearrangement is favoured by methyl substitution and actually becomes more of an S_N1-type mechanism when 2-methyl-2-nitropropane is involved, as the alkyl cation transfer step occurs in two steps.

The unimolecular chemistry of the proton-bound pairs involving 2-methyl-2-nitropropane is also affected by a low isomerization barrier between protonated 2-methyl-2-nitropropane and protonated t-butyl nitrite. This results in a mixture of nitro-nitro and nitro-nitrite proton-bound pairs in the ion source. Addition of a neutral nitroalkane to the protonated species (to make a proton-bound pair) raises the interconversion barrier between the two types of proton-bound pairs, but does not prevent their interconversion. The nitrite isomer of the proton-bound pair can dissociate by loss of t-butanol to form an ionic complex between a nitroalkane and NO^+. It can also dissociate by a simple bond

cleavage into 2-methyl-2-nitropropane and protonated t-butyl nitrite. Given results from calculations showing a low isomerization barrier between the nitro and nitrite isomer of protonated 2-methyl-2-nitropropane, the actual product ion of m/z 104 appearing in the mass spectrum is a mixture of both.

Variational transition state study of the dissociations of $(CH_3NO_2)((CH_3)_3CNO_2)H^+$ and $(CH_3CH_2NO_2)((CH_3)_3CNO_2)H^+$ show that the transition states are located close to products. $\Delta(\Delta S^{\ddagger})$ and $\Delta(\Delta S)$ are similar for the dissociations of $(CH_3NO_2)((CH_3)_3CNO_2)H^+$ but deviation becomes larger in the case of $(CH_3CH_2NO_2)((CH_3)_3CNO_2)H^+$. Therefore, one should be cautious in assuming $\Delta(\Delta S^{\ddagger}) = \Delta(\Delta S)$ in competitive dissociation reactions of proton-bound pairs.

References

(1) DePetris, G. *Acc. Chem. Res.* **2002**, *35*, 305.

(2) Ferguson, E. E.; Fehsenfeld, F. C.; Albritton, D. L. Ion chemistry of the earth's atmosphere. In *Gas Phase Ion Chemistry*; Bowers, M. T., Ed.; Academic Press: New York, 1979; Vol. 1.

(3) Anicich, V. G.; Wilson, P. F.; McEwan, M. J. *J. Am. Soc. Mass Spectrom.* **2006**, *17*, 544.

(4) McEwan, M. J.; Anicich, V. G. *Mass Spectrom. Rev.* **2007**, *26*, 281.

(5) Postma, R.; Ruttink, P. J. A.; Baar, B. v.; Terlouw, J. K.; Holmes, J. L.; Burgers, P. C. *Chem. Phys. Lett.* **1986**, *123*, 409.

(6) Bouma, W. J.; Nobes, R. H.; Radom, L. *J. Am. Chem. Soc.* **1983**, *105*, 1743.

(7) Terlouw, J. K.; Heerma, W.; Dijkstra, G. *Org. Mass Spectrom.* **1981**, *16*, 326.

(8) Burgers, P. C.; Holmes, J. L.; Terlouw, J. K.; Baar, B. v. *Org. Mass Spectrom.* **1985**, *20*, 202.

(9) Mazyar, O. A.; Mayer, P. M.; Baer, T. *Int. J. Mass Spectrom. Ion Proc.* **1998**, *167/168*, 398.

(10) Nibbering, N. M. M. *J. Am. Soc. Mass Spectrom.* **2004**, *15*, 956.

(11) Burgers, P. C.; Holmes, J. L.; Mommers, A. A.; Szulejko, J. E.; Terlouw, J. K. *Org. Mass Spectrom.* **1984**, *19*, 442.

(12) Burgers, P. C.; Holmes, J. L.; Hop, C. E. C. A.; Terlouw, J. K. *Org. Mass Spectrom.* **1986**, *21*, 549.

(13) Holmes, J. L.; Hop, C. E. C. A.; Terlouw, J. K. *Org. Mass Spectrom.* **1986**, *21*, 776.

(14) Holmes, J. L.; Aubry, C.; Mayer, P. M. *Assigning Structures to Ions in Mass Spectrometry*; CRC Press: Boca Raton, 2007.

(15) Beynon, J. H.; Job, B. E.; Williams, A. E. *Z. Naturforsch.* **1965**, *20a*, 883.

(16) Meyerson, S.; Corbin, J. L. *J. Am. Chem. Soc.* **1965**, *87*, 3045.

(17) Young, D. C. *Computational Chemistry: A Practical Guide for Applying Techniques to Real-World Problems*; Wiley-Interscience: New York, 2001.

(18) Koch, W.; Holthausen, M. C. *A Chemist's Guide to Density Functional Theory*; Wiley-VCH: New York, 2000.

(19) Solomons, T. W. G. *Organic Chemistry*, 6th ed.; John Wiley & Sons: New York, 1996.

(20) Bohme, D. K.; Young, L. B. *J. Am. Chem. Soc.* **1970**, *92*, 7354.

(21) Bohme, D. K.; Mackay, G. L.; Payzant, J. D. *J. Am. Chem. Soc.* **1974**, *96*, 4027.

(22) Olmstead, W. N.; Brauman, J. I. *J. Am. Chem. Soc.* **1977**, *99*, 4219.

(23) Brauman, J. I.; Olmstead, W. N.; Lieder, C. A. *J. Am. Chem. Soc.* **1974**, *96*, 4030.

(24) Dougherty, R. C. *Org. Mass Spectrom.* **1974**, *8*, 85.

(25) Dougherty, R. C.; Dalton, J.; Roberts, J. D. *Org. Mass Spectrom.* **1974**, *8*, 77.

(26) Dougherty, R. C.; Roberts, J. D. *Org. Mass Spectrom.* **1974**, *8*, 81.

(27) Fridgen, T. D.; Burkell, J. L.; Wilsily, A. N.; Braun, V.; Wasylycia, J.; McMahon, T. B. *J. Phys. Chem. A* **2005**, *109*, 7519.

(28) Fridgen, T. D.; McMahon, T. B. *J. Phys. Chem. A* **2003**, *107*, 668.

(29) Li, C.; Ross, P.; Szulejko, J. E.; McMahon, T. B. *J. Am. Chem. Soc.* **1996**, *118*, 9360.

(30) Johannessen, A.; Krankowsky, D. *J. Geophys. Res.* **1972**, *77*, 2888.

(31) Johannessen, A.; Krankowsky, D.; Arnold, F.; Riedler, W.; Friedrich, M.; Folkestad, K.; Skovli, G.; Thrane, E. V.; Troim, J. *Nature* **1972**, *235*, 215.

(32) Beauchamp, J. L.; Caserio, M. C. *J. Am. Chem. Chem.* **1972**, *94*, 2638.

(33) Beauchamp, J. L.; Caserio, M. C.; McMahon, T. B. *J. Am. Chem. Soc.* **1974**, *96*, 6243.

(34) Feng, W. Y.; Lifshitz, C. *Int. J. Mass Spectrom. Ion Proc.* **1995**, *149/150*, 13.

(35) Mafune, F.; Kohno, J.; Kondow, T. *J. Phys. Chem.* **1996**, *100*, 10041.

(36) Zhang, X.; Yang, X.; Castleman, A. W. *Chem. Phys. Lett.* **1991**, *185*, 298.

(37) Bouchoux, G.; Choret, N. *Rapid Commun. Mass Spectrom.* **1997**, *11*, 1799.

(38) Fridgen, T. D.; McMahon, T. B. *J. Phys. Chem. A* **2002**, *106*, 9648.

(39) Raghavachari, K.; Chandrasckhar, J.; Burnier, R. C. *J. Am. Chem. Soc.* **1984**, *106*, 3124.

(40) Sheldon, J. C.; Currie, G. J.; Bowie, J. H. *J. Chem. Soc. Perkin Trans.* **1986**, *27*, 941.

(41) Audier, H. E.; Monteiro, C.; Mourgues, P.; Robin, D. *Rapid Commun. Mass Spectrom.* **1989**, *3*, 84.

(42) Dang, T. T.; Bierbaum, V. M. *Int. J. Mass Spectrom. Ion Proc.* **1992**, *117*, 65.

(43) Graul, S. T.; Squires, R. R. *Int. J. Mass Spectrom. Ion Proc.* **1987**, *81*, 183.

(44) Karpas, Z.; Meot-Ner, M. *J. Phys. Chem.* **1989**, *93*, 1859.

(45) Kleingeld, J. C.; Nibbering, N. M. M. *Org. Mass Spectrom.* **1982**, *17*, 136.

(46) Fridgen, T. D.; Keller, J. D.; McMahon, T. B. *J. Phys. Chem. A* **2001**, *105*, 3816.

(47) Ochran, R. A.; Annamalai, A.; Mayer, P. M. *J. Phys. Chem. A* **2000**, *104*, 8505.

(48) Ochran, R. A.; Mayer, P. M. *Eur. Mass Spectrom.* **2001**, *7*, 267.

(49) Ruggiero, G. D.; Williams, I. H. *J. Chem. Soc., Perkin Trans. 2* **2002**, *2*, 591.

(50) Fridgen, T. D.; McMahon, T. B. *J. Am. Chem. Soc.* **2001**, *123*, 3980.

(51) Atkins, P.; DePaula, J. *Physical Chemistry*, 7th ed.; W.H. Freeman and Company: New York, 2002.

(52) Marcus, R. A.; Rice, O. K. *J. Phys. Colloid Chem.* **1951**, *55*, 894.

(53) Marcus, R. A. *J. Chem. Phys.* **1952**, *20*, 359.

(54) Rosenstock, H. M.; Wallenstein, M. B.; Wahrhaftig, A. L.; Eyring, H. *Proc. Nat. Acad. Sci.* **1952**, *38*, 667.

(55) Baer, T.; Hase, W. L. *Unimolecular Reaction Dynamics: Theory and Experiments*; Oxford University Press: New York, 1996.

(56) Baer, T.; Mayer, P. M. *J. Am. Soc. Mass Spectrom.* **1997**, *8*, 103.

(57) Lorquet, J. C.; Leyh, B. Statistical Theories in Mass Spectrometry. In *Encyclopedia of Mass Spectrometry*; Gross, M. L., Caprioli, R., Eds.; Elsevier: Oxford, 2003; Vol. 1.

(58) Holmes, J. L.; Mayer, P. M. *J. Phys. Chem.* **1995**, *99*, 1366.

(59) Mayer, P. M. Mass Spectrometry. In *Encyclopedia of Chemical Physics and Physical Chemistry*; Moore, J. H., Spencer, N. D., Eds.; Institute of Physics: Bristol, 2001; Vol. 2; pp 1147.

(60) Rennie, E. E.; Mayer, P. M. *J. Chem. Phys.* **2004**, *120*, 10561.

(61) Cooks, R. G.; Beynon, J. H.; Caprioli, R. M.; Lester, G. R. *Metastable Ions*; Elsevier: Amsterdam, 1973.

(62) Traeger, J. C.; Mommers, A. A. *Org. Mass Spectrom.* **1987**, *22*, 592.

(63) Holmes, J. L. *Org. Mass Spectrom.* **1985**, *20*, 169.

(64) Goldberg, N.; Schwarz, H. *Acc. Chem. Res.* **1994**, *27*, 347.

(65) McLafferty, F. W. *Science* **1990**, *247*, 925.

(66) Schalley, C. A.; Hornung, G.; Schroder, D.; Schwarz, H. *Chem. Soc. Rev.* **1998**, *27*, 91.

(67) Wesdemiotis, C.; McLafferty, F. W. *Chem. Rev.* **1987**, *87*, 485.

(68) Danis, P. O.; Wesdemiotis, C.; McLafferty, F. W. *J. Am. Chem. Soc.* **1983**, *105*, 7454.

(69) Frisch, M. J.; Trucks, G. W.; Schlegel, H. B.; Scuseria, G. E.; Robb, M. A.; Cheeseman, J. R.; Zakrzewski, V. G.; Montgomery, J. A.; Stratmann, R. E.; Burant, J. C.; Dapprich, S.; Millam, J. M.; Daniels, A. D.; Kudin, K. N.; Strain, M. C.; Farkas, O.; J. Tomasi; Barone, V.; Cossi, M.; Cammi, R.; Mennucci, B.; Pomelli, C.; Adamo, C.; Clifford, S.; Ochterski, J.; Petersson, G. A.; Ayala, P. Y.; Cui, Q.; Morokuma, K.; Malick, D. K.; Rabuck, A. D.; Raghavachari, K.; Foresman, J. B.; Cioslowski, J.; Ortiz, J. V.; Stefanov, B. B.; Liu, G.; Liashenko, A.; Piskorz, P.; Komaromi, I.; Gomperts, R.; Martin, R. L.; Fox, D. J.; Keith, T.; Al-Laham, M. A.; Peng, C. Y.; Nanayakkara, A.; Gonzalez, C.; Challacombe, M.; Gill, P. M. W.; Johnson, B.; Chen, W.; Wong, M. W.; Andres, J. L.; Gonzalez, C.; Head-Gordon, M.; Replogle, E. S.; Pople, J. A. GAUSSIAN 98 Rev. A.6. In *GAUSSIAN 98 Rev. A.6*; Gaussian Inc.: Pittsburgh PA, 1998.

(70) Frisch, M. J.; Trucks, G. W.; Schlegel, H. B.; Scuseria, G. E.; Robb, M. A.; Cheeseman, J. R.; Montgomery, J. A.; Vreven, T.; Kudin, K. N.; Burant, J. C.; Millam, J. M.; Iyengar, S. S.; Tomasi, J.; Barone, V.; Mennucci, B.; Cossi, M.; Scalmani, G.; Rega, N.; Petersson, G. A.; Nakatsuji, H.; Hada, M.; Ehara, M.; Toyota, K.; Fukuda, R.; Hasegawa, J.; Ishida, M.; Nakajima, T.; Honda, Y.; Kitao, O.; Nakai, H.; Klene, M.; Li, X.; Knox, J. E.; Hratchian, H. P.; Cross, J. B.; Bakken, V.; Adamo, C.; Jaramillo, J.; Gomperts, R.; Stratmann, R. E.; Yazyev, O.; Austin, A. J.; Cammi, R.; Pomelli, C.; Ochterski, J. W.; Ayala, P. Y.; Morokuma, K.; Voth, G. A.; Salvador, P.; Dannenberg, J. J.; Zakrzewski, V. G.; Dapprich, S.; Daniels, A. D.; Strain, M. C.; Farkas, O.; Malick, D. K.; Rabuck, A. D.; Raghavachari, K.; Foresman, J. B.; Ortiz, J. V.; Cui, Q.; Baboul, A. G.; Clifford, S.; Cioslowski, J.; Stefanov, B. B.; Liu, G.; Liashenko, A.; Piskorz, P.; Komaromi, I.; Martin, R. L.; Fox, D. J.; Keith, T.; Al-Laham, M. A.; Peng, C. Y.; Nanayakkara, A.; Challacombe, M.; Gill, P. M. W.; Johnson, B.; Chen, W.; Wong, M. W.; Gonzalez, C.; Pople, J. A. GAUSSIAN 03 Rev. C.02. In *GAUSSIAN 03 Rev. C.02*; Gaussian Inc.: Wallingford CT, 2004.

(71) Scott, A. P.; Radom, L. *J. Phys. Chem.* **1996**, *100*, 16502.

(72) Curtiss, L. A.; Raghavachari, K.; Redfern, P. C.; Rassolov, V.; Pople, J. A. *J. Chem. Phys.* **1998**, *109*, 7764.

(73) Baboul, A. G.; Curtiss, L. A.; Redfern, P. C. *J. Chem. Phys.* **1999**, *110*,7650.

(74) Grabowy, J. A. D.; Mayer, P. M. *Eur. J. Mass Spectrom.* **2004**, *10*, 899.

(75) Beyer, T.; Swinehart, D. R. *ACM Commun.* **1973**, *16*, 379.

(76) Grabowy, J. A. D.; Mayer, P. M. *Can. J. Chem.* **2005**, *83*, 1864.

(77) Linstrom, P. J.; Mallard, W. G. *Eds, NIST Chemistry WebBook, NIST Standard Reference Database Number 69*; National Institute of Standards and Technology: Gaithersburg, 2005 (http://webbook.nist.gov).

(78) Reiche, F.; Abel, B.; Beck, R. D.; Rizzo, T. R. *J. Chem. Phys.* **2000**, *112*, 8885.

(79) Larson, J. W.; McMahon, T. B. *J. Am. Chem. Soc.* **1982**, *104*, 6255.

(80) Gerbaux, P.; Wantier, P.; Nam, P. C.; Nguyen, M. T.; Bouchoux, G.; Flammang, R. *Eur. J. Mass Spectrom.* **2004**, *10*, 889.

(81) Dechamps, N.; Gerbaux, P.; Flammang, R.; Bouchoux, G.; Nam, P.-C.; Nguyen, M.-T. *Int. J. Mass Spectrom.* **2004**, *232*, 31.

(82) Wodtke, A. M.; Hintsa, E. J.; Lee, Y. T. *J. Phys. Chem.* **1986**, *90*, 3549.

(83) Wodtke, A. M.; Hintsa, E. J.; Lee, Y. T. *J. Chem. Phys.* **1986**, *84*, 1044.

(84) Dewar, M. J. S.; Ritchie, J. P. *J. Org. Chem.* **1985**, *50*, 1031.

(85) McKee, M. L. *J. Am. Chem. Soc.* **1986**, *108*, 5784.

(86) McKee, M. L. *J. Phys. Chem.* **1989**, *93*, 7365.

(87) Saxon, R. P.; Yoshimine, M. *Can. J. Chem.* **1992**, *70*, 572.

(88) Manaa, M. R.; Fried, L. E. *J. Phys. Chem. A* **1998**, *102*, 9884.

(89) Arenas, J. F.; Centeno, S. P.; López-Tocón, I.; Peláez, D.; Soto, J. *Thermochem.* **2003**, *630*, 17.

(90) Nguyen, M. T.; Le, H. T.; Hajgato, B.; Veszpremi, T.; Lin, M. C. *J. Phys. Chem. A* **2003**, *107*, 4286.

(91) Packwood, T. J.; Page, M. *Chem. Phys. Lett.* **1993**, *216*, 180.

(92) Khrapkovskii, G. M.; Nikolaeva, E. V.; Chachkov, D. V.; Shamov, A. G. *Rus. J. Gen. Chem.* **2004**, *74*, 908.

(93) McLuckey, S. A.; Cameron, D.; Cooks, R. G. *J. Am. Chem. Soc.* **1981**, *130*, 1313.

(94) Zheng, X.; Cooks, R. G. *J. Phys. Chem. A* **2002**, *106*, 9939.

(95) Grabowy, J. A. D.; Mayer, P. M. *J. Am. Soc. Mass Spectrom.* **2005**, *16*, 2039.

Part B

Internal Excitation in keV Ion-Target Collisions

5 Introduction

5.1 Gas-Phase Collisions

The study of the decomposition of gas-phase ions by collisional activation is almost as old as mass spectrometry itself. The first mass spectrometrist, J. J. Thomson[1] observed a residual signal from $H_2^{+\cdot}$ as early as 1913, although it was not till 1919 that Aston[2] explained the signal as a result of collisional activation. Since then, all mass spectrometrists have put strong emphasis in avoiding collisional processes by maintaining a low pressure in the mass spectrometer.

Collisions in mass spectrometers were revived when Jennings[3] and McLafferty[4] reported their collision-induced dissociation mass spectra as a result of air being leaked into the vacuum chamber of the mass spectrometer. Collisional effects on metastable ion decomposition were observed. Although these spectra were obtained purely by accident, McLafferty[5] illustrated a few years later the usefulness of collisions in ion structure determination and initiated the widespread use of collision-induced dissociations (CID) in mass spectrometry.

CID is often considered as a two-step process. The first step excites the ions by converting some of the ion translational energy into internal energy, and the second step results in the dissociation of the ions with energy above the dissociation threshold.

$$(AB)^{+\cdot} + X + \Delta E \rightarrow (AB)^{+\cdot *} + X' \qquad (5.1)$$

$$(AB)^{+\cdot *} \rightarrow A^{+} + B^{\cdot} \qquad (5.2)$$

In the above schemes, $(AB)^{+\cdot}$ and X represent the precursor ion and the target gas, respectively, in the pre-collision states. $(AB)^{+\cdot *}$ and X' are the collision partners in the post-collision states and ΔE is the change in the kinetic energy of the system. After some time, the excited precursor ion $(AB)^{+\cdot *}$ can dissociate into fragments, A^{+} and $B^{\cdot}$.

When the precursor ion (i.e. $AB^{+\cdot}$) is polyatomic, the second step illustrates the competition of unimolecular dissociations. If the internal energy is statistically distributed among all internal degrees of freedom (which is usually the case), the relative amount of fragments from the competing channels can be related to the activation energy and the activation entropy by statistical rate theory such as RRKM theory.[6,7] This second step is really looking at the chemistry of collisionally activated ions and is similar to the study of nitroalkane proton-bound pairs in Part A of this thesis, except that we were looking at competitive dissociations of metastable ions (i.e. ions that are excited in the ion source rather than collisionally activated ions).

In the second part of the thesis, I will discuss how ions are excited upon collisions (i.e. the first step in the two-step process) by means of emission spectroscopy. By studying the emissions from the collisionally-activated ion and its fragments, it allows us

to investigate and identify the population of the excited states after collisions, which can provide insights into ion-target collisions occurring in the mass spectrometer. The objective of this project is to study quantitatively the emission changes at various collision conditions. The systems that I have studied involve collisions of $N_2^{+\cdot}$ and $CO_2^{+\cdot}$ with a neutral target gas at keV ion translational energy. The interests in the study of these two ions are two-fold. First of all, these two ions are of atmospheric importance. They are common species in the atmosphere and collisions with these ions could be related to atmospheric reactions or atmospheric phenomenon such as aurora. Secondly, because these ions are of atmospheric interest, there is a lot of information available on them; therefore, it is a good starting point for my study by emission spectroscopy. Future goals will extend the study to larger polyatomic ions.

5.1.1 Hard-Sphere Collision Theory

The simplest collision theory is the so-called hard-sphere collision theory.[8] It is derived by treating molecules as hard spheres. In an interaction potential, there are two distinct parts, an attractive potential at large interatomic distances and a repulsive potential at small distances. Figure 5.1a shows a typical two-dimensional plot of an interaction potential between an atomic ion and an atomic target. This picture represents one approach vector of the projectile and target and can be extended into three dimensions (Figure 5.1b). A polyatomic projectile will contain too many degrees of freedom to be drawn pictorially. The mathematical form of the attractive potential will depend on the diffuseness of the charge on the projectile ion and on the nature of the

interaction; for example, r^{-2} for ion-dipole, r^{-3} for ion-quadrupole and r^{-4} for ion-induced dipole, where r is the distance between the projectile and the target. For targets such as helium, the attractive part of the potential can often be ignored. But for polyatomic and polarizable targets, it must be considered. A strong attractive potential can increase significantly the relative velocities of the two species. The repulsive part of the interaction potential can also have an impact. It can contribute significantly to the scattering effect and change as a function of e^{-r}.

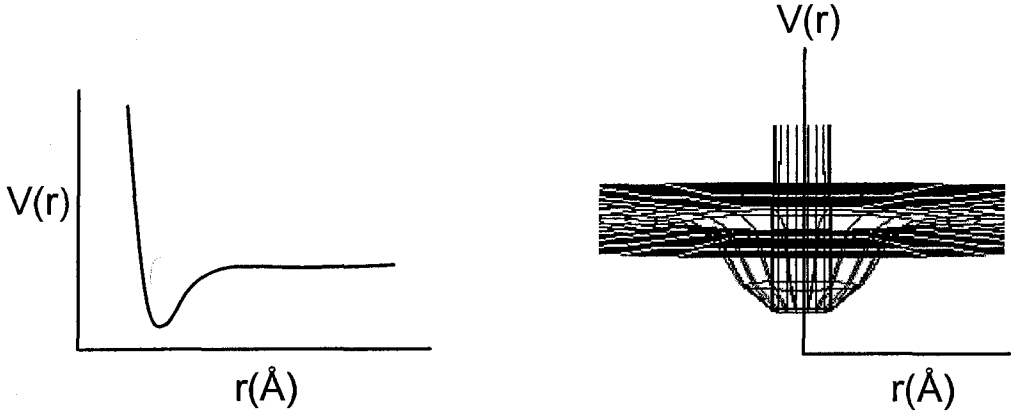

Figure 5.1 (a) A two-dimensional plot and (b) a three-dimensional plot of an interaction potential *V(r)*, for an ion-target system as a function of ion-target separation, *r*.

One of the terms that is commonly used in collision theory is the impact parameter, *b*. In the hard-sphere collision model, *b* is the distance of closest approach of the two collision particles (see Figure 5.2). But in reality, with the involvement of intermolecular forces, the impact parameter is no longer as clearly cut. Relative values of impact parameter, however, provide a good indication as to the type of collisions taking

place: large values of b for "soft" collisions, small values for "hard" collisions and $b = 0$ for head-on collisions.

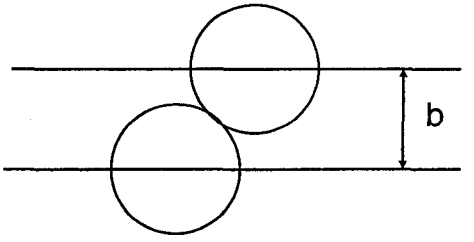

Figure 5.2 Hard-sphere collision model.

5.1.2 Classification of Collision Processes

Collision processes can be classified in different ways based on the nature, the property or the result of the collisions. One type of classification is based on whether there is any conversion between different forms of energy. *Elastic* collisions are those in which there is no change in the internal energy states of any species and therefore, the resultant kinetic energy and the angle of both particles must be conserved. A classical picture of this type of collisions is the billiard ball collision. Of course, because there are intrinsic chemical properties to the colliding particles, chemical reactions are rarely elastic. These collisions are said to be *inelastic* and include all those in which there is a change in the internal state of the system. In the CID process, the first step of the mechanism is always inelastic as it converts some of the ion kinetic energy into internal energy of the ion and/or the target. Therefore, in this thesis, inelastic collisions will be the centre of the discussion. When inelastic reactions are exothermic, they are said to be *superelastic*. These processes lead to an increase in velocity in the products.

It is common to classify collision processes into high or low energy collisions by their translational energy (i.e. the lab-frame collision energy). To mass spectrometrists, ions in sector instruments typically have translational energy ranging from 1 to 8 keV. This type of collision is referred to as *high-energy collisions*. Those that are carried out in quadrupole or ion trap mass spectrometers have a collision energy range of 1 to 200 eV and are usually referred to as *low-energy collisions*. *Intermediate-energy collisions* often refer to those that are in between.

5.1.3 Frame of Reference

There are two frames of reference that are commonly used in collisions: laboratory and center-of-mass. Most of the discussion in this thesis can be described using the laboratory frame of reference but it is important to point out the difference between the two, in particular between the laboratory and the centre-of-mass collision energy.

For most mass spectrometric collision experiments, the target gas can be assumed to be at rest in the laboratory frame of reference. Therefore, the laboratory collision energy is simply taken as the kinetic energy of the ion. Figure 5.3a shows pictorially the pre-collision fast projectile-resting target situation where X marks the centre-of-mass point in the lab frame. The post-collision picture is shown in Figure 5.3b.

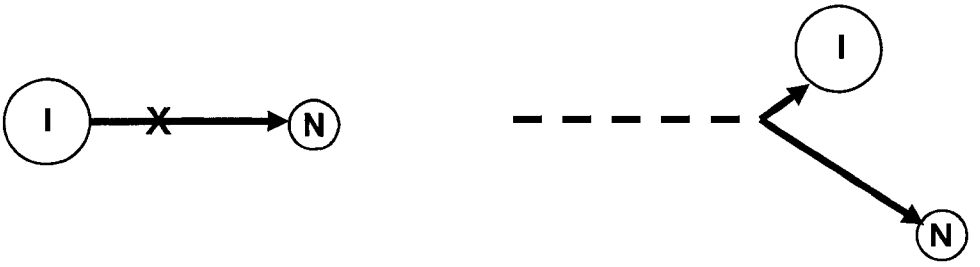

(a) (b)

Figure 5.3 (a) A precollision and (b) a postcollision picture of a fast ion-resting neutral target collision viewed in the laboratory frame of reference.

By definition, the centre of mass of the two collision partners is the point in space at which the mechanical moments of the two collision partners are equal and opposite.

$$m_I(R_C - R_I) + m_N(R_C - R_N) = 0 \qquad (5.3)$$

where R_C, R_I and R_N are the instantaneous position vectors of the centre of mass, the projectile ion and the neutral target, respectively, in the laboratory frame of reference. Because of the conservation of momentum, the total laboratory kinetic energy of the fast particle undergoing collision with a stationary target is not available for conversion into internal energy of the products. The available energy is termed the relative kinetic energy, KE_{com}. It is equal to the total kinetic energy in the centre of mass reference frame since total linear momentum in the centre of mass is zero by definition.

$$KE_{com} = \frac{1}{2} m_I (r_I')^2 + \frac{1}{2} m_N (r_N')^2 \qquad (5.4)$$

where r_I' and r_N' are the ion and target velocities in the centre-of-mass reference frame. It can be shown that when replacing r_I' and r_N' with the initial velocity of the colliding particles in the laboratory frame, the following equation is derived. KE_{com} is also known as the centre-of-mass collision energy.[9,10]

$$KE_{com} = \frac{1}{2}\left(\frac{m_I m_N}{m_I + m_N}\right) v_i^2 = \left(\frac{m_N}{m_I + m_N}\right) KE_{lab} \qquad (5.5)$$

The limitations that relative kinetic energy places on energy interconversions in collisions are most important in low-energy collisions. For high-energy collisions, the energy converted from one form to another is only a few percent of the laboratory energy. The centre-of-mass collision energy, however, would indicate that collision systems involving heavier targets will have more available energy for interconversions.

Figure 5.4 shows the same collision in Figure 5.3 viewed in the centre-of-mass frame of reference which is equivalent to "sitting" on the centre of mass of the system and watching the collision partners approach each other from opposite directions prior to collision and recede from each other in opposite directions after they have interacted. The post-collision picture shows only one of many possible outcomes. All of the possible post-collision velocities of the ion and the target can be visualized by rotating them by 360°, forming the so-called Newton velocity diagram[9-11] (Figure 5.5). Post-collision vectors that fall on the two circles represent elastic collisions whereas those that fall inside and outside the circles indicate inelastic and superelastic collisions, respectively. An inelastic collision is illustrated in Figure 5.5.

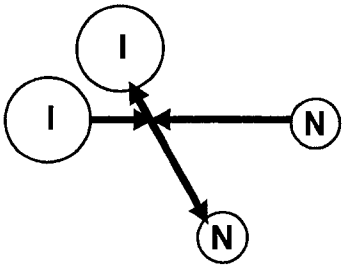

Figure 5.4 Picture of the same collision in Figure 5.3 viewed in the centre-of-mass frame of reference.

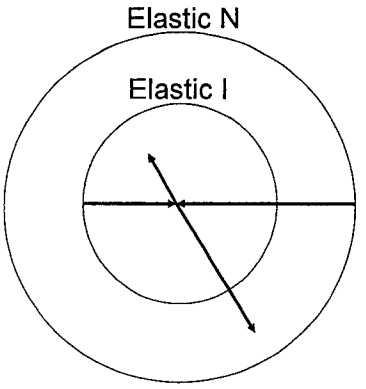

Figure 5.5 The Newton velocity diagram for the collision in Figure 5.4.

5.2 Mechanisms of Collisional Excitation

A number of collisional activation mechanisms have been proposed for the transfer of energy from translation to internal modes under the range of ion translational energy used in today's mass spectrometers. Most of these mechanisms were first given by Durup[12] in 1970 and have been augmented in a subsequent review by McLuckey.[10] In this section, only those that are relevant to my study will be described.

5.2.1 Vertical Excitations

Vertical transition is a concept widely used to explain photon excitation. When collisions occur in a very short time (i.e. 10^{-14}s or less), the Franck-Condon principle[13,14] is expected to be obeyed. This principle states that because the nuclei are so much more massive than the electrons, an electronic transition takes place faster than the nuclei can respond. Therefore, the nuclear positions are virtually the same immediately before and

after the transition and result in a vertical transition. This is illustrated in Figure 5.6 for a diatomic molecule. Suppose that a diatomic molecule has very similar potential energy curves in two different electronic states, as illustrated by the lowest two curves in Figure 5.6. When starting from $v = 0$ in the ground electronic state, the most probable transition will be to the $v = 0$ of the excited state. This can be viewed by the largest overlap between the two wavefunctions and will result in only one predominant peak in the electronic spectrum. On the other hand, if the potential energy surface of the excited state is somewhat different, as shown by the second excited electronic state, several vibrational states will now have a partial overlap with the $v = 0$ of the ground electronic state, resulting in a long vibrational progression.

The relative probability of transition to different vibrational levels of an excited electronic state can be expressed mathematically by the square of the overlap integral and is known as the Franck-Condon factor (FC).

$$FC = \left\langle \int \psi'_v \psi''_v dR \right\rangle^2 \qquad (5.6)$$

ψ'_v and ψ''_v represent the wavefunction of an upper and a lower state, respectively and the most probable transition is therefore given by the largest overlap integral between the two wavefunctions.

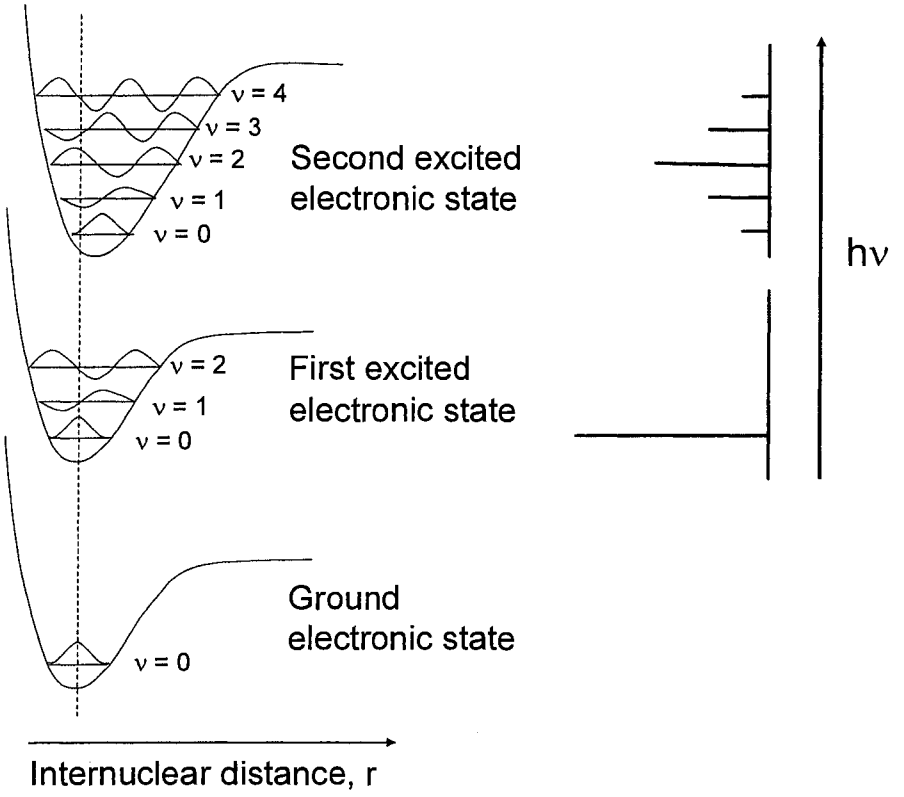

Figure 5.6 Diagram illustrating the source of vibrational structure in electronic spectra. When the two wells are very similar, one predominant peak will result. When they are different, it can yield a long vibrational progression.

As McLuckey pointed out, in most MS/MS experiments with present-day instrumentation, interaction time tends to be longer than 10^{-14}s for many polyatomic ions, in particular those that are greater than a few hundred mass units. However, this mechanism may still be important for very light precursor ions (e.g. < 50 amu) in the keV collision energy range.[10]

5.2.2 *Curve Crossings*

Curve crossing is the other mechanism that can result in electronic transitions. This mechanism is most frequently credited for electronic transitions in the collisional activation of polyatomic species, wherein a net transition occurs at an avoided crossing along the ion-target coordinate.[10,15,16] Figure 5.7 illustrates this mechanism by showing a simplified diagram in which there are only two adiabatic potential energy curves, one for the ground state and one for an excited state. As the collision partners approach each other, the energy of the collision complex increases along the adiabatic curve of the ground state. At a point where this surface is close to those of a higher excited state, the surface may cross through nonadiabatic interactions that bring about radiationless transitions from the ground to an electronic excited state of the collision complex. When the collision partners then separate, this excited state correlates with the excited state of the reactants.

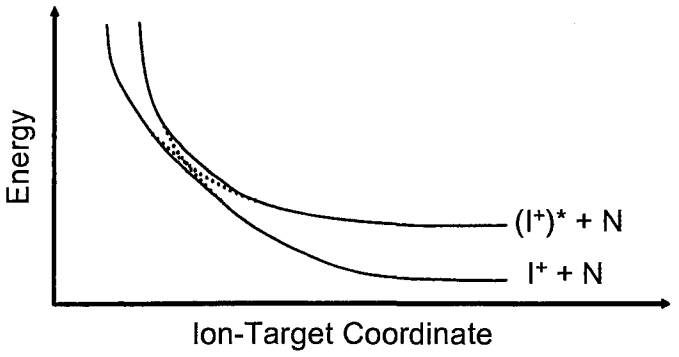

Figure 5.7 Simplified diagram illustrating curve crossing during ion-target collisions.

According to the Massey adiabatic criteria,[17,18] if the interaction time is long enough, the electrons in the collision complex will be able to relax into their lowest energy state at the crossing point and therefore, the complex will continue along the ground state potential energy curve, resulting in no excitation. Similarly, if the energy required for the transition (ΔE) is large, crossing is unlikely. However, while the energy difference between the states can be large when the two particles are far apart, it can be sufficiently small at the crossing point which would allow for the transition. Massey incorporated these conditions in the following expression, which is commonly referred as the Massey parameter, ξ.

$$\xi = \frac{a\Delta E}{h\nu} \qquad (5.7)$$

ΔE is the internal energy change in the electronic transition, a is the collision interaction distance, ν is the relative velocity of the two species and h is Planck's constant. When $\xi >> 1$, the system behaves adiabatically and crossing over to the excited state is unlikely.

Landau, Zener and Stueckelberg expressed the probability (P) of crossing-over in terms of the slope (dV/dr) difference at the crossing point and the relative velocity (ν) of the two colliding species.[19-21]

$$P = e^{-2\delta} \qquad (5.8)$$

where

$$\delta = \frac{(2\pi)^{3/2} U^2(R)}{\left(\left|\frac{dV_i}{dr} - \frac{dV_f}{dr}\right|\right) h\nu} \qquad (5.9)$$

$U(R)$ is the potential describing the particular kind of transition involved in the energy transfer at the crossing point and h is Planck's constant. For instance, if the transition is optically allowed, U follows a $\mu^2 r^{-3}$ dependence, where μ is the dipole moment of the optical transition.

In a simple case at which there is only a crossing point between two states (as in Figure 5.7), the total probability for the system to result in the excited state is $2P(1\text{-}P)$. The term $P(1\text{-}P)$ takes into account the fact that the crossing point is encountered twice for each collision, the first time when the colliding particles approach each other before the collision and the second time as they recede from each other after the collision. Therefore, in order to result in the excited state, it has to cross at only one of the two occasions. The factor 2 is to take into account that there are two ways to achieve this (i.e. cross, not cross and not cross then cross). Since the probability is a function of $P(1\text{-}P)$, we can expect the probability to be at the maximum when $P = 0.5$. Therefore, there will be a set of conditions that lead to a maximum in this probability. An ion velocity that leads to a maximum probability is v_{max}.

5.2.3 Impulsive Collision

A mechanism that will lead to only vibrational excitation is impulsive collision. It is based on momentum transfer and involves an elastic collision between the target and part of the ion with some of the recoil energy distributed into vibration. The repulsive part of the potential is sampled, resulting in momentum transfer and scattering. We can

consider its extreme case in which an ion consisting of two non-interacting parts, a "participant" group P and a "spectator" group S, has negligible force constant between them. Upon collision with the target, momentum transfer occurs to only group P and not group S. In this case, there is a net internal momentum change in PS^+ and therefore, a part of the incident kinetic energy is transformed into vibrational excitation energy of PS^+.

5.2.4 Combined Electronic and Vibrational Excitations

Of course, in a vertical transition, vibrational excitation can accompany direct electronic excitation when an excited electronic state is populated in excited vibrational states. This is regarded as indirect vibrational excitation.

We have dealt with electronic and vibrational excitation separately in the previous sections. It is also possible for a direct vibrational excitation proceeding in concert with an electronic transition. Both Durup[12] and McLuckey[10] have suggested that an impulsive collision can occur in concert with curve crossing. This situation would be expected from curve crossing on the repulsive part of the potential for an ion that does not behave like a rigid structure. In this case, the relative position of the P and the S groups can change while going through the curve-crossing mechanism, leading to both electronic and vibrational excitation.

5.2.5 *Summary*

I have discussed several mechanisms for keV collisional activation. In the case where only electronic transitions occur, one would expect the collision time to be shorter than the time for the nuclei to react. On the other hand, vibrational transitions would become more favourable at lower collision energy.

McLuckey has used the Massey adiabatic criterion to estimate the ion translational energy leading to maximum transition probability for different projectile masses.[10] When ΔE is 2 eV (typical of an electronic transition), the lab-frame ion translational energy giving rise to the maximum transition probability is at around 30 keV, which is above the typical range of a sector mass spectrometer. On the other hand, when ΔE is 0.1 eV (typical of a vibrational transition), it is below, at around 300 eV. Therefore, we can expect from these approximate numbers that within the typical energy range in a sector mass spectrometer, as the ion velocity (v) increases, the probability for an electronic transition will increase while that for a vibrational transition will decrease.

5.3 Methods for Collision Studies

There are two major experimental strategies used for studying excitation by collisions. One of them is based on detecting post-collision ions. The translational energy change of the projectile or the fragment ions can be measured at zero scattering angle. Alternatively, one can obtain energy loss or CID mass spectra at different

scattering angles. The other strategy, on the other hand, is based on observing photon emissions from collisionally-activated species. The former is known as translational energy spectroscopy and angle-resolved mass spectrometry and the latter is usually referred to as collision-induced emission spectroscopy.

5.3.1 Translational Energy Spectroscopy (TES)

(i) TES by fragment ion detection

When collisions result in fragment ions, the translational energy of the fragment ions can be monitored to obtain information regarding ion excitation. In this method, the measurement of energy deposition into internal modes can be effected by detecting the momentum distribution of dissociation ions.

A simple mass spectrometer can consist of an ion source, a magnetic sector and a detector.[22] The magnetic sector separates the ions according to their momentum by magnetic field according to the relationship

$$mv = rBze \qquad (5.10)$$

where m and v are the mass and the velocity of the ions, r is the radius of the circular path by which the ions pass through the magnet, B is the magnetic field, z is the ion charge and e is the elementary charge. The velocity of ions with uniform translational kinetic energy (eV) is given by the following equation:

$$v = \left(\frac{2zeV}{m}\right)^{\frac{1}{2}} \qquad (5.11)$$

Therefore, equation 5.11 can be written as

$$\frac{m}{z} = \frac{B^2 r^2 e}{2V} \qquad (5.12)$$

Because V is determined by the accelerating voltage and therefore can be held constant, ions with a particular mass-to-charge ratio, m/z, can be made selectively through the analyzer for a given value of B. However, when the fully-accelerated molecular ions M_1^+ dissociate in the field-free region (before the magnetic analyzer), the magnetic sector will not transmit the product ion M_2^+ at the m/z value given by equation 5.12, because M_2^+ only has $m_2/m_1 \cdot eV_{acc}$ translational kinetic energy. The magnet will therefore select M_2^+ at an apparent mass, $(m/z)_{app}$, and this apparent mass can easily be shown[23] to be approximately

$$\left(\frac{m}{z}\right)_{app} = \left(\frac{m_2}{z_2}\right)^2 \left(\frac{z_1}{m_1}\right) \qquad (5.13)$$

In the derivation of equation 5.13, the inelastic energy transfer in the collision is neglected. This energy transfer, ΔE, results in the decrease in laboratory ion translational energy as a result of energy conversion to internal modes. ΔE can be determined by comparing the position of the fragment peak with respect to a nearby primary ion peak.

A useful modification to the instrument is to add a selection magnet immediately after the ion source to select only the ions of interest.[24] The use of an electrostatic sector to detect energy loss is also common. Several groups have used the sequence of ion

source, magnetic sector, electrostatic sector and detector in their studies.[25,26] The electrostatic sector which is an energy analyzer measures directly the ion translational energy using electric field. As a result, the peak displacement in the obtained spectrum directly reflects the energy change.

Many studies have been performed on $N_2^{+\cdot}$ since the collisional dissociation of fast $N_2^{+\cdot}$ ions was first reported in 1923.[27-35] Figure 5.8 shows the laboratory momentum distribution of forward- and backward-scattered N^+ arising from collisions of 10 keV $N_2^{+\cdot}$ on He plotted against *W*, the kinetic energy of the dissociation products with respect to their centre of mass.[28] Peak g corresponds to N_2^{2+} while peak h corresponds to N^+. The broad N^+ peak is nearly symmetric and when compared to the sharp peak of N^{2+} ions produced in the ion source (used as a marker to calibrate the mass scale), the displacement of the N^+ peak corresponds to an energy loss of 8 ± 2 eV.

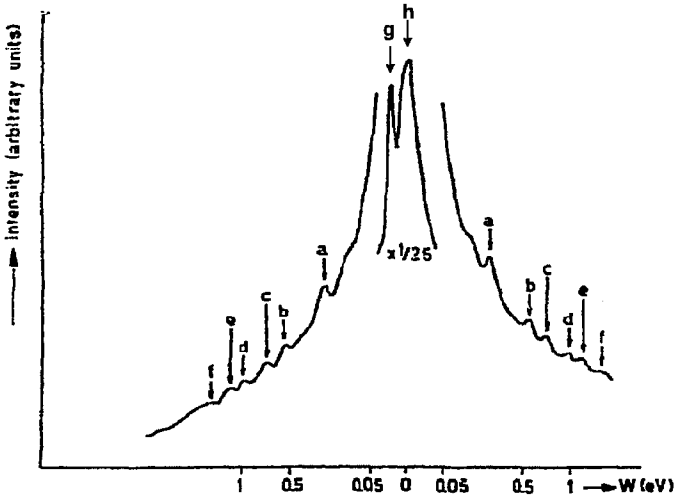

Figure 5.8 High-resolution scan of the N^+ fragments from the CID of 10-keV $N_2^{+\cdot}$/He collisions (reproduced with permission).[28]

The broad feature of the N^+ band is the result of energy conversion from the internal energy of the excited parent molecule into translational energy of the dissociation fragments with respect to their center of mass. This amount of energy is designated as e_d. For diatomic ions, it is equivalent to the excess energy of the excited parent molecule relative to the dissociation limit corresponding to the resulting fragments. The shoulder peaks labelled from a to f represent N^+ fragments with different amounts of energy release, e_d. These values are compared to the excess energies of the vibrational levels v' = 4-9 of the $N_2^{+\cdot}$ C $^2\Sigma_u^+$ state relative to the first dissociation limit obtained from spectroscopic data. The agreement suggests that the N^+ fragments come from the predissociation of v' = 4-9 of the C $^2\Sigma_u^+$ state, which also implies that the predissociation extends over a rather wide range of vibrational levels. The authors suggested that the continuous spectrum underlying the structure in Figure 5.8 could be resulted from collisional excitation to the repulsive part of the D $^2\Pi_g$ state of $N_2^{+\cdot}$.

Similar conclusions were obtained in a recent study by Fuentes and Martinez.[36] They obtained translational energy spectra of N^+ resulting from 3.0 keV and 4.0 keV $N_2^{+\cdot}$ collisions with He and Ar and presented their results in both laboratory and centre-of-mass frame. The displacement of the N^+ peak corresponds to an energy loss of 8.5 ± 0.8 eV. For both collision systems, they identified excitation to the C $^2\Sigma_u^+$ state as the most important transitions involved in the production of N^+. In addition, they also observed a secondary maximum in the case of Ar target while it is either slight or absent for He target. They attributed this broad distribution to the dissociation of the D $^2\Pi_g$ state. The results would suggest that dissociation from the D $^2\Pi_g$ state is more important with Ar

target than for He target. The wide skirts of their peaks indicate that a considerable range of energies is involved.

(ii) TES by precursor ion detection

Information can also be obtained by looking at the translational energy change in the precursor ions. This method is also applicable when excitation results in no fragment ions. Collision studies involving an atomic ion and a neutral molecule are also common. This combination allows studies on the excitation of neutral molecules and at the same time, it ensures no dissociation of the precursor ions.

Instruments have been under constant development as resolution is highly demanded for this type of experiments to differentiate near-by excited states. The Brenton group, for example, constructed an energy-loss spectrometer that can provide an energy resolution of 0.02 eV on a beam of 3 keV energy.[37,38] This resolution is substantially higher than previous instruments for keV collisions.[39-41] Their instrument consists of an ion source, a magnet for mass selection, a pair of symmetrical electrostatic analyzers for TES experiments and a third smaller ESA located before the detector to eliminate artifact signals.

Using this instrument, they studied excitation processes in H_2, N_2 and O_2 molecules with H^+ and $H_2^{+\cdot}$ projectile ions to look into the validity of quantum selection rules for collisions.[38] Based on spin conservation, H^+ projectile ions possessing singlet

symmetry can only access singlet excited states whereas $H_2^{+\cdot}$ possessing doublet symmetry can enable excitation of both singlet and triplet states of the target.

Figure 5.9 presents their TES spectra of keV H^+/N_2 and $H_2^{+\cdot}/N_2$ collisions. For H^+/N_2 collisions, only transitions to singlet excited states were observed while both singlet and triplet excited states were observed for $H_2^{+\cdot}/N_2$ collisions. Therefore, spin conservation was obeyed. However, the prominent transitions for H^+/N_2 collisions are X $^1\Sigma_g^+ \rightarrow$ a $^1\Pi_g$ and X $^1\Sigma_g^+ \rightarrow$ w $^1\Delta_u$, both of which break the dipole electronic selection rules that are applied to optical spectroscopy. Excitation to a $^1\Pi_g$ state should be symmetry forbidden since g-g and u-u transitions are disallowed. Similarly, for excitation to w $^1\Delta_u$, the orbital angular momentum changes by 2, which also breaks the selection rule $\Delta\Lambda=0, \pm1$. Similar results were obtained from several other collision systems. As a result, it was concluded that not all selection rules that are normally applied to optical spectroscopy are obeyed in collisional excitation.

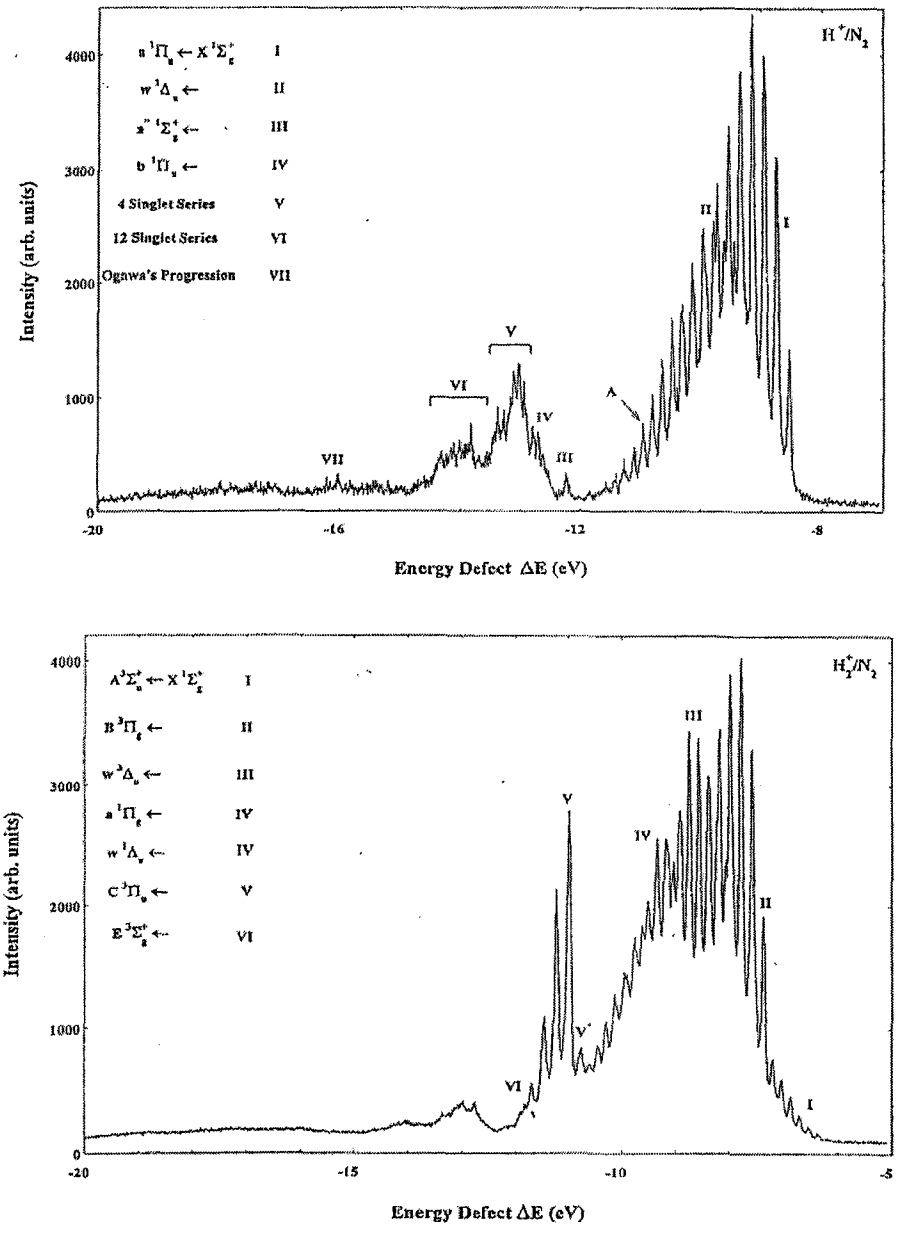

Figure 5.9 TES spectra of 3-keV H^+ and $H_2^{+\cdot}$ projectile ions scattered off N_2 (reproduced with permission).[38]

(iii) Double Translational Energy Spectroscopy (DTES)

Recently, there is some interest in studying electron capture by multiply-charged ions using translational energy spectroscopy. As the ion beam can sometimes contain metastable content, the Gilbody group uses double translational energy spectroscopy (DTES) (first demonstrated by Huber et al.[42]) to resolve the ground state and the metastable state of the ion beam.[43,44] An ion beam of C^{2+}, for example, is known to contain $(1s^2 2s^2)^1S$ ground state and $(1s^2 2s2p)^3P$ metastable C^{2+} ions. In the DTES approach, an intense beam of C^{3+} ions was first obtained from an ECR ion source and were mass selected by a magnet. These ions collide with He target gas and, through electron capture, produces $(1s^2 2s^2)^1S$ ground and some excited states of C^{2+}. These peaks are resolved in TES by their energy change. As a result, ^1S ground or ^3P metastable ions can be selected by an electric field and then passed on to another electrostatic analyzer to study their electron capture process by a second stage of TES. Figure 5.10 illustrates a comparison between energy change spectra for one-electron capture in 4 keV C^{2+}/Ar collisions obtained with a C^{2+} beam containing (a) a mixture of ground and metastable content, (b) only ground state and (c) only ^3P metastable ions. Collision product channels resulting from the respective ^1S ground and ^3P metastable states can clearly be distinguished this way.

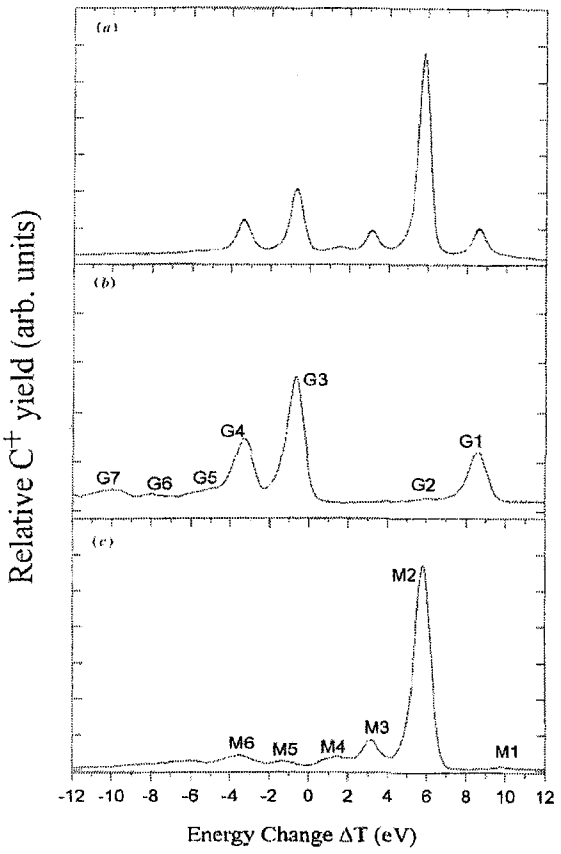

Figure 5.10 Energy change spectra for 4-keV C^{2+}/Ar collisions obtained with a C^{2+} beam containing (a) a mixture of ground and metastable content, (b) only ground state and (c) only ^3P metastable ions (reproduced with permission).[45]

5.3.2 Angle-Resolved Mass Spectrometry

A variation to translational energy spectroscopy is angle-resolved mass spectrometry. This method relates impact parameter for a collision to the internal energy deposited by assuming that hard collisions deposit more energy than soft collisions.

The Cooks group tested this hypothesis by installing an angle-resolving slit to their double focusing mass spectrometer[46] and comparing energy-loss spectra and CID mass spectra at different scattering angles (typically between 0 and 2 degrees). For

Ar^+/Ar collisions, four peaks were observed in the TES spectrum; one elastic and three inelastic scattering peaks.[46] The energy loss of each peak was correlated to an excited state of Ar target. When small scattering angles are sampled, the elastic scattering peak is much more intense than the inelastic peaks. As the scattering angle increases, the absolute intensity decreases for all peaks but the relative intensity of the inelastic peaks increases. Similarly, CID mass spectra were obtained at different scattering angles for ethyl isobutyl ether. Two prominent CID peaks were observed. At larger scattering angles, the relative peak intensity of m/z 29 increases. As a result, the higher-energy process ($59^+ \rightarrow 29^+$) is favoured over the lower-energy process ($59^+ \rightarrow 31^+$).

They have also generated the breakdown curves for several molecular ions (e.g. 1-propanol, methanol, methane and carbon disulfide) from the relative fragment ion intensities in the CID mass spectra as a function of scattering angles.[47] The similarity of these curves with those calculated by QET is given as qualitative proof that selecting scattering angle does select internal energy of the projectile ion. The effectiveness of target is probed by comparing results for methanol molecular ions on He, N_2 and Freon. The scattering angle giving rise to equal intensities of the two fragment ions were determined for each target. These laboratory scattering angles were 0.44, 0.49 and 0.59 respectively. Helium is the most effective target in terms of the degree of internal excitation for a given laboratory scattering angle. But considering their large difference in mass, their laboratory scattering angles are considerably similar.

The Cooks group has also extended their studies to include the effects of variation of the projectile translational energy.[48] An attempt was made to investigate whether the reduced scattering angle, defined as $\tau = E\theta$, can be used to relate scattering angles at different ion translational energies. Energy loss spectra of the same $E\theta$ are similar for Ar^+/Ar collision. As $E\theta$ increases, so does the abundance of high-energy loss peaks. Similar behaviour was observed for the CID of nitromethane molecular ions. At low $E\theta$, the lowest energy dissociation ($CH_3NO_2^{+\cdot} \rightarrow NO_2^+ + CH_3^{\cdot}$) dominates but as $E\theta$ increases, the higher energy dissociation ($CH_3NO_2^{+\cdot} \rightarrow NO^+ + CH_3O^{\cdot}$) starts to compete, as does $NO_2^+ \rightarrow NO^+$. The same $E\theta$ results in similar CID mass spectrum. This feature provides the flexibility that either the kinetic energy or the scattering angle can be adjusted. However, Boyd et al. later pointed out that the relationship should be proportional to $E\theta^2$ instead.[49]

On the other hand, concerns regarding contribution of scattering by kinetic energy release (KER) have also been raised.[50-53] It is generally agreed that both impact parameters and KER contribute to scattering of the precursor ions. However, separating KER and collision scattering is infeasible. As a result, it would be difficult for angle-resolved mass spectrometry to yield direct information on the internal excitation of projectile ions.

5.3.3 Collision-Induced Emission Spectroscopy (CIE)

Laser-induced fluorescence spectroscopy has been widely used to obtain information on the electronic states of polyatomic ions. A similar approach can be realized by exciting the ions with collisions instead of laser pulses. In this case, observation of the resultant emissions gives information on the electronic states that are accessible by collisions as well as insights to the collision process. This type of spectroscopy is often carried out in a mass spectrometer for the study of ion-neutral collisions where projectile ions collide with a neutral target gas in a collision cell. The photon emissions are subsequently detected by a photomultiplier tube or a charge-coupled device detector.

Early experiments were carried out to acquire laboratory data on reactions that occur in the Earth's atmosphere, especially on charge transfer processes. Collision systems involving N_2, O_2 and CO_2 have been investigated by several groups. In addition to the measurement of cross sections for various charge transfer processes, emphasis is also placed on the determination of vibrational state distributions in the excited electronic states. In an effort to better understand the nature of collisions, the observed vibrational state distributions are often compared to those obtained from theory. The most commonly used model is the vertical transition model. Synthetic spectra can be constructed from knowledge of the Franck-Condon factors and are compared to experimental observations. Moore and Doering have studied the vibrational distribution of the $N_2^{+\cdot}$ B state by observing the relative band intensities of the $\Delta v = -1$ sequence of

the B→X emission resulting from charge transfer process between various atomic / diatomic ions and N_2 target.[54] They concluded that the observed vibrational distributions depend heavily on the laboratory velocity of the reactant ion but very little on its chemical nature. They observed that when the velocity is below 10^8 cm/s (i.e. ~ 5 keV for H^+ precursor ion), the vibrational distributions no longer agree with the vertical transition model. This was explained as distortion of the target molecule electron cloud by the impinging ion at low velocities.[54,55] This explanation, however, could not explain the similar behaviour in direct excitation process observed in $N_2^{+\cdot}$/target collisions.[56] In this case, the charge resides on the precursor ion; therefore, the ion-induced distortion explanation cannot be used.

Kelly et al. explained it with a more general qualitative curve-crossing model and the assumption that deviations from vertical transitions during collisions are caused by short-range, repulsive interaction between the projectile and the target and these short-range interactions result in direct translational-vibrational excitation in both the initial and final electronic states of the diatomic molecule.[57-59] The fact that short-range forces are involved means that the reaction occurs at small impact parameters. As such, the diatomic molecule cannot be regarded as being isolated. In other words, distortion occurs by chemical forces that are operative in any short-range encounter between the two collision particles.

Similarly, charge transfer process with CO_2 has been studied by several groups.[60-65] The B→X and A→X emissions are the dominant emissions observed in the

wavelength range of 200-500 nm. At high velocity, the vibrational energy distribution in $CO_2^{+\cdot}$ (A) was found to be independent of velocity whereas at velocity below 4 x 10^7 cm/s, the relative populations of the low vibrational states increases monotonically with decreasing projectile ion velocity.[60] In the study of Ne^+/CO_2 charge transfer, the B→X and A→X emissions are monitored as a function of translational energy. It was found that below 2 keV, the ratio of B→X to A→X decreases with translational energy.[62]

Collisions involving multiply-charged ions have also been studied by emission spectroscopy and similar conclusions were reached. Ehbrecht et al. studied the charge transfer process between CO^{2+} and a series of neutral targets (Ar, N_2, H_2, D_2 and CO) at 60-2000 eV projectile energy.[66] The charge transfer process results in CO^+ ($B\ ^2\Sigma^+$), and the B → X emission was detected. At 2 keV, the vibrational distributions in CO^+ were found to be similar to those predicted by the Franck-Condon principle while at lower energy, an increase in the population of higher vibrational states was observed, especially from collisions with Ar. In the case of $CO_2^{+\cdot}/N_2$ and $CO_2^{+\cdot}$/CO collisions where emission from the ionized targets was also observed, a comparison was made with the analogous product emission from charge transfer with singly-charged projectiles (i.e. Ar^+/N_2 and Ar^+/CO collisions). Pronounced deviations from the Franck-Condon prediction in the latter case was explained as the difference in the crossing radius between the entrance and the exit channel potentials. Whenever the crossing radius is large, the vibrational distribution in the product deviates only little from the Franck-Condon prediction and vice versa. CO^{2+}/CO collision is a special case as CO^+(B) can be resulted from both

electron capture of the CO^{2+} projectile and ionization of the CO target. Isotopic-labelled reagent was used to differentiate the two emission bands.

$$^{13}CO^{2+} + {}^{12}CO \rightarrow {}^{13}CO^{+}\,(B) + {}^{12}CO^{+} \quad \text{(electron capture)} \qquad (5.14)$$

$$^{13}CO^{2+} + {}^{12}CO \rightarrow {}^{12}CO^{+}\,(B) + {}^{13}CO^{+} \quad \text{(ionization)} \qquad (5.15)$$

Experimental observation showed that the ionization process was more favourable. This was rationalized by considering the electronic rearrangement involved. It was suggested that the ionization process involving CO^{2+} ($^3\Pi$) which can be effected by a one-electron process is expected to be more probable than a two-electron process.

A major advantage with collision-induced emission spectroscopy over translational energy spectroscopy is the higher resolution and sensitivity and therefore, this technique was chosen to be implemented in my experiments. As mentioned above, previous studies heavily focus on charge-transfer processes and small wavelength range (usually on only a single emission band). In the present project, I studied emissions from direct excitation process involving $N_2^{+\cdot}$ and $CO_2^{+\cdot}$ as a function of projectile ion translational energy and over a broader range of wavelengths (190 nm - 1020 nm) than has previously been reported (typically spectra have been reported for wavelengths ranging from 380 nm – 392 nm[67,68] to 180 nm – 850 nm[69]). By observing also the emissions from the dissociated products, excited states that involve a very different amount of energy deposition can be compared.

6 Methods of Study

6.1 The Modified VG-ZAB Mass Spectrometer

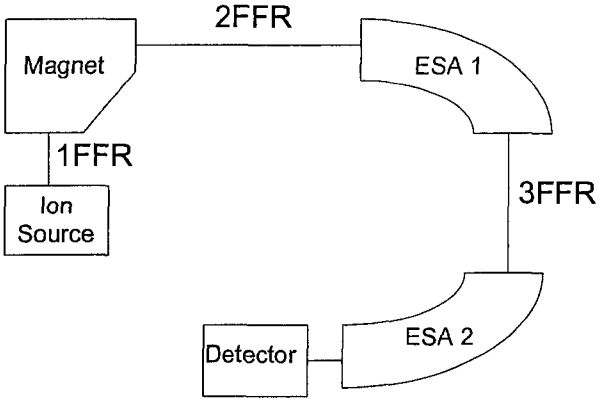

Figure 6.1 Schematic diagram of the modified VG-ZAB mass spectrometer used in this research work.

The mass spectrometer used for the experiments is a modified VG-ZAB triple-focusing mass spectrometer. Figure 6.1 shows the schematic diagram of this instrument, which is the same as shown in Figure 2.1. It consists of an ion source, a magnetic mass analyzer and two electrostatic analyzers (ESA). The region between the first and the second electrostatic analyzer is the third field-free region. Originally a double-focusing mass spectrometer,[70,71] the third field-free region (3FFR) and ESA2 were later added to allow for mass spectrometric studies of fragment ions.[72]

The 3FFR (Figure 6.2) consists of a 1 m long box differentially pumped by two six-inch diffusion pumps and ending in a second electrostatic analyzer. The box contains

a lens assembly used to create a near parallel beam of ions through the 3FFR after the focal point of ESA1. Another set is placed at the end of the box to focus the ion beam before entering the second ESA. Two optically correct rails run along the bottom of the box, allowing collision cells and other experimental hardware to be precisely located in the ion beam path. Two collision cells and a repeller have been installed for carrying out a wide variety of typical tandem mass spectrometric experiments such as collision-induced dissociation, collision-induced dissociative ionization, charge transfer, charge stripping and neutralization-reionization mass spectrometry (NRMS). The 3FFR also contains an experimental zone for this work. A fused silica window of 1 cm diameter (Optikon WU-25) was embedded in the lid of the 3FFR to allow photons to exit and be detected. The goal of this project is to study the change of emissions from the collisionally-activated ions at various collision energies. In this respect, it is necessary to be able to control precisely the ion translational energy. Therefore, some sort of deceleration components need to be installed. It has been attempted in the lab to simply put another collision cell under the observation window and decelerate the ions by putting a voltage on it. This turned out to be impractical as many of the ions were scattered away, resulting in an almost total loss of signal.

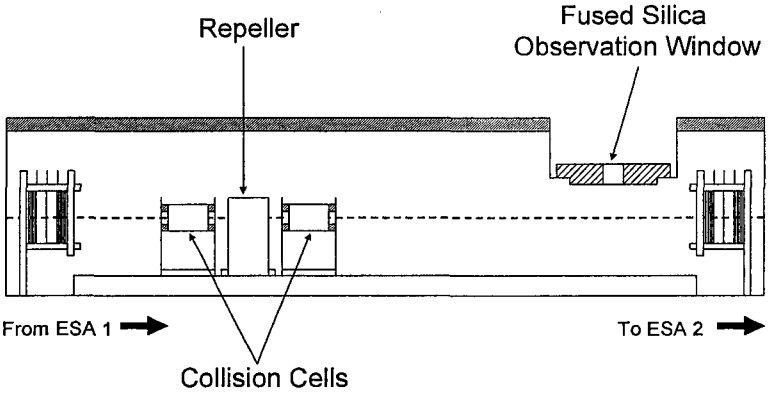

Figure 6.2 The inside of the third field-free region.

6.2 Deceleration-Reacceleration Lens Assembly

There are various applications in mass spectrometry in which it is necessary to decelerate ions. An example is to link an electric sector to a quadrupole analyzer in a hybrid instrument. Traditionally, many deceleration systems involve creating an exponentially decaying retarding potential field that normally requires a complex lens assembly, often incorporating 40 or more electrodes. Using the SIMION ion simulation program, O'Connor et al. successfully illustrated that deceleration lens assembly need not be very complicated to maintain high transmission of ions through the system.[73] From their evaluation, they found that the ratio of the initial beam diameter to the electrode aperture diameter is the most significant criterion in determining the performance of ion deceleration lenses, not the complexity of the retarding field. Therefore, it is advantageous to constrain the ion beam near the central axis of the lens assembly. They proposed doing so by preceding the deceleration stage by an Einzel lens.

Enlightened by their findings, I have designed a similar lens and have simulated it at different conditions using the SIMION 6.0 program.[74] Figure 6.3 presents the schematic diagram of my Einzel lens and the deceleration-reacceleration lens assembly.

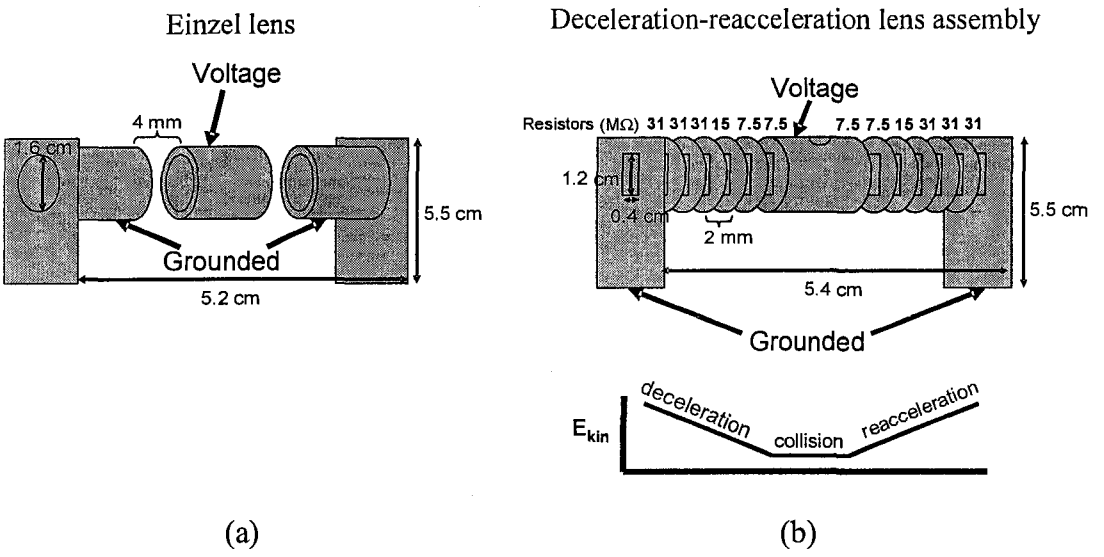

Figure 6.3 Dimensions of the (a) Einzel lens and the (b) deceleration-reacceleration lens assembly with a schematic diagram demonstrating the behaviour of the ion kinetic energy in the assembly.

The Einzel lens (Figure 6.3a) consists of three 16-mm internal diameter aluminum cylindrical tubes with a thickness of 4.7 mm and a length of 14 mm. On each end of the Einzel lens is a rectangular aluminum ground plate (55 x 30 mm with a circular opening of 16-mm diameter). The cylindrical tubes are separated by 4-mm spacers and the whole assembly is connected by four ceramic rods and mounted on a stainless steel plate on the two optically correct rails.

The collision chamber (Figure 6.3b) is a 16-mm internal diameter aluminum cylindrical tube with a thickness of 4.7 mm and a length of 16 mm. A 6-mm diameter circular hole is drilled at the top of the tube and covered by a fused silica (UV grade) window (Edmund Optics, 10 mm diameter, 1mm thickness) for photon transmission. On each side of the collision cell are six circular plates made of brass (2.54 cm diameter with

a slit of 12 x 4 mm) and an aluminum rectangular ground plate (55 x 30 mm with a slit of 12 x 4 mm). The plates are separated by 2-mm spacers and are mounted on two ceramic rods. The whole assembly is mounted on a stainless steel plate which is subsequently mounted onto the two parallel rails running along the bottom of the 3FFR. A number of 33 MΩ and 15 MΩ resistors (Electrosonics VR 37J 33M and VR 37J 15M) are soldered between plates to create a gradual voltage drop before the collision cell and a gradual voltage gain after the collision cell when a voltage is applied to the collision cell. The net result is a deceleration-reacceleration lens assembly, which allows us to decelerate the ions for collisions and reaccelerate them for detection at the ESA and detector. An illustration of the change in kinetic energy across the lens is shown in Figure 6.3b. The resistances between the lens plates are also shown. They are arranged in such a way that the difference in resistance is smaller when closer to the collision cell. This is to reduce the field penetration effect.

Ion trajectory modeling with the SIMION 6.0 program[74] showed that a high deceleration voltage applied to the cell (such as 7900 V for an 8 keV ion beam) resulted in a very scattered ion beam (Figure 6.4a). However, with the installation of an Einzel lens to focus the ion beam before it enters the deceleration lens, ion scattering is significantly reduced (Figure 6.4b).

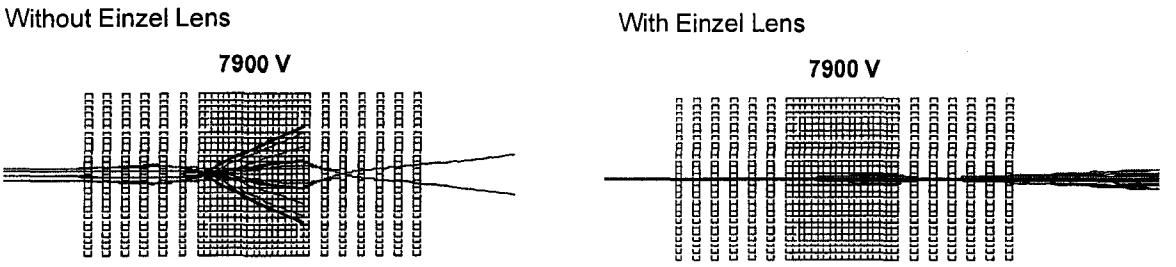

Figure 6.4 SIMION modeling of the behaviour of an 8 keV ion beam in the deceleration-reacceleration lens assembly with an applied voltage of 7900 V, (a) without and (b) with the use of an Einzel lens.

6.3 Characterization of the Lens Assembly

To characterize the deceleration-reacceleration lens, the beam-resolving slits of the mass spectrometer were set for high resolution and an 8 keV $N_2^{+\cdot}$ beam was passed through the lens. The intensity, energy and energy spread (full peak width at half maximum) of the beam were measured as a function of applied voltage (Figure 6.5). Ions can be decelerated to 3 keV without much intensity loss (Figure 6.5a). The reaccelerated main beam energy is within 0.4% of the original 8 keV (Figure 6.5b). This small difference can be considered insignificant when comparing ion energy difference in the range of keV. The energy spread of the reaccelerated beam does not change significantly with the use of the lens (Figure 6.5c).

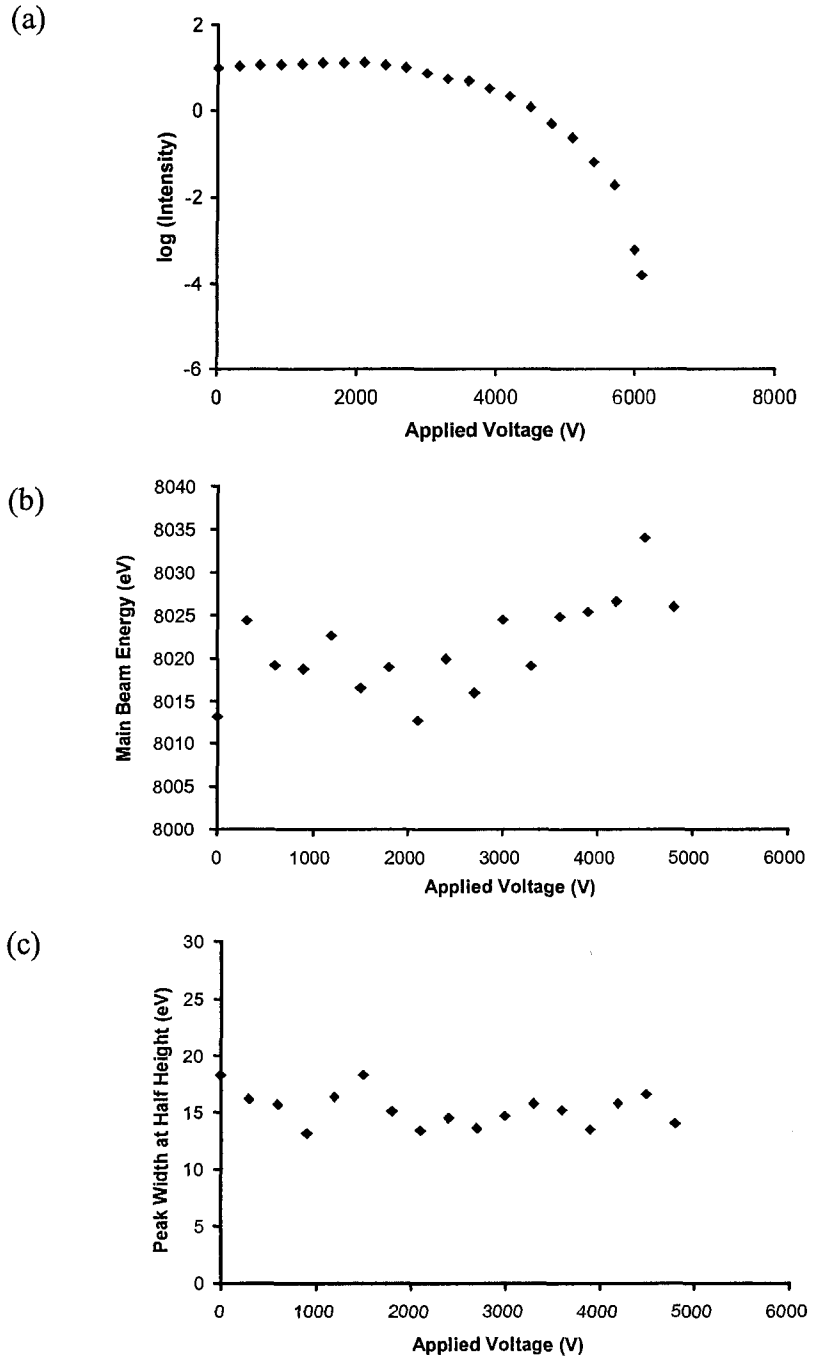

Figure 6.5 The plot of the (a) intensity, (b) energy and (c) energy spread of a reaccelerated 8 keV $N_2^{+\cdot}$ beam with different applied voltages on the deceleration-reacceleration lens assembly.

To correlate ion translational energies with applied voltage, a simple metastable ion experiment was performed. Figure 6.6a illustrates how the energy of the ions dissociated in the collision cell is shifted with applied voltage. When an 8 keV ion dissociates in half before the collision cell, the resultant daughter ion translational energy is 4 keV, which after deceleration and reacceleration by 2 keV, remains 4 keV. However, when the ion dissociates inside the collision cell, the energy of the daughter ion is again half of the decelerated parent ion, and upon reacceleration will result in a different energy than those formed outside the collision cell. This energy shift allows the determination of the actual translational energy of the ion in the collision cell. Figure 6.6b shows the metastable ion spectra of the methanol-acetonitrile proton-bound pair at a few different applied voltages. The pair dissociates primarily via three channels to form $CH_3OH_2^+$, CH_3CNH^+ and $CH_3CNCH_3^+$. At 0 V applied voltage, the peaks for protonated methanol (m/z 33), protonated acetonitrile (m/z 42) and $CH_3CNCH_3^+$ (m/z 56) were observed. By increasing the applied voltage, the two more abundant peaks (m/z 42 and 56) were shifted (m/z 32 was too small to reliably measure). The intensity of these peaks also seems reasonable if one considers the time the ions spend outside relative to inside the lens. By measuring the energy shift of these two peaks, the ion translational energy inside the collision cell can be calculated, resulting in the correlation plot of ion translational energy vs. applied voltage (Figure 6.6c). The calibration plot has a very good linear correlation with a slope close to -1 ($y = -1.01x + 8027$, $R^2 = 1.000$).

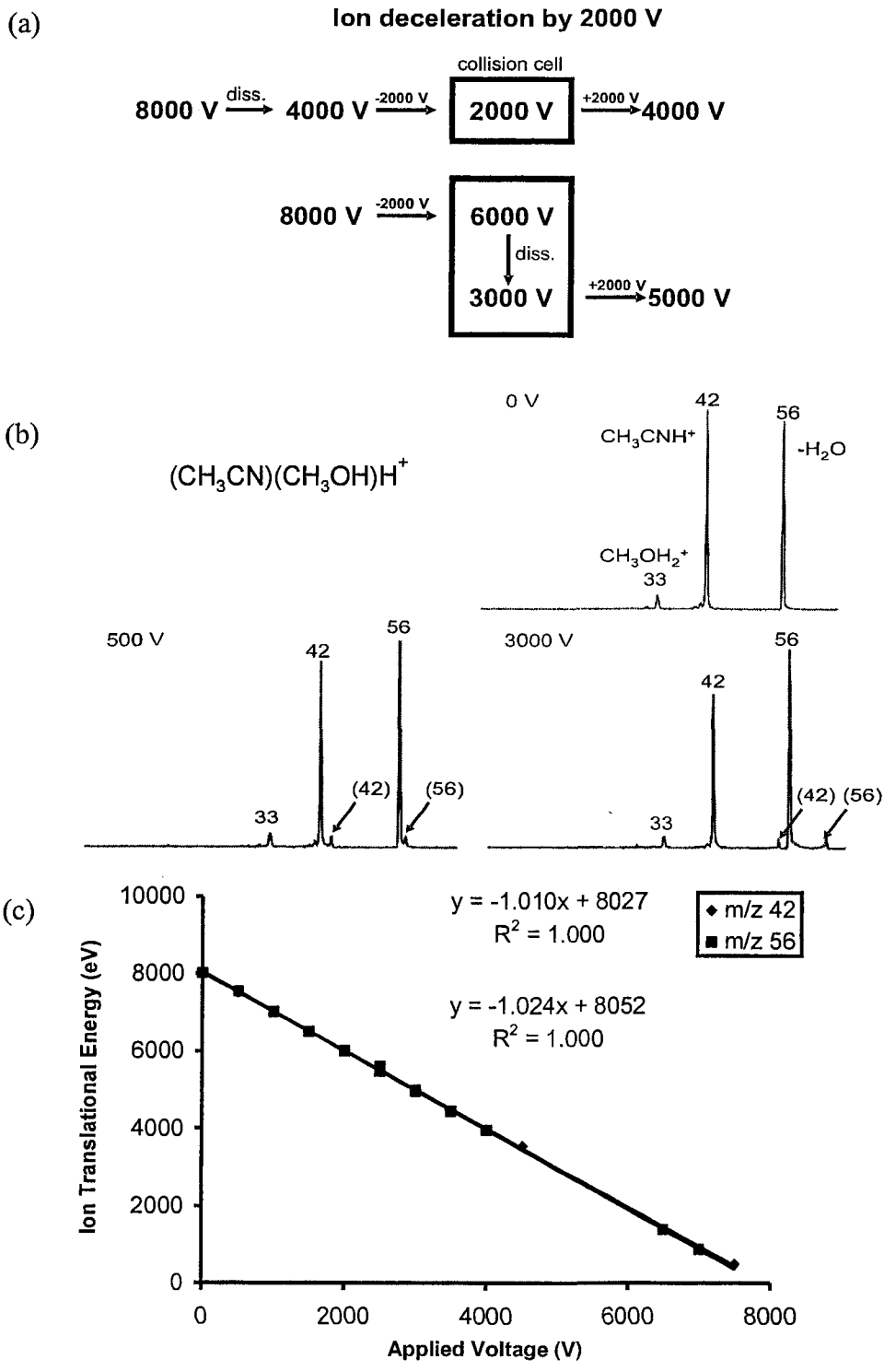

Figure 6.6 (a) An illustration of how fragment ion kinetic energy is shifted with an applied voltage on the collision cell. (b) Metastable ion (MI) mass spectra of the methanol-acetonitrile proton-bound pair at a few different applied voltages. (c) A correlation plot of ion translational energy with applied voltage.

Two ways of decelerating the ions to the desired ion translational energy were compared. One way is to decelerate an 8 keV ion beam to the desired ion translational energy with the deceleration-acceleration lens only (Figure 6.7a). The other way is to use a lower accelerating voltage on the VG ZAB ion source (which can be changed at 1 kV intervals), and then fine-tune to the desired ion translational energy with the deceleration lens (Figure 6.7b). Figure 6.7a and b illustrate the difference between these two approaches with a $N_2^{+\cdot}$ ion beam. The second method appears to be better for obtaining ions at low ion translational energy.

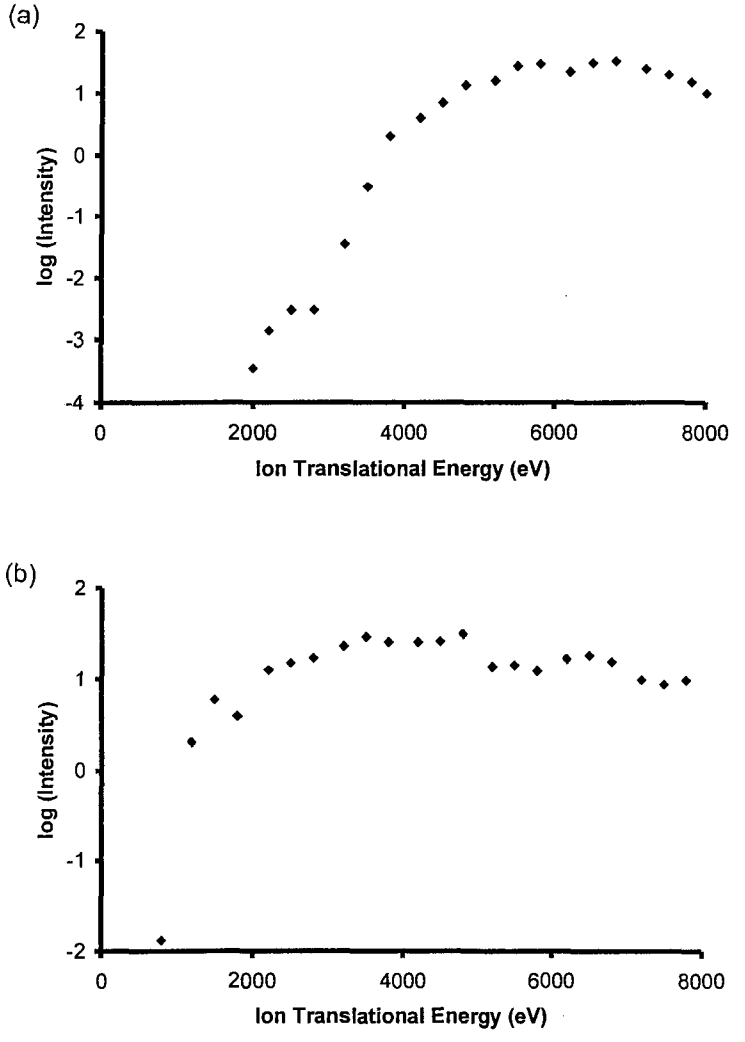

Figure 6.7 The intensity of the reaccelerated 8 keV $N_2^{+\cdot}$ beam (a) after deceleration by the deceleration-reacceleration lens assembly only and (b) after using the ion source accelerating voltage to drop the translational energy to 7, 6, 5, 4 and 3 keV and then obtaining intermediate values and values less than 3 keV with the deceleration-reacceleration lens assembly.

6.4 Photon Detection System

Photons from the collisionally-activated ions are dispersed by an Acton SpectraPro 275 spectrograph (27.5 cm focal length, 1200 g mm^{-1} holographic grating) and detected with an Andor thermoelectrically cooled charge-coupled device (CCD) detector (Andor DV401-UV, front-illuminated with UV coating). The CCD detector can be cooled to -42 °C with air and to -49 °C when water cooling is used.

Wavelength calibration of the detection system was performed so that the wavelength appeared on the screen corresponded to the true wavelength. A total of seven wavelengths from the mercury lamp and the He-Ne gas laser were used for the calibration. Two parameters (offset and acquisition pixel width) in the data acquisition program were adjusted for each wavelength. These two parameters basically set the wavelength scale by specifying the centre value and the wavelength range as detected by the CCD detector. The optimized values are presented in Table 6.1 and the correlation plot in Figure 6.8. After wavelength calibration, the observed spectral window decreases from 78 nm when the grating is set at 225 nm to 55 nm when the grating is at 995 nm. Based on the calibration results, the uncertainty of the wavelength is ± 0.5 nm.

Table 6.1 The optimized values of the offset and the acquisition pixel width parameters for each of the seven wavelengths.

Light Source	Wavelength (nm)	Offset (pixels)	Acquisition pixel width (μm)
Hg lamp	289.36	-19.5	24.60
	302.15	-20.0	24.50
	334.15	-18.8	24.35
	404.66	-18.8	23.85
	435.83	-16.4	23.80
	546.08	-16.7	23.07
He-Ne gas laser	632.80	-13.0	22.53

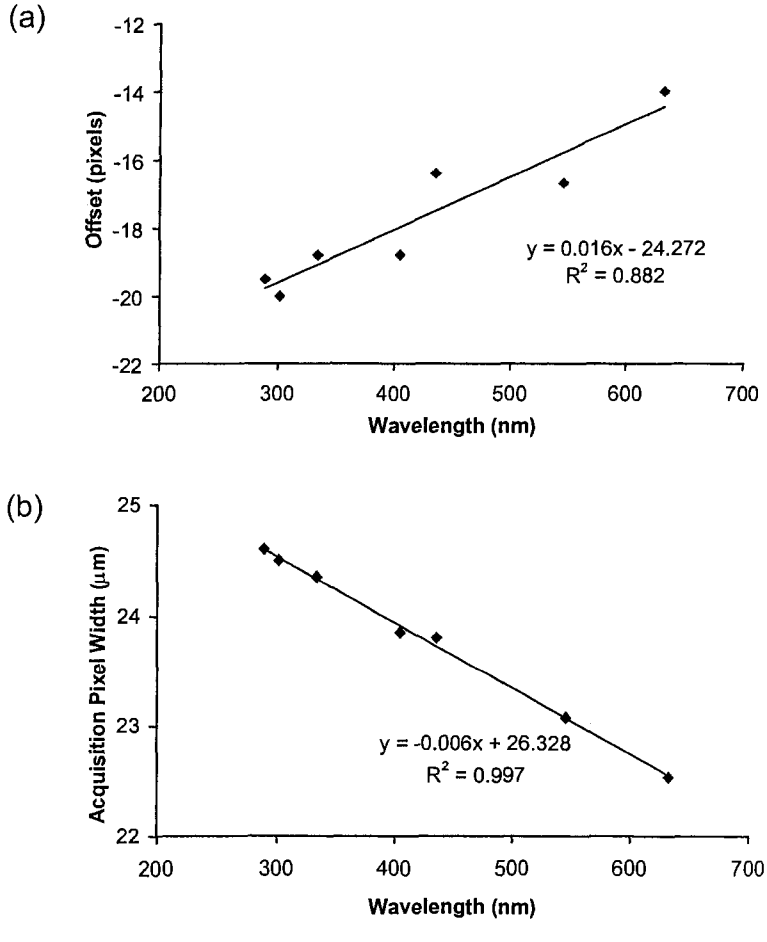

Figure 6.8 Correlation plots of (a) the offset parameter and (b) the acquisition pixel width parameter as a function of wavelength.

Bandpass refers to the full width at half maximum (FWHM) of a spectral peak. It is one way of measuring an instrument's ability to separate adjacent spectral lines. A bandpass of 3 nm, for example, will have difficulty separating two peaks that are only 1 nm apart. Bandpass is related to resolution in a sense that lower bandpass corresponds to higher resolution. In principle, when a light source emits a monochromatic photon and is analyzed by a perfect spectrometer, the output should show only a perfect line at that wavelength. In reality, spectrometers are not perfect and produce an apparent spectral broadening. The line profile will have a finite width and is known as the instrumental bandpass. This is not the only factor that contributes to the bandpass. The entrance and/or the exit slit can also play a role. In fact, most spectrometers are not routinely used at the limit of their resolution and therefore, it is usually the influence of the slits that dominates the line profile.

The full width at half maximum (FWHM) of the peaks from several wavelengths from the Hg lamp and the He-Ne gas laser were monitored at various entrance slit widths (Table 6.2, Figure 6.9). In all cases, the peak width decreases as the slit narrows, indicating that the slit is the dominant contribution to the peak width in these cases. As a result, spectral resolution can be increased with narrower slit width, at the expense of signal intensity. The peak width follows a linear relationship with respect to slit widths (Figure 6.9). They can serve as a reference for the minimum width of a spectral peak. Peaks that are much narrower than these peaks can be regarded as artifacts or spectral spikes resulting from cosmic rays.

Table 6.2 Peak width at half maximum at different slit widths for five wavelengths.

Slit Width	Peak width at half maximum for each of the following wavelengths (nm)				
(mm)	334.15	404.66	435.83	546.08	632.80
3.0	8.58	8.74	8.85	8.72	8.29
2.5	7.46	7.39	7.60	7.49	6.98
2.0	6.04	6.07	6.22	6.26	5.73
1.5	4.61	4.85	4.92	5.11	4.44
1.0	3.49	3.75	3.79	4.02	3.04
0.5	2.98	2.65	3.11	3.34	1.69

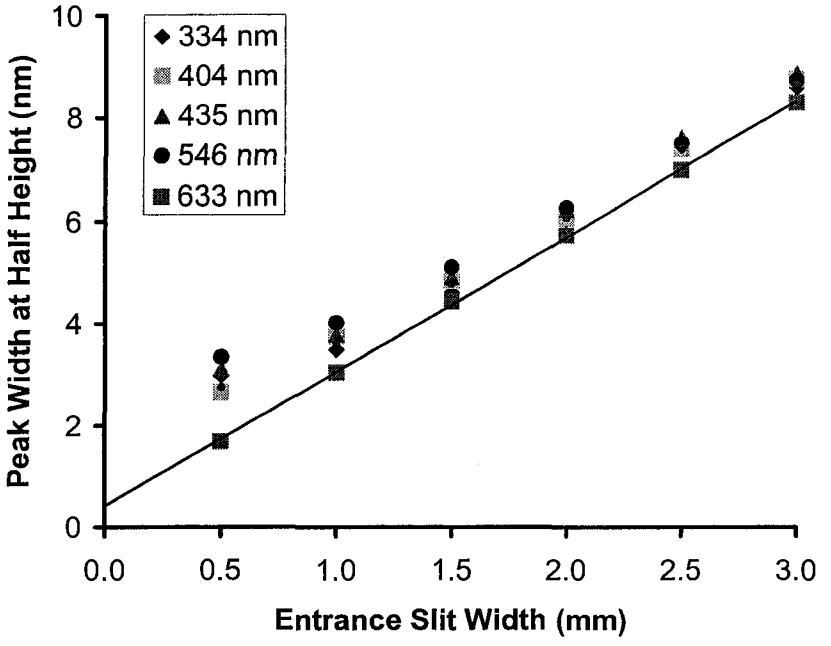

Figure 6.9 Plot of peak width at half maximum at different entrance slit width for five wavelengths.

6.5 Instrumental Setup

The instrumental setup in the third field-free region is shown in Figure 6.10. The deceleration-reacceleration lens assembly was installed underneath the optical window whereas the spectrograph and the CCD detector were installed right above it to disperse and detect photons. The Einzel lens is put at a distance of 28.4 cm away from the deceleration-reacceleration collision cell assembly. This distance is not critical but it signifies the maximum distance away from the collision cell that the Einzel lens can be placed in the third field-free region. SIMION simulations have shown that a smaller voltage is required on the Einzel lens and better ion beam focusing is obtained when the Einzel lens is placed farther away from the deceleration-reacceleration lens.

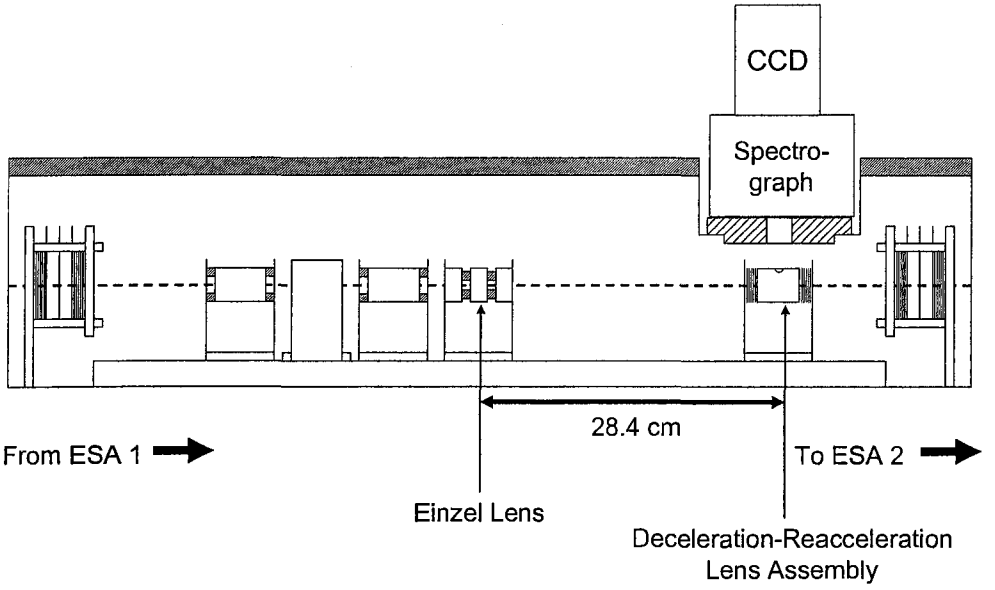

Figure 6.10 Instrumental setup of the lenses and the photon detection system in the third field-free region of the VG ZAB mass spectrometer.

6.6 Experimental Procedure

The precursor ions are generated by electron ionization (with 80-90 eV electrons) in the ion source, mass selected by the magnetic analyzer, energy selected by the first electrostatic analyzer and collide with the target gas in the deceleration-reacceleration lens assembly at a collision gas pressure that reduces the pre-cell ion flux by 10% (i.e. single collision condition).[75] The entrance slit of the spectrograph (unless otherwise noted) is set to 3.0 mm to maximize emission signal intensity resulting in a spectral resolution of 8.5 nm (full width at half maximum for atomic lines). Emission spectra were collected by the thermoelectrically-cooled charge-coupled device (CCD) cooled to a temperature of -35 °C. The offset and the acquisition pixel width parameters were set to values determined from the wavelength calibration (as described in Section 6.4). Optical emissions from 190-1020 nm were recorded by the Andor MCD 2.63.1.8 program and were recorded in 14 separate segments, each being 50-70 nm wide. Two accumulations of 15, 30 or 60 minutes were collected for each segment at full vertical binning reading mode and each of the 14 segments was background subtracted. Background spectra were collected prior to the signal acquisition at exactly the same conditions except without an ion beam. Spectral spikes resulting from cosmic rays were removed digitally by the program. Horizontal binning was performed manually in the ASCII file by combining data from every 10 pixel columns (for $N_2^{+\cdot}$/He collisions) and 20 pixel columns (for all other collision systems) and the overlapping portion of the spectrum at the two ends of each window was averaged. When comparing absolute emission intensities at different collision energies, the plotted values are normalized to the flux of the ion beam at 8 keV.

6.7 Theoretical Procedure

Adiabatic potential energy curves of the collision complex $N_2^{+\cdot}$-He and $N_2^{+\cdot}$-Ar as a function of collision coordinate were calculated at the CISD/6-311+G(2df) level of theory. Figure 6.11 shows the collision trajectory between a target atom and an $N_2^{+\cdot}$ ion as defined in the calculations. When the diatomic ion $N_2^{+\cdot}$ lies along the y axis, the collision trajectory of the target atom follows a path above and parallel to the x axis separated by β angstroms. This parameter is directly related to impact parameters. α is defined as the distance between the target atom and the z-axis. Single-point energy calculations were performed as a function of α, from 0 to 3 Å (for He) and from 0 to 4 Å (for Ar) in steps of 0.1 Å. Several trajectories with different β were sampled (β varies from 0.5 to 0.8 Å for $N_2^{+\cdot}$/He and from 0.9 to 1.5 Å for $N_2^{+\cdot}$/Ar collisions). With the collision trajectory as defined, the collision complex always possess C_{2v} symmetry.

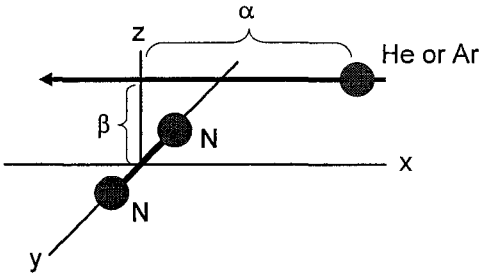

Figure 6.11 The collision trajectory between a target atom (He or Ar) and an $N_2^{+\cdot}$ ion.

The potential energy curves of $N_2^{+\cdot}$-He collision complex with β = 0.8 Å were also calculated using time-dependent density function theory (TD B3-LYP/6-311+G(2df)) and were compared to that from CISD calculations. Both sets of results are

in good agreement. It is therefore believed that CISD calculations yield reasonable results for the collisions in this study.

Figure 6.12 shows the orbitals of $N_2^{+\cdot}$ corresponding to the term symbols written on the left hand side. There are two possible orbital arrangements for each term symbol and each of these orbital arrangements has its own irreducible representation. As a result, an electronic state can be composed of more than one irreducible representation. For example, when an atomic orbital of the target atom interacts with the ground state of $N_2^{+\cdot}$ ($X\ ^2\Sigma_g^+$), the resultant collision complex (in C_{2v} symmetry) will have an A_1 representation but that with $A\ ^2\Pi_u$ will have A_1 and B_1 representations.

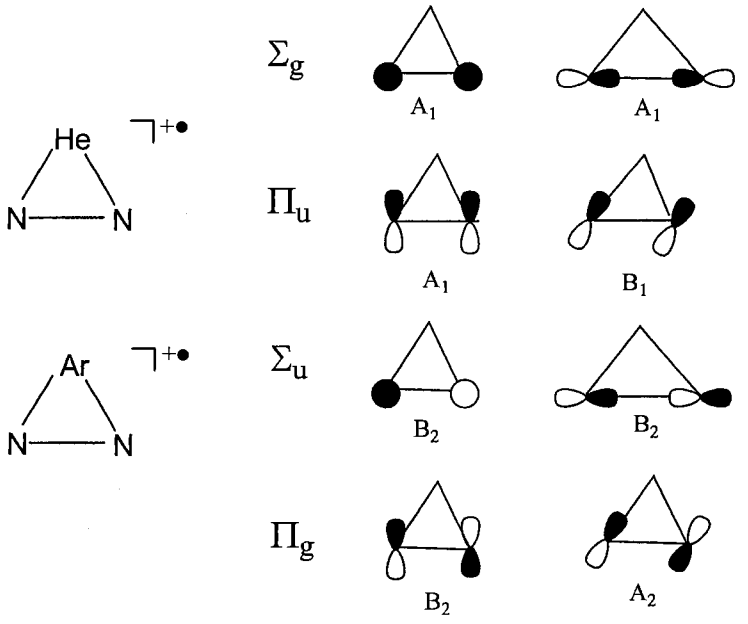

Figure 6.12 Irreducible representations of the $N_2^{+\cdot}$-He and $N_2^{+\cdot}$-Ar collision complexes (in C_{2v} symmetry).

Potential energy curves of different individual representations were averaged as they yield similar potential energy curves from my calculations. They will be presented as averaged results for each particular electronic state of the collision complex.

7 Results & Discussion

7.1 The $N_2^{+\cdot}$ Ion Beam

The $N_2^{+\cdot}$ ion beam was generated by electron ionization (EI) on N_2 using 80-90 eV electrons. At such electron energy, the ionization process could result in $N_2^{+\cdot}$ being formed in excited electronic states. Information regarding the electron configuration and the relative energy of some of the electronic states are given in Table 7.1. It is worthwhile noting that the ordering of the $3\sigma_g$ and $1\pi_u$ orbitals for N_2 has been a matter of controversy. The photoelectron spectrum of N_2 shows that the π_u orbital is lower in energy than $3\sigma_g$.[76] However, if this is the ordering for all electronic states, it cannot explain why the $N_2^{+\cdot}$ D $^2\Pi_g$ electronic state is lower in energy than the C $^2\Sigma_u^+$ electronic state. Calculations for N_2 show that the energy of the π_u orbital is higher than that of σ_g, with the two types of orbital very close in energy.[77] One of the explanations to the discrepancy is that the orbital energy shifts when an electron is removed.

Table 7.1 The electron configuration and the relative energy of several electronic states of $N_2^{+\cdot}$.

Electronic States	Electron Configuration	Relative Energy[a,b] (eV)
N_2		
$X\ ^1\Sigma_g^+$	$(1\sigma_g)^2(1\sigma_u)^2(2\sigma_g)^2(2\sigma_u)^2(1\pi_u)^4(3\sigma_g)^2$	0
$A\ ^3\Sigma_u^+$	$(1\sigma_g)^2(1\sigma_u)^2(2\sigma_g)^2(2\sigma_u)^2\ (1\pi_u)^3(3\sigma_g)^2(1\pi_g)^1$	6.2
$B\ ^3\Pi_g$	$(1\sigma_g)^2(1\sigma_u)^2(2\sigma_g)^2(2\sigma_u)^2(1\pi_u)^4(3\sigma_g)^1(1\pi_g)^1$	7.3
$C\ ^3\Pi_u$	$(1\sigma_g)^2(1\sigma_u)^2(2\sigma_g)^2(2\sigma_u)^1(1\pi_u)^4(3\sigma_g)^2(1\pi_g)^1$	11.1
$N_2^{+\cdot}$		
$X\ ^2\Sigma_g^+$	$(1\sigma_g)^2(1\sigma_u)^2(2\sigma_g)^2(2\sigma_u)^2(1\pi_u)^4(3\sigma_g)^1$	15.6 (0)
$A\ ^2\Pi_u$	$(1\sigma_g)^2(1\sigma_u)^2(2\sigma_g)^2(2\sigma_u)^2(1\pi_u)^3(3\sigma_g)^2$	16.7 (1.1)
$B\ ^2\Sigma_u^+$	$(1\sigma_g)^2(1\sigma_u)^2(2\sigma_g)^2(2\sigma_u)^1(1\pi_u)^4(3\sigma_g)^2$	18.8 (3.2)
$D\ ^2\Pi_g$	$(1\sigma_g)^2(1\sigma_u)^2(2\sigma_g)^2(2\sigma_u)^2(1\pi_u)^2(3\sigma_g)^2(1\pi_g)^1$	22.1 (6.5)
$C\ ^2\Sigma_u^+$	$(1\sigma_g)^2(1\sigma_u)^2(2\sigma_g)^2(2\sigma_u)^2(1\pi_u)^3(3\sigma_g)^1(1\pi_g)^1$	23.6 (8.0)

[a] Relative energy is given with respect to the ground state of N_2. Values relative to the ground state of $N_2^{+\cdot}$ are given in brackets.
[b] from reference 78.

With an electron energy of 59 eV, the $N_2^{+\cdot}$ ion population can be up to 60% A $^2\Pi_u$ and about 14% B $^2\Sigma_u^+$ state (the amount of C $^2\Sigma_u^+$ state is almost negligible, <0.2%).[79] The lifetimes of the B and C states are 60 ns and 100 ns respectively,[28,80,81] whereas the time required for the ions to reach the collision chamber ranges from 14 to 27 μs, depending on the accelerating voltage. Ions that are formed initially in the B and C states will therefore undergo spontaneous radiative decay to the ground state before arriving at the collision cell. The A $^2\Pi_u$ state of $N_2^{+\cdot}$ has a lifetime of 8-15 μs, depending on the vibrational level.[82] Therefore, considerable amount of $N_2^{+\cdot}$ A $^2\Pi_u$ may be involved in the collision events. However, $N_2^{+\cdot}$ A $^2\Pi_u \rightarrow$ X $^2\Sigma_g^+$ emissions could not be detected in the absence of target gas. Any signal observed from the $N_2^{+\cdot}$ A $^2\Pi_u$ state in the emission spectrum must therefore have resulted from collisions.

The fraction of $N_2^{+\cdot}$ A $^2\Pi_u$ generated in the ion source increases with electron energy. For example, the fraction of $N_2^{+\cdot}$ in the A $^2\Pi_u$ state increases from 21% at 19 eV electron energy to 43% at 26 eV and 57% at 59 eV.[79] I therefore have compared emission spectra of 8 keV $N_2^{+\cdot}$/He collisions with $N_2^{+\cdot}$ produced at different electron energies (i.e. 45, 90 and 150 eV). From the spectra (Figure 7.1), little difference is observed with respect to the relative peak intensities. The electron energy as well as the distribution of the excited ions generated in the ion source should therefore have no effect on the relative intensities of the peaks in my study.

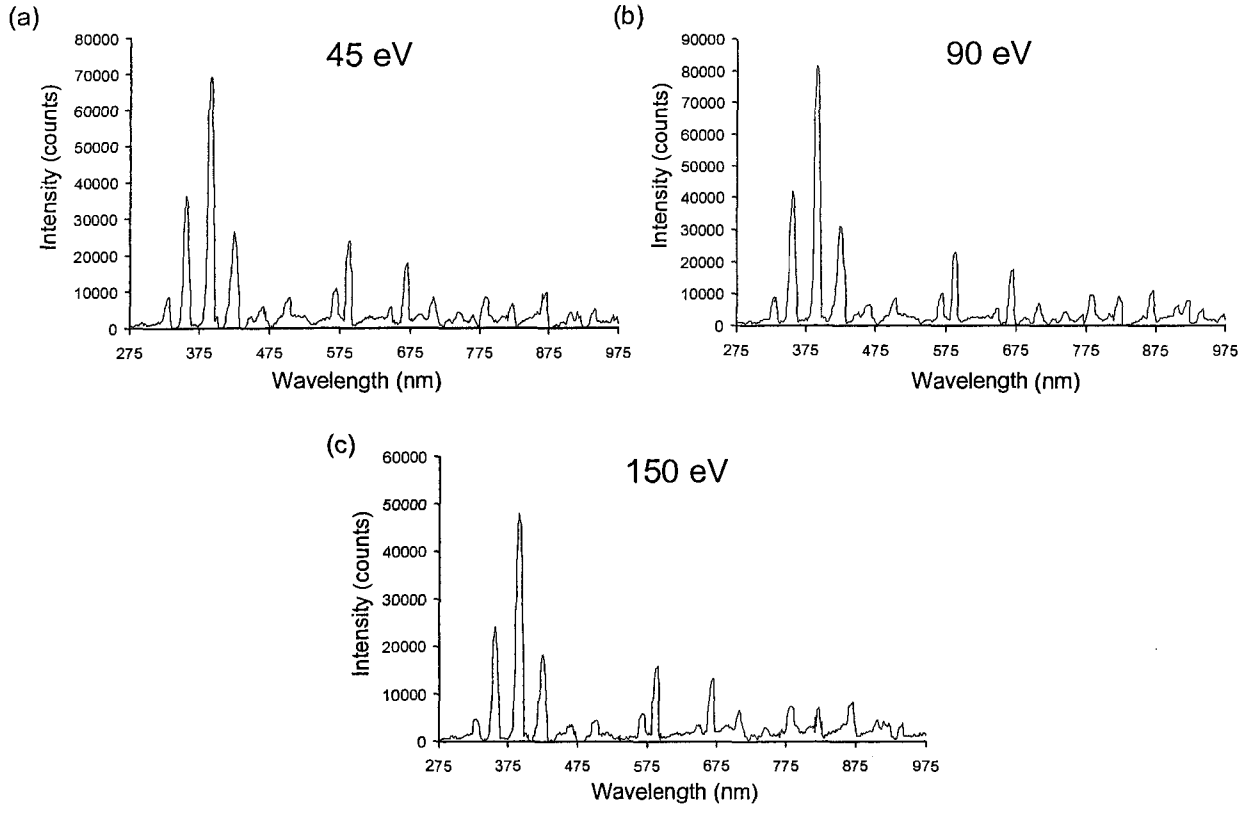

Figure 7.1 CIE spectra of 8 keV $N_2^{+\cdot}$/He collisions when N_2 was ionized with (a) 45 eV, (b) 90 eV and (c) 150 eV electron energy. (Note that the signal collected at each electron energy has not been normalized to the same ion flux.)

7.2 CIE of $N_2^{+\cdot}$/He

Emission spectra over the wavelength range of 190-1020 nm were obtained from $N_2^{+\cdot}$/He collisions at different projectile ion translational energies. The 8 keV $N_2^{+\cdot}$/He spectrum is presented in Figure 7.2 and the others (7 keV to 2 keV) in Figure 7.3. All ion translational energies were obtained by varying the source accelerating voltage, except at 2 keV which was obtained from a 3 keV ion beam with +1 kV voltage applied to the collision cell. The prominent feature at low wavelength is the $\Delta v = +2, +1, 0, -1, -2$ vibrational transition progression in the $N_2^{+\cdot}$ $B\ ^2\Sigma_u^+ \rightarrow X\ ^2\Sigma_g^+$ electronic transition.[78] The $A\ ^2\Pi_u \rightarrow X\ ^2\Sigma_g^+$ electronic transition ($\Delta v = +3, +2, +1$) is also observed but the peaks are weaker due to the longer lifetime of the $A\ ^2\Pi_u$ state. The other peaks arise from the emissions of the excited N^+ and $N^\cdot$ fragments, resulting from the dissociation of $N_2^{+\cdot}$ with higher internal energy. Emissions from the helium target gas are also observed. A summary of the peak and transition assignments is presented in Table 7.2.

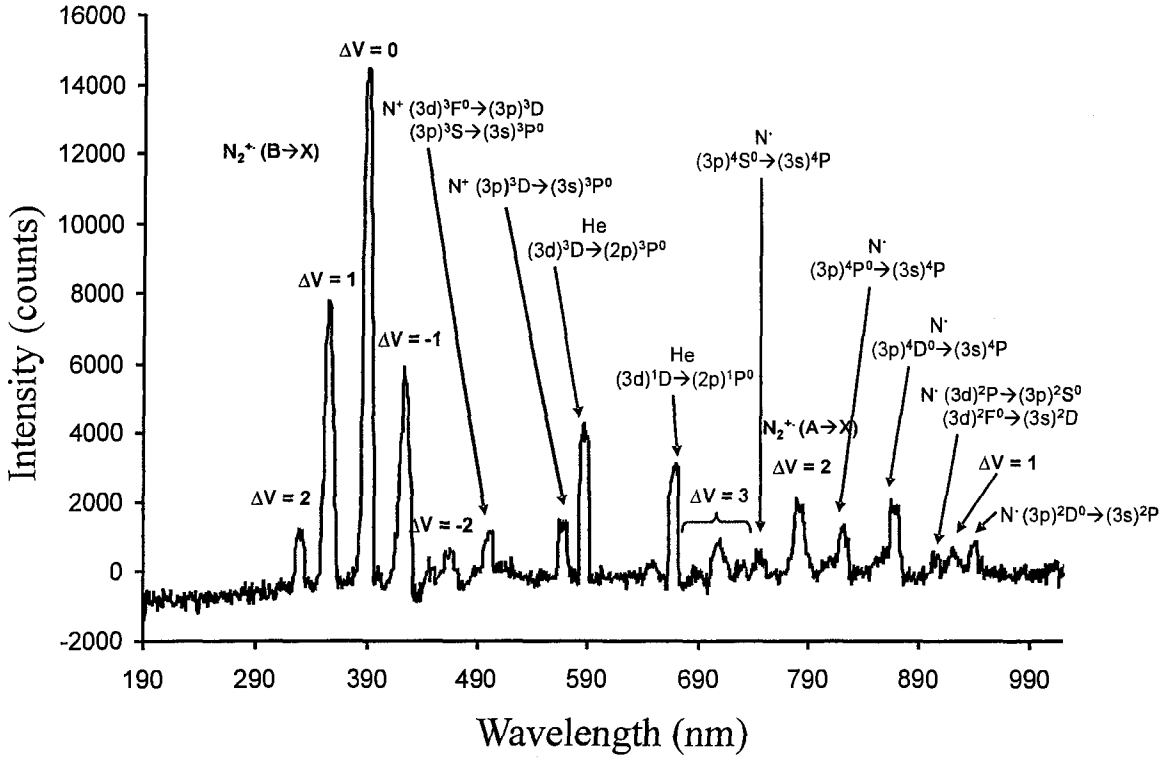

Figure 7.2 CIE spectrum (190-1020 nm) of $N_2^{+\cdot}$/He collisions at 8 keV ion translational energy. Collision gas pressure corresponded to 90% ion beam transmission (accumulation time per section: 30 mins).

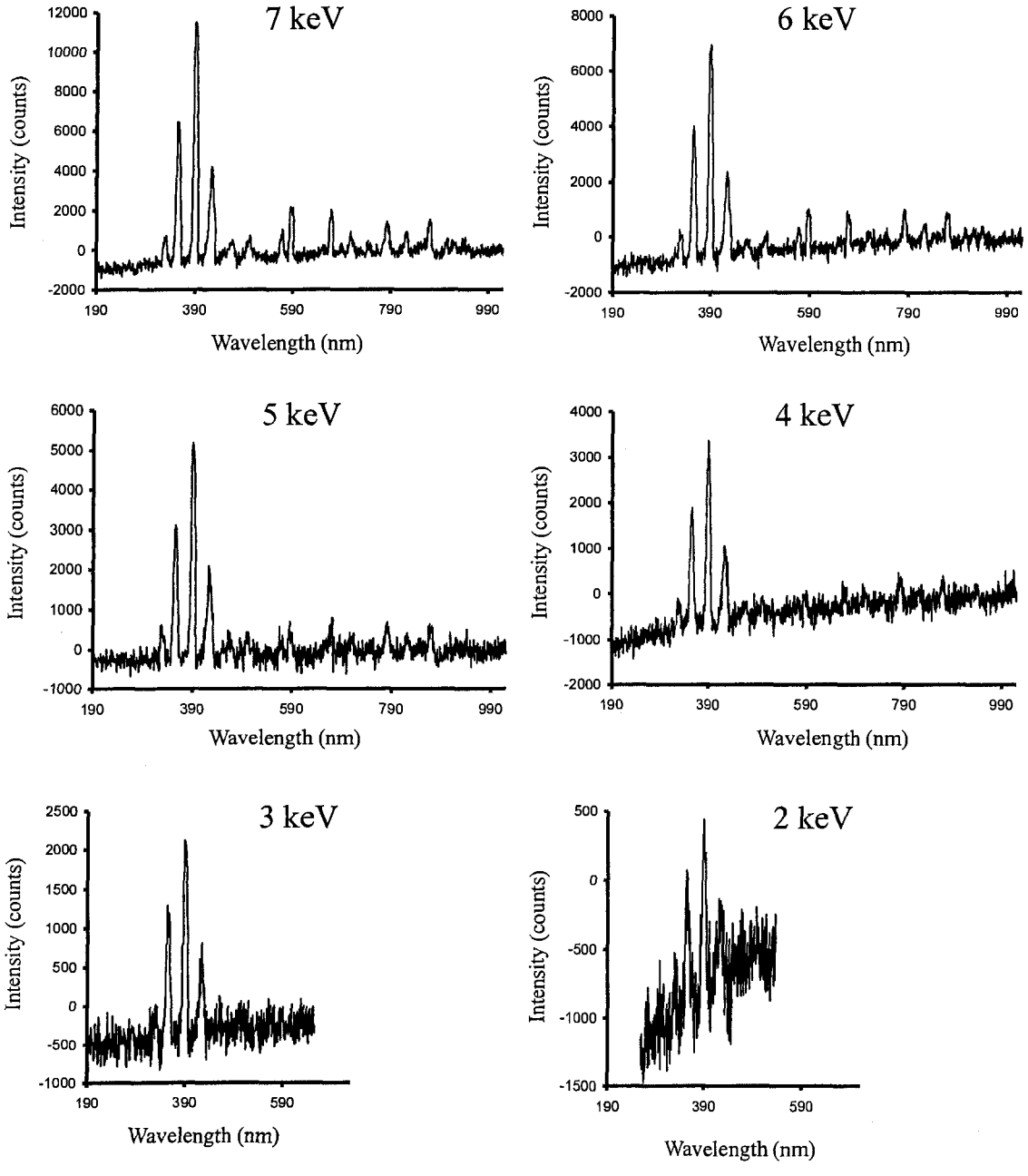

Figure 7.3 CIE spectra (190-1020 nm) of $N_2^{+\cdot}$/He collisions at other projectile ion translational energies (7 keV to 2 keV). Collision gas pressure corresponded to 90% ion beam transmission (accumulation time per section: 30 mins).

Table 7.2 Observed emissions in Figure 7.2 and 7.3 and their corresponding radiative lifetimes.

Transition			v'-v''	τ (ns)[a]	λ (nm)	Ref.
$N_2^{+\cdot}$	$B\ ^2\Sigma_u^+ \rightarrow X\ ^2\Sigma_g^+$	$\Delta v = +2$		~60	331	78,80,81
		+1			356	
		0			390	
		-1			425	
		-2			467	
$N_2^{+\cdot}$	$A\ ^2\Pi_u \rightarrow X\ ^2\Sigma_g^+$	$\Delta v = +3$	3-0	8000-15000	691	78,82
		+3	4-1		710	
		+3	5-2		730	
		+2	2-0		785	
		+1	1-0		922	
N^+	$(3d)\ ^3F^0 \rightarrow (3p)\ ^3D$			8	503	83,84
	$(3p)\ ^3S \rightarrow (3s)\ ^3P^0$			13	503	
	$(3p)\ ^3D \rightarrow (3s)\ ^3P^0$			18	570	
N	$(3p)\ ^4S^0 \rightarrow (3s)\ ^4P$			31	748	83,84
	$(3p)\ ^4P^0 \rightarrow (3s)\ ^4P$			44	822	
	$(3p)\ ^4D^0 \rightarrow (3s)\ ^4P$			52	872	
	$(3d)\ ^2P \rightarrow (3p)\ ^2S^0$			39	906	
	$(3p)\ ^2F^0 \rightarrow (3s)\ ^2D$			37	906	
	$(3p)\ ^2D^0 \rightarrow (3s)\ ^2P$			46	941	
He	$(3d)\ ^3D \rightarrow (2p)\ ^3P^0$			14	590	83,84
	$(3d)\ ^1D \rightarrow (2p)\ ^1P^0$			16	671	

[a] Lifetimes from references.[80-83]

As shown in Figure 7.2 and 7.3, the relative intensities of the spectral peaks appear to be constant with changing ion translational energy. The only difference is the decrease in signal to noise ratio. To better show these observations, the absolute emission intensities of $N_2^{+\cdot}$, N^+ and $N^\cdot$ at various collision energies vs. that at 8 keV is plotted in Figure 7.4a. The plotted values have been normalized to the flux of the 8 keV $N_2^{+\cdot}$ beam to correct for any difference in ion flux between experiments. The $A\ ^2\Pi_u \rightarrow X\ ^2\Sigma_g^+$ peaks are not plotted since they are weak and their assignment remains uncertain. Figure 7.4a clearly shows that the absolute emission intensities decrease with decreasing ion translational energy.

A similar plot is made for the relative intensities (Figure 7.4b). All the points fall along the y = x line, indicating that relative intensities from $N_2^{+\cdot}$, N^+ and $N^\cdot$ do not change with ion translational energy. An expanded view of the N^+ and $N^\cdot$ emission region of Figure 7.4b can be seen in Figure 7.4c. Based on repetitive experiments, the uncertainty to the relative intensities is estimated to be ± 0.04. We can conclude from these results that as the ion translational energy decreases, the population in the excited states also decreases, but the relative population distribution in these states remains constant.

(a)

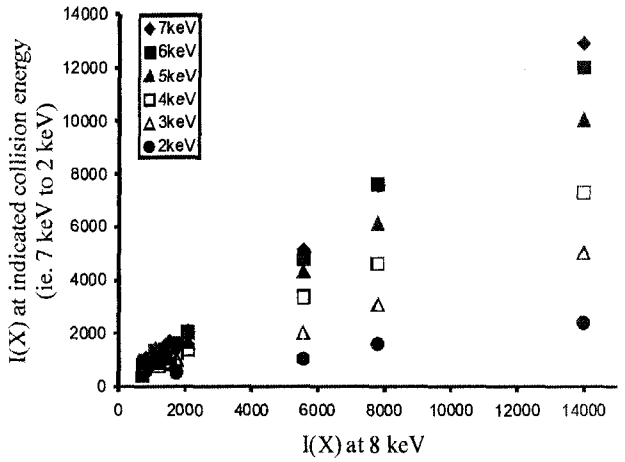

(b)

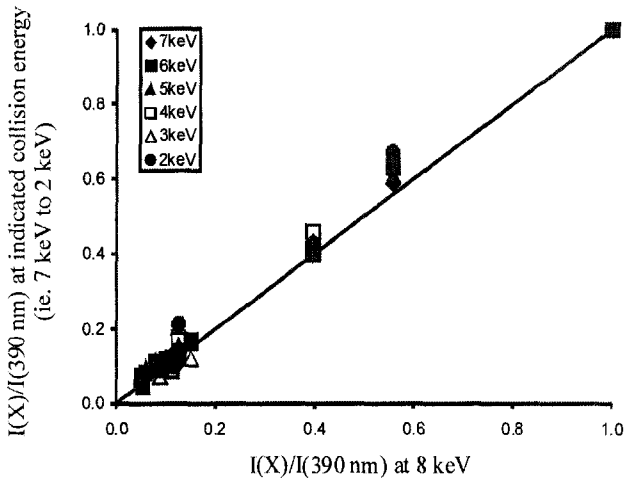

(c)

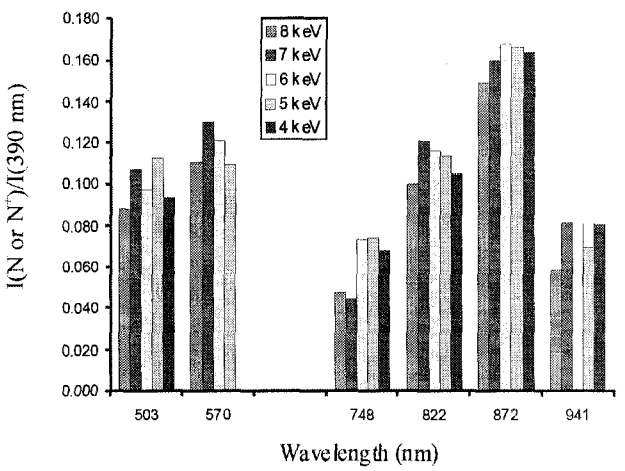

Figure 7.4 Plot of (a) the absolute emission intensities, (b) the relative emission intensities of $N_2^{+\cdot}$, N^+ and $N^\cdot$ at various ion translational energies vs. those at 8 keV. I(X) represents the intensity of $N_2^{+\cdot}$, N^+, and $N^\cdot$ and I(390 nm) the intensity of the B $^2\Sigma_u^+ \rightarrow$ X $^2\Sigma_g^+$ ($\Delta v = 0$) transition of $N_2^{+\cdot}$. Uncertainties, based on replicate measurements, are represented by the size of the symbols in the figures. (c) Relative emission intensities of N^+ and $N^\cdot$ in bar graph format.

A number of possible sources of error have been considered. It is possible that ion scattering could be responsible for the decrease in absolute intensities at lower translational energy. A worst case scenario has the collision occurring at the beginning of the collision cell. The projectile ions need to be scattered by over 20° from the ion beam in order to miss the optical window. Based on the absolute differential cross sections for direct scattering of O^+ by He,[85] even at translational energies as low as 1.5 keV, scattering decreases by three orders of magnitude from 0.24° to 4.67° laboratory angle. Therefore, scattering over 20° is negligible. Similarly, in order for ions to be scattered at a large enough angle so that they cannot exit the collision cell (and thus not be transmitted by the electrostatic analyzer, the scattering angle needs to be over 3.5°. From the differential cross sections of O^+/He collisions, about 98% of the ions would pass through the exit slit even at 1.5 keV ion translational energy. Therefore, it should be valid to use ion flux to normalize the absolute intensity and 10% beam reduction as a reference point for collision conditions at different ion translational energies. As most of the precursor ions are detected, the 10% beam reduction is therefore expected to be mainly due to dissociations.

Another potential major error comes from the lifetimes of the different emitting species. Since an $N_2^{+\cdot}$ ion at 8 keV and 2 keV translational energies takes only 26 ns and 51 ns respectively to fly through the observation region, only a portion of the emission from the excited species may be observed. If we simply take the relative intensities from the CIE spectra, we are assuming the same lifetime for all. The best way is to correct for the relative amounts by calculating the fraction of the total emission that occurs under the

observation window and correcting the peak intensity accordingly based on the lifetime. This way, the relative amount for longer-lived species, for example, would be increased because we have observed a smaller fraction of the total amount from the emitting species and vice versa. However, correcting for the lifetime is not simple because the exact point of collisions is not known. Therefore, two situations were considered for comparison purposes. The first assumes all collisions taking place at the beginning of the collision cell while the other one considers collisions occurring when the ions enter the observation region. The life-time corrected plot for the relative intensities in these two situations are shown in Figure 7.5 a and b, respectively. Figure 7.5b is essentially the same as Figure 7.4b while for Figure 7.5a, it was found that one of the emitting states is affected significantly due to its short lifetime (~ 8 ns for N^+ (3d) $^3F^0 \rightarrow$ (3p) ^3D). However, there is no reason for this one particular excited state species to be preferentially generated at high translational energy indicating that this treatment is indeed an extreme correction for radiative lifetime and that the vast majority of collision events take place under the window. Therefore for $N_2^{+\cdot}$/He collisions, lifetime constraints do not affect the previously stated conclusions. The intensities of the emissions from the target gas cannot be directly compared with those from the projectile ions or fragments since the spatial distribution of collisions across the collision cell is unknown.

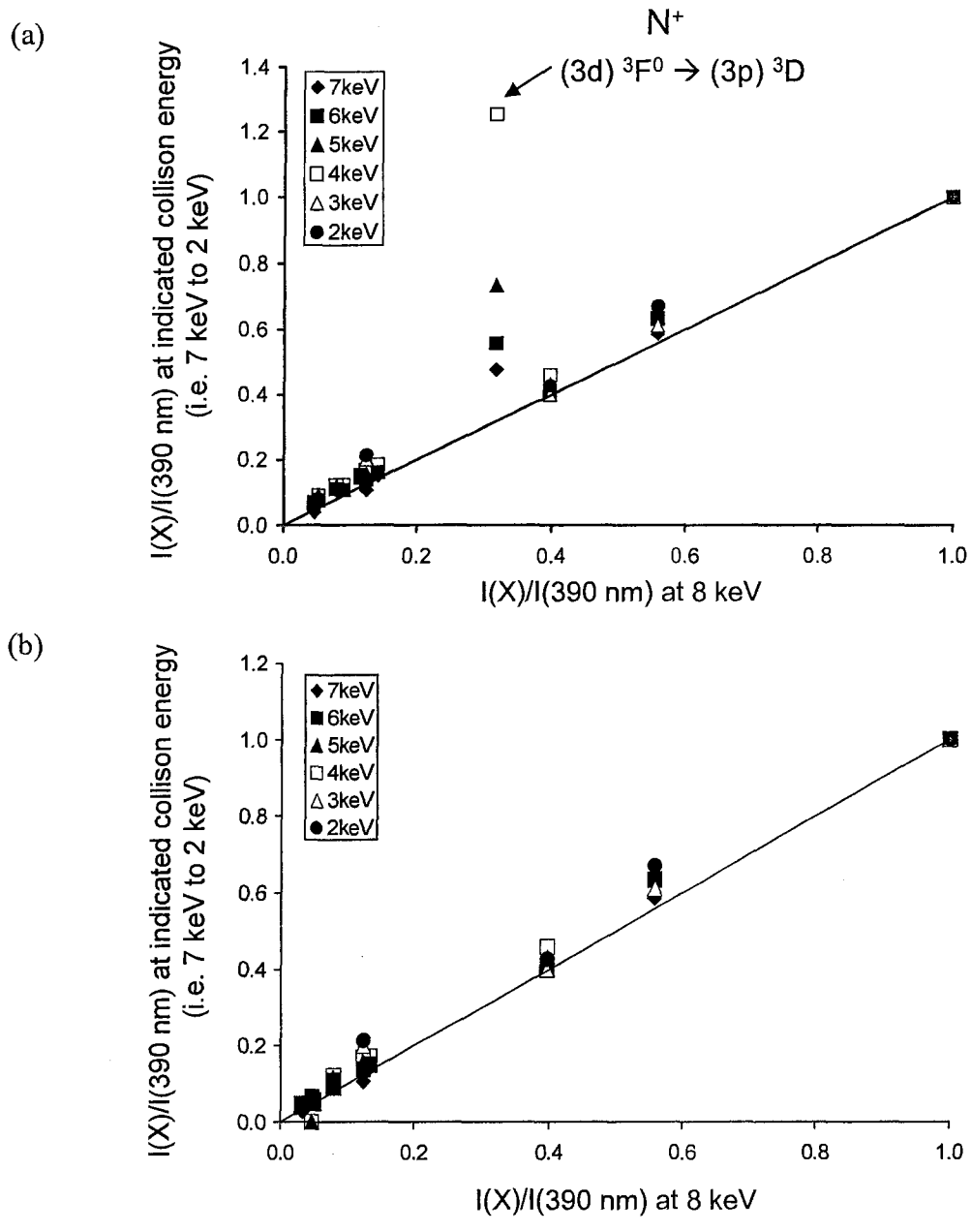

Figure 7.5 Plot of the lifetime-corrected relative emission intensities of $N_2^{+\cdot}$, N^+ and $N^\cdot$ at various ion translational energies vs. those at 8 keV when all collisions were assumed to take place when the ions enter (a) the collision cell and (b) the observation region. I(X) represents the intensity of $N_2^{+\cdot}$, N^+, and $N^\cdot$ and I(390 nm) the intensity of the B $^2\Sigma_u^+ \rightarrow$ X $^2\Sigma_g^+$ ($\Delta v = 0$) transition of $N_2^{+\cdot}$. Uncertainties, based on replicate measurements, are represented by the size of the symbols in the figures.

When the vertical transition model (as described in the introduction) is applied to collision processes, the electronic transitions are assumed to take place simultaneously and in competition with each other, since collisions deposit a range of energy rather than a finite and precise energy as in photon excitation. As a result, we would expect higher excited states to be less populated as collision energy decreases; thus, emissions from the fragments were expected to decrease with decreasing collision energy. However, from my results, this is obviously not the case, and thus a different explanation needs to be invoked. If we apply the curve-crossing model, as ion translational energy (i.e. ion velocity) increases, the Landau-Zener model predicts a higher probability to cross to higher-excited states (Equation 5.8 and 5.9). The intricate succession of non-adiabatic interactions that follows can then lead to a consistent population distribution in the excited states. This would also suggest that when the ion translational energy is changed, the observed emission always comes from excited states arising from the same crossing points. By looking at the relative intensities of the vibrational progression of an emission band, it is often concluded that it resembles the distribution as would be expected from the Frank-Condon factors and therefore, vertical transitions.[54,56,86,87] However, as de Froidmont et al.[88] pointed out, the analogy with photon excitation could be superficial and misleading. In fact, the Franck-Condon picture which is based on the grounds of short excitation time is a cause leading to vertical transitions but is not necessarily limited to only vertical transitions. De Froidmont et al. carried out a theoretical study of the keV collisions of H_3^+ with He.[88] They concluded from their adiabatic potential energy curves that a very complicated sequence of non-adiabatic interactions is involved in

transforming kinetic energy into electronic energy. As a result, they believe that the curve-crossing model is a better picture for collisional excitation.

To conclude this section, my emission results on the $N_2^{+\cdot}$/He collisions agree with the curve-crossing model. That is, when ion translational energy increases, the probability of crossing over to the excited states also increases, which results in more excited-state species (i.e. more emissions), but the relative distribution of these species remain the same.

7.3 CIE of $N_2^{+\cdot}$/Ar

Similar experiments were carried out for keV $N_2^{+\cdot}$/Ar collisions to see if any difference appears when a heavier target gas such as argon is used in the collisions. As the emission intensities from $N_2^{+\cdot}$ are considerably lower for $N_2^{+\cdot}$/Ar collisions than for $N_2^{+\cdot}$/He collisions, increase of the accumulation time is necessary to obtain a good CIE spectrum. Emission intensity increases in a linear fashion with accumulation time. The emission spectra at 8 keV and at other projectile ion translational energies (i.e. from 6 keV to 2 keV) are presented in Figure 7.6 and 7.7, respectively. A summary of the peak and transition assignments is tabulated in Table 7.3.

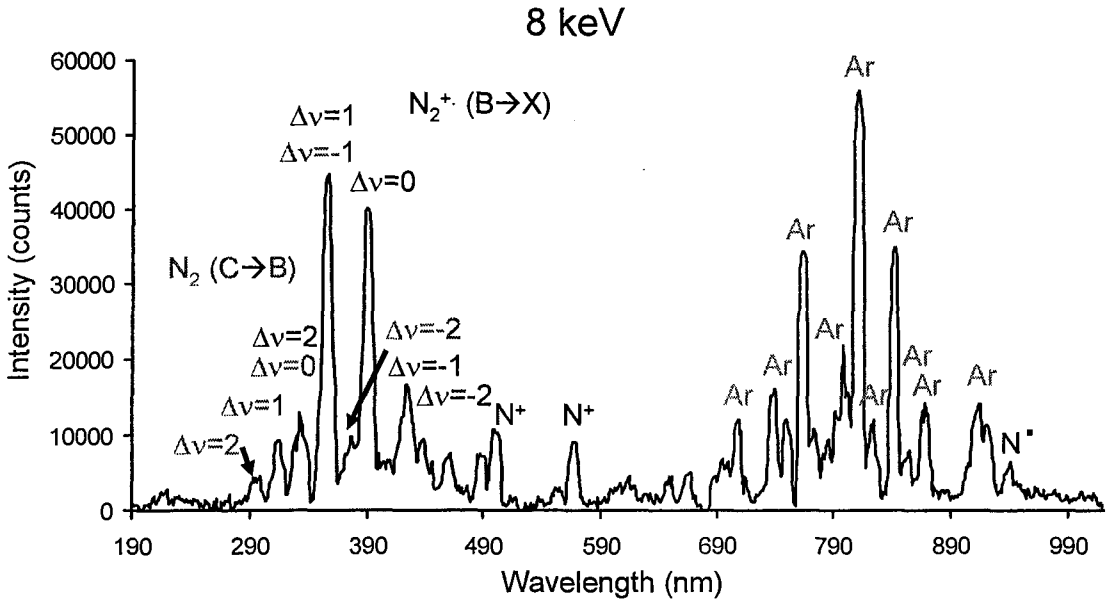

Figure 7.6 CIE spectrum (190-1020 nm) of $N_2^{+\cdot}$/Ar collisions at 8 keV ion translational energy. Collision gas pressure corresponded to 90% ion beam transmission (accumulation time per section: 2 hours).

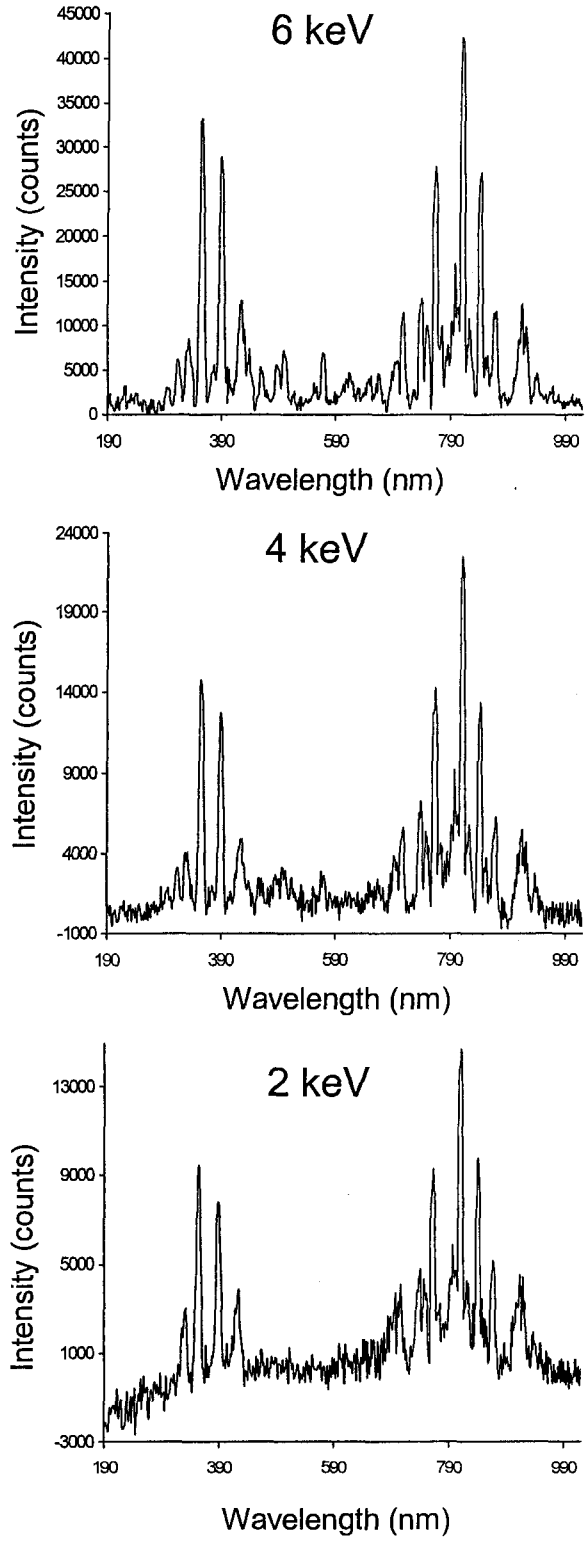

Figure 7.7 CIE spectra (190-1020 nm) of $N_2^{+\cdot}$/Ar collisions at 6 keV, 4 keV and 2 keV ion translational energies. Collision gas pressure corresponded to 90% ion beam transmission (accumulation time per section: 2 hours).

Table 7.3 Observed emissions in Figure 7.6 and 7.7 and their corresponding radiative lifetimes.

Transition			τ (ns)[a]	λ (nm)	Ref.
$N_2^{+\cdot}$	$B\ ^2\Sigma_u^+ \rightarrow X\ ^2\Sigma_g^+$	$\Delta v = +2$	~ 60	332	78,80,81
		+1		356	
		0		390	
		-1		424	
		-2		465	
N_2	$C\ ^3\Pi_u \rightarrow B\ ^3\Pi_g$	$\Delta v = +2$	~ 39	296	78,89
		+1		314	
		0		333	
		-1		352	
		-2		376	
N^+	$(3d)\ ^3F^0 \rightarrow (3p)\ ^3D$		8	503	83,84
	$(3p)\ ^3S \rightarrow (3s)\ ^3P^0$		13	503	
	$(3p)\ ^3D \rightarrow (3s)\ ^3P^0$		18	570	
N	$(3p)\ ^2D^0 \rightarrow (3s)\ ^2P$		46	941	83,84
Ar	$(4p')\left[\frac{1}{2}\right]_1 \rightarrow (4s)\left[\frac{3}{2}\right]_2$		149	697	83,84,90
	$(4p')\left[\frac{3}{2}\right]_2 \rightarrow (4s)\left[\frac{3}{2}\right]_2$		253	707	
	$(4p')\left[\frac{3}{2}\right]_2 \rightarrow (4s)\left[\frac{3}{2}\right]_1$			738	
	$(4p)\left[\frac{1}{2}\right]_0 \rightarrow (4s)\left[\frac{3}{2}\right]_1$		21	752	
	$(4p)\left[\frac{3}{2}\right]_2 \rightarrow (4s)\left[\frac{3}{2}\right]_2$		36	764	
	$(4p)\left[\frac{3}{2}\right]_1 \rightarrow (4s)\left[\frac{3}{2}\right]_2$			773	
	$(4p)\left[\frac{5}{2}\right]_2 \rightarrow (4s)\left[\frac{3}{2}\right]_2$		108	802	

Ar	$(4p)\left[\frac{5}{2}\right]_3 \rightarrow (4s)\left[\frac{3}{2}\right]_2$	30	812
	$(4p')\left[\frac{1}{2}\right]_1 \rightarrow (4s')\left[\frac{1}{2}\right]_1$		826
	$(4p)\left[\frac{5}{2}\right]_2 \rightarrow (4s)\left[\frac{3}{2}\right]_1$		843
	$(4p')\left[\frac{3}{2}\right]_1 \rightarrow (4s')\left[\frac{1}{2}\right]_1$		853
	$(4p)\left[\frac{3}{2}\right]_1 \rightarrow (4s')\left[\frac{1}{2}\right]_0$		868
	$(4p)\left[\frac{1}{2}\right]_1 \rightarrow (4s)\left[\frac{3}{2}\right]_2$	53	913
	$(4p)\left[\frac{3}{2}\right]_1 \rightarrow (4s')\left[\frac{1}{2}\right]_1$		922

[a] Lifetimes from references.[80,81,83,89]

Similar to $N_2^{+\cdot}$/He collisions, the prominent feature is also the $\Delta v = +2, +1, 0, -1, -2$ vibrational transition progression of the $N_2^{+\cdot}$ $B\ ^2\Sigma_u^+ \rightarrow X\ ^2\Sigma_g^+$ electronic transition. In addition, a vibrational transition progression in the N_2 $C\ ^3\Pi_u \rightarrow B\ ^3\Pi_g$ electronic transition was also observed. Previously, when He was used as the target gas, the charge transfer process was unlikely because of the high ionization energy of He. A conversion of 9.01 eV from translational to internal energy is required for electron transfer to occur.

$$N_2^{+\cdot} + He \rightarrow N_2 + He^+ \qquad \Delta E = 9.01 \text{ eV} \qquad (7.1)$$

To produce $N_2(C)$ from charge transfer, 20.1 eV must be converted from translational to internal energy. In comparison, the charge transfer process with Ar is much more favourable. Only 0.18 eV is needed to produce $N_2(X)$ and 11.3 eV to produce $N_2(C)$.

$$N_2^{+\cdot}(X) + Ar \rightarrow N_2(X) + Ar^+ \qquad \Delta E = 0.18 \text{ eV} \qquad (7.2)$$

$$N_2^{+\cdot}(X) + Ar \rightarrow N_2(C) + Ar^+ \qquad \Delta E = 11.3 \text{ eV} \qquad (7.3)$$

The electron configurations of the electronic states of N_2 and $N_2^{+\cdot}$ suggest that the N_2 C $^3\Pi_u$ state is produced via either N_2 B $^3\Pi_g$ or $N_2^{+\cdot}$ B $^2\Sigma_u^+$, depending on whether the electron transfer takes place before or after electronic excitation (Figure 7.8).

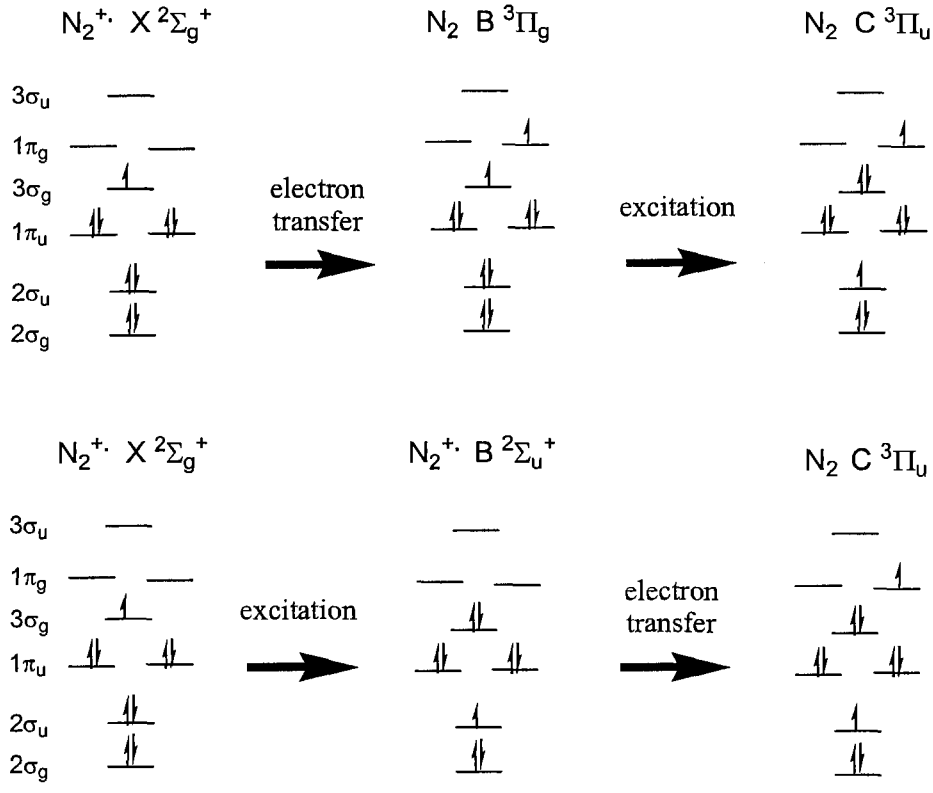

Figure 7.8 Electronic configuration of the electronic states suggests that the N_2 C $^3\Pi_u$ state is produced via either N_2 B $^3\Pi_g$ or $N_2^{+\cdot}$ B $^2\Sigma_u^+$.

The relative intensities of the $N_2^{+\cdot}$ B $^2\Sigma_u^+ \rightarrow$ X $^2\Sigma_g^+$ transitions in Figure 7.6 and 7.7 may appear to be different from what was observed from the $N_2^{+\cdot}$/He collisions[91] as the $\Delta v = 1$ peak is now the most dominant peak in the vibrational progression. This is believed to have resulted from the overlap of the N_2 and $N_2^{+\cdot}$ emissions as some of their wavelengths are very close. A higher-resolution spectrum with the entrance slit width reduced to 1.0 mm was obtained at this wavelength region, in an attempt to separate them (Figure 7.9). At this slit width, spectral resolution is increased to 3.2 nm. The $\Delta v = 0$ (at 330 nm) of N_2 C $^3\Pi_u \rightarrow$ B $^3\Pi_g$ and the $\Delta v = 2$ (at 335 nm) of N_2^+ B $^2\Sigma_u^+ \rightarrow$ X $^2\Sigma_g^+$ are obviously separated but the peak at 355 nm is not. However, the peak intensity of the $\Delta v = 1$ vibrational transition of the $N_2^{+\cdot}$ B $^2\Sigma_u^+ \rightarrow$ X $^2\Sigma_g^+$ electronic transition is now lower than $\Delta v = 0$. This now better resembles the $N_2^{+\cdot}$/He spectrum and may indicate that the two peaks are on the verge of separation.

At 2 keV ion translational energy, N_2 C $^3\Pi_u \rightarrow$ B $^3\Pi_g$ emissions were not observed. Kelly et al. studied emissions (310-435 nm) from $N_2^{+\cdot}$/Ar collisions with $N_2^{+\cdot}$ translational energy ranges from 100 eV to 1 keV.[58] Within this energy range, no N_2 C $^3\Pi_u \rightarrow$ B $^3\Pi_g$ was observed. This indicates that at low translational energy, the probability of forming N_2 C $^2\Pi_u$ is small, precluding our observation of the weak $\Delta v = 2$, 1 bands at 2 keV.

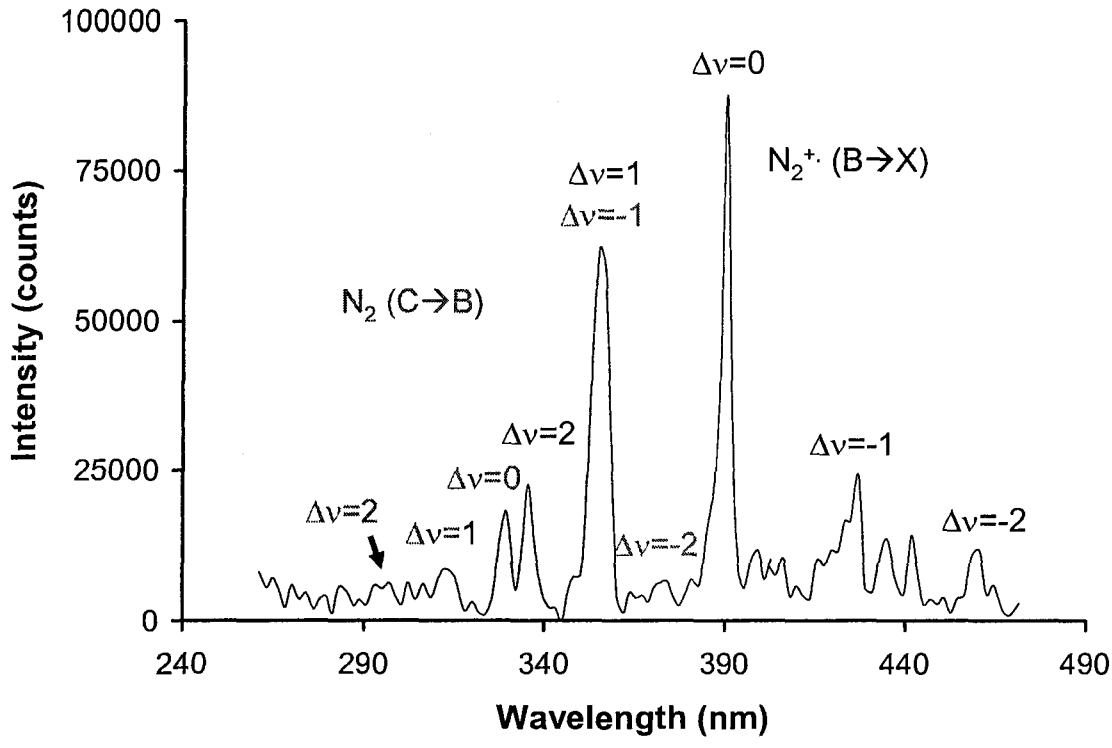

Figure 7.9 CIE spectrum (260 to 470 nm) of 8 keV $N_2^{+\cdot}$/Ar collisions obtained with an entrance slit width of 1.0 mm (accumulation time per section: 10 hours). The expected position of the $\Delta v = 2$ and $\Delta v = -2$ bands of the N_2 C $^3\Pi_u \rightarrow$ B $^3\Pi_g$ transition are labelled.

The emissions from the excited N^+ fragments resulting from the dissociation of $N_2^{+\cdot}$ can also be observed but those from the excited $N^\cdot$ are not obvious. This is because of the presence of many intense peaks from Ar in the high wavelength region. The only unambiguous $N^\cdot$ peak (i.e. free from Ar interference) is the (3p) $^2D^0 \rightarrow$ (3s) ^2P transition observed at 941 nm.

As shown in Figure 7.6 and 7.7, the relative intensities of the spectral peaks appear to be constant with changing ion translational energy. The only difference is the decrease in signal to noise ratio with decreasing ion translational energy. Similar to the

$N_2^{+\cdot}$/He collisions, the relative intensities of the spectral peaks are also compared. Due to the spectral congestion of the strong Ar emissions, some of the weaker emission peaks from the N· fragments are overlapped by the Ar atomic lines. Only those that are clearly uninterfered can therefore be selected for the comparison. The relative intensity of $N_2^{+\cdot}$, N^+ and N· at various collision energies vs. that at 8 keV is plotted in Figure 7.10a. Like $N_2^{+\cdot}$/He collisions, they also appear to be constant. All the points fall along the y = x line, indicating that the relative intensities from $N_2^{+\cdot}$, N^+ and N· do not change with ion translational energy.

The relative intensity has also been corrected for the difference in lifetime. Figure 7.10b presents the plot when all collisions were assumed to take place at the beginning of the collision cell as the worst case scenario. One of the emitting states is affected significantly due to its short lifetime (~ 8 ns for N^+ (3d) $^3F^0 \rightarrow$ (3p) ^3D). As for $N_2^{+\cdot}$/He collisions, this indicates that this treatment is an extreme correction for radiative lifetime and that the vast majority of collision events take place under the window. It can therefore be concluded that as ion translational energy decreases from 8 keV to 2 keV, the relative intensity of the peaks from the $N_2^{+\cdot}$/Ar collisions do not change, which agrees once again with the curve-crossing model.

(a)

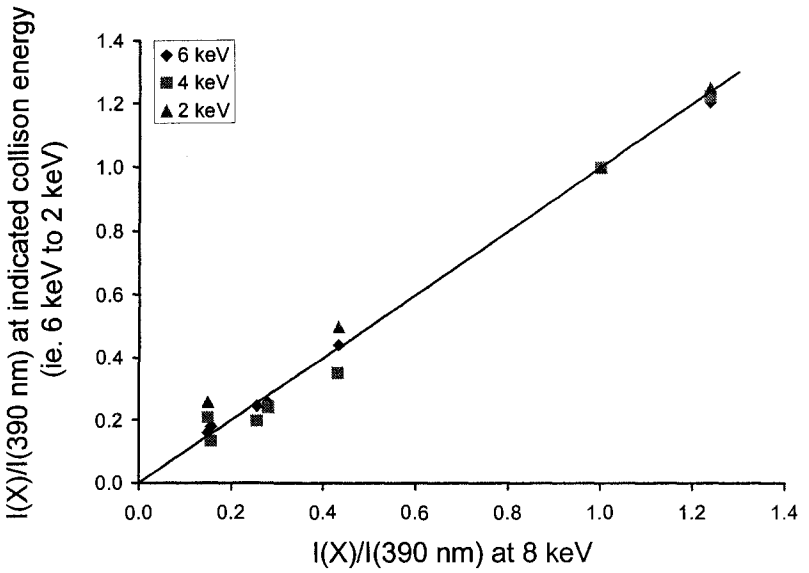

(b)

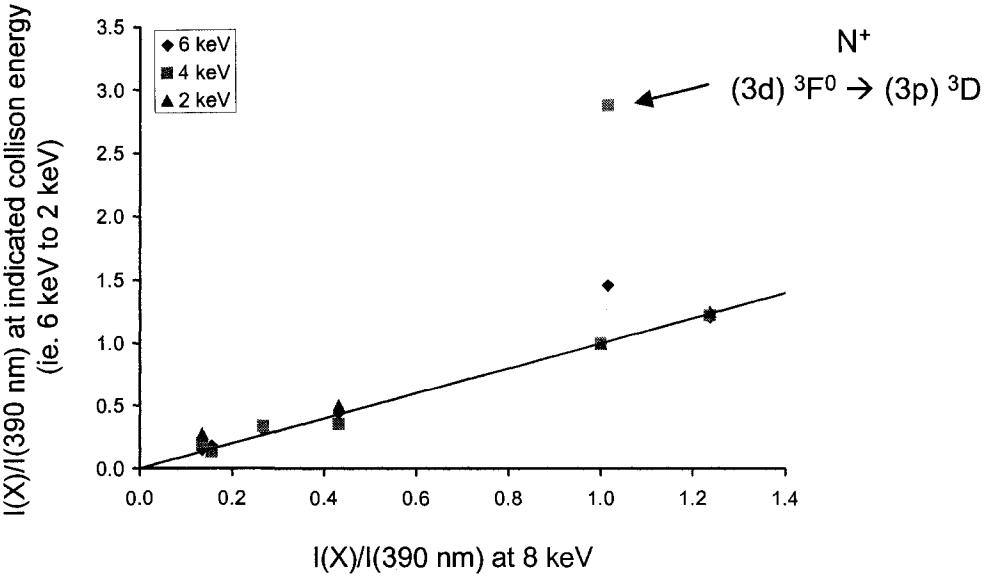

Figure 7.10 (a) Plot of the relative emission intensities of $N_2^{+\cdot}$, N^+ and $N^\cdot$ at various ion translational energies vs. those at 8 keV. (b) Lifetime-corrected relative intensity plot assuming all collisions take place when the ions enter the collision cell. I(X) represents the intensity of $N_2^{+\cdot}$, N^+, and $N^\cdot$ and I(390 nm) the intensity of the B $^2\Sigma_u^+ \rightarrow$ X $^2\Sigma_g^+$ (Δv = 0) transition of $N_2^{+\cdot}$.

7.4 Comparison of $N_2^{+\cdot}$/He and $N_2^{+\cdot}$/Ar Collisions

The $N_2^{+\cdot}$ B $^2\Sigma_u^+$ → X $^2\Sigma_g^+$ emission intensities of keV $N_2^{+\cdot}$/He and $N_2^{+\cdot}$/Ar collisions at 90% beam transmission were compared on the same day. Table 7.4 tabulates the photon counts of the peak at 356 nm ($\Delta v = +1$) and 390 nm ($\Delta v = 0$) arising from both collisions. Emissions were collected with an accumulation time of 30 minutes and 1 hour. It is clear that $N_2^{+\cdot}$/He collisions result in emission intensities that are about four times stronger (based on $\Delta v = 0$) . The difference could not have been caused by ion scattering. Even though a stronger scattering effect would be expected with argon, comparison of scattering cross sections of O· by He and Ar shows that 99% and 98%, respectively would have exited the collision cell.[92] This difference is too small to have any significant impact on the emission intensities. The charge-transfer process can reduce the amount of $N_2^{+\cdot}$ B $^2\Sigma_u^+$ state being formed. In order for the signal to decrease by 2-4 times, 50-75% of the $N_2^{+\cdot}$ ion beam needs to be neutralized upon collisions. A careful neutralization-reionization study of $N_2^{+\cdot}$ finds that the charge transfer efficiency between $N_2^{+\cdot}$ and Ar is only about 5%.[93]

Table 7.4 Emission intensity (in photon counts) of the $\Delta v = +1$ (356 nm) and $\Delta v = 0$ (390 nm) transitions of $N_2^{+\cdot}$ B $^2\Sigma_u^+$ → X $^2\Sigma_g^+$ from 8 keV $N_2^{+\cdot}$/He and $N_2^{+\cdot}$/Ar collisions.

Accumulation Time	$N_2^{+\cdot}$/He		$N_2^{+\cdot}$/Ar	
	I(356 nm)	I(390 nm)	I(356 nm)	I(390 nm)
30 mins	391	721	173	165
1 hour	698	1247	384	364

Figure 7.11 presents the adiabatic potential energy curves of the $N_2^{+\cdot}$-He and $N_2^{+\cdot}$-Ar collision complex at different β values calculated at the CISD/6-311+G(2df) level of theory. As the excited states of He and Ar are higher in energy than those of $N_2^{+\cdot}$, the lowest excited states of the collision complex are composed of the interaction of the ground state of He or Ar with various electronic states of $N_2^{+\cdot}$. A small dip (~0.2 eV) is observed in the $N_2^{+\cdot}$-Ar potential energy curves at around 2.1 Å. This indicates a slightly stronger interaction between Ar and $N_2^{+\cdot}$ and is in agreement with other computational and spectroscopic studies of the $N_2^{+\cdot}$-He and $N_2^{+\cdot}$-Ne complexes.[94]

In all cases, the $N_2^{+\cdot}$ $X\ ^2\Sigma_g^+$ state crosses with only the $C\ ^2\Sigma_u^+$ state, not $A\ ^2\Pi_u$ or $B\ ^2\Sigma_u^+$ state. Therefore, excitation to the $B\ ^2\Sigma_u^+$ state will normally require curve-crossing first to $C\ ^2\Sigma_u^+$ state and then from $C\ ^2\Sigma_u^+$ state to either $A\ ^2\Pi_u$ or $B\ ^2\Sigma_u^+$ state. This result would agree with translational energy loss experiments in which the $C\ ^2\Sigma_u^+$ state was identified as the most important transitions involved in the production of N^+.[28,36]

(a)

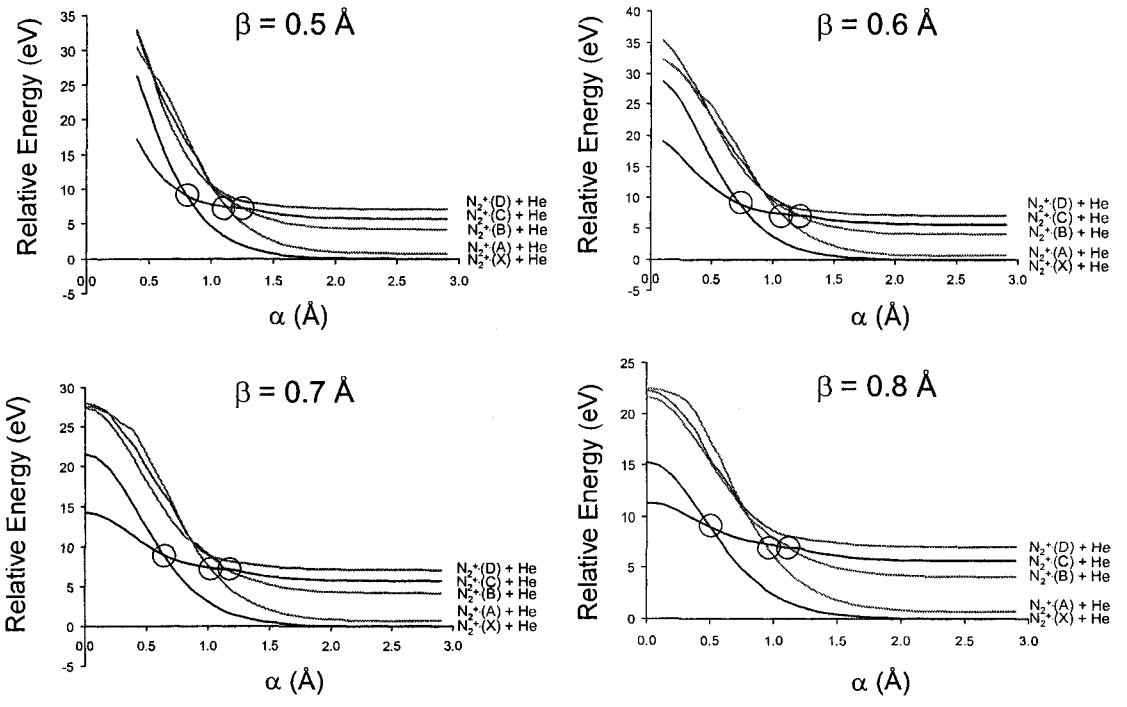

(b)

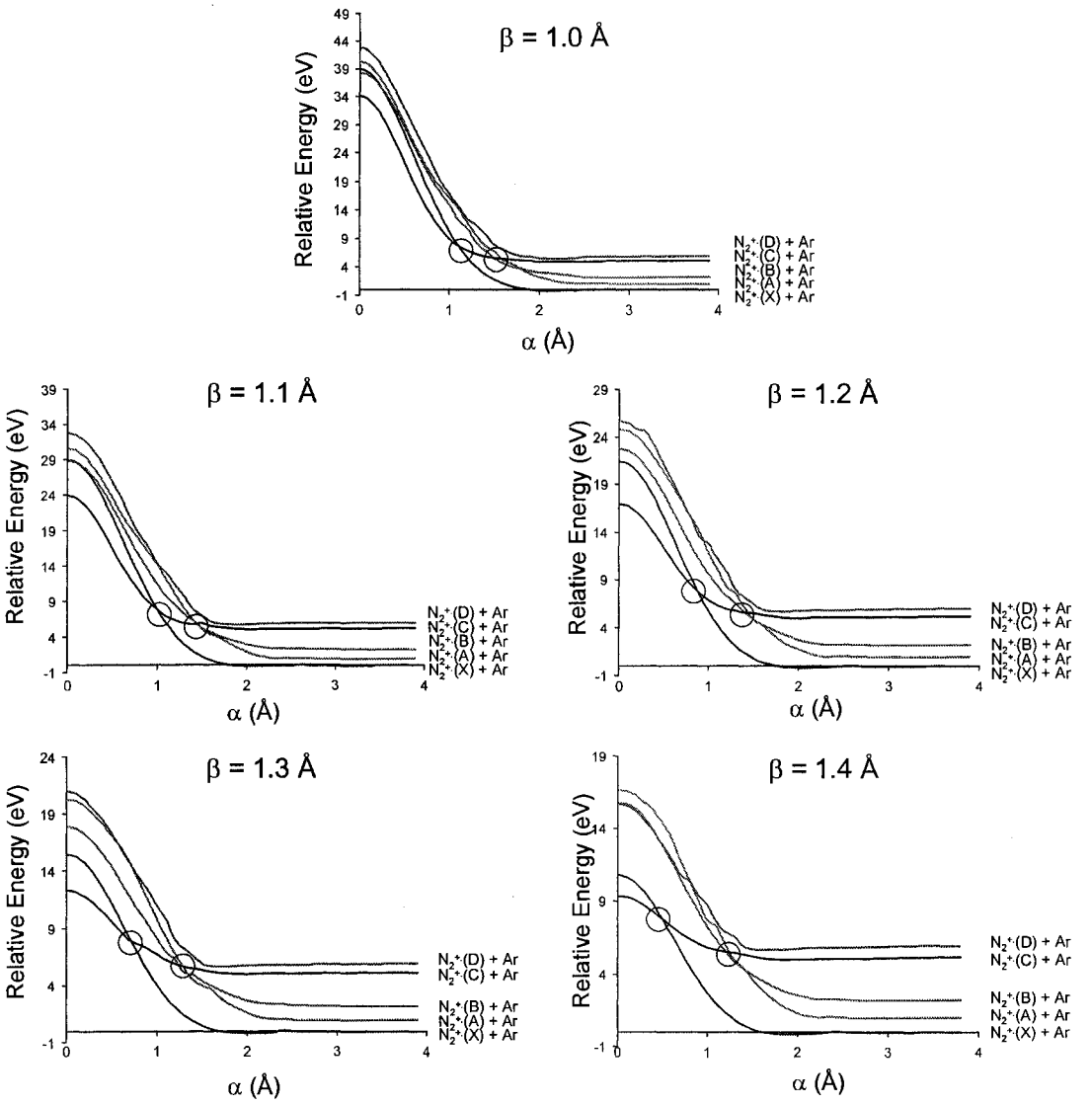

Figure 7.11 Adiabatic potential energy curves of the (a) $N_2^{+\cdot}$-He and (b) $N_2^{+\cdot}$-Ar collision complex at different β values calculated at the CISD/6-311+G(2df) level of theory. The location of the crossing points is circled.

Due to nuclear and electronic interaction, a lower β (i.e. smaller impact parameter) leads to crossing at a larger collision distance (i.e. α). As a result, the distance between the ion and the target and the potential energy at the crossing point is almost constant with respect to β. According to the Landau-Zener model, the probability (P) of crossing over to another electronic state is reflected in terms of the slope (dV/dr) difference at the crossing point and the ion velocity (v).

$$P = e^{-2\delta} \quad \text{where} \quad \delta = \frac{(2\pi)^{3/2} U^2(R)}{\left(\left|\frac{dV_i}{dr} - \frac{dV_f}{dr}\right|\right) h\mathrm{v}} \qquad (7.4)$$

Larger differences in slopes represent higher probability of crossing-over. A comparison was therefore made to the slope differences at different β parameters for both collision systems (Table 7.5).

Table 7.5 Slope difference at the crossing points of the potential energy curves calculated at the CISD/6-311+G(2df) level of theory.

	Slope difference at crossing point		
β (Å)	X→C	C→A	C→B
$N_2^{+\cdot}$/He			
0.5	20	19	7
0.6	17	21	8
0.7	15	17	6
0.8	18	15	6
Average	18	18	6
$N_2^{+\cdot}$/Ar			
1.0	10	10	8
1.1	9	10	6
1.2	9	9	6
1.3	9	8	5
1.4	6	8	6
Average	9	9	6

The slope differences at the X-C crossing point are larger for $N_2^{+\cdot}$/He than for $N_2^{+\cdot}$/Ar whereas those at the C-B crossing point are similar in both cases. Based on this picture, the formation of ions in the B $^2\Sigma_u^+$ state is more probable in $N_2^{+\cdot}$/He collisions because more ions first cross over to the C $^2\Sigma_u^+$ state upon collisions with He target and subsequently, to the B $^2\Sigma_u^+$ state.

From the relative intensities between the fragments and $N_2^{+\cdot}$, the ratio of the emissions from the fragments to the $N_2^{+\cdot}$ B $^2\Sigma_u^+ \rightarrow$ X $^2\Sigma_g^+$ emissions is higher for $N_2^{+\cdot}$/Ar collisions than for $N_2^{+\cdot}$/He collisions. This agrees with conclusions from Martinez and Fuentes who measured higher dissociation cross sections for $N_2^{+\cdot}$/Ar collisions.[36,95]

7.5 CIE of $N_2^{+\cdot}/O_2$

Emission spectra of 8 keV $N_2^{+\cdot}/O_2$ collisions was also obtained. In the two previous sections, we have looked at $N_2^{+\cdot}$ ions colliding with He and Ar. The charge-transfer process is highly unfavourable in the first case as helium possesses a very high ionization energy (IE = 24.59 eV). Argon, on the other hand, has a much lower ionization energy (IE = 15.76 eV) and N_2 C $^3\Pi_u \rightarrow$ B $^3\Pi_g$ emissions resulting from charge-transfer process were indeed observed. Oxygen has an even lower ionization energy (IE = 12.07 eV) and therefore, charge-transfer processes are expected to be favoured considerably, resulting in $O_2^{+\cdot}$ and N_2.

$$N_2^{+\cdot} + O_2 \rightarrow N_2 + O_2^{+\cdot} \quad \Delta E = -3.51 \text{ eV} \qquad (7.5)$$

$$N_2^{+\cdot} + O_2 \rightarrow N_2 + O_2^{+\cdot}(b) \quad \Delta E = 2.67 \text{ eV} \qquad (7.6)$$

The 8 keV $N_2^{+\cdot}/O_2$ spectrum is presented in Figure 7.12. The prominent feature of the $N_2^{+\cdot}$ B $^2\Sigma_u^+ \rightarrow$ X $^2\Sigma_g^+$ emissions in the previous collision systems of study no longer dominates the spectrum. The difference is even more drastic when taking into account the difference in their radiative lifetimes (60 ns for $N_2^{+\cdot}$ B $^2\Sigma_u^+ \rightarrow$ X $^2\Sigma_g^+$ and 1100 ns for $O_2^{+\cdot}$ b $^4\Sigma_g^- \rightarrow$ a $^4\Pi_u$). This is largely due to the competition of the charge-transfer process (which is now less endothermic than the direct excitation of $N_2^{+\cdot}$), resulting in the formation of $O_2^{+\cdot}$ and the $O_2^{+\cdot}$ b $^4\Sigma_g^- \rightarrow$ a $^4\Pi_u$ emission. The other peaks arise from the emissions of the excited fragments ($N^\cdot$ and $O^\cdot$), resulting from the dissociation of $N_2^{+\cdot}$ or $O_2^{+\cdot}$ of higher internal energy. A summary of the peak and transition assignments is tabulated in Table 7.6. Figure 7.13 shows the electron configuration of the X $^3\Sigma_g^-$ state of O_2 and the b $^4\Sigma_g^-$ state of $O_2^{+\cdot}$.

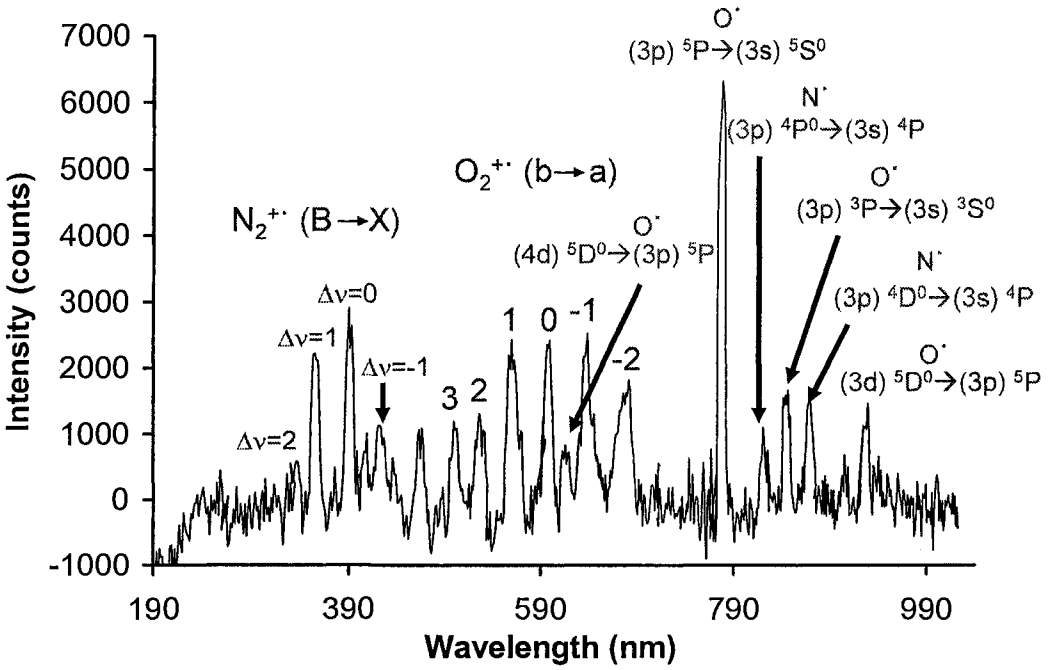

Figure 7.12 CIE spectra (190-1020 nm) of $N_2^{+\cdot}/O_2$ collisions at 8 keV ion translational energy. Collision gas pressure corresponded to 90% ion beam transmission (accumulation time per section: 30 mins).

Table 7.6 Observed emissions in Figure 7.2 and 7.3 and their corresponding radiative lifetimes.

Transition			τ (ns)[a]	λ (nm)	Ref.
$N_2^{+\cdot}$	B $^2\Sigma_u^+ \rightarrow$ X $^2\Sigma_g^+$	Δν = +2	~60	334	78,80,81
		+1		356	
		0		390	
		-1		424	
		-2		467	
$O_2^{+\cdot}$	b $^4\Sigma_g^- \rightarrow$ a $^4\Pi_u$	Δν = +3	~1100	500	96,97
		+2		528	
		1		561	
		0		598	
		-1		639	
		-2		680	
N	(3p) $^4P^0 \rightarrow$ (3s) ^4P		44	821	83,84
	(3p) $^4D^0 \rightarrow$ (3s) ^4P		52	870	
O	(4d) $^5D^0 \rightarrow$ (3p) ^5P			616	83,84
	(3p) $^5P \rightarrow$ (3s) $^5S^0$		27	779	
	(3p) $^3P \rightarrow$ (3s) $^3S^0$		31	843	
	(3d) $^5D^0 \rightarrow$ (3p) ^5P		22	928	

[a] Lifetimes from references.[80-83,97]

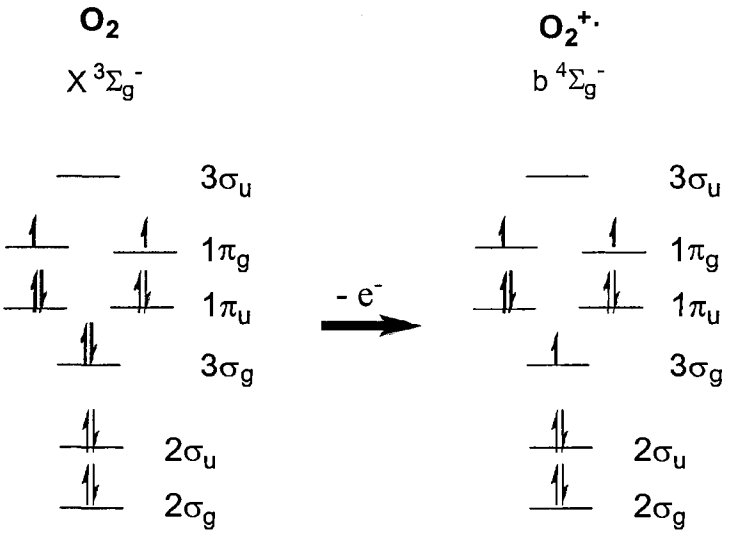

Figure 7.13 Electronic configuration of the X $^3\Sigma_g^-$ state of O_2 and the b $^4\Sigma_g^-$ of $O_2^{+\cdot}$.

7.6 The $CO_2^{+\cdot}$ Ion Beam

The $CO_2^{+\cdot}$ ion beam was generated by electron ionization (EI) on CO_2 using 80-90 eV electrons. Such electron energy could produce some $CO_2^{+\cdot}$ in the excited electronic states. However, the radiative lifetimes of the A $^2\Pi_u$ and B $^2\Sigma_u^+$ states of $CO_2^{+\cdot}$ are 116 and 145 ns, respectively.[98,99] When compared to the time required for the ions to reach the collision chamber which ranges from 17 to 34 μs, depending on the accelerating voltage, virtually all ions that are formed initially in the A or B state would have returned to the ground state by the time it collides with the target gas. The valence electron configuration and the relative energy of these electronic states are tabulated in Table 7.7.

Table 7.7 The valence electron configuration and the relative energy of several electronic states of $CO_2^{+\cdot}$.

Electronic States	Valence Electron Configuration	Relative Energy[a,b] (eV)
CO_2		
$X\ ^1\Sigma_g^+$	$(4\sigma_g)^2(3\sigma_u)^2(1\pi_u)^4(1\pi_g)^4$	0
$CO_2^{+\cdot}$		
$X\ ^2\Pi_g$	$(4\sigma_g)^2(3\sigma_u)^2(1\pi_u)^4(1\pi_g)^3$	13.8 (0)
$A\ ^2\Pi_u$	$(4\sigma_g)^2(3\sigma_u)^2(1\pi_u)^3(1\pi_g)^4$	17.3 (3.5)
$B\ ^2\Sigma_u^+$	$(4\sigma_g)^2(3\sigma_u)^1(1\pi_u)^4(1\pi_g)^4$	18.1 (4.3)
$C\ ^2\Sigma_g^+$	$(4\sigma_g)^1(3\sigma_u)^2(1\pi_u)^4(1\pi_g)^4$	19.4 (5.6)

[a] Relative energy is given with respect to the ground state of CO_2. Values relative to the ground state of CO_2^+ are given in brackets.
[b] from reference 100.

7.7 CIE of $CO_2^{+\cdot}$/He

Emission spectra over the wavelength range of 190-1020 nm were obtained from $CO_2^{+\cdot}$/He collisions at 8 keV ion translational energy (Figure 7.14). A summary of the peak and transition assignments is presented in Table 7.8. The prominent feature at low wavelength consists of two emission bands. The furthest left peak is the $\Delta v = 0$ of $CO_2^{+\cdot}$ $B\ ^2\Sigma_u^+ \rightarrow X\ ^2\Pi_g$ electronic transition. Immediately to the right is the $\Delta v = +3, +2, +1, 0, -1, -2, -3$ vibrational transition progression in the $CO_2^{+\cdot}$ $A\ ^2\Pi_u \rightarrow X\ ^2\Pi_g$ electronic transition. The other peaks arise from the emissions of the excited $O^{\cdot}$ fragment and the target gas, He. The single sharp peak for the $B\ ^2\Sigma_u^+ \rightarrow X\ ^2\Pi_g$ transitions and the broad vibrational progression in the $A\ ^2\Pi_u \rightarrow X\ ^2\Pi_g$ transition indicate a similar geometry between the $B\ ^2\Sigma_u^+$ and the ground electronic state while that for the $A\ ^2\Pi_u$ electronic state is substantially different, consistent with previous experimental results by fluorescence and photoelectron spectroscopy.[100-104] The $X\ ^2\Pi_g$, $A\ ^2\Pi_u$ and $B\ ^2\Sigma_u^+$ states of $CO_2^{+\cdot}$ all have linear and symmetric geometries, with CO bond lengths of 1.1768, 1.2274 and 1.1805 Å, respectively.[101,102]

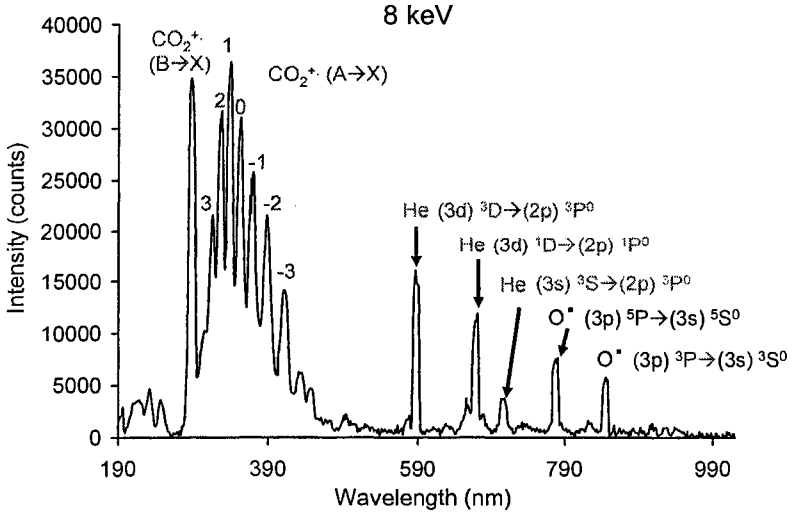

Figure 7.14 CIE spectra (190-1020 nm) of $CO_2^{+\cdot}$/He collisions at 8 keV projectile ion translational energy. Collision gas pressure corresponded to 90% ion beam transmission (accumulation time per section: 30 mins).

Table 7.8 Observed emissions in Figure 7.14 and their corresponding radiative lifetimes.

Transition[a]				τ (ns)[b]	λ (nm)	Ref.
$CO_2^{+\cdot}$	$B\ ^2\Sigma_u^+ \rightarrow X\ ^2\Pi_g$	(n,0,0)→(n,0,0)	(Δν = 0)	~145	288	98,99,101
	$A\ ^2\Pi_u \rightarrow X\ ^2\Pi_g$	(n,0,0)→(n-5,0,0)	(Δν = 5)	~120	294	98-100,102-105
		(n,0,0)→(n-4,0,0)	(Δν = 4)		304	
		(n,0,0)→(n-3,0,0)	(Δν = 3)		315	
		(n,0,0)→(n-2,0,0)	(Δν = 2)		326	
		(n,0,0)→(n-1,0,0)	(Δν = 1)		338	
		(n,0,0)→(n,0,0)	(Δν = 0)		351	
		(n,0,0)→(n+1,0,0)	(Δν = -1)		368	
		(n,0,0)→(n+2,0,0)	(Δν = -2)		386	
		(n,0,0)→(n+3,0,0)	(Δν = -3)		405	
		(n,0,0)→(n+4,0,0)	(Δν = -4)		427	
		where n = 0, 1, 2,.....				
		(n,0,0)→(n-2,0,2)	(Δν = 2)*	---	361	64,100,103,104
		(n,0,0)→(n-1,0,2)	(Δν = 1)*		375	
		(n,0,0)→(n,0,2)	(Δν = 0)*		392	
		(n,0,0)→(n+1,0,2)	(Δν = -1)*		411	
		(n,0,0)→(n+2,0,2)	(Δν = -2)*		434	
		where n = 0, 1, 2,.....				
$O^{\cdot}$	$(3p)\ ^5P \rightarrow (3s)\ ^5S^0$			27	779	83,84
	$(3p)\ ^3P \rightarrow (3s)\ ^3S^0$			31	845	
He	$(3d)\ ^3D \rightarrow (2p)\ ^3P^0$			14	587	83,84
	$(3d)\ ^1D \rightarrow (2p)\ ^1P^0$			16	669	
	$(3s)\ ^3S \rightarrow (2p)\ ^3P^0$			65	707	

[a] Transition written in notation (ν_1, ν_2, ν_3). For $CO_2^{+\cdot}$, ν_1 = symmetric stretch, ν_2 = bending mode and ν_3 = asymmetric stretch.
[b] Lifetimes from references.[83,98,99]

Figure 7.15 presents the emission spectrum (262-442 nm) obtained at higher resolution (with an entrance slit width of 1.0 mm), resulting in a spectral resolution of 3.0 nm (full width at half maximum). The vibrational progression in the A $^2\Pi_u \rightarrow$ X $^2\Pi_g$ transition is better resolved, including several peaks at low wavelength corresponding to the $\Delta v = 5$, 7 and 8 of the A $^2\Pi_u \rightarrow$ X $^2\Pi_g$ transition. The peak for the $\Delta v = 6$ transition likely overlaps with the B $^2\Sigma_u^+ \rightarrow$ X $^2\Pi_g$ emission, giving rise to the tailing on one side of the peak. In addition, another vibrational progression marked by asterisks was observed (see Table 7.8 for the assignments).

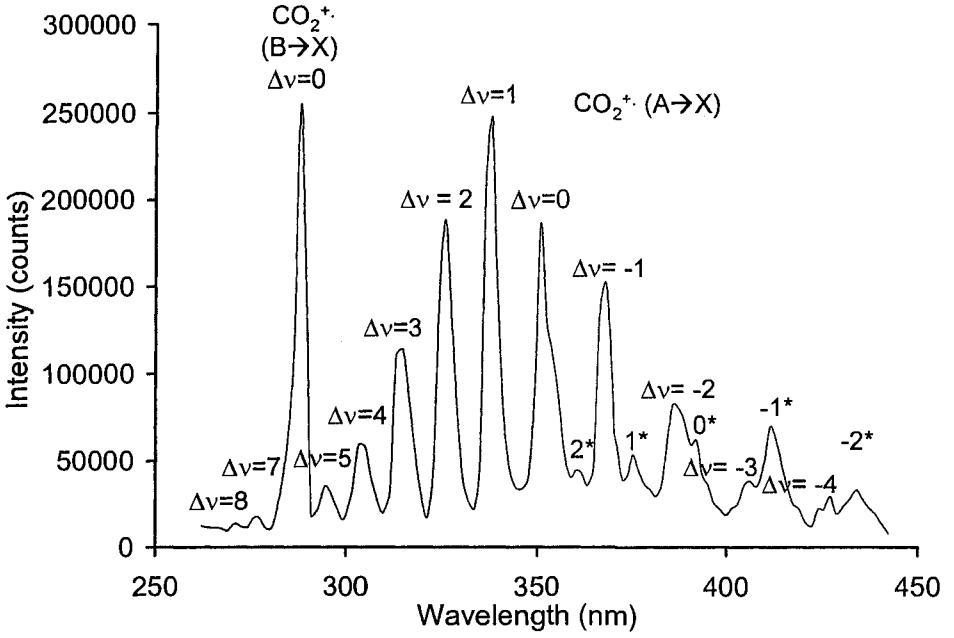

Figure 7.15 CIE spectrum (262 to 442 nm) of 8 keV $CO_2^{+\cdot}$/He collisions obtained with an entrance slit width of 1.0 mm (accumulation time per section: 10 hours).

The emission spectra over the wavelength range of 190-536 nm and 768-875 nm from 7 keV to 2 keV ion translational energy are presented in Figure 7.16. These are the energy ranges that contain emissions from the precursor ion $CO_2^{+\cdot}$ and its fragments.

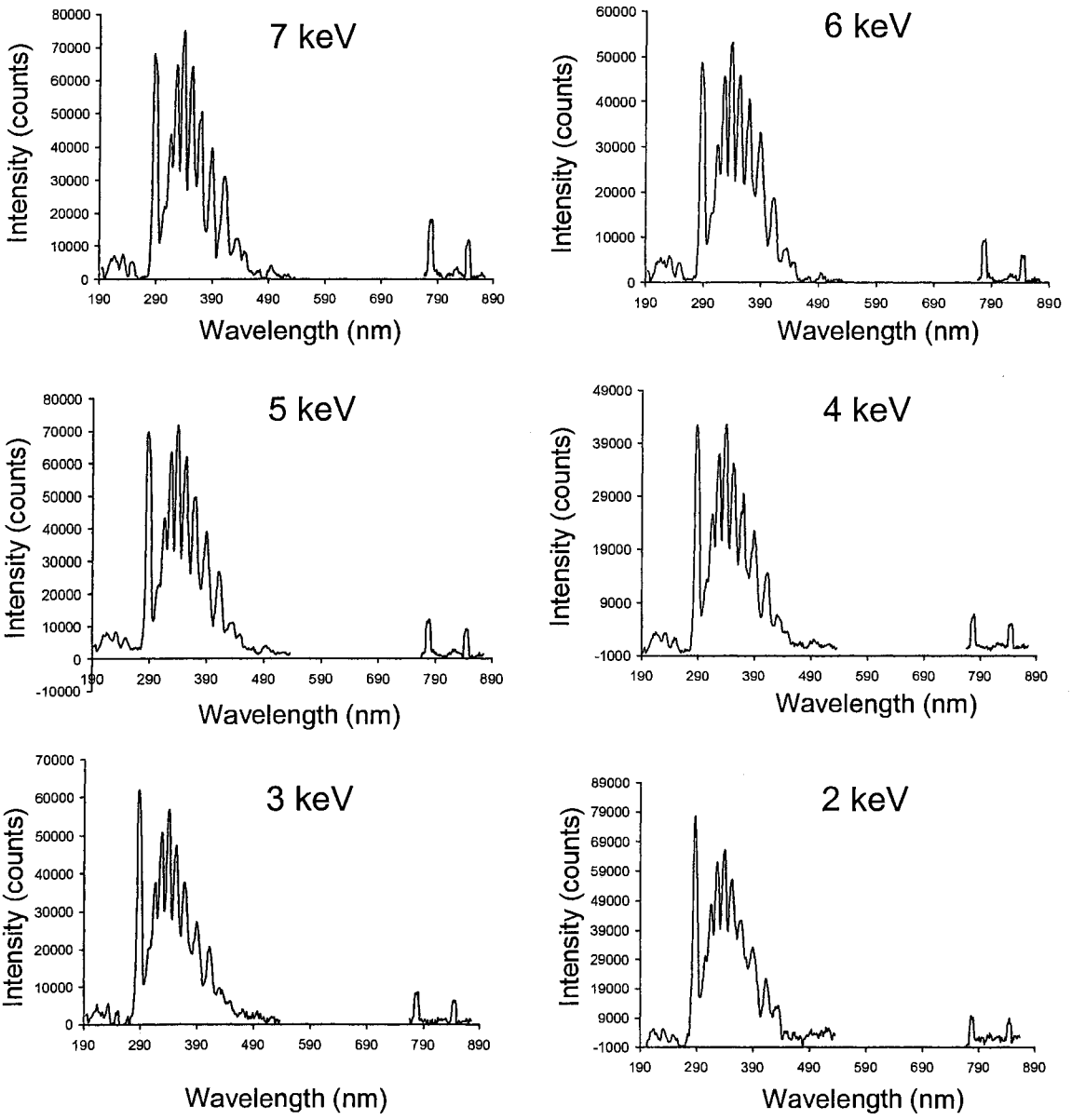

Figure 7.16 CIE spectra (190-536 nm and 768-875 nm) of $CO_2^{+\cdot}$/He collisions at various projectile ion translational energies. Collision gas pressure corresponds to 90% ion beam transmission (accumulation time per section: 1 hour (7 keV to 4 keV), 3 hours (3 keV) and 5 hours (2 keV)).

$CO_2^{+\cdot}$ presents an interesting case for the study as within the wavelength range of 190-1020 nm, two emission bands can result from the direct excitation of $CO_2^{+\cdot}$ in addition to emissions from fragment ions and neutrals. In comparison to $N_2^{+\cdot}$, emissions from the fragments are also comparatively stronger, providing a more reliable comparison of the relative intensities at different ion translational energies. The relative intensities of the fragment ions may appear to decrease slightly as the ion translational energy decreases. However, these spectra (Figure 7.14 and 7.16) are the raw data obtained directly from experiments (i.e. without lifetime correction). As the radiative lifetime of $CO_2^{+\cdot}$ and its fragments are relatively different (120-145 ns vs. 27-31 ns), it is important in this case to consider lifetime correction. The relative intensities after lifetime correction are tabulated in Table 7.9 and the lifetime-corrected plots for the relative intensity of $CO_2^{+\cdot}$ and $O^{\cdot}$ can be found in Figure 7.17 for visualization. Once again, two situations were taken into consideration. Figure 7.17b presents the plot when all collisions were assumed to take place at the beginning of the collision cell while Figure 7.17c presents the plot at which all collisions were assumed to take place when they enter the observation region. Most of the points fall along the y = x line, indicating these relative intensities do not change with ion translational energy. This is in agreement with the curve-crossing mechanism.

There are two points that result in larger deviations. These points correspond to $\Delta v = 3$ and $\Delta v = 2$ of the $CO_2^{+\cdot}$ A $^2\Pi_u \rightarrow$ X $^2\Pi_g$ emission. This is interpreted as the growing importance of vibrational excitation in addition to electronic excitation at lower ion translational energy. Based on the collision cross section of CO_2,[14] the interaction

time between $CO_2^{+\cdot}$ and He is estimated to be near 10^{-14} s at 2 keV ion translational energy, bringing it closer to the vibrational period of about 2 x 10^{-14} s. At these ion translational energies, the collision time is no longer much shorter than the time of a vibrational period. Therefore, the Franck-Condon principle no longer holds. The increase in vibrational excitation with decreasing ion translational energy is opposite of what was observed in the charge transfer process with CO_2 [60] but is consistent with the direct excitation process involving $N_2^{+\cdot}$ precursor ions.[54,58] Kelly et al.[57-59] proposed that the reaction occurs at small impact parameters, in which short-range, repulsive interaction between the projectile and the target result in direct translational-vibrational excitation.

The B $^2\Sigma_u^+ \rightarrow$ X $^2\Pi_g$ emission appears to increase with respect to the A $^2\Pi_u \rightarrow$ X $^2\Pi_g$ ($\Delta v = 1$) emission on the 3 keV and 2 keV CIE spectra. This is primarily due to vibrational excitation in the A $^2\Pi_u$ state as the peak for the B $^2\Sigma_u^+ \rightarrow$ X $^2\Pi_g$ emission overlaps with several peaks from the broad vibrational progression of the A $^2\Pi_u \rightarrow$ X $^2\Pi_g$ transition ($\Delta v = 5$, 6 and 7) (see Figure 7.14 and 7.16). Corrections were made to deconvolute the two components, resulting in consistent relative intensities for the B $^2\Sigma_u^+ \rightarrow$ X $^2\Pi_g$ emission as a function of ion translational energy (Table 7.9).

Table 7.9 Relative intensities after lifetime correction.[a]

Ion Translational Energy (keV)	$CO_2^{+\cdot}$ B→X[b] 288 nm	$CO_2^{+\cdot}$ A→X 315 nm	326 nm	338 nm	351 nm	368 nm	386 nm	O· 779 nm	845 nm
8	0.97	0.58	0.87	1.00	0.86	0.71	0.59	0.37	0.07
7	0.94	0.58	0.85	1.00	0.85	0.67	0.52	0.41	0.09
6	0.95	0.57	0.86	1.00	0.86	0.76	0.62	0.35	0.07
5	0.97	0.59	0.88	1.00	0.86	0.72	0.58	0.33	0.07
4	0.97	0.60	0.89	1.00	0.84	0.69	0.54	0.35	0.07
3	0.99	0.65	0.89	1.00	0.85	0.67	0.50	0.36	0.06
2	0.94	0.73	0.95	1.00	0.84	0.67	0.51	0.33	0.06

[a] Lifetime corrections were performed by treating all collisions occurring when the ions enter the observation region.

[b] Relative intensity has been corrected by subtracting the overlapping contribution from the A→X emission (see text).

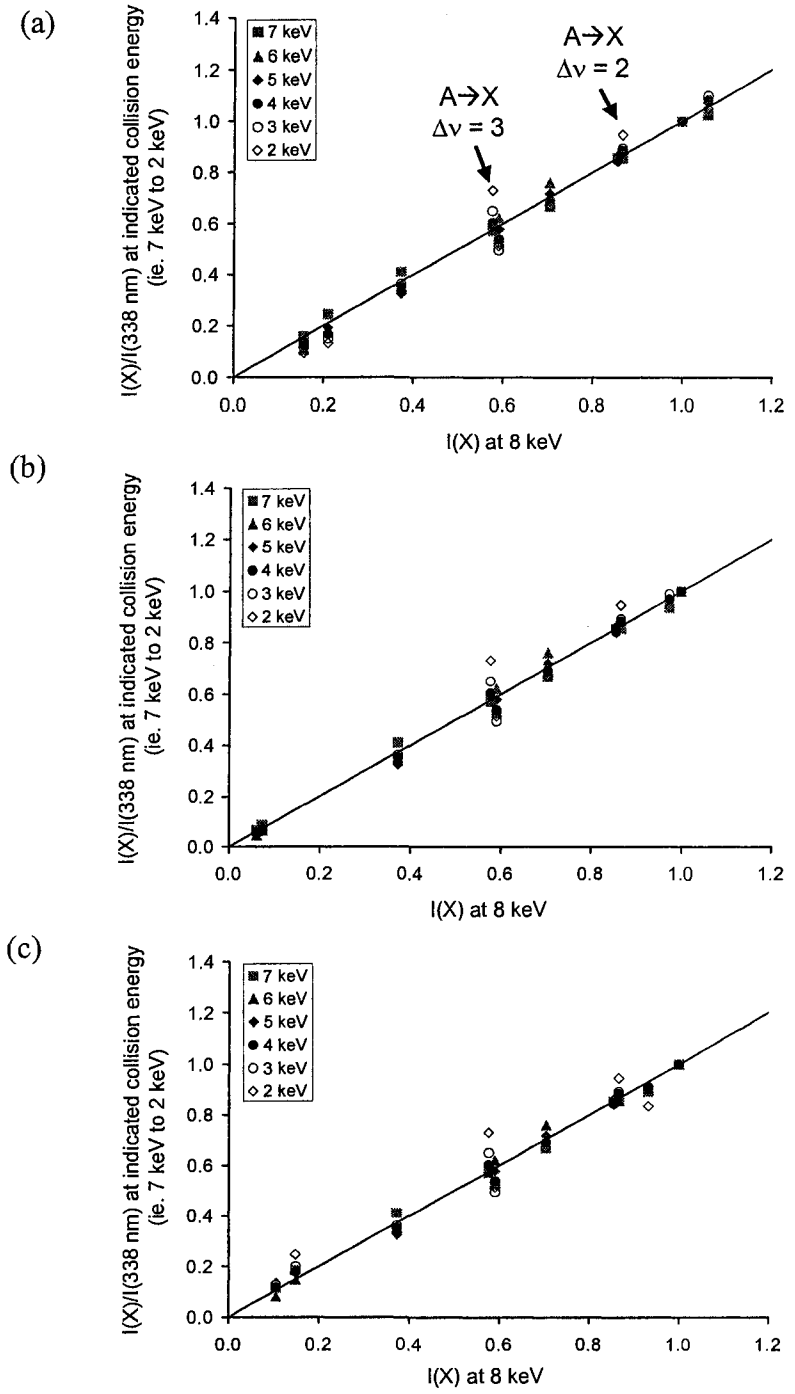

Figure 7.17 (a) Plot of relative emission intensities of $CO_2^{+\cdot}$ and $O^{\cdot}$ at various ion translational energies vs. those at 8 keV. (b,c) Lifetime-corrected relative emission intensities when all collisions were assumed to take place when the ions enter (b) the collision cell and (c) the observation region. I(X) represents the intensity of $CO_2^{+\cdot}$ and $O^{\cdot}$ and I(338 nm) the intensity of $\Delta v = 1$ of $CO_2^{+\cdot}$ $A\ ^2\Pi_u \rightarrow X\ ^2\Pi_g$ transition.

Rigorous checks have been performed to ensure that the observation was not an artifact. The increase in relative intensities was observed in all repetitive experiments and at different data acquisition times. Identical CIE spectra obtained from 4 keV ion translational energy and 5 keV ion translational energy with 1 kV deceleration voltage on the deceleration-reacceleration lens assembly confirm that the relative intensity difference could not have been an instrumental artifact from the lens assembly.

As a conclusion, the emission results on the $CO_2^{+\cdot}$/He collisions agree better with the curve-crossing model than the vertical transition model. Below 3 keV, the higher vibrational transitions of A $^2\Pi_u \rightarrow$ X $^2\Pi_g$ emission starts to increase, indicating that the collision time is no longer much shorter than a vibrational period. The importance of vibrational excitation increases at this energy range. The current system does not allow studies of lower ion translational energy as the emission signals become too weak for detection. The second phase of instrumental modification (by installing optics, for example) to increase detection sensitivity would be needed.

7.8 Vibrational Distribution of the A $^2\Pi_u$ State of $CO_2^{+\cdot}$ after Collisions

Figure 7.15 was used to estimate the vibrational distribution of the A $^2\Pi_u$ state of $CO_2^{+\cdot}$ after collisions. Each peak in the CIE spectrum is composed of several individual components corresponding to transitions between different vibrational states. For example, the peak of $\Delta v = 0$ contains contribution from transitions 0-0, 1-1, 2-2 etc. A number of Gaussian functions and the Franck-Condon factors between the A and X state

of $CO_2^{+\cdot}$ from McCallum and Nicholls[106] were therefore used to fit for the vibrational population (from (0,0,0) to (7,0,0)). The following equation illustrates this approach in the generic form.

$$H(\lambda) = \frac{N_i}{(\lambda_{i,j})^4} \cdot \frac{FC_{i,j}}{FC_{tot}} \cdot G(\lambda) + \frac{N_{i+1}}{(\lambda_{i+1,j+1})^4} \cdot \frac{FC_{i+1,j+1}}{FC_{tot}} \cdot G(\lambda) + \frac{N_{i+2}}{(\lambda_{i+2,j+2})^4} \cdot \frac{FC_{i+2,j+2}}{FC_{tot}} \cdot G(\lambda) + \ldots \quad (7.7)$$

where $H(\lambda)$ represents the peak to be fitted by a number of smaller Gaussian functions $G(\lambda)$, each of them scaled by the Franck-Condon factor between two vibrational states (e.g. $FC_{i,j}$ for transition from the (i,0,0) of the A state to the (j,0,0) of the X state) and the population N of the emitting vibrational state. FC_{tot} is the sum of the Franck-Condon factors used and $\lambda_{i,j}$ is the wavelength of the emission. Figure 7.18 shows the results of the fits. The relative vibrational population from (0,0,0) to (7,0,0) is tabulated in Table 7.10. My results are generally similar to those produced by electron impact on jet-cooled CO_2 and photoelectron spectroscopy.[107]

To determine if the differences in these populations cause any dramatic differences in the resulting emission spectrum, spectra (330-370 nm) were synthesized from the vibrational distributions obtained from the three methods (Figure 7.19). All three spectra exhibit similar vibrational patterns; however, the relative intensity of the $\Delta v = 0$ and -1 bands appears to be higher for CIE than for PES. The small difference appears to be due to a larger population in the ground vibrational state obtained from the CIE results and could be a result of intramolecular vibrational redistribution (IVR) prior to emission. The vibrational distribution in the A $^2\Pi_u$ state as a result of collisions therefore resembles those predicted by the Franck-Condon factors, an indication that for 8 keV

$CO_2^{+\cdot}$/He collisions, the collision time is indeed short enough in comparison to the vibrational period that the Franck-Condon principle can be applied to predict the relative intensity of an emission band resulting from collisional activation.

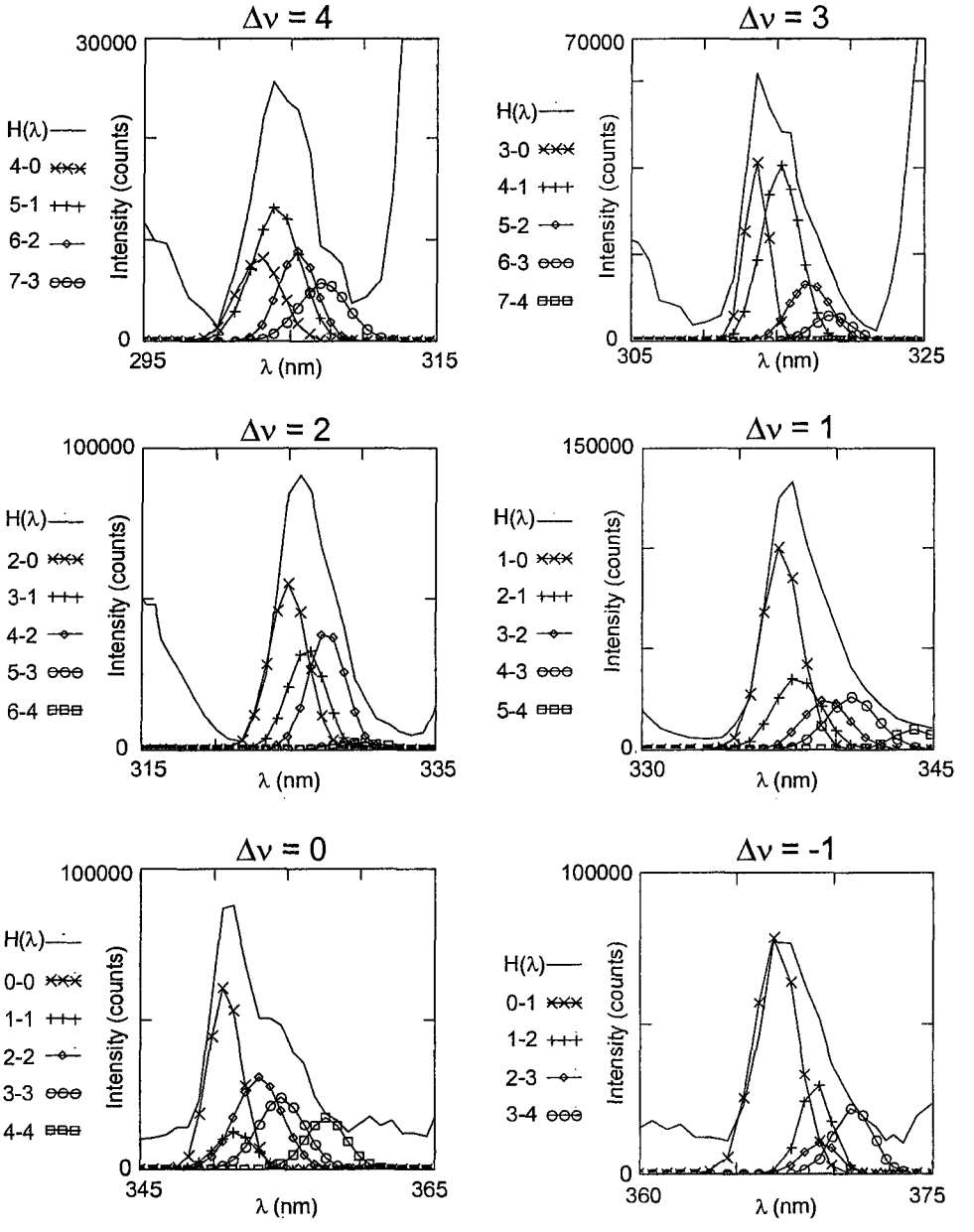

Figure 7.18 Peaks of the A $^2\Pi_u \rightarrow$ X $^2\Pi_g$ emission of $CO_2^{+\cdot}$ in the CIE spectrum fitted with Gaussian functions representing transitions between different vibrational states in the ground and excited states. The experimental data is shown as H(λ) and individual vibrational transitions from (i,0,0) of the A $^2\Pi_u$ state to (j,0,0) of the X $^2\Pi_g$ state are listed as i-j.

Table 7.10 Relative vibrational populations of the $CO_2^{+\cdot}$ ($A\ ^2\Pi_u$) state.

Method	Electron Energy (eV)	Vibrational level (i,0,0) 0	1	2	3	4	5	6	7	Ref.
CIE		17	12	15	18	19	9	5	4	This work
EI	30	12	26	21	19	13	6	2	1	107
	50	13	23	22	20	13	6	2	1	
	100	13	23	21	19	14	6	2	1	
	300	14	23	23	20	14	5	2	1	
PES		8	18	28	18	12	9	4	2	107,108

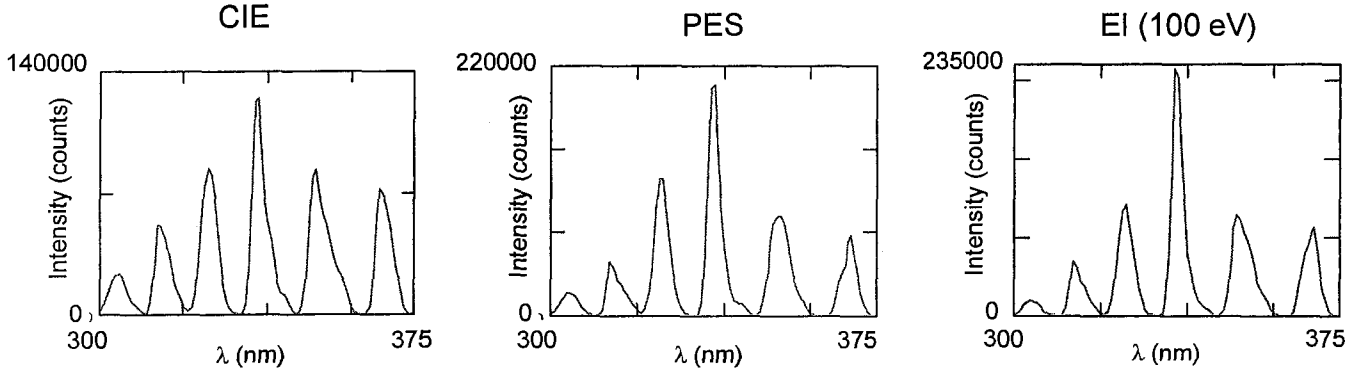

Figure 7.19 Relative intensities of the $CO_2^{+\cdot}$ $A\ ^2\Pi_u \rightarrow X\ ^2\Pi_g$ emission that would be expected using the vibrational distribution from CIE, PES and EI (at 100 eV electron energy).

8 Conclusions

While the mechanism for photon excitation is well known, that for collisional electronic excitation is often divided between vertical transitions and curve crossings, especially for small molecules and ions. Based on the short collision time involved in keV collisions, a number of authors often immediately invoke the Franck-Condon principle and vertical transitions. Several studies on the relative intensities of an emission band have confirmed the Franck-Condon picture. However, in my experiments, I monitored the population distribution of the excited states by observing emissions from the precursor ions and its fragments. While the A $^2\Pi_u \rightarrow$ X $^2\Pi_g$ emission band of $CO_2^{+\cdot}$ demonstrates similar Franck-Condon behaviour above 3 keV ion translational energy, the fact that the relative intensities between the fragments and the precursor ions stay constant with respect to ion translational energy in the studied collision systems ($N_2^{+\cdot}$/He, $N_2^{+\cdot}$/Ar and $CO_2^{+\cdot}$/He) cannot be accounted for by vertical transitions. Based on the vertical model, intensities from the fragments (i.e. a higher-energy process) would be expected to increase as collision energy or ion velocity increases. I have looked into ion scattering and other instrumental effects but none of them can account for this behaviour. On the other hand, if we look at curve crossings, a complicated sequence of non-adiabatic interactions could be involved in transforming kinetic energy into electronic energy. Based on the Landau-Zener model, increasing collision energy will increase the probability of crossing over to the excited states and therefore, will not necessarily favour

higher-energy processes. The Franck-Condon principle which is purely based on the grounds of short transition time can also be applied to the curve-crossing model. Therefore, linking the Franck-Condon principle immediately to vertical transitions for collisional excitation could be misleading.

Below 3 keV ion translational energy, changes to the relative intensities in the $CO_2^{+\cdot}$ emission band were observed. This is an indication that the Franck-Condon principle starts to break down as the collision time becomes comparable to the vibrational period of $CO_2^{+\cdot}$ at this ion translational energy. The gradual increase of the relative intensities at lower wavelengths of the $CO_2^{+\cdot}$ $A\ ^2\Pi_u \rightarrow X\ ^2\Pi_g$ emission therefore indicates the growing importance of vibrational excitation at lower translational energy.

A comparison was made between different target gases. In $N_2^{+\cdot}$/He, $N_2^{+\cdot}$/Ar and $N_2^{+\cdot}/O_2$ collisions, each of the targets differs significantly by their ionization energy and hence, different importance of the charge-transfer process. Adiabatic potential energy surfaces calculated at the CISD/6-311+G(2df) level of theory for $N_2^{+\cdot}$/He and $N_2^{+\cdot}$/Ar indicate that excitation to the A and B states involves curve-crossing first to the $C\ ^2\Sigma_u^+$ state. These results seem to agree with those obtained from translational energy spectroscopy. The difference in emission intensities from the $B\ ^2\Sigma_u^+ \rightarrow X\ ^2\Sigma_g^+$ emission of $N_2^{+\cdot}$ in the two systems can be accounted for by the slope difference at the crossing point and the higher relative emission intensity observed from the N^+ and $N^\cdot$ fragments in $N_2^{+\cdot}$/Ar collisions also agree with the dissociative cross section measurements by Fuentes and Martinez.[95]

References

(1) Thomson, J. J. *Rays of Positive Electricity and Their Application to Chemical Analysis*; Longmans, Green: London, 1913.

(2) Aston, F. W. *Proc. Cambridge Philos. Soc.* **1919**, *19*, 317.

(3) Jennings, K. R. *Int. J. Mass Spectrom. Ion Phys.* **1968**, *1*, 227.

(4) Haddon, W. K.; McLafferty, F. W. *J. Am. Chem. Soc.* **1968**, *90*, 4745.

(5) McLafferty, F. W.; Bente, P. F.; Kornfeld, F. C.; Tsai, S.-C.; Howe, I. *J. Am. Chem. Soc.* **1973**, *95*, 2120.

(6) Baer, T.; Hase, W. L. *Unimolecular reaction dynamics, theory and experiments*; Oxford University Press: New York, 1996.

(7) Baer, T.; Mayer, P. M. *J. Am. Soc. Mass Spectrom.* **1997**, *8*, 103.

(8) Laidler, K. J.; Meiser, J. H. *Physical Chemistry*; Houghton Mifflin Company: Boston, 1999.

(9) Cooks, R. G. *Collision Spectroscopy*; Plenum Press: New York, 1978.

(10) McLuckey, S. A. *J. Am. Soc. Mass Spectrom.* **1992**, *3*, 599.

(11) Shirts, R. B. Collision Theory and Reaction Dynamics. In *Gaseous Ion Chemistry and Mass Spectrometry*; Futrell, J. H., Ed.; Wiley: New York, 1986.

(12) Durup, J. Recent developments in mass spectrometry. In *Mechanisms of collision-induced dissociation of fast ions*; Ogata, K., Hayakawa, T., Eds.; University of Tokyo Press: Tokyo, 1970; pp 921.

(13) Condon, E. U. *Amer. J. Phys.* **1947**, *15*, 366.

(14) Atkins, P. *Physical Chemistry*; W.H. Freeman and Company: New York, 1998.

(15) Reid, C. J. *Int. J. Mass Spectrom. Ion Processes* **1990**, *101*, 35.

(16) Reid, C. J. *Int. J. Mass Spectrom. Ion Processes* **1991**, *105*, 191.

(17) Massey, H. S. W. *Rep. Prog. Phys.* **1949**, *12*, 248.

(18) Massey, H. S. W.; Burhop, E. H. S. *Electronic and ionic impact phenomena*; Clarendon Press: Oxford, 1952.

(19) Landau, L. D. *Phys. Zeits. Sowjetunion* **1932**, *2*, 46.

(20) Stueckelberg, E. C. G. *Helv. Phys. Acta* **1932**, *5*, 370.

(21) Zener, C. *Proc. R. Soc A* **1932**, *137*, 696.

(22) Gibson, D. K.; Los, J.; Schopman, J. *Physica* **1968**, *40*, 385.

(23) McGowan, W.; Kerwin, L. *Can. J. Phys.* **1963**, *41*, 316.

(24) Asselt, N. P. F. B. v.; Maas, J. G.; Los, J. *Chem. Phys.* **1974**, *5*, 429.

(25) Fournier, P. G. A. "Methodes de spectroscopie sans largeur Doppler de niveaux excites de systemes moleculaires simples"; Colloques Internationaux du C.N.R.S., 1973, Paris.

(26) Beynon, J. H.; Cooks, R. G.; Amy, J. W.; Baitinger, W. E.; Ridley, T. E. *Anal. Chem.* **1973**, *45*, 1023A.

(27) Fournier, P.; Pernot, A.; Durup, J. *J. Phys. (Paris)* **1971**, *32*, 533.

(28) Fournier, P.; VandeRunstraat, C. A.; Govers, T. R.; Schopman, J.; deHeer, F. J.; Los, J. *Chem. Phys. Lett.* **1971**, *9*, 426.

(29) Hagstrum, H. D.; Tate, J. T. *Phys. Rev.* **1941**, *59*, 354.

(30) Hippel, J. A.; Fox, R. E.; Condon, E. U. *Phys. Rev.* **1946**, *67*, 347.

(31) Kuprianov, S. E. *Sov. Phys. Tech. Phys.* **1964**, *9*, 659.

(32) Moran, T. F.; Petty, F. C.; Hedrick, A. F. *J. Chem. Phys.* **1969**, *51*, 2112.

(33) Smyth, H. D. *Proc. R. Soc. A* **1923**, *104*, 121.

(34) Smyth, H. D. *Rev. Mod. Phys.* **1931**, *3*, 347.

(35) Wankenne, H.; Momigny, J. *Int. J. Mass Spectrom. Ion Phys.* **1971**, *7*, 227.

(36) Fuentes, B. E.; Martinez, H. *Int. J. Mass Spectrom.* **2004**, *238*, 55.

(37) Lock, C. M.; Brenton, A. G. *Rapid Commun. Mass Spectrom.* **1998**, *11*, 1155.

(38) Lock, C. M.; Brenton, A. G.; Mathur, D. *Int. J. Mass Spectrom. Ion Processes* **1997**, *165/166*, 119.

(39) Moore, J. H.; Doering, J. P. *J. Chem. Phys.* **1970**, *52*, 1693.

(40) Park, J. T.; Schowengerdt, F. D. *Rev. Sci. Instr.* **1969**, *40*, 753.

(41) Illies, A. J.; Bowers, M. T. *Chem. Phys.* **1982**, *65*, 281.

(42) Huber, B. A.; Kahlert, H. J.; Wiesemann, K. *J. Phys. B* **1984**, *17*, 2883.

(43) Gilbody, H. B. *Nucl. Instr. and Meth. in Phys. Res. B* **1999**, *154*, 113.

(44) Gilbody, H. B.; McCullough, R. W. *J. Phys.: Conf. Ser.* **2004**, *2*, 199.

(45) Greenwood, J. B.; Burns, D.; McCullough, R. W.; Geddes, J.; Gilbody, H. B. *J. Phys. B., At. Mol. Opt. Phys.* **1996**, *29*, 5867.

(46) Laramee, J. A.; Carmody, J. J.; Cooks, R. G. *Int. J. Mass Spectrom. Ion Phys.* **1979**, *31*, 333.

(47) Laramee, J. A.; Hemberger, P. H.; Cooks, R. G. *Int. J. Mass Spectrom. Ion Phys.* **1980**, *33*, 231.

(48) Hubik, A. R.; Hemberger, P. H.; Laramee, J. A.; Cooks, R. G. *J. Am. Chem. Soc.* **1980**, *102*, 3997.

(49) Boyd, R. K.; Kingston, E. E.; Brenton, A. G.; Beynon, J. H. *Proc. R. Soc. Lond. A* **1984**, *392*, 59.

(50) Moore, C.; Mason, R. S.; Jennings, K. R.; Evans, S. *Int. J. Mass Spectrom. Ion Processes* **1988**, *86*, 109.

(51) Singh, S.; Harris, F. M.; Boyd, R. K.; Beynon, J. H. *Int. J. Mass Spectrom. Ion Processes* **1985**, *66*, 131.

(52) Todd, P. J.; Warmack, R. J.; McBay, E. H. *Int. J. Mass Spectrom. Ion Phys.* **1983**, *50*, 299.

(53) Waddell, D. S.; Boyd, R. K.; Brenton, A. G.; Beynon, J. H. *Int. J. Mass Spectrom. Ion Processes* **1986**, *68*, 71.

(54) Moore, J. H.; Doering, J. P. *Phys. Rev.* **1969**, *177*, 218.

(55) Lipeles, M. *J. Chem. Phys.* **1969**, *51*, 1252.

(56) Bregman-Reisler, H.; Doering, J. P. *Phys. Rev. A* **1974**, *9*, 1152.

(57) Kelley, J. D.; Bearman, G. H.; Harris, H. H.; Leventhal, J. J. *Chem. Phys. Lett.* **1977**, *50*, 295.

(58) Kelley, J. D.; Bearman, G. H.; Harris, H. H.; Leventhal, J. J. *J. Chem. Phys.* **1978**, *68*, 3345.

(59) Leventhal, J. J. The emission of light from excited products of charge exchange reactions. In *Gas Phase Ion Chemistry*; Bowers, M. T., Ed.; Academic Press: Orlando, 1984; Vol. 3.

(60) Bregman-Reisler, H.; Doering, J. P. *Chem. Phys. Lett.* **1974**, *27*, 199.

(61) Bregman-Reisler, H.; Doering, J. P. *J. Chem. Phys.* **1975**, *62*, 3109.

(62) Haugh, M. J.; Birely, J. H. *J. Chem. Phys.* **1974**, *60*, 264.

(63) Moore, J. H. *J. Geophys. Res.* **1975**, *80*, 3727.

(64) Parker, J. E.; Milner, R. G.; Robertson, A. M. *Int. J. Mass Spectrom. Ion Phys.* **1977**, *24*, 429.

(65) Sim, W.; Haugh, M. *J. Chem. Phys.* **1976**, *65*, 1616.

(66) Ehbrecht, A.; Mustafa, N.; Ottinger, C.; Herman, Z. *J. Chem. Phys.* **1996**, *105*, 9833.

(67) Moore, J. H.; Doering, J. P. *Phys. Rev.* **1968**, *174*, 178.

(68) Moore, J. H.; Doering, J. P. *Phys. Rev.* **1969**, *182*, 176.

(69) Bearman, G. H.; Earl, J. D.; Pieper, R. J.; Harris, H. H.; Leventhal, J. J. *Phys. Rev. A* **1976**, *13*, 1734.

(70) Holmes, J. L.; Mommers, A. A.; Terlouw, J. K.; Hop, C. E. C. A. *Int. J. Mass Spectrom. Ion Processes* **1986**, *68*, 249.

(71) Burgers, P. C.; Holmes, J. L.; Szulejko, J. E.; Mommers, A. A.; Terlouw, J. K. *Org. Mass Spectrom.* **1983**, *18*, 254.

(72) Holmes, J. L.; Mayer, P. M.; Mommers, A. A. *Int. J. Mass Spectrom. Ion Processes* **1994**, *135*, 213.

(73) O'Connor, P. J.; Leroi, G. E.; Allison, J. *J. Am. Soc. Mass Spectrom.* **1991**, *2*, 322.

(74) Dahl, D. A. *SIMION 3D Version 6.0*; Idaho National Engineering Laboratory: Idaho Falls, 1995.

(75) Holmes, J. L. *Org. Mass Spectrom.* **1985**, *20*, 169.

(76) Gardner, J. L.; Samson, J. A. R. *J. Chem. Phys.* **1975**, *62*, 1447.

(77) Ermler, W. C.; McLean, A. D. *J. Chem. Phys.* **1980**, *73*, 2297.

(78) Lofthus, A.; Krupenie, P. H. *J. Phys. Chem. Ref. Data* **1977**, *6*, 113.

(79) Maier, W. B. *J. Chem. Phys.* **1974**, *61*, 3459.

(80) Bennett, R. G.; Dalby, F. W. *J. Chem. Phys.* **1959**, *31*, 434.

(81) Hesser, J. E.; Dressler, K. *J. Chem. Phys.* **1966**, *45*, 3149.

(82) Holland, R. F.; Maier, W. B. *J. Chem. Phys.* **1972**, *56*, 5229.

(83) Wiese, W. L.; Smith, M. W.; Glennon, B. M. *Atomic Transition Probabilities*; National Bureau of Standards: Washington, D.C., 1966; Vol. I.

(84) Bashkin, S.; Stoner, J. O. *Atomic energy levels & grotrian diagrams 1*; North-Holland Publishing Company: New York, 1975.

(85) Lindsay, B. G. *J. Geophys. Res.* **2004**, *109*, A08305.

(86) Birely, J. H. *Phys. Rev. A* **1974**, *10*, 550.

(87) Obase, H.; Tsuji, M.; Nishimura, Y. *Chem. Phys. Lett.* **1984**, *105*, 214.

(88) deFroidmont, Y.; Lorquet, A. J.; Lorquet, J. C. *J. Phys. Chem.* **1991**, *95*, 4220.

(89) Dumont, M. N.; Remy, F. *J. Chem. Phys.* **1982**, *76*, 1175.

(90) Norlen, G. *Physica Scripta* **1973**, *8*, 249.

(91) Poon, C.; Mayer, P. M. *J. Phys. Chem. A* **2007**, *111*, 777.

(92) Smith, G. J.; Gao, R. S.; Lindsay, B. G.; Smith, K. A.; Stebbings, R. F. *Phys. Rev. A* **1996**, *53*, 1581.

(93) Rennie, E. E.; Mayer, P. M. *J. Chem. Phys.* **2004**, *120*, 10561.

(94) Maier, J. P. *Mass Spectrom. Rev.* **1992**, *11*, 119.

(95) Martinez, H.; Fuentes, B. E. *Nucl. Instr. and Meth. in Phys. Res. B* **2005**, *241*, 459.

(96) Krupenie, P. H. *J. Phys. Chem. Ref. Data* **1972**, *1*, 423.

(97) Baird, N. C.; Gupta, R. R.; Taylor, K. F. *J. Am. Chem. Soc.* **1979**, *101*, 4531.

(98) Bloch, M.; Turner, D. W. *Chem. Phys. Lett.* **1975**, *30*, 344.

(99) Maier, J. P.; Thommen, F. *Chem. Phys.* **1980**, *51*, 319.

(100) Wang, L.-S.; Reutt, J. E.; Lee, Y. T.; Shirley, D. A. *J. Electron. Spectrosc. Relat. Phenom.* **1988**, *47*, 167.

(101) Gauyacq, D.; Horani, M.; Leach, S.; Rostas, J. *Can. J. Phys.* **1975**, *53*, 2040.

(102) Gauyacq, D.; Larcher, C.; Rostas, J. *Can. J. Phys.* **1975**, *57*, 1634.

(103) Liu, J.; Chen, W.; Hsu, C.-W.; Hochlaf, M.; Evans, M.; Stimson, S.; Ng, C. Y. *J. Chem. Phys.* **2000**, *112*, 10767.

(104) Liu, J.; Hochlaf, M.; Ng, C. Y. *J. Chem. Phys.* **2000**, *113*, 7988.

(105) Judge, D. L.; Bloom, G. S.; Morse, A. L. *Can. J. Phys.* **1969**, *47*, 489.

(106) McCallum, J. C.; Nicholls, R. W. *J. Phys. B: Atom. Molec. Phys.* **1971**, *4*, 1096.

(107) Tokue, I.; Shimada, H.; Masuda, A.; Ito, Y.; Kume, H. *J. Chem. Phys.* **1990**, *93*, 4812.

(108) Brundle, C. R.; Turner, D. W. *Int. J. Mass Spectrom. Ion Phys.* **1969**, *2*, 195.

Claims to Original Research

1. The nitro-nitrite isomerization of protonated nitroalkanes was investigated by theoretical calculations. This represents the first study in which the effect of protonation on this isomerization process was explored. Comparison between protonated nitromethane and protonated 2-methyl-2-nitropropane demonstrates the effect of methyl substituents in lowering the isomerization barrier. By extending the study to the isomerization of 2-methyl-2-nitroproapane proton-bound dimers, it was observed that an additional neutral molecule bound to the proton increases the isomerization barrier by 57 kJ mol^{-1}. The difference can be related to solvation effect and raises questions as to the feasibility of nitro-nitrite isomerization in larger proton-bound cluster ions and in solution.

2. Competing rearrangement reactions of nitroalkane proton-bound pairs were studied by mass spectrometry and their potential energy surfaces were probed by theoretical calculations. In addition to a simple bond cleavage process in which the proton-bound pairs dissociate into neutral and protonated nitroalkanes, the nitroalkane proton-bound pairs can also rearrange via an internal S_N2 rearrangement to lose nitrous acid and via a nitro-nitrite isomerization to lose t-butanol. This is the first study in which nitroalkane proton-bound pairs are studied by experiment or theory. Study of the dissociations of nitroalkane proton-bound pairs by variational transition state theory finds that $\Delta(\Delta S^{\ddagger})$ is not necessarily the same as $\Delta(\Delta S)$. Therefore, one

should be careful in making such assumption as in the kinetic method for the determination of proton affinity.

3. The VG ZAB mass spectrometer in the lab was modified by installing an Einzel lens and a deceleration-reacceleration collision cell assembly to allow for the control of the translational energy of precursor ions and for the study of collision-induced emissions as a function of ion translational energy. This represents the first time collision-induced emission study as a function of ion translational energy has been carried out on a commercial mass spectrometer.

4. Collision-induced emission spectra of keV $N_2^{+\cdot}$/He, $N_2^{+\cdot}$/Ar and $CO_2^{+\cdot}$/He collisions were collected at different ion translational energy from a wavelength range of 190-1020 nm. This is the first time collision-induced emissions were collected over such a broad wavelength. This allows both emissions from the precursor ions and the fragments to be observed. By observing the relative emission intensity of these two groups, it was suggested that these processes were excited by curve crossings, even though the relative intensity within the $CO_2^{+\cdot}$ band agrees with the Franck-Condon factors as a result of short transition time at high collision energy. The study of $CO_2^{+\cdot}$/He collisions also represent the first time collision-induced emissions were collected from the direct excitation of $CO_2^{+\cdot}$ precursor ions over a range of ion translational energy.

List of Publications

1. C. Poon and P. M. Mayer, "Competing rearrangement reactions in small gas-phase ionic complexes: The internal S_N2 and nitro-nitrite rearrangements in nitroalkane proton-bound pairs", Int. J. Mass Spectrom. 255-256 (2006) 93-101.

2. C. Poon and P. M. Mayer, "Experimental evidence for the curve crossing mechanism for collisional excitation in keV $N_2^{+\cdot}$/He collisions by emission spectroscopy", J. Phys. Chem. A. 111 (2007) 777-782.

3. C. Poon, Y. Lin and P. M. Mayer, "Comparison of keV $N_2^{+\cdot}$/He and $N_2^{+\cdot}$/Ar collisions by emission spectroscopy and theory", submitted to J. Phys. Chem. A.

4. C. Poon and P. M. Mayer, "Should a Franck-Condon or a curve-crossing picture be applied to ion-target collisional activation? A case study of keV $CO_2^{+\cdot}$/He collisions by emission spectroscopy", submitted to J. Am. Soc. Mass Spectrom.

Appendix A

Fortran Code for the RRKM Program

```
* Calculation of Density and Sum of States and Unimolecular Rate Constants
* with the use of the Beyer-Swinehart scheme for Direct Count
*
* This FORTRAN program was adapted from the BASIC version quoted in
* P.M. Mayer and T. Baer, J. Am. Soc. Mass Spectrom. 1997, 8, 103-115.
*  by Paul M. Mayer (Chem Dept, U of Ottawa, Ottawa, Canada K1N 6N5)
*   25/7/97
*
* The variables:
* Eo   the activation energy
* MIN and IMIN are the minimum energy for which you want a k printed
* MAX and IMAX are the maximum energy for which you want a k calc and print
* NUM and INUM is the interval you want the k printed at
* Nfreq is the number of vibrational frequencies for both ion and ts
* w(100) is the array into which freqs are put
* p(32000) is the density of states vector in which densities are put
* N(32000) is the sum of states vector in which sums are put
* RATE(32000) is the rate constant vector into which k's are put
* LOGRATE(32000) is the vector into which is put log10(k)
* QMolc, QTs are the ion and ts partition functions at 600K
* UMolc, UTs are the ion and ts internal energies at 600K
*
* The constants:
*  H=3.3364E-11 is Planck's constant in cm-1 sec
*  Kb=1.3807E-23 in Boltzman's constant in J/K
*  Na=6.022E23 is Avogadro's number
*  HJ=6.6262E-34 is Planck's constant in Jsec
*  c=2.9979E10 is the speed of light in cm/sec
*  T is temperature in Kelvin
*
* STEP 1. Variable declaration:
*
    INTEGER IEo,Nfreq,IMIN,INCR,IMAX,ITMAX,J,I,T,v(100)
    REAL w(100),LOGRATE(32000)
    DOUBLE PRECISION p(32000)
    DOUBLE PRECISION N(32000)
    DOUBLE PRECISION RATE(32000)
```

```
      REAL Eo,MAX,MIN,NUM,QMolc,UMolc,QTs,UTs,Sts
      REAL H,Kb,Na,HJ,c,Sigma,B
      CHARACTER Title*80,Name*6
*
* STEP 2. Reading in the stuff
*
      WRITE (*,'("input file name")')
      READ (*,'(a6)') Name
      OPEN (UNIT=8, FILE=Name, STATUS='OLD')
      READ (8,'(a80)') Title
      READ (8,*) Eo,MIN,MAX,NUM,Sigma
      READ (8,*) Nfreq
      READ (8,*) (w(I),I=1,Nfreq)
      READ (8,*) B
*
* STEP 3. Converting input energies to integral wavenumbers
*
      Eo=Eo*8065.5          !converting to cm-1
      IEo=NINT(Eo)          ! converting to an integer
      MAX=MAX*8065.5        ! converting to cm-1
      IMAX=NINT(MAX)        ! converting to an integer
      ITMAX=IMAX-IEo        ! defining transition state maximum energy
      MIN=MIN*8065.5
      IMIN=NINT(MIN)
*
*       Converting input frequencies to integers
*
      DO 20 J=1,Nfreq,1
      v(J)=NINT(w(J))
20    CONTINUE
*
*       Converting rotational constant (GHz) to wavenumbers
*
      Kb=1.3807E-23
      Na=6.022E23
      HJ=6.6262E-34
      c=2.9979E10
      T=600
*
      B=B*(1.0E9/c)
*
* STEP 4. Initializing p and N vectors
*
      DO 40 J=1,32000,1
        p(J)=3*SQRT(1/(B*J))     !(p with internal rotor densities)
        N(J)=0
```

```
40   CONTINUE
*
* STEP 5. Convoluting in the vibrational density of states
*
    DO 200 J=1,Nfreq,1
      DO 100 I=v(J),IMAX,1
       IF ((I-v(J)) .EQ. 0) THEN
         p(I)=p(I)+0
       ELSE
        p(I) = p(I) + p(I - v(J))
       END IF
100    CONTINUE
200  CONTINUE
*
* STEP 6. Calculating ion partition function and internal energy
*
    QMolc=1
    UMolc=0
    DO 250 I=1,Nfreq,1
      QMolc=QMolc*(1/(1-EXP(-w(I)/417.0)))     !calcing molc partion fcn
      UMolc=UMolc + (w(I)/(EXP(w(I)/417.0)-1)) ! calcing molc int nrg
250  CONTINUE
*
* STEP 7. Calculating sum of states of transition state
*
    READ (8,*) Nfreq
    READ (8,*) (w(I),I=1,Nfreq)
    READ (8,*) B
*
* making TS frequencies integers
*
    DO 270 J=1,Nfreq,1
    v(J)=NINT(w(J))
270  CONTINUE
*
* converting rotational constant to wavenumbers from GHz
*
      B=B*(1.0E9/c)
*
* STEP 7a. Adding to N vector the internal rotor sums
*
    DO 285 J=1,32000,1
      N(J)=N(J)+2*3*SQRT(J/B)
285   CONTINUE
*
* STEP 7c.  Convoluting in the vibrational sums
```

```
*
    DO 400 J=1,Nfreq,1
      DO 300 I=v(J),ITMAX,1
        N(I) = N(I) + N(I-v(J))
300     CONTINUE
400   CONTINUE
*
* STEP 8. Calculating ts partition function and internal energy at 600K
*
    QTs=1
    UTs=0
    DO 450 I=1,Nfreq,1
      QTs=QTs*(1/(1-EXP(-w(I)/417.0)))     !calcing molc partion fcn
      UTs=UTs + (w(I)/(EXP(w(I)/417.0)-1)) ! calcing molc int nrg
450   CONTINUE
*
* STEP 9. Calculating rate constant at specific intervals
*
    H=3.3364E-11
    DO 500 J=1,ITMAX,1
    RATE(J)=(Sigma*N(J))/(H*p(J+IEo))
    LOGRATE(J) = LOG10(RATE(J))
500   CONTINUE
*
* STEP 10. Calculating entropy of activation at 600K
*
    Sts= ((Kb*LOG(Qts/QMolc)) + (HJ*c*(UTs-UMolc))/T)*Na
*
* STEP 11. Printing it off
*
    PRINT '("RRKM k(E) vs E using the Direct Count method")'
    PRINT 550, Title
550   FORMAT (1X,A80)
    PRINT 560, Sts
560   FORMAT ('entropy of activation (J/K/mol) at 600K is', 1PG15.7E2)
    PRINT 600
600   FORMAT (' E        RATE        Log10RATE      p          N')
*
    INCR=INT((IMAX-IMIN)/(NUM-1))
    DO 800 J=IMIN-IEo,IMAX-IEo,INCR
    PRINT 700, (J+IEo)/8065.5, RATE(J), LOGRATE(J),  p(J+IEo),  N(J)
700   FORMAT (1PG10.4E2,E15.7E2,1PG13.4E2,E20.7E3,E20.7E3)
800   CONTINUE
    END
```

Appendix B

Archive Entries for B3-LYP/6-31+G(d) Optimized Geometries

A. NITRO-NITRITE ISOMERIZATION

CH_3NO_2
N-N= 1.243789407281D+02 E-N=-8.226990743263D+02 KE= 2.428211084906D+02
1\1\GINC-MS3\FOpt\RB3LYP\6-31+G(d)\C1H3N1O2\POON\08-Jan-2004\0\\#B3LYP
/6-31+G(D) OPT FREQ\\CH3NO2\\0,1\C,0.4371801804,1.2260110789,0.2646031
947\H,0.4163621715,1.3701538333,1.3436802158\H,1.4351160084,1.33198235
06,-0.1575261428\H,-0.2604407758,1.9100382208,-0.224784116\N,-0.047821
8738,-0.1624819891,-0.0283098099\O,-0.8715259744,-0.644611595,0.745021
4192\O,0.3866053032,-0.7092467743,-1.0388739762\\Version=x86-Linux-G98
RevA.7\HF=-245.0247967\RMSD=5.699e-09\RMSF=1.241e-04\Dipole=0.4857018,
1.384149,0.2935954\PG=C01 [X(C1H3N1O2)]\\@
Zero-point correction= 0.050030
Frequencies -- 28.5467 481.1956 607.2178
Frequencies -- 658.7891 924.0448 1121.3462
Frequencies -- 1144.7336 1416.3934 1442.2008
Frequencies -- 1483.7843 1495.7208 1641.0844
Frequencies -- 3099.4555 3191.7594 3224.2981

CH_3ONO (trans)
1\1\GINC-MS10\FOpt\RB3LYP\6-31+G(d)\C1H3N1O2\POON\04-Sep-2005\0\\#B3LY
P/6-31+G(D) OPT FREQ GEOM=CHECK GUESS=CHECK\\CH3NO2\\0,1\C,1.322166012
6,0.9216476434,0.3716796087\H,1.6448214758,0.9602544372,1.415475674\H,
2.1908417917,0.861707499,-0.289344417\H,0.7206560153,1.8026107511,0.12
80309005\N,-0.7722758413,0.0524548505,-0.25145434\O,-1.4211948615,-0.9
222300076,-0.4038390518\O,0.5357718028,-0.2679753051,0.1883316231\\Ver
sion=x86-Linux-G98RevA.7\HF=-245.0189504\RMSD=3.261e-09\RMSF=1.065e-04
\Dipole=0.7290056,0.7941653,0.188233\PG=C01 [X(C1H3N1O2)]\\@
Zero-point correction= 0.048276
Frequencies -- 99.2708 225.5697 372.2591
Frequencies -- 594.1585 841.4630 1060.8633
Frequencies -- 1172.7964 1209.2203 1470.9411
Frequencies -- 1501.9539 1523.5133 1754.4307
Frequencies -- 3063.4472 3150.2683 3150.7492

CH_3ONO (cis)
1\1\GINC-MS10\FOpt\RB3LYP\6-31+G(d)\C1H3N1O2\POON\27-Oct-2004\0\\#B3LY
P/6-31+G(D) OPT=(MAXCYCLES=150) FREQ\\3methylONO\\0,1\O,-0.7277662033,
0.,-0.5018386047\N,-0.5629220893,0.,0.8852024305\O,0.5707844914,0.,1.2
493255068\C,0.4840728376,0.,-1.285338814\H,1.0781614061,0.8937888161,-
1.0731960624\H,1.0781614061,-0.8937888161,-1.0731960624\H,0.1355484833

,0.,-2.3178872223\\Version=x86-Linux-G98RevA.7\State=1-A'\HF=-245.0197
992\RMSD=6.291e-09\RMSF=3.482e-05\Dipole=0.4906802,0.,-0.8160233\PG=CS
[SG(C1H1N1O2),X(H2)]\\@
Zero-point correction= 0.048629
Frequencies -- 186.8198 343.4270 368.3674
Frequencies -- 680.7327 860.2469 1000.5588
Frequencies -- 1160.2663 1192.0154 1454.6981
Frequencies -- 1496.2312 1507.1754 1688.1152
Frequencies -- 3070.0962 3145.5396 3191.4351

CH_3NO_2 → CH_3ONO (TS)
1\1\GINC-SFNODE1\Freq\RB3LYP\6-31+G(d)\C1H3N1O2\HPC1392\22-Feb-2005\1\
\#B3LYP/6-31+G(D) OPT=(TS,EF,CALCALL)\\methyl CH3NO2\\0,1\C\H,1,B2\H,1
,B3,2,A3\H,1,B4,2,A4,3,D4,0\N,1,B5,2,A5,4,D5,0\O,5,B6,1,A6,2,D6,0\O,5,
B7,1,A7,2,D7,0\\B2=1.08223779\B3=1.08488256\B4=1.08593609\B6=1.2045853
1\A3=116.49435545\A4=115.74362313\A6=151.18036232\D4=-139.75747486\D6=
142.18831331\B5=1.97105505\B7=1.29807337\A5=96.56065187\A7=73.20324709
\D5=-93.7883295\D7=-97.6951437\\Version=Sun64-SVR4-Unix-G98RevA.9\HF=-
244.9168469\RMSD=6.864e-09\RMSF=1.955e-05\Dipole=0.5786013,1.5983982,0
.4430011\DipoleDeriv=0.4914789,0.2082615,-0.0224143,0.0839779,0.721482
2,0.0344772,-0.0302055,0.0865347,0.1952603,0.0749372,-0.037579,-0.0001
16,-0.0603112,-0.0134292,-0.0243982,-0.0023505,-0.0180999,0.0408263,0.
0146431,-0.0581156,0.0286235,-0.0231016,-0.03374,-0.0266091,0.0263452,
-0.0123377,0.0662123,0.002782,-0.0321116,-0.0377916,-0.0611795,-0.0795
118,-0.0068417,-0.045575,-0.00845,0.064092,1.4231463,0.379302,0.413642
,0.2615631,0.2898541,0.1617998,0.7082776,0.31005,0.2191407,-1.0694521,
-0.3779209,-0.2051292,-0.6609914,-0.4916906,-0.160924,-0.7158589,-0.30
30056,-0.3410573,-0.9375331,-0.0818361,-0.1768148,0.4600439,-0.3929643
,0.0224969,0.059368,-0.054689,-0.2444732\Polar=41.6444607,9.8692368,41
.8736692,4.8204903,5.6382902,24.5234814\PG=C01 [X(C1H3N1O2)]\NImag=1\\
Zero-point correction= 0.045542
Frequencies -- -824.9238 113.0440 191.4864
Frequencies -- 415.0459 731.5399 892.8092
Frequencies -- 907.5783 1227.6706 1258.0766
Frequencies -- 1447.3618 1485.0717 1597.8312
Frequencies -- 3134.4171 3271.1991 3317.6579

$CH_3NO_2H^+$
1\1\GINC-MS3\FOpt\RB3LYP\6-31+G(d)\C1H4N1O2(1+)\POON\08-Jan-2004\0\\#B
3LYP/6-31+G(D) OPT FREQ\\CH3NO2\\1,1\C,0.5550174737,1.1855726292,0.473
8421006\H,0.2799228113,1.3497003201,1.5142207122\H,1.6333503069,1.0637
789258,0.3281052427\H,0.1716531925,1.9591741468,-0.1995638042\N,-0.081
762803,-0.0954375715,0.0637134857\O,0.180111019,-0.4142413493,-1.19862
77389\O,-0.7513872562,-0.7788115114,0.757505607\H,-0.2724816352,-1.273
6032818,-1.4028320994\\Version=x86-Linux-G98RevA.7\HF=-245.3104581\RMS
D=3.328e-09\RMSF=1.366e-04\Dipole=0.267231,0.2748349,-0.2731218\PG=C01
[X(C1H4N1O2)]\\@
Zero-point correction= 0.061785
Frequencies -- 64.8893 450.3060 552.3170
Frequencies -- 600.6186 662.9092 814.4497
Frequencies -- 1052.5459 1141.9597 1246.9772

Frequencies -- 1414.3840 1435.3456 1457.9032
Frequencies -- 1470.9353 1783.1894 3077.5661
Frequencies -- 3165.2264 3236.1438 3492.9020

CH_3ONOH^+ (cis)
1\1\GINC-SFNODE8\FOpt\RB3LYP\6-31+G(d)\C1H4N1O2(1+)\HPC1396\16-Apr-200
5\0\\#B3LYP/6-31+G(D) OPT FREQ GUESS=CHECK GEOM=CHECK\\methylnitriteH+
TSqstcalc ircfopt\\1,1\C,-0.2363953218,1.5466897604,0.8077250617\H,-0.
0926807856,1.4395184357,1.8829654475\H,0.6228441075,1.9720684103,0.290
2304149\H,-1.1800581857,2.0312375658,0.5601036023\N,0.5130357363,-0.29
4603589,-0.4209892666\O,0.3018601339,-1.4821951689,-0.8265476385\O,-0.
4221640231,0.132207748,0.3085884566\H,-0.5605522464,-1.8608384843,-0.4
890515129\\Version=Sun64-SVR4-Unix-G98RevA.9\HF=-245.291209\RMSD=6.894
e-09\RMSF=3.506e-04\Dipole=-0.5899377,0.1666652,0.4134039\PG=C01 [X(C1
H4N1O2)]\\@
Zero-point correction= 0.061096
Frequencies -- 121.0666 249.1200 346.9791
Frequencies -- 580.6611 814.3504 892.7844
Frequencies -- 1152.0566 1155.2604 1295.8677
Frequencies -- 1353.5884 1455.3704 1466.5072
Frequencies -- 1485.2046 1506.6548 3106.8454
Frequencies -- 3232.5001 3241.8513 3361.1969

CH_3ONOH^+ (trans)
1\1\GINC-MS10\FOpt\RB3LYP\6-31+G(d)\C1H4N1O2(1+)\POON\27-Oct-2004\0\\#
B3LYP/6-31+G(D) OPT=(MAXCYCLES=150) FREQ\\methylOHNO+\\1,1\O,-
0.7054439279,0.,-0.5084034684\N,-
0.6719290035,0.,0.735096483\O,0.5409889484,0.
,1.193927182\C,0.5396560931,0.,-1.3640419561\H,1.0967516645,0.90863332
25,-1.1300053857\H,1.0967516645,-0.9086333225,-1.1300053857\H,0.118532
2856,0.,-2.3660194023\H,0.4691706879,0.,2.1804168208\\Version=x86-Linu
x-G98RevA.7\State=1-A'\HF=-245.2929669\RMSD=4.356e-09\RMSF=1.597e-04\D
ipole=0.6714111,0.,0.4089476\PG=CS [SG(C1H2N1O2),X(H2)]\\@
Zero-point correction= 0.061594
Frequencies -- 155.0863 323.7481 418.0038
Frequencies -- 683.0901 754.5655 817.3651
Frequencies -- 1131.3482 1168.3796 1228.5853
Frequencies -- 1291.6899 1434.7258 1466.4819
Frequencies -- 1480.6430 1566.2027 3100.7477
Frequencies -- 3213.1897 3257.2595 3545.4594

$CH_3O(H)(NO)^+$ (cis)
N-N= 1.181277426428D+02 E-N=-8.025092498476D+02 KE= 2.430106184338D+02
1\1\GINC-SFNODE7\FOpt\RB3LYP\6-31+G(d)\C1H4N1O2(1+)\HPC1396\17-Apr-200
5\0\\#B3LYP/6-31+G(D) OPT FREQ GUESS=CHECK GEOM=CHECK\\ch3no2ohno+TS-q
stcalc ircropt\\1,1\C,-0.5323952885,1.7355241985,-0.3856648792\H,-0.25
72509282,2.0302348594,0.6266689582\H,0.2262045319,2.034373676,-1.11198
61188\H,-1.5108079753,2.1551190073,-0.6381348263\N,0.8478047097,-0.679
0869844,0.4904490035\O,0.6437096611,-1.7585951006,0.5198543277\O,-0.68
22508755,0.2812249379,-0.362263726\H,-0.8900771505,-0.0603025413,-1.25
64265763\\Version=Sun64-SVR4-Unix-G98RevA.9\HF=-245.3170813\RMSD=7.743

e-09\RMSF=2.964e-05\Dipole=0.3242748,-0.2476051,-0.3575498\PG=C01 [X(C
1H4N1O2)]\\@
Zero-point correction= 0.059173
Frequencies -- 43.8488 120.8597 161.1284
Frequencies -- 261.9256 483.2730 571.2158
Frequencies -- 941.1778 1069.3087 1162.0092
Frequencies -- 1338.0197 1472.8468 1497.4376
Frequencies -- 1506.4981 2231.7873 3080.7839
Frequencies -- 3172.9154 3207.5355 3651.4675

$CH_3O(H)(NO)^+$ (trans)
1\1\GINC-SFNODE2\FOpt\RB3LYP\6-31+G(d)\C1H4N1O2(1+)\HPC1418\22-Feb-200
5\0\\#B3LYP/6-31+G(D) OPT FREQ\\CH3NO2OHNO+\\1,1\C,0.4326401624,0.9738
245824,1.2547845142\H,0.7181320746,0.8401998336,2.302780443\H,1.335442
7168,0.9620341591,0.6392911324\H,-0.140027166,1.8914348428,1.104971262
7\N,-0.5128714545,-0.6906112849,-1.0287842236\O,0.3891329351,-0.370523
7819,-1.5720609716\O,-0.3483863721,-0.1932798127,0.8679637762\H,-1.245
2609223,-0.1919085797,1.2585172054\\Version=Sun64-SVR4-Unix-G98RevA.9\
HF=-245.3183611\RMSD=5.698e-09\RMSF=2.609e-06\Dipole=-0.4279332,0.1724
451,-0.1324531\PG=C01 [X(C1H4N1O2)]\\@
Zero-point correction= 0.059311
Frequencies -- 108.6319 111.5579 151.8295
Frequencies -- 323.7207 462.2024 593.2738
Frequencies -- 944.1198 1072.1415 1149.7907
Frequencies -- 1333.0435 1469.2797 1497.1237
Frequencies -- 1501.7752 2219.0617 3072.4679
Frequencies -- 3163.9777 3185.7929 3674.6887

$CH_3NO_2H^+ \rightarrow CH_3ONOH^+$ (TS)
1\1\GINC-SFNODE1\Freq\RB3LYP\6-31+G(d)\C1H4N1O2(1+)\HPC1392\22-Feb-200
5\1\\#B3LYP/6-31+G(D) OPT=(TS,EF,CALCALL,MAXCYCLES=200)\\CH3NO2H+ to
methylnitrite
TS\\1,1\C\H,1,R2\H,1,R3,2,A3\H,1,R4,2,A4,3,D4,0\N,1,R5,2,
A5,3,D5,0\O,5,R6,1,A6,2,D6,0\O,5,R7,1,A7,6,D7,0\H,6,R8,5,A8,1,D8,0\\R2
=1.08728231\R3=1.0873431\R4=1.08822816\R5=2.27430804\R6=1.31210965\R7=
1.21832291\R8=0.99793491\A3=119.95645823\A4=119.42923766\A5=104.285923
97\A6=164.23334054\A7=78.36782887\A8=109.18564195\D4=-166.9250396\D5=9
3.24420337\D6=-130.81433959\D7=163.09533438\D8=161.26682229\\Version=S
un64-SVR4-Unix-G98RevA.9\HF=-245.2203128\RMSD=8.634e-09\RMSF=6.496e-06
\Dipole=0.2000016,1.6433473,0.3180878\DipoleDeriv=0.2870452,0.1806079,
-0.0123916,0.1329007,1.2510443,0.1202025,-0.0278051,0.0104614,0.304215
8,0.137365,-0.0121519,0.0042146,-0.0255351,0.017593,0.0061552,0.000996
4,0.0505421,0.2201303,0.194153,0.0425564,-0.0238414,-0.0008361,0.04473
53,-0.0251883,-0.031012,-0.0370022,0.1480069,0.1805318,-0.0770171,0.01
78669,-0.0316084,0.0520059,-0.0195088,0.0231416,-0.0460466,0.1443102,0
.2413736,-0.6251094,-0.4064197,-0.2894827,0.9252067,0.6145583,-0.29550
98,1.1208756,0.8263333,-0.1404829,0.0616456,-0.029373,0.3213406,-1.163
9933,-0.7476433,0.017539,-0.2532187,-0.2467543,-0.2399934,0.4098372,0.
3440069,-0.1237633,-0.6039457,0.0562502,0.215481,-0.800864,-0.6240412,
0.3400082,0.0196315,0.1059362,0.0169838,0.4773547,-0.004825,0.0971693,
-0.0447478,0.2277994\Polar=22.0119925,0.2253983,42.3939799,-4.052545,5

.992718,27.2759142\PG=C01 [X(C1H4N1O2)]\NImag=1\\
Zero-point correction= 0.055754
Frequencies -- -574.6416 44.1929 107.1515
Frequencies -- 269.4438 552.2758 643.5531
Frequencies -- 705.9656 735.7249 1107.9700
Frequencies -- 1330.3122 1358.1295 1429.4327
Frequencies -- 1438.4310 1589.1829 3125.8596
Frequencies -- 3320.7962 3325.0202 3389.6572

$CH_3NO_2H^+ \rightarrow CH_3O(H)(NO)^+$ (TS)
1\1\GINC-SFNODE8\Freq\RB3LYP\6-31+G(d)\C1H4N1O2(1+)\HPC1396\15-Apr-200
5\1\\#B3LYP/6-31+G(D) OPT=(TS,EF,CALCALL)\\ch3no2ohno+TS-qst freq\\1,1
\C\H,1,R2\H,1,R3,2,A3\H,1,R4,2,A4,3,D4,0\N,1,R5,2,A5,3,D5,0\O,5,R6,1,A
6,2,D6,0\O,5,R7,1,A7,6,D7,0\H,7,R8,5,A8,1,D8,0\\R2=1.08740224\R3=1.087
40294\R4=1.08616817\R5=2.48447285\R6=1.16213688\R7=1.41404506\R8=0.995
9518\A3=119.47018424\A4=119.82439923\A5=83.2848377\A6=175.72318001\A7=
67.51113622\A8=113.36845653\D4=-169.24219248\D5=78.34831721\D6=-61.596
31634\D7=181.11524595\D8=-180.11557233\\Version=Sun64-SVR4-Unix-G98Rev
A.9\HF=-245.2281669\RMSD=5.451e-09\RMSF=1.557e-05\Dipole=-0.5375765,1.
8051447,-0.3140634\DipoleDeriv=0.275068,-0.0722307,0.0281703,0.0282096
,0.9184497,0.0164421,0.0281918,-0.0418568,0.2431174,0.1287892,-0.01399
47,-0.0040399,0.0043963,0.0036671,0.0053174,-0.0048509,0.0870015,0.188
4688,0.1700784,0.0690673,-0.0282406,0.006835,0.0038198,0.0012731,-0.02
74047,-0.0551019,0.1470227,0.1784271,-0.0805687,0.0247301,-0.0219617,0
.0896608,-0.012786,0.0247548,-0.0470377,0.150393,1.0499091,-0.1473103,
0.5409005,-0.684549,1.0228822,-0.3977493,0.5403108,-0.083998,0.4343258
,-0.2162189,0.0713248,-0.1474248,0.7090641,-1.08354,0.4119926,-0.14623
48,0.0397748,-0.0481335,-0.9504547,0.0130981,-0.3821222,-0.0864146,-0.
2636588,-0.0499691,-0.3828962,0.0078798,-0.5161266,0.3644021,0.1606141
,-0.031973,0.0444194,0.3087215,0.0254787,-0.031871,0.0933375,0.4009324
\Polar=28.4758248,-5.0603595,58.1175484,5.1193287,-2.9244929,22.655187
2\PG=C01 [X(C1H4N1O2)]\NImag=1\\
Zero-point correction= 0.054611
Frequencies -- -395.8293 32.5314 75.8380
Frequencies -- 244.0178 491.1860 544.9471
Frequencies -- 608.5205 622.5639 883.3413
Frequencies -- 1237.8406 1295.1837 1429.1061
Frequencies -- 1437.9769 1842.5817 3130.1773
Frequencies -- 3326.2227 3333.5178 3435.8078

$(CH_3)_3CNO_2$
1\1\GINC-SFNODE9\FOpt\RB3LYP\6-31+G(d)\C4H9N1O2\HPC1397\18-Apr-2004\0\
\#B3LYP/6-31+G(D) OPT=(MAXCYCLES=150) FREQ\\3methyl (CH3)3CNO2\\0,1\C,
-0.0069392722,0.011894719,-0.5644642362\N,-0.0047034261,0.0082181831,0
.9904641138\C,1.4671090088,0.0113596815,-0.9943771881\C,-0.7406518015,
1.257319212,-1.057644027\C,-0.7210215733,-1.2776814978,-0.9942653812\O
,0.552918504,-0.9388283822,1.5411974048\O,-0.5506382832,0.9344250381,1
.5833339756\H,1.9816584536,0.912644492,-0.6432117448\H,1.9898895262,-0
.8667941239,-0.6072933398\H,1.5167675468,-0.0044769773,-2.0884791286\H
,-0.7353517317,1.2482396381,-2.1534190925\H,-1.7794263201,1.2760260547
,-0.7169788721\H,-0.2534671448,2.1749802142,-0.7170477459\H,-0.2063092

944,-2.1605885069,-0.6071809601\H,-1.7587332746,-1.2908416429,-0.64301
97351\H,-0.7313237157,-1.3288423648,-2.0883642267\\Version=Sun64-SVR4-
Unix-G98RevA.9\HF=-362.9777101\RMSD=5.644e-09\RMSF=4.320e-05\Dipole=0.
0011653,-0.0016614,-1.6160497\PG=C01 [X(C4H9N1O2)]\\@
Zero-point correction= 0.134771
Frequencies -- 36.0538 196.2212 255.1200
Frequencies -- 263.9773 285.4702 289.9423
Frequencies -- 354.9205 369.5472 385.5022
Frequencies -- 524.7491 559.1013 737.3241
Frequencies -- 802.2150 859.0525 945.8002
Frequencies -- 947.1392 985.9258 1062.6877
Frequencies -- 1062.8072 1217.5342 1266.1799
Frequencies -- 1289.6809 1398.9692 1420.4176
Frequencies -- 1426.9352 1462.8058 1495.7313
Frequencies -- 1506.7456 1513.1395 1520.7768
Frequencies -- 1522.1082 1543.5965 1623.0006
Frequencies -- 3059.0920 3060.0193 3067.9858
Frequencies -- 3124.9878 3125.3896 3134.2948
Frequencies -- 3149.7095 3150.9669 3154.1634

$(CH_3)_3CONO$ (trans)
1\1\GINC-SFNODE5\FOpt\RB3LYP\6-31+G(d)\C4H9N1O2\HPC1418\25-Nov-2004\0\
\#B3LYP/6-31+G(D) OPT FREQ GEOM=CHECK GUESS=CHECK\\3methyl (CH3)3CNO2\
\0,1\C,-0.00143764,0.7561487162,0.0249709753\C,0.0032682212,0.87916139
15,1.552100997\C,1.3938344518,0.9509007051,-0.577157621\C,-1.018348407
,1.7076170647,-0.6076860162\H,0.7096284878,0.1776957284,2.0064509671\H
,-0.9950387402,0.6816553895,1.957807944\H,0.2963347661,1.8949026193,1.
8418021988\H,1.3694428555,0.8025721168,-1.6623477474\H,2.1162209097,0.
2515105953,-0.1453999993\H,1.7446123489,1.9702117783,-0.3783636553\H,-
2.0214653295,1.5258596601,-0.2081565324\H,-1.0494712618,1.5762284308,-
1.6942313241\H,-0.7409614029,2.7453908528,-0.3911147657\N,0.2704174467
,-1.6251949783,0.1200444426\O,-0.1771904976,-2.6759092119,-0.206432355
5\O,-0.5210750669,-0.5756694866,-0.3585836688\\Version=Sun64-SVR4-Unix
-G98RevA.9\HF=-362.974429\RMSD=2.945e-09\RMSF=1.337e-05\Dipole=0.27148
7,1.2633353,0.2196476\PG=C01 [X(C4H9N1O2)]\\@
Zero-point correction= 0.132601
Frequencies -- 103.2009 160.9144 199.9310
Frequencies -- 205.8653 263.0951 267.9189
Frequencies -- 336.1777 342.5547 370.9315
Frequencies -- 465.6537 487.6807 583.8304
Frequencies -- 790.1171 826.7487 931.9096
Frequencies -- 938.6671 967.4726 977.4463
Frequencies -- 1059.2867 1067.0817 1222.6026
Frequencies -- 1277.2819 1295.9656 1422.1496
Frequencies -- 1423.6359 1449.9249 1495.9001
Frequencies -- 1510.6041 1510.7607 1521.7096
Frequencies -- 1522.0186 1542.8163 1723.3404
Frequencies -- 3052.7065 3053.7004 3061.2579
Frequencies -- 3119.1812 3120.4300 3129.1228
Frequencies -- 3132.4716 3134.5469 3136.4131

$(CH_3)_3CONO$ (cis)
1\1\GINC-MS10\FOpt\RB3LYP\6-31+G(d)\C4H9N1O2\POON\22-Oct-2004\0\\#B3LY
P/6-31+G(D) OPT=(MAXCYCLES=150) FREQ\\3methylONO\\0,1\C,-0.3904323815,
-0.0330967951,-0.5151981351\O,-0.4840125294,0.1213241138,0.969318618\N
,0.6259738079,0.1510235693,1.7955168999\O,1.6887167019,0.0454288519,1.
2614897469\C,0.3574652678,1.1554111673,-1.1309019875\H,-0.0604607956,2
.1007865315,-0.7680138545\H,1.4264311191,1.1347998358,-0.9113695659\H,
0.2316476092,1.126547944,-2.2199605799\C,0.2329727841,-1.3872818304,-0
.873891797\H,1.3009965332,-1.4265838991,-0.6522454478\H,-0.270884496,-
2.1961497685,-0.3336106004\H,0.1001528865,-1.5647107476,-1.9479526535\
C,-1.871231774,0.0000837851,-0.9060498056\H,-2.3322593286,0.9467197936
,-0.6059617742\H,-1.9687267083,-0.105256518,-1.9925764648\H,-2.4189902
337,-0.8180398445,-0.4271439269\\Version=x86-Linux-G98RevA.7\HF=-362.9
692985\RMSD=3.740e-09\RMSF=8.795e-06\Dipole=-0.3711082,-0.0915709,-1.0
849182\PG=C01 [X(C4H9N1O2)]\\@

Zero-point correction=		0.132731	
Frequencies --	93.5827	195.4385	211.6699
Frequencies --	234.7327	241.4918	266.2830
Frequencies --	308.8666	372.7854	397.2684
Frequencies --	432.5985	489.3529	671.0540
Frequencies --	769.8342	826.1503	926.7541
Frequencies --	937.1974	954.2535	981.0365
Frequencies --	1058.3094	1064.7053	1211.9947
Frequencies --	1273.8837	1282.4944	1422.3860
Frequencies --	1424.0290	1449.3748	1494.8735
Frequencies --	1511.1680	1512.0380	1519.2750
Frequencies --	1526.1460	1546.0254	1669.5129
Frequencies --	3053.2449	3055.1859	3062.4350
Frequencies --	3116.3373	3116.4455	3126.9541
Frequencies --	3133.8979	3159.4234	3161.6496

$(CH_3)_3CNO_2$ → $(CH_3)_3CONO$ (TS)
1\1\GINC-SFNODE6\Freq\RB3LYP\6-31+G(d)\C4H9N1O2\HPC1418\24-Nov-2004\1\
\#B3LYP/6-31+G(D) OPT=(TS,EF,CALCALL) GEOM=CHECK GUESS=CHECK\\3methyl
(CH3)3CNO2\\0,1\C\C,1,R2\C,1,R3,2,A3\C,1,R4,2,A4,3,D4,0\H,2,R5,1,A5,3,
D5,0\H,2,R6,1,A6,5,D6,0\H,2,R7,1,A7,5,D7,0\H,3,R8,1,A8,2,D8,0\H,3,R9,1
,A9,8,D9,0\H,3,R10,1,A10,8,D10,0\H,4,R11,1,A11,2,D11,0\H,4,R12,1,A12,1
1,D12,0\H,4,R13,1,A13,11,D13,0\N,1,R14,2,A14,3,D14,0\O,14,R15,1,A15,2,
D15,0\O,14,R16,1,A16,15,D16,0\\R2=1.4895295\R3=1.495398\R4=1.49475043\
R5=1.09197277\R6=1.09040264\R7=1.10518099\R8=1.09281505\R9=1.09039426\
R10=1.10583369\R11=1.0895763\R12=1.09278106\R13=1.10497583\R14=2.31561
258\R15=1.22162604\R16=1.28137637\A3=117.68660546\A4=118.42847869\A5=1
11.91598413\A6=112.06943524\A7=106.53934999\A8=112.05897872\A9=112.536
87685\A10=106.6484078\A11=112.46563452\A12=111.68410475\A13=106.764404
37\A14=96.72826911\A15=163.87253444\A16=75.03533406\D4=-147.96427229\D
5=-46.11030013\D6=-124.18456114\D7=117.38785334\D8=161.9359179\D9=-123
.96163911\D10=116.99483615\D11=-35.164273\D12=-123.54784111\D13=119.63
267694\D14=92.99259302\D15=-133.09800475\D16=-142.29310501\\Version=Su
n64-SVR4-Unix-G98RevA.9\HF=-362.8907502\RMSD=2.576e-09\RMSF=4.504e-05\
Dipole=0.7594461,2.834495,0.3813508

Zero-point correction=		0.129233

Frequencies -- -507.2672 26.3035 75.4778
Frequencies -- 186.7828 206.7697 229.9090
Frequencies -- 234.8532 259.7735 273.3759
Frequencies -- 395.2134 401.8620 430.8551
Frequencies -- 766.3387 781.4623 878.9108
Frequencies -- 889.6545 987.3346 1028.3027
Frequencies -- 1054.6490 1131.8706 1210.8075
Frequencies -- 1312.7341 1320.5841 1409.6117
Frequencies -- 1416.6379 1429.4599 1453.2758
Frequencies -- 1480.0521 1490.0711 1495.5026
Frequencies -- 1506.7466 1527.9340 1537.0321
Frequencies -- 2978.3853 2988.7136 2998.1412
Frequencies -- 3120.6335 3126.5790 3129.8615
Frequencies -- 3180.6783 3184.9099 3188.5872

$(CH_3)_3CNO_2H^+$

1\1\GINC-SFNODE7\FOpt\RB3LYP\6-31+G(d)\C4H10N1O2(1+)\HPC1397\20-Apr-20
04\0\\#B3LYP/6-31+G(D) OPT=(MAXCYCLES=150) FREQ\\3methylH+\\1,1\C,-0.0
302914027,-0.0520544375,-0.646996992\N,-0.0305895375,-0.0524240938,0.9
260269717\C,1.4547956015,-0.0507293629,-1.0536638878\C,-0.761476461,1.
2405071698,-1.0538305612\C,-0.7683082641,-1.3188463085,-1.0634128192\O
,0.5838091798,1.0022186391,1.4680687889\O,-0.5140916041,-0.8821938426,
1.6166937818\H,1.478244416,-0.0879836382,-2.1475750586\H,1.9718905628,
0.855871502,-0.7317262311\H,1.9810701243,-0.9328703153,-0.6764428302\H
,-0.8053687402,1.242445451,-2.1477454027\H,-1.788451384,1.2633406292,-
0.6766909107\H,-0.2278198004,2.1374712964,-0.7319296267\H,-0.264842892
4,-2.2261433905,-0.7177294685\H,-1.8059183721,-1.3282991379,-0.7178129
086\H,-0.7790472263,-1.3373830821,-2.1574676931\H,0.5283126271,0.90705
8605,2.4522563247\\Version=Sun64-SVR4-Unix-G98RevA.9\HF=-363.2814336\R
MSD=7.979e-09\RMSF=6.302e-05\Dipole=0.1989985,0.3416167,0.4867815\PG=C
01 [X(C4H10N1O2)]\\@

Zero-point correction= 0.146065
Frequencies -- 38.9737 194.0718 246.5503
Frequencies -- 259.1880 262.1834 286.3309
Frequencies -- 324.6635 344.4627 375.3639
Frequencies -- 476.2837 494.9144 597.2017
Frequencies -- 710.7703 719.5867 757.2324
Frequencies -- 933.7979 941.8111 997.1477
Frequencies -- 1043.6838 1058.2094 1112.1662
Frequencies -- 1165.5541 1244.7503 1287.4223
Frequencies -- 1413.2240 1425.5996 1436.5865
Frequencies -- 1464.1916 1488.6700 1500.9038
Frequencies -- 1504.3924 1514.4992 1516.6291
Frequencies -- 1538.1454 1753.9948 3073.4366
Frequencies -- 3073.8474 3079.4053 3146.7973
Frequencies -- 3147.1167 3154.3932 3157.9565
Frequencies -- 3168.0484 3171.4945 3513.3060

$(CH_3)_3C^+\cdots NO_2H$

1\1\GINC-SFNODE1\FOpt\RB3LYP\6-31+G(d)\C4H10N1O2(1+)\HPC1471\02-Jul-20
05\0\\#B3LYP/6-31+G(D) OPT=TIGHT FREQ GUESS=CHECK GEOM=CHECK\\3nitrite

isoTS (tempA,oxygen pointing)\\1,1\C,1.4301602328,-0.0447177503,-0.000
0562748\C,1.465949565,-0.7785446741,-1.2730168963\C,1.4663879735,-0.77
23827656,1.2764191409\C,1.4853950606,1.4196097995,-0.0035633321\H,2.54
47923294,-0.9214677407,-1.4894576164\H,1.0178879505,-1.7729866089,-1.2
176121204\H,1.0699430876,-0.1968479524,-2.1107472983\H,1.0714484787,-0
.1863844943,2.1116456987\H,2.5452974171,-0.9151276105,1.4926496924\H,1
.0175721542,-1.766755328,1.2261063416\H,0.4248995451,1.7506796658,-0.0
037887771\H,1.9329452406,1.836296948,0.9039816437\H,1.9321525324,1.832
0531148,-0.9134254223\N,-1.497169091,0.0276504433,0.0002822769\O,-2.44
94494104,-0.938444706,0.0001373603\O,-1.9039023664,1.1510996346,-0.000
1112064\H,-3.3372978751,-0.4980401829,-0.0002331377\\Version=Sun64-SVR
4-Unix-G98RevA.9\HF=-363.2747341\RMSD=7.847e-10\RMSF=2.064e-06\Dipole=
1.5525216,-0.1806932,-0.0003192\PG=C01 [X(C4H10N1O2)]\\@

Zero-point correction=	0.139351		
Frequencies --	30.3793	32.3440	74.7404
Frequencies --	90.0040	105.6532	124.9998
Frequencies --	162.0412	195.2238	225.9153
Frequencies --	409.0007	410.2677	434.3253
Frequencies --	671.7192	731.7689	760.7769
Frequencies --	761.5653	857.7298	985.9543
Frequencies --	1002.1605	1002.7042	1025.2229
Frequencies --	1126.0699	1320.2243	1336.0896
Frequencies --	1364.7118	1370.1651	1377.7267
Frequencies --	1396.1313	1429.5400	1445.8146
Frequencies --	1457.2129	1509.4623	1518.0776
Frequencies --	1527.5447	1697.6768	2946.2689
Frequencies --	2964.8343	2977.5438	3096.0626
Frequencies --	3106.4557	3109.8154	3163.0865
Frequencies --	3174.9751	3180.7609	3477.2009

$(CH_3)_3C^+\cdots O(H)NO$

1\1\GINC-SFNODE8\FOpt\RB3LYP\6-31+G(d)\C4H10N1O2(1+)\HPC1532\19-Apr-20
05\0\\#B3LYP/6-31+G(D) OPT FREQ GEOM=CHECK GUESS=CHECK\\3methyl nitrit
e TS ircropt\\1,1\C,1.677768043,0.1910825723,0.04519959\C,1.7639758732
,-0.7911317256,-1.0356891402\C,1.9640933794,-0.2207023878,1.4237754466
\C,1.2416421794,1.5615206627,-0.2271755584\H,2.4463785346,-1.618004954
9,-0.8148185595\H,0.744224941,-1.234397812,-1.0552968838\H,1.943629936
9,-0.355934241,-2.0213710304\H,1.4416846061,0.382507209,2.1722600149\H
,3.0460379014,-0.013096183,1.560385312\H,1.833249003,-1.2935813287,1.5
912625871\H,0.130641342,1.5043631436,-0.1832390321\H,1.5385722946,2.27
33196654,0.5488792573\H,1.493205456,1.9130415975,-1.2311988386\N,-2.07
67903118,0.2665074877,-0.1314977812\O,-1.4700716776,-1.0223069475,-0.0
303698207\O,-3.2507600359,0.2489783757,-0.0882743404\H,-2.1983149751,-
1.6817556641,0.0661129026\\Version=Sun64-SVR4-Unix-G98RevA.9\HF=-363.2
749127\RMSD=5.485e-09\RMSF=1.023e-04\Dipole=2.1991994,-0.2501585,0.177
2592\PG=C01 [X(C4H10N1O2)]\\@

Zero-point correction=	0.138232		
Frequencies --	19.3882	25.2429	55.9503
Frequencies --	62.6288	91.9971	94.3953
Frequencies --	125.2789	209.8471	222.2403
Frequencies --	408.3623	410.5229	438.0675

Frequencies -- 562.9718 668.6246 724.9572
Frequencies -- 760.5922 834.6306 854.5268
Frequencies -- 993.8682 1003.4611 1026.9321
Frequencies -- 1129.1089 1316.7876 1324.9970
Frequencies -- 1336.8311 1358.1253 1371.5405
Frequencies -- 1390.2931 1424.2471 1439.6074
Frequencies -- 1455.2063 1511.9824 1516.8516
Frequencies -- 1529.0156 1782.5202 2922.3689
Frequencies -- 2943.4214 2968.8866 3100.9508
Frequencies -- 3101.9194 3104.8101 3168.4931
Frequencies -- 3170.3713 3176.7935 3537.0673

$(CH_3)_3CO(H)(NO)^+$
1\1\GINC-SFNODE7\FOpt\RB3LYP\6-31+G(d)\C4H10N1O2(1+)\HPC1532\17-Apr-20
05\0\\#B3LYP/6-31+G(D) OPT FREQ GEOM=CHECK GUESS=CHECK\\3methyl nitrit
e TS ircropt\\1,1\C,0.4478862812,-0.8079699734,-0.0315635103\C,0.48422
14414,-0.9869345256,1.4830494559\C,1.7755825338,-1.1639968642,-0.70419
04385\C,-0.7446286473,-1.4837079,-0.6959809886\H,0.6347910865,-2.04541
54848,1.7193813439\H,1.3120272179,-0.4306945928,1.9386197685\H,-0.4569
515202,-0.6767609516,1.9501028532\H,1.7465349602,-0.9598128463,-1.7780
929809\H,1.9611122974,-2.234824421,-0.562533815\H,2.6190947482,-0.6257
345783,-0.255593342\H,-1.6913558807,-1.2040951316,-0.2214774524\H,-0.7
90220461,-1.2477076655,-1.7635350542\H,-0.6401639525,-2.568490795,-0.5
945120097\N,-1.350268218,1.5612104578,0.2514296419\O,0.2685498544,0.67
76273789,-0.3332037542\O,-1.2765014071,2.6402078141,0.0200385582\H,1.0
42251797,1.1780372986,0.0050676523\\Version=Sun64-SVR4-Unix-G98RevA.9\
HF=-363.2853659\RMSD=9.337e-09\RMSF=2.424e-05\Dipole=-0.3198925,1.2341
472,0.3496114\PG=C01 [X(C4H10N1O2)]\\@
Zero-point correction= 0.143121
Frequencies -- 39.5366 64.6514 107.8788
Frequencies -- 208.8184 220.2054 266.8797
Frequencies -- 275.2477 326.8702 338.2441
Frequencies -- 408.8855 429.9748 448.1244
Frequencies -- 509.0726 582.0070 707.9250
Frequencies -- 794.8405 928.2043 938.4904
Frequencies -- 984.6327 1038.1082 1052.7751
Frequencies -- 1158.9366 1176.1951 1278.0223
Frequencies -- 1339.7416 1428.1073 1436.6019
Frequencies -- 1459.9663 1494.9417 1498.2943
Frequencies -- 1503.0635 1522.0448 1526.5223
Frequencies -- 1535.4793 2175.6040 3053.4074
Frequencies -- 3057.5304 3067.3786 3120.7522
Frequencies -- 3124.9940 3134.4038 3139.0110
Frequencies -- 3146.7229 3151.6155 3622.3064

$(CH_3)_3CNO_2H^+ \rightarrow (CH_3)_3C^+\cdots NO_2H$ (TS)
1\1\GINC-SFNODE4\Freq\RB3LYP\6-31+G(d)\C4H10N1O2(1+)\HPC1396\16-Feb-20
05\1\\#B3LYP/6-31+G(D) OPT=(TS,EF,CALCALL)\\3methyl nitrite int\\1,1\C
\C,1,B2\C,1,B3,2,A3\C,1,B4,2,A4,3,D4,0\H,2,B5,1,A5,4,D5,0\H,2,B6,1,A6,
4,D6,0\H,2,B7,1,A7,4,D7,0\H,3,B8,1,A8,2,D8,0\H,3,B9,1,A9,2,D9,0\H,3,B1
0,1,A10,2,D10,0\H,4,B11,1,A11,2,D11,0\H,4,B12,1,A12,2,D12,0\H,4,B13,1,

A13,2,D13,0\N,1,B14,2,A14,4,D14,0\O,14,B15,1,A15,2,D15,0\O,14,B16,1,A1
6,2,D16,0\H,15,B17,14,A17,1,D17,0\\B2=1.47455477\B3=1.47140577\B4=1.47
337796\B5=1.10786388\B6=1.09350212\B7=1.0925128\B8=1.09428533\B9=1.109
05671\B10=1.09145235\B11=1.10151417\B12=1.09112935\B13=1.1019568\B15=1
.3619947\B16=1.18921495\B17=0.9908642\A3=119.82780239\A4=119.20737958\
A5=105.3427009\A6=112.65260235\A7=113.50426092\A8=112.42807755\A9=104.
91203729\A10=114.03587715\A11=109.35106672\A12=113.91358501\A13=108.88
530013\A14=93.10819425\A15=120.66012708\A16=123.19222487\A17=108.24013
066\D4=168.77877894\D5=93.86541932\D6=-151.24413219\D7=-23.05888879\D8
=-153.49458283\D9=92.67893847\D10=-24.97270481\D11=65.33617103\D12=188
.34459981\D13=-48.04475921\D14=94.67596788\D15=77.5313333\D16=-100.991
43611\D17=-178.74747265\B14=2.65628048\\Version=Sun64-SVR4-Unix-G98Rev
A.9\HF=-363.2744036\RMSD=4.144e-09\RMSF=4.317e-05\Dipole=0.3241927,-1.
2956337,0.1451663\DipoleDeriv=0.990534,-0.0950064,-0.0563199,-0.042748
3,1.0247941,-0.034518,0.0096837,-0.064751,0.9515269,-0.0548469,0.05169
8,-0.1391696,0.0079168,-0.2419517,0.2645538,-0.0680346,0.1811341,-0.51
03775,-0.3422656,0.1689756,0.2125187,0.2693296,-0.2303836,-0.144158,0.
2802821,-0.1158317,-0.23799,-0.5926933,-0.1122322,-0.1956176,-0.003094
6,-0.1745122,0.0130357,-0.0048765,0.0525305,0.0057611,0.1408701,0.0098
596,0.0523245,0.0254188,0.0801406,-0.1032953,0.0083742,-0.0083108,0.13
22022,0.0505009,-0.0696313,0.0577466,-0.0520513,0.0993646,-0.0686057,0
.0224109,-0.0032925,0.1044099,0.0026888,0.0235611,0.0093785,0.019167,0
.1258643,-0.0703216,-0.0115133,-0.0077132,0.0861736,0.0535037,0.026276
1,-0.0387249,-0.0566039,0.1249541,0.0716468,-0.0693538,0.0494084,0.084
0635,0.1177083,-0.0053125,0.0156773,-0.1077992,0.0828054,0.0535347,-0.
0239895,0.0152204,0.1657734,0.0800172,-0.0267596,-0.0210365,-0.0830156
,0.1160086,0.0010385,-0.0285709,-0.0386158,0.0303011,0.1970526,0.01126
99,0.0317286,0.028585,0.1484935,-0.0407353,-0.0548912,-0.070947,0.0623
91,0.0733503,-0.0011035,0.0434191,-0.0121313,0.1036885,-0.003433,0.002
4231,-0.0125945,-0.0030021,0.191553,0.0090215,0.0253158,-0.0200103,0.0
961239,0.0404502,-0.0615438,0.0123339,0.0376573,1.5497112,0.3256235,0.
326759,0.2554756,0.6578666,0.037502,0.3153744,0.0750868,0.0986785,-0.7
7717337,-0.2530524,-0.1097342,-0.7151525,-0.7844208,-0.1365033,-0.10631
61,-0.0487017,-0.264681,-0.8868307,-0.1232476,-0.1771402,0.4220572,-0.
5308989,0.1034892,-0.1717902,-0.0263009,-0.1090898,0.200883,0.0600576,
-0.0371253,0.0646562,0.302064,0.0163185,-0.0376693,0.0113455,0.3662057
\Polar=69.1395529,0.2158404,76.1140067,2.2931521,-0.7283896,57.3562298
\PG=C01 [X(C4H10N1O2)]\NImag=1\\

Zero-point correction= 0.139586

Frequencies --	-65.7476	31.2042	68.8349
Frequencies --	75.2610	94.4177	166.8164
Frequencies --	169.8059	196.0703	217.4657
Frequencies --	406.7534	414.2718	431.9992
Frequencies --	664.7768	718.3176	774.6751
Frequencies --	789.8499	849.8556	973.1353
Frequencies --	987.1598	1009.4607	1031.0627
Frequencies --	1129.0642	1314.2795	1329.2055
Frequencies --	1361.0467	1377.7421	1384.9146
Frequencies --	1392.8796	1438.2349	1458.4469
Frequencies --	1462.9240	1503.5254	1514.8206
Frequencies --	1530.7437	1721.5553	2971.9049

Frequencies -- 2986.3542 3022.9361 3062.1012
Frequencies -- 3108.4755 3112.5255 3174.5640
Frequencies -- 3175.4412 3182.5018 3483.6467

$(CH_3)_3C^+\cdots NO_2H \rightarrow (CH_3)_3C^+\cdots O(H)NO$ (TS)
1\1\GINC-SFNODE1\Freq\RB3LYP\6-31+G(d)\C4H10N1O2(1+)\HPC1471\27-Jun-20
05\1\\#B3LYP/6-31+G(D) OPT=(TS,EF,CALCALL,MAXCYCLES=200) FREQ\\3nitrit
eisoTS (tempA,oxygen pointing)\\1,1\C\C,1,R2\C,1,R3,2,A3\C,1,R4,2,A4,3
,D4,0\H,2,R5,1,A5,3,D5,0\H,2,R6,1,A6,5,D6,0\H,2,R7,1,A7,5,D7,0\H,3,R8,
1,A8,2,D8,0\H,3,R9,1,A9,8,D9,0\H,3,R10,1,A10,8,D10,0\H,4,R11,1,A11,2,D
11,0\H,4,R12,1,A12,11,D12,0\H,4,R13,1,A13,11,D13,0\N,1,R14,2,A14,3,D14
,0\O,14,R15,1,A15,2,D15,0\O,14,R16,15,A16,1,D16,0\H,15,R17,14,A17,1,D1
7,0\\R5=1.10733349\R6=1.0983581\R7=1.09120692\R8=1.09681916\R9=1.10878
295\R10=1.09119173\R11=1.10872349\R12=1.09229946\R13=1.0967035\A5=106.
69741883\A6=110.61979238\A7=114.11137238\A8=111.6859472\A9=105.4551761
\A10=114.22212479\A11=104.87265651\A12=114.14875904\A13=112.16685774\D
5=-64.50721694\D6=113.16315663\D7=-120.11952253\D8=-145.55824257\D9=-1
13.00118104\D10=128.1191453\D11=78.89332519\D12=117.59688826\D13=-113.
40365684\R2=1.46704688\R3=1.46776377\R4=1.46565227\R16=1.18453815\R17=
0.98904817\A3=119.98180635\A4=120.23127779\A16=114.89254064\A17=107.93
214077\D4=-182.73513596\D16=-178.13911946\D17=178.24783278\R14=3.16896
672\R15=1.39005646\A14=87.67391003\A15=98.25769998\D14=-86.7275608\D15
=45.03103952\\Version=Sun64-SVR4-Unix-G98RevA.9\HF=-363.2739722\RMSD=6
.064e-09\RMSF=2.270e-05\Dipole=0.0361076,-1.9678702,0.0334365\DipoleDe
riv=1.0383465,-0.1136832,-0.023349,-0.0333648,0.5026763,0.0178814,0.05
2126,-0.0122551,1.0351868,-0.0622837,0.0260321,-0.3127706,-0.0363701,-
0.1573967,0.1690602,-0.1089741,0.1022032,-0.5855138,-0.3194955,0.12846
79,0.233788,0.2455499,-0.1644036,-0.162922,0.3503811,-0.0888528,-0.328
3167,-0.5886009,0.0316609,-0.2287948,0.2768091,-0.0881628,0.1557527,-0
.1113916,0.0426397,-0.0720029,0.1310963,0.0297498,0.1153636,0.039061,0
.1014265,-0.0743168,0.0272193,-0.0389536,0.1563872,0.0817033,-0.047946
5,0.1237979,-0.0331557,0.1599614,-0.0386836,0.0273867,-0.0025417,0.137
5495,0.0067658,0.0067704,0.0319046,0.0102857,0.1189813,-0.0419941,-0.0
054512,-0.007443,0.0780504,0.0567883,0.0276683,-0.0293426,-0.0399049,0
.1283371,0.0739579,-0.088873,0.0497343,0.1325595,0.1050912,-0.0414695,
0.0163634,-0.1102697,0.0935192,0.0381648,-0.0544979,0.0089384,0.186822
6,0.0705406,-0.0257806,-0.0208683,-0.0662471,0.1285862,0.0090527,-0.04
03326,-0.0205277,0.034115,0.1981502,-0.0086513,0.0163895,-0.0937604,0.
0876277,-0.0756743,-0.0500372,-0.0420444,0.1106999,0.071519,0.0098038,
0.0436407,-0.0511268,0.110254,-0.0452468,0.0284137,-0.0174332,0.035834
1,0.1579788,-0.0040817,0.0347505,-0.0815837,0.1117067,-0.004938,-0.028
2267,0.0307007,0.0243532,0.8080654,-0.2280086,0.7986908,-0.377259,0.56
16952,-0.4034608,0.800037,-0.2708784,0.8625088,-0.7585406,0.1521015,-0
.4916153,-0.202743,-0.2473493,-0.2114546,-0.4616762,0.1523321,-0.76425
68,-0.3222557,-0.0003204,-0.2596807,0.518997,-0.6372325,0.5485259,-0.2
896722,0.0393335,-0.3625334,0.3251346,0.0576855,-0.048269,0.0350816,0.
1897736,0.0462971,-0.046431,0.0750476,0.3185586\Polar=64.0465785,-1.19
65949,62.8126404,6.0092831,-1.2493541,64.4258909\PG=C01 [X(C4H10N1O2)]
\NImag=1\\
Zero-point correction= 0.138293
Frequencies -- -48.5884 17.5530 49.2771

Frequencies --	57.8128	75.7940	95.3683
Frequencies --	119.3340	135.9490	180.3621
Frequencies --	401.6148	407.5536	438.9256
Frequencies --	627.5029	700.7835	756.5514
Frequencies --	792.0265	834.6035	901.4639
Frequencies --	996.5873	1001.7457	1012.3546
Frequencies --	1127.2423	1318.9812	1322.0325
Frequencies --	1338.8160	1365.6276	1375.8947
Frequencies --	1376.6148	1434.0484	1446.4474
Frequencies --	1461.2449	1510.4366	1515.2429
Frequencies --	1525.5029	1742.7312	2974.6731
Frequencies --	2980.1733	2992.5290	3078.4257
Frequencies --	3088.8294	3090.3766	3169.9672
Frequencies --	3177.0044	3180.8384	3506.8101
Frequencies --	-48.6025	17.5540	49.2771
Frequencies --	57.8128	75.7932	95.3719
Frequencies --	119.3350	135.9410	180.3618
Frequencies --	401.6151	407.5546	438.9249
Frequencies --	627.5016	700.7851	756.5368
Frequencies --	792.0262	834.6029	901.4639
Frequencies --	996.5879	1001.7479	1012.3553
Frequencies --	1127.2423	1318.9824	1322.0288
Frequencies --	1338.8160	1365.6267	1375.8958
Frequencies --	1376.6144	1434.0482	1446.4473
Frequencies --	1461.2450	1510.4385	1515.2431
Frequencies --	1525.5021	1742.7354	2974.6730
Frequencies --	2980.1708	2992.5192	3078.4293
Frequencies --	3088.8301	3090.3744	3169.9676
Frequencies --	3177.0069	3180.8396	3506.8426

$(CH_3)_3C^+\cdots O(H)(NO) \rightarrow (CH_3)_3CO(H)(NO)^+$ (TS)

1\1\GINC-SFNODE9\Freq\RB3LYP\6-31+G(d)\C4H10N1O2(1+)\HPC1397\03-Feb-20
05\1\\#B3LYP/6-31+G(D) OPT=(TS,EF,CALCALL,MAXCYCLES=200)\\3methyl nitr
ite int\\1,1\C\C,1,R2\C,1,R3,2,A3\C,1,R4,2,A4,3,D4,0\H,2,R5,1,A5,3,D5,
0\H,2,R6,1,A6,5,D6,0\H,2,R7,1,A7,5,D7,0\H,3,R8,1,A8,2,D8,0\H,3,R9,1,A9
,8,D9,0\H,3,R10,1,A10,8,D10,0\H,4,R11,1,A11,2,D11,0\H,4,R12,1,A12,11,D
12,0\H,4,R13,1,A13,11,D13,0\N,1,R14,2,A14,3,D14,0\O,14,R15,1,A15,2,D15
,0\O,14,R16,1,A16,15,D16,0\H,15,R17,14,A17,1,D17,0\\R2=1.48046401\R3=1
.4815089\R4=1.48031086\R5=1.1059815\R6=1.09188351\R7=1.09184256\R8=1.0
9247417\R9=1.10576301\R10=1.09256245\R11=1.09201372\R12=1.0917715\R13=
1.10579888\R14=3.42041182\R15=1.55061113\R16=1.15062751\R17=0.98500566
\A3=118.9560755\A4=119.08784115\A5=105.41941142\A6=112.96842813\A7=112
.94416854\A8=112.90647082\A9=105.51836251\A10=113.10136316\A11=112.942
64325\A12=112.90999101\A13=105.42081073\A14=88.65715994\A15=30.8322153
2\A16=143.0503478\A17=107.58254125\D4=159.83354984\D5=-79.26504789\D6=
116.38094368\D7=-116.37479066\D8=-163.01230916\D9=-116.01025999\D10=12
7.87223294\D11=36.70903108\D12=127.24100212\D13=-116.23407749\D14=-119
.36004644\D15=112.14022051\D16=-4.51229688\D17=-176.53385863\\Version=
Sun64-SVR4-Unix-G98RevA.9\HF=-363.2723385\RMSD=5.959e-09\RMSF=2.581e-0
5\Dipole=0.834043,-1.1869884,-0.0705183\DipoleDeriv=0.8951058,-0.02522
09,0.0055728,-0.2610352,1.4443757,0.0006991,0.0467952,-0.082728,0.9040

866,-0.0564492,0.0303787,-0.0410198,0.0608778,-0.1972893,0.2080892,-0.
0432116,0.1518408,-0.4407606,-0.3818226,0.1614068,0.1625198,0.26493,-0
.2613825,-0.0912444,0.1553928,-0.0462381,-0.1161057,-0.245961,-0.16735
96,-0.1183628,-0.1878113,-0.3313836,-0.1452378,-0.1108648,-0.0939915,-
0.1139336,0.1402488,0.0162344,0.017523,0.0147426,0.0513594,-0.0892079,
-0.0034994,-0.0081285,0.1222774,0.0367646,-0.0661379,0.0200957,-0.0591
526,0.0893927,-0.0666318,0.0177355,-0.0084575,0.0813457,-0.0037106,0.0
302941,0.0061169,0.0199816,0.1220687,-0.0715002,-0.0098508,-0.0115647,
0.0822649,0.0622721,0.0039054,-0.0423804,-0.058977,0.1231075,0.0585851
,-0.0377395,0.0404639,0.0252123,0.1247514,0.0047575,0.0068757,-0.07044
47,0.0521293,0.0558063,0.0195758,0.0139121,0.1303988,0.0862402,-0.0455
106,-0.0188526,-0.095591,0.0857449,-0.0149958,-0.0097872,-0.0551409,0.
0269581,0.0459899,0.0236525,0.0205279,0.0719632,0.1309817,-0.0080431,0
.0261205,-0.0480945,0.0279346,0.0531304,-0.0291718,0.0216097,0.0215798
,0.1326072,0.065739,0.0122259,0.0389498,0.0247569,0.1065882,0.0202912,
-0.0265854,0.0870277,0.084799,0.0540557,-0.023512,0.0093336,0.1258431,
1.0602536,-1.099813,-0.1517118,-1.2274638,2.1945581,0.1205788,-0.15340
26,0.1029616,0.1543647,-1.0967328,1.079746,0.0881182,0.480943,-1.28352
87,-0.018332,0.1739229,-0.2202786,-0.4068651,-0.0246219,-0.1040614,0.0
353847,0.8717429,-1.5079843,-0.0713624,-0.0873452,0.2343211,0.0486178,
0.197956,0.16661,0.0145687,0.0666896,0.0704459,0.0129995,0.0274433,-0.
017163,0.3236066\Polar=66.4242979,-11.8657836,81.9193659,-1.5689986,0.
2625708,56.8652004\PG=C01 [X(C4H10N1O2)]\NImag=1\\

Zero-point correction= 0.138934

Frequencies --	-116.2110	17.7367	52.4271
Frequencies --	77.8122	129.5552	182.3845
Frequencies --	187.2355	215.2936	217.1825
Frequencies --	327.2309	414.5139	417.5598
Frequencies --	458.5722	494.2143	755.5536
Frequencies --	788.5451	814.0656	819.8122
Frequencies --	992.4481	1038.9215	1041.3782
Frequencies --	1123.6067	1220.1537	1325.0881
Frequencies --	1325.6001	1396.7169	1397.8555
Frequencies --	1419.4154	1431.8670	1471.7420
Frequencies --	1473.3412	1505.5341	1507.0075
Frequencies --	1542.9380	1892.0655	2998.0429
Frequencies --	2999.3957	3013.7340	3117.2631
Frequencies --	3123.3653	3128.8034	3177.4678
Frequencies --	3184.5613	3187.3267	3579.6090

B. PROTON-BOUND DIMER REARRANGEMENT

Structure 1 $(CH_3NO_2)_2H^+$

1\1\GINC-SFNODE0\FOpt\RB3LYP\6-31+G(d)\C2H7N2O4(1+)\HPC1397\09-Jan-200
4\0\\#B3LYP/6-31+G(D) OPT FREQ\\CH3NO2 Dimer\\1,1\C,1.8769637103,2.402
7981464,1.4541197634\H,1.7852508379,2.4923082863,2.5344099121\H,2.9118
165834,2.2812513362,1.1243345844\H,1.4110513488,3.2352241578,0.9201974
954\N,1.1448271986,1.1685016494,1.0551438125\O,1.1866912959,0.91803639
35,-0.2095173306\O,0.5695026916,0.4741791425,1.8398121632\H,0.61042968
24,-0.0072422544,-0.4737611792\O,0.0545470016,-1.1589283453,-0.9540290
564\N,-1.2110671677,-1.1631095908,-0.9766346422\O,-1.8840281293,-0.240
1592842,-0.5847347641\C,-1.8402366895,-2.3984350206,-1.5275026083\H,-2
.9184502567,-2.2634423104,-1.4804360515\H,-1.4760884543,-2.5128488276,
-2.5509537712\H,-1.4943949604,-3.234196805,-0.9153062094\\Version=Sun6
4-SVR4-Unix-G98RevA.9\HF=-490.3799885\RMSD=9.569e-09\RMSF=3.671e-06\Di
pole=0.5358894,0.3434993,0.1155062\PG=C01 [X(C2H7N2O4)]\\@

Zero-point correction=	0.110797		
Frequencies --	32.0103	47.7221	51.0641
Frequencies --	60.7846	71.1045	133.0564
Frequencies --	155.6042	199.4989	454.5857
Frequencies --	502.7659	603.1283	613.6743
Frequencies --	632.6152	657.9238	883.5224
Frequencies --	900.1893	1096.4604	1116.5235
Frequencies --	1147.6903	1149.4989	1171.6869
Frequencies --	1284.6781	1360.2386	1418.5804
Frequencies --	1430.2286	1463.7738	1472.7889
Frequencies --	1476.4847	1479.2439	1480.6213
Frequencies --	1547.7239	1701.8725	1797.1871
Frequencies --	3092.9672	3098.6510	3182.3936
Frequencies --	3188.4614	3238.2137	3238.8612

Structure 2 $CH_3NO_2\cdots CH_3NO_2H^+$

1\1\GINC-SFNODE7\FOpt\RB3LYP\6-31+G(d)\C2H7N2O4(1+)\HPC1471\27-Jul-200
4\0\\#B3LYP/6-31+G(D) OPT FREQ GEOM=CHECK GUESS=CHECK\\CH3NO2 TSa\\1,1
\N,0.2519802894,1.8547351749,-0.0391359697\O,0.2503280156,1.8250683627
,1.2880566369\O,1.2575338259,1.8476452218,-0.6608578661\H,1.1879926251
,1.7077352186,1.584716476\O,0.7178529796,-0.9523170771,0.3481782564\N,
-0.154475126,-1.7356472519,-0.0382234615\O,-1.227024906,-1.3762619508,
-0.5217423902\C,0.0921085914,-3.2020845452,0.1195358632\H,-0.460278439
8,-3.7188139989,-0.6634332895\H,1.1668603334,-3.3674575222,0.068602289
2\H,-0.2938879566,-3.4758701897,1.1054250376\C,-1.1077776097,1.8415530
115,-0.6156223875\H,-1.0283413558,2.2517555764,-1.6215749287\H,-1.3861
952882,0.7723958677,-0.6316874894\H,-1.7641912736,2.4067523358,0.04690
99737\\Version=Sun64-SVR4-Unix-G98RevA.9\HF=-490.3621942\RMSD=4.550e-0
9\RMSF=1.368e-05\Dipole=0.0252803,1.0735005,0.3980313\PG=C01 [X(C2H7N2
O4)]\\@

Zero-point correction=	0.113068		
Frequencies --	30.9742	34.6135	41.4084
Frequencies --	59.5718	80.5965	99.9940
Frequencies --	132.8895	214.3048	457.7407
Frequencies --	481.7316	517.3228	607.4080

Frequencies -- 612.0558 637.5073 660.9098
Frequencies -- 826.4591 925.5381 1062.6334
Frequencies -- 1125.7238 1149.1364 1150.3295
Frequencies -- 1249.2563 1418.5470 1423.9118
Frequencies -- 1442.9257 1459.5768 1471.6423
Frequencies -- 1473.8375 1475.7479 1489.5665
Frequencies -- 1612.8954 1782.7900 2977.5597
Frequencies -- 3099.1885 3158.9301 3195.0815
Frequencies -- 3234.3423 3235.5938 3520.9402

Structure 2b $CH_3NO_2\cdots CH_3NO_2H^+$ (higher energy intermediate)
1\1\GINC-SFNODE4\FOpt\RB3LYP\6-31+G(d)\C2H7N2O4(1+)\HPC1418\02-Apr-200
4\0\\#B3LYP/6-31+G(D) OPT=(MAXCYCLES=120) FREQ GUESS=CHECK
GEOM=CHECK\
\CH3NO2-CH3NO2H (INTERM1) from *ch3no2int1-lyp2a\\1,1\C,3.5461514065,-
0.6523818285,0.1255065532\H,3.5458722154,-1.2180283535,1.0584187487\H,
3.6419250539,-1.3349934164,-0.7214851196\H,4.304479792,0.1270682556,0.
109656032\N,2.2078224424,0.005926975,0.0047472885\O,1.2080074821,-0.72
61583227,0.0908646831\O,2.1510623041,1.2131843802,-0.1780212574\C,-1.3
102472553,1.0456408766,-0.195100024\H,-1.375710977,1.8103870752,0.5777
590535\H,-1.4558244797,1.4160038164,-1.2106025218\H,-0.3514862164,0.48
34942827,-0.1246949769\N,-2.355896084,0.055270946,0.0908189498\O,-2.85
23144685,-0.138877072,1.1494625615\O,-2.6753347814,-0.6871124875,-0.97
03949414\H,-3.339529095,-1.3601633791,-0.6757424263\\Version=Sun64-SVR
4-Unix-G98RevA.9\HF=-490.3582089\RMSD=1.583e-09\RMSF=9.855e-06\Dipole=
-1.6956961,-0.4823713,-0.2885694\PG=C01 [X(C2H7N2O4)]\\@
Zero-point correction= 0.112644
Frequencies -- 9.3724 21.6803 24.8684
Frequencies -- 34.8720 54.7002 69.5177
Frequencies -- 149.8661 281.2382 462.3811
Frequencies -- 479.7087 553.5450 608.3957
Frequencies -- 616.8732 655.9585 658.3054
Frequencies -- 827.5609 925.8122 1050.4019
Frequencies -- 1124.7665 1145.8798 1148.3126
Frequencies -- 1240.4493 1414.8893 1421.7064
Frequencies -- 1432.9906 1448.6610 1465.4419
Frequencies -- 1472.7162 1476.5976 1487.4892
Frequencies -- 1621.1707 1765.6544 2858.8129
Frequencies -- 3102.4522 3150.5396 3192.9524
Frequencies -- 3235.4327 3235.5404 3517.3450

Structure 3 $CH_3NO_2CH_3^+\cdots HONO$
1\1\GINC-SFNODE5\FOpt\RB3LYP\6-31+G(d)\C2H7N2O4(1+)\HPC1471\12-Mar-200
4\0\\#B3LYP/6-31+G(D) OPT=(MAXCYCLES=120) FREQ\\methyl interm 2 (with
HONO rather than HNO2, and position up for HONO)\\1,1\C,0.9174041294,0
.9474506749,2.0523127807\H,0.1887668236,1.3472394459,2.7570184022\H,1.
8616728542,0.6604843101,2.5135944167\H,1.074366081,1.6358209925,1.2139
83599\N,0.347787406,-0.2862056678,1.4474493149\O,0.9954910238,-1.21571
22188,1.0908804161\O,-0.9592467927,-0.2383976316,1.3107408342\C,-1.568
2834998,-1.3898191496,0.6116794133\H,-1.1669558703,-1.4205215609,-0.40
3114805\H,-1.3480397668,-2.3004469138,1.1714630423\H,-2.6265531861,-1.

1388280023,0.6323265232\N,0.4201252465,1.1449083521,-2.3047371101\O,0.
438855942,0.87210481,-1.1442283397\O,-0.3670569926,0.2461896459,-2.999
5113332\H,-0.3177147238,0.5460669425,-3.9312623955\\Version=Sun64-SVR4
-Unix-G98RevA.9\HF=-490.3622171\RMSD=4.980e-09\RMSF=5.499e-05\Dipole=-
0.3945967,-0.0652456,1.0934463\PG=C01 [X(C2H7N2O4)]\\@

Zero-point correction= 0.111763

Frequencies --	13.3280	36.1526	56.9970
Frequencies --	60.3223	96.0418	102.9718
Frequencies --	118.9850	174.3655	206.6488
Frequencies --	298.0910	442.9310	599.0628
Frequencies --	626.1725	656.4378	696.9897
Frequencies --	867.8477	890.0864	924.0037
Frequencies --	1096.5886	1144.4814	1158.8877
Frequencies --	1210.5751	1270.7499	1342.5866
Frequencies --	1422.6627	1464.1126	1473.7612
Frequencies --	1475.7475	1481.0340	1487.6476
Frequencies --	1727.5879	1739.9694	3082.7158
Frequencies --	3096.5284	3186.6539	3201.5539
Frequencies --	3234.9257	3238.6667	3653.6076

Structure 7 $(CH_3CH_2NO_2)_2H^+$

1\1\GINC-SFNODE9\FOpt\RB3LYP\6-31+G(d)\C4H11N2O4(1+)\HPC1471\03-Jul-20
04\0\\#B3LYP/6-31+G(D) OPT FREQ GUESS=CHECK GEOM=CHECK\\ethylint 1\\1,
1\C,3.1304393736,-1.3395327635,0.3112063184\H,2.9021001182,-1.81701891
44,1.2695836613\N,1.835853967,-0.6536305208,-0.0710327398\C,4.30340906
12,-0.382950791,0.3671891505\O,0.8256430857,-1.4134226176,-0.145295791
8\O,1.784637608,0.5332445042,-0.2866451681\H,4.157404027,0.3983722088,
1.1175724318\H,5.1892923712,-0.9628142769,0.6457509135\H,4.4935233789,
0.0854657347,-0.6020273103\C,-3.2369841449,0.8896130933,-0.6022044563\
H,-2.959599671,1.4091847205,-1.5261253113\N,-1.9228391855,0.345910382,
-0.0867585363\C,-3.9313310846,1.7667246295,0.4180493403\O,-1.488142533
8,0.5973000742,0.9972980373\O,-1.3089127101,-0.4184925619,-0.927825477
4\H,-3.3327542503,2.6435619877,0.6785322171\H,-4.8658603313,2.11432897
89,-0.0337935421\H,-4.1786779,1.21613294,1.3295207445\H,-0.3348372033,
-0.786027664,-0.522481419\H,3.2392378956,-2.1314070318,-0.436678961\H,
-3.7999347351,-0.0078979121,-0.8810094088\\Version=Sun64-SVR4-Unix-G98
RevA.9\HF=-569.0255184\RMSD=5.693e-09\RMSF=1.315e-06\Dipole=-0.7074341
,-0.0786527,-0.1820746\PG=C01 [X(C4H11N2O4)]\\@

Zero-point correction= 0.167880

Frequencies --	20.5347	34.1649	40.6341
Frequencies --	46.3085	48.3738	117.2789
Frequencies --	132.8014	173.1343	234.0457
Frequencies --	237.4062	285.2305	298.1454
Frequencies --	484.6481	532.2643	571.8085
Frequencies --	582.7608	616.3938	626.8171
Frequencies --	806.5221	809.9383	835.4559
Frequencies --	861.5299	988.6355	995.1709
Frequencies --	1121.1675	1128.2473	1147.1246
Frequencies --	1159.0670	1160.7543	1277.8721
Frequencies --	1304.9091	1307.2874	1319.3203
Frequencies --	1373.8946	1378.0185	1432.7206

Frequencies --	1445.9325	1450.8740	1470.7683
Frequencies --	1483.5299	1507.5586	1508.9112
Frequencies --	1515.9062	1517.7966	1551.0135
Frequencies --	1699.8705	1800.6264	3078.6915
Frequencies --	3079.4966	3088.3509	3094.6760
Frequencies --	3133.2679	3138.8954	3149.5660
Frequencies --	3151.8527	3166.1291	3166.4866

Structure 8 $CH_3CH_2NO_2\cdots CH_3CH_2NO_2H^+$

1\1\GINC-SFNODE5\FOpt\RB3LYP\6-31+G(d)\C4H11N2O4(1+)\HPC1471\01-Sep-20
04\0\\#B3LYP/6-31+G(D) OPT FREQ\\ethylint 1\\1,1\N,-0.4129284553,1.881
2781035,-1.7992355673\C,-0.5798490655,1.7255129046,-0.3272563394\O,0.8
555478676,2.0302762558,-2.1853373947\O,-1.2881539202,1.8311660387,-2.5
987714797\O,0.3721687703,-1.276492415,-0.0812262615\N,0.3862242736,-1.
5001079886,1.1381603202\C,0.7355905331,-2.8956881339,1.5944647152\H,1.
2033574942,-2.7718494397,2.5717650714\O,0.09809993,-0.6601427989,1.984
0956286\H,-0.2773288285,0.6695800826,-0.1625737303\H,0.859796694,2.065
1455423,-3.1744334747\C,0.2758248983,2.6876481564,0.4913098627\H,0.056
479324,2.4694170827,1.5407323849\H,1.343549284,2.5283204869,0.32882394
16\H,0.0175281397,3.7312959167,0.2905103653\H,-1.656241099,1.826574944
7,-0.1796456903\C,-0.5325247639,-3.7484806772,1.6642778112\H,-1.249068
3854,-3.3346219317,2.3796653629\H,-1.0043006346,-3.8393279594,0.681632
4538\H,-0.250669082,-4.7503251631,2.0029662994\H,1.4482755731,-3.27481
05112,0.8612235056\\Version=Sun64-SVR4-Unix-G98RevA.9\HF=-569.0018136\
RMSD=3.239e-09\RMSF=7.855e-06\Dipole=0.2183534,1.316614,-1.4429159\PG=
C01 [X(C4H11N2O4)]\\@

Zero-point correction=		0.170052	
Frequencies --	10.0592	20.2998	21.5791
Frequencies --	26.8985	45.5690	50.4452
Frequencies --	77.6986	140.7380	226.5017
Frequencies --	233.9299	271.8156	274.9788
Frequencies --	471.9057	473.9700	544.6721
Frequencies --	604.8571	618.6309	681.2674
Frequencies --	730.7991	769.6189	827.4050
Frequencies --	829.8863	887.1834	968.7962
Frequencies --	985.2128	1064.0040	1115.5447
Frequencies --	1124.1854	1163.2172	1206.6826
Frequencies --	1284.6178	1318.4895	1361.0086
Frequencies --	1385.0425	1415.0196	1424.1990
Frequencies --	1444.6052	1452.3841	1473.8439
Frequencies --	1498.8028	1505.8831	1511.1110
Frequencies --	1516.1056	1523.2686	1609.1453
Frequencies --	1747.8165	2900.4623	3072.2436
Frequencies --	3082.2362	3124.5559	3149.0589
Frequencies --	3152.0849	3158.1773	3164.9593
Frequencies --	3180.3882	3196.2867	3524.1698

Structure 9 $CH_3CH_2NO_2CH_2CH_3^+\cdots HONO$

1\1\GINC-SFNODE7\FOpt\RB3LYP\6-31+G(d)\C4H11N2O4(1+)\HPC1471\30-Jun-20
04\0\\#B3LYP/6-31+G(D) OPT FREQ\\ethyl interm 2\\1,1\C,-1.9039260887,-
0.7831066178,0.5468077575\H,-1.8764104211,-0.3950864892,1.5669364362\N

,-0.4533802092,-0.8534293837,0.1504454539\O,0.4064394434,-1.2450820015
,0.8746928508\O,-0.228254447,-0.4732723159,-1.08345202\C,1.2030012438,
-0.5175201371,-1.5624272121\H,1.8133159554,-0.1382433216,-0.7415544295
\H,1.1503104259,0.213503639,-2.3689728735\N,0.2748421803,2.921448953,1
.2534645952\O,0.083855715,1.8257153827,0.8246035183\O,1.479655955,3.41
96429554,0.7955734408\H,1.5430216394,4.3101130223,1.1993907626\C,1.574
7750648,-1.9086202968,-2.0331933837\H,1.608179825,-2.6341109204,-1.215
9913508\H,0.8960075031,-2.2602834638,-2.8153466732\H,2.5812218708,-1.8
481541382,-2.4639254853\C,-2.5279466011,-2.1807827117,0.4644563304\H,-
2.02685773,-2.8829651373,1.1359927578\H,-3.5704439792,-2.084132514,0.7
835722193\H,-2.5177513079,-2.5673766765,-0.5583361466\H,-2.3598226229,
-0.0652545705,-0.134338832\\Version=Sun64-SVR4-Unix-G98RevA.9\HF=-569.
008453\RMSD=6.454e-09\RMSF=4.066e-06\Dipole=-0.4952806,-0.4477597,-0.4
118749\PG=C01 [X(C4H11N2O4)]\\@

Zero-point correction=		0.168892	
Frequencies --	20.2495	28.2377	34.5913
Frequencies --	37.9081	54.4240	74.3435
Frequencies --	89.3224	94.4914	117.6490
Frequencies --	204.4715	230.4523	273.1131
Frequencies --	324.4837	366.4251	467.4874
Frequencies --	585.8241	652.6319	694.1441
Frequencies --	710.6181	765.3845	796.0121
Frequencies --	825.0492	881.9688	926.6397
Frequencies --	958.9362	966.3762	1098.1123
Frequencies --	1115.5018	1134.0448	1197.2190
Frequencies --	1214.9210	1315.3968	1323.2877
Frequencies --	1342.5603	1352.5358	1400.5145
Frequencies --	1435.3620	1439.9826	1490.8733
Frequencies --	1499.7821	1505.6509	1506.6306
Frequencies --	1517.8020	1520.7788	1723.6320
Frequencies --	1728.5823	3070.5706	3076.5016
Frequencies --	3128.2475	3130.7976	3142.2371
Frequencies --	3154.9084	3158.0434	3163.1364
Frequencies --	3204.1527	3206.5435	3655.5838

Structure 10 $((CH_3)_2CHNO_2)_2H^+$
1\1\GINC-SFNODE8\FOpt\RB3LYP\6-31+G(d)\C6H15N2O4(1+)\HPC1418\18-Apr-20
04\0\\#B3LYP/6-31+G(D) OPT FREQ\\2methyldimer (from mp2)\\1,1\C,-0.792
6211384,0.0565579674,-3.3119077359\N,-0.7272366259,-0.1344188631,-1.79
86599251\C,0.6403702281,0.1236001569,-3.8502457384\C,-1.6435532562,1.2
93338105,-3.6133326343\H,-1.2939406395,-0.8613007938,-3.6254002754\O,-
0.1906332433,0.8419180585,-1.1449600589\O,-1.1395712849,-1.1187665973,
-1.25663487\H,1.2236848732,-0.7578625965,-3.5673062562\H,0.5755656974,
0.1489086225,-4.9426419557\H,1.1526958719,1.0280032701,-3.5121854182\H
,-1.7642880015,1.3472462088,-4.699935767\H,-2.6401036584,1.2210114715,
-3.1671572784\H,-1.1544534419,2.2097251091,-3.2732188588\H,-0.13159304
4,0.6205045961,-0.0565986288\O,-0.0604242027,0.5371786871,1.3192888341
\N,0.7454915106,-0.3419864384,1.739617718\O,1.393750503,-1.0438473739,
0.996023083\C,0.8729847468,-0.4856120855,3.2538512098\C,-0.4882461844,
-0.8955618059,3.820142972\H,1.6018533648,-1.2928167683,3.3465960447\C,
1.4200299552,0.8266528528,3.8205831104\H,-1.2269470625,-0.0994505559,3

.6949968998\H,-0.86023843,-1.8150527757,3.3573394998\H,-0.3604543797,-
1.0854062736,4.8904823798\H,0.7048324937,1.6435994869,3.6925662574\H,1
.5926909289,0.6807938775,4.8915335649\H,2.3741509517,1.1012208913,3.35
9942235\\Version=Sun64-SVR4-Unix-G98RevA.9\HF=-647.66687\RMSD=7.064e-0
9\RMSF=2.258e-05\Dipole=-0.2217094,0.2012002,-0.6530618\PG=C01 [X(C6H1
5N2O4)]\\@

Zero-point correction= 0.224650

Frequencies --	11.9639	27.3050	31.0831
Frequencies --	39.7494	51.5553	104.9698
Frequencies --	122.1011	127.7980	214.1429
Frequencies --	215.4567	246.8351	248.6533
Frequencies --	264.2019	271.1744	297.1808
Frequencies --	328.7316	335.3328	363.7709
Frequencies --	507.2178	514.2083	605.5480
Frequencies --	629.5085	727.3435	737.6878
Frequencies --	816.0874	847.5349	870.2757
Frequencies --	884.1168	961.6327	964.2234
Frequencies --	966.0309	968.0679	1091.5933
Frequencies --	1116.6309	1142.4482	1147.5176
Frequencies --	1192.1636	1200.5199	1213.4185
Frequencies --	1272.1358	1282.9225	1349.3449
Frequencies --	1356.4631	1363.0816	1411.4507
Frequencies --	1425.9593	1425.9817	1437.3743
Frequencies --	1453.8106	1480.2219	1500.4590
Frequencies --	1502.6108	1504.5955	1506.6637
Frequencies --	1514.8936	1517.2181	1527.8187
Frequencies --	1529.4548	1551.3320	1685.1822
Frequencies --	1807.5542	3070.1467	3072.2815
Frequencies --	3072.6254	3074.4141	3136.3995
Frequencies --	3137.9521	3143.1228	3144.8614
Frequencies --	3146.4982	3148.0368	3156.3936
Frequencies --	3161.3929	3165.0748	3168.4851

Structure 11 $(CH_3)_2CHNO_2\cdots(CH_3)_2CHNO_2H^+$

1\1\GINC-SFNODE10\FOpt\RB3LYP\6-31+G(d)\C6H15N2O4(1+)\HPC1418\31-Aug-2
004\0\\#B3LYP/6-31+G(D) OPT FREQ\\2methylint a\\1,1\N,-0.1872192111,1.
8734314172,-2.1983005283\C,-0.303644905,1.7893380927,-0.6909497778\O,0
.9763205931,1.4101843837,-2.6690933782\O,-1.0145267382,2.2825430006,-2
.9426807849\O,0.1867122426,-1.3110973813,0.0472828049\N,0.1208006738,-
1.2645873288,1.2809456511\C,0.2597408824,-2.5709697898,2.0621702739\H,
0.1524050577,-2.246340248,3.0983981262\O,-0.0494159931,-0.2219880464,1
.9103571072\H,-0.0971408103,0.7202377033,-0.504381123\H,0.9481416741,1
.4952621794,-3.6542040591\C,-1.7107322895,2.1824996103,-0.2801581874\H
,-2.4715360833,1.5706830932,-0.7731524915\H,-1.7824444972,2.0073803982
,0.7970436189\H,-1.9172543253,3.2396235978,-0.4737351766\C,0.824280488
3,2.6376255348,-0.0705679969\H,0.7551100693,2.4828028732,1.0097243362\
H,1.8140236487,2.3145852936,-0.3995525961\H,0.6838002181,3.7014504958,
-0.2852629887\C,-0.8791578507,-3.5060323358,1.6547034318\H,-0.81979810
13,-4.4084320255,2.2715168754\H,-1.8586788731,-3.0469196594,1.82345114
71\H,-0.7935178534,-3.7978972348,0.6042302006\C,1.6539429103,-3.144155
8443,1.8048725463\H,2.4399413982,-2.4337340229,2.080905774\H,1.7765080

29,-4.0390360127,2.423299075\H,1.7760739595,-3.4285423107,0.755855691\
\Version=Sun64-SVR4-Unix-G98RevA.9\HF=-647.6442082\RMSD=5.749e-09\RMSF
=5.956e-06\Dipole=0.2722168,1.2506798,-1.7416007\PG=C01 [X(C6H15N2O4)]
\\@

Zero-point correction= 0.226102

Frequencies --	18.4162	22.7426	28.2212
Frequencies --	37.2902	42.7063	54.2719
Frequencies --	68.3800	83.2129	211.2410
Frequencies --	215.5560	244.2107	247.8008
Frequencies --	264.5995	266.1679	304.9641
Frequencies --	323.1641	337.1385	360.8905
Frequencies --	475.6594	519.9644	551.9047
Frequencies --	592.9984	629.4457	703.0645
Frequencies --	733.6572	741.4582	856.3029
Frequencies --	860.0655	899.5303	960.9573
Frequencies --	962.3548	966.8251	975.1671
Frequencies --	1076.7852	1122.8644	1126.4332
Frequencies --	1151.3158	1173.8236	1200.3601
Frequencies --	1207.5231	1323.6303	1341.9562
Frequencies --	1369.9280	1377.1667	1413.5340
Frequencies --	1416.7616	1425.7492	1431.5896
Frequencies --	1451.6186	1460.1390	1497.9087
Frequencies --	1504.3489	1505.3135	1508.3866
Frequencies --	1515.2540	1519.5583	1525.4135
Frequencies --	1530.9405	1603.5689	1749.5574
Frequencies --	2971.7066	3066.5954	3069.0591
Frequencies --	3075.1332	3078.8899	3133.8574
Frequencies --	3138.1682	3140.1052	3149.8626
Frequencies --	3152.6247	3156.4691	3160.4219
Frequencies --	3160.6492	3173.8749	3528.0254

Structure 12 $(CH_3)_2CHNO_2CH(CH_3)_2^+\cdots HONO$
1\1\GINC-SFNODE8\FOpt\RB3LYP\6-31+G(d)\C6H15N2O4(1+)\HPC1418\22-Apr-20
04\0\\#B3LYP/6-31+G(D) OPT FREQ\\2methyl interm 2\\1,1\C,-1.807143556,
-0.9058966114,0.2985815563\H,-1.7531262688,-0.6889360006,1.3684780809\
N,-0.3161543923,-0.8871188357,-0.0736320585\O,0.5216549199,-1.31268705
21,0.6616129047\O,-0.0541449546,-0.4259673043,-1.2627357867\C,1.412284
5932,-0.4104658579,-1.7960680185\H,1.1661400054,0.0477408748,-2.755753
8721\N,0.004209345,2.533537056,2.3239802989\O,-0.2575778357,1.61587197
96,1.6141356736\O,1.0632014884,3.2686402648,1.8032533675\H,1.195292078
5,3.9903069318,2.4520307312\C,-2.5898975162,0.155695419,-0.4579925165\
H,-3.6028473658,0.1636186938,-0.0422517886\H,-2.162580511,1.1518020973
,-0.3207299032\H,-2.6628586043,-0.0681213863,-1.5252473289\C,-2.288248
1826,-2.347303152,0.064323734\H,-3.3203035911,-2.4063539217,0.42369850
75\H,-2.2822591444,-2.6012629849,-1.0001454443\H,-1.6910924274,-3.0721
265258,0.6242813575\C,2.2706490222,0.5174245781,-0.9578854267\H,1.7731
349144,1.4733920479,-0.7728167106\H,2.5752994093,0.0723473244,-0.00871
66836\H,3.1764681355,0.7220242173,-1.5412287772\C,1.90613979,-1.832364
9576,-1.9856176239\H,1.1790553101,-2.4436571081,-2.5289082977\H,2.8110
403503,-1.7770507428,-2.6024758802\H,2.1744791927,-2.3180506726,-1.044
8311738\\Version=Sun64-SVR4-Unix-G98RevA.9\HF=-647.6481818\RMSD=2.596e

-09\RMSF=2.002e-06\Dipole=-0.1150208,-0.2862959,-0.6145004\PG=C01 [X(C
6H15N2O4)]\\@

Zero-point correction= 0.224375

Frequencies --	13.7061	24.0688	30.0973
Frequencies --	35.8817	47.3249	64.2540
Frequencies --	71.6029	89.9849	108.3425
Frequencies --	166.6869	211.2762	225.7232
Frequencies --	230.4307	241.1334	251.3842
Frequencies --	275.7810	348.4845	365.9413
Frequencies --	415.2156	469.0684	494.1188
Frequencies --	535.0100	646.3252	665.8404
Frequencies --	683.4031	710.4678	847.9789
Frequencies --	866.7111	890.8818	902.2735
Frequencies --	941.1575	959.0606	960.5771
Frequencies --	963.3107	1090.3366	1120.1858
Frequencies --	1151.0059	1166.1146	1190.8807
Frequencies --	1213.2357	1214.9215	1338.0248
Frequencies --	1340.8639	1373.6252	1380.5990
Frequencies --	1403.3170	1424.8316	1430.5457
Frequencies --	1446.6513	1452.8643	1501.9966
Frequencies --	1502.5049	1505.5606	1507.5576
Frequencies --	1513.0712	1516.3574	1528.1961
Frequencies --	1530.2466	1698.4782	1737.0846
Frequencies --	3068.2744	3071.4108	3072.6069
Frequencies --	3078.9557	3127.1230	3132.2259
Frequencies --	3135.2253	3140.6007	3146.9030
Frequencies --	3152.3163	3159.2706	3166.7839
Frequencies --	3168.6493	3175.3535	3660.7928

Structure 13 $((CH_3)_3CNO_2)_2H^+$

1\1\GINC-SFNODE9\FOpt\RB3LYP\6-31+G(d)\C8H19N2O4(1+)\HPC1397\19-Apr-20
04\0\\#B3LYP/6-31+G(D) OPT=(MAXCYCLES=150) FREQ\\3methyldimer\\1,1\C,-
0.8821022946,0.3298707777,-3.2952592892\N,-0.7967064581,0.113200188,-1
.7536204082\C,0.575445305,0.3931522847,-3.7855689113\C,-1.6439239671,-
0.8612322189,-3.8676583055\C,-1.6255437277,1.6618781581,-3.4939289446\
O,-0.1988886681,1.0593512867,-1.1037228179\O,-1.24025881,-0.8488687313
,-1.1987846517\H,1.1147482831,-0.5337733343,-3.566168595\H,0.548079418
7,0.51830003,-4.8724552093\H,1.1142482084,1.2403636717,-3.3552688413\H
,-2.6596185149,-0.9310588873,-3.4683048016\H,-1.7154585389,-0.71501166
1,-4.9495733994\H,-1.1260264697,-1.8071733964,-3.687340421\H,-1.717166
4337,1.8264012224,-4.5719447294\H,-2.6349135374,1.6263876205,-3.071704
0857\H,-1.0791541437,2.5036578959,-3.0628819934\H,-0.125926918,0.82255
47156,-0.0250482277\O,-0.0233020019,0.7198845937,1.3570430615\N,0.7487
455269,-0.2043393569,1.7442367162\O,1.3326646438,-0.9240350687,0.96578
61643\C,0.9095579845,-0.3658407532,3.2838557107\C,-0.5006118106,-0.649
1144918,3.8269182998\C,1.8713963321,-1.524501802,3.5303152068\C,1.4659
441462,0.9751565089,3.790570223\H,-1.1858959782,0.1771420464,3.6240100
953\H,-0.9124945405,-1.5739563166,3.4096966079\H,-0.4228833901,-0.7746
680475,4.9113231853\H,1.4903400949,-2.4671455235,3.1281225329\H,2.8601
510118,-1.3348420256,3.1037801394\H,1.9842004846,-1.6377971604,4.61292
94405\H,1.600397414,0.893675992,4.873599882\H,2.4414335631,1.197679685

5,3.3458130289\H,0.7789733871,1.8003702315,3.5890632474\\Version=Sun64
-SVR4-Unix-G98RevA.9\HF=-726.3040616\RMSD=6.383e-09\RMSF=2.495e-06\Dip
ole=-0.2566561,0.2666525,-0.706569\PG=C01 [X(C8H19N2O4)]\\@

Zero-point correction= 0.280162

Frequencies --	20.9071	22.8138	26.1200
Frequencies --	41.4227	55.4201	99.1063
Frequencies --	118.3522	122.6679	196.1029
Frequencies --	200.6208	258.5804	259.3750
Frequencies --	260.8194	270.1423	287.3272
Frequencies --	290.8330	297.1296	302.4215
Frequencies --	352.7318	355.8028	358.7785
Frequencies --	382.8773	385.1005	394.5848
Frequencies --	511.4926	518.6985	531.5288
Frequencies --	539.3770	719.7809	732.1621
Frequencies --	776.9094	787.5586	800.6643
Frequencies --	842.7765	938.9228	942.2920
Frequencies --	945.0981	946.5107	993.9691
Frequencies --	996.6301	1061.7228	1062.6888
Frequencies --	1063.2069	1064.0669	1155.6083
Frequencies --	1188.8475	1207.0246	1251.3404
Frequencies --	1258.8281	1263.1532	1273.3421
Frequencies --	1292.3556	1328.1492	1424.3221
Frequencies --	1425.9637	1430.2258	1435.8556
Frequencies --	1447.6242	1463.4091	1477.5000
Frequencies --	1493.8581	1495.8305	1503.6812
Frequencies --	1505.9554	1507.0411	1509.1686
Frequencies --	1519.0077	1520.7489	1520.9472
Frequencies --	1522.5733	1540.1019	1542.1729
Frequencies --	1556.1462	1679.4524	1820.0052
Frequencies --	3069.2145	3070.2356	3072.1028
Frequencies --	3072.6226	3077.7051	3079.0812
Frequencies --	3139.9270	3140.9924	3144.2848
Frequencies --	3144.6596	3149.4709	3152.6640
Frequencies --	3156.0454	3157.1912	3160.0167
Frequencies --	3163.3733	3163.6497	3167.1732

Structure 14 $(CH_3)_3C^+\cdots HONO\cdots O_2NC(CH_3)_3$

1\1\GINC-SFNODE2\FOpt\RB3LYP\6-31+G(d)\C8H19N2O4(1+)\HPC1471\10-Jul-20
05\0\\#B3LYP/6-31+G(D) OPT FREQ\\3nitro-nitrite step a min. structure\
\1,1\C,-0.7135157693,0.8122669108,-4.2309124945\O,-0.0935166441,-0.274
8555324,-1.3749194326\C,0.374638095,0.0315982612,-4.8082539042\C,-2.07
03086621,0.2509603066,-4.1904827406\C,-0.4572392998,2.1222839787,-3.62
89182467\N,0.8862374118,-1.1938201273,-1.7505443374\H,0.037219367,-0.7
089155504,-5.540283839\H,1.2119798226,0.6306862565,-5.1733949572\H,0.7
554517206,-0.559816243,-3.9393385821\H,-2.6688763872,0.6387158435,-3.3
614471072\H,-2.5533814785,0.60819109,-5.1226507614\H,-2.0848486556,-0.
8416896524,-4.2294906094\H,-0.2193468341,1.8708191715,-2.5728822166\H,
0.4106521889,2.640251098,-4.0430676157\H,-1.3451513515,2.7612998496,-3
.5952412028\O,-0.6281725658,-0.3474068866,1.3209424901\N,0.2388518673,
0.1562477563,2.0609422258\O,1.1715046646,0.8175762328,1.6351443117\C,0
.0941280322,-0.1009029095,3.5876023804\C,0.1687487835,-1.6256293107,3.

7652161099\C,1.234158851,0.6169786247,4.3055553008\C,-1.2812139113,0.4
550755018,3.9862404274\H,-0.6432947344,-2.1304339695,3.2363466461\H,1.
1270941665,-2.0215454911,3.4128345302\H,0.0817134562,-1.851575782,4.83
27277632\H,2.2130820101,0.2444284647,3.992305734\H,1.2044658356,1.6972
805948,4.1391823827\H,1.1257350561,0.4332324324,5.3793595581\H,-1.4241
795477,0.2825343012,5.0576154203\H,-1.3417478246,1.534031111,3.8074253
043\H,-2.0871478659,-0.044976914,3.443928045\O,1.3564038454,-1.8184902
238,-0.8613776415\H,-0.2211750134,-0.3098869153,-0.3713125271\\Version
=Sun64-SVR4-Unix-G98RevA.9\HF=-726.2771724\RMSD=4.386e-09\RMSF=4.910e-
06\Dipole=-1.4452657,1.2090366,-4.0925898\PG=C01 [X(C8H19N2O4)]\\@

Zero-point correction= 0.274826

Frequencies --	12.0847	17.2717	21.3676
Frequencies --	26.0339	32.2866	43.6583
Frequencies --	55.4200	78.5157	87.4773
Frequencies --	100.1319	113.6886	129.3012
Frequencies --	194.0891	200.5602	205.5650
Frequencies --	212.9991	260.8232	266.0990
Frequencies --	272.0166	293.4022	298.6105
Frequencies --	358.0077	381.2295	385.8476
Frequencies --	406.7513	411.1945	434.9200
Frequencies --	527.4088	551.0844	637.7588
Frequencies --	721.5385	737.8950	767.7068
Frequencies --	796.1970	846.1119	862.1281
Frequencies --	919.5204	943.7653	946.7059
Frequencies --	971.4154	991.9656	993.7107
Frequencies --	1004.7157	1034.5916	1063.5457
Frequencies --	1064.8759	1129.2834	1204.9253
Frequencies --	1263.3711	1286.8166	1325.6048
Frequencies --	1337.3437	1357.5860	1372.5711
Frequencies --	1390.7077	1394.7286	1424.1513
Frequencies --	1427.1142	1433.1510	1435.2815
Frequencies --	1442.8729	1456.2953	1466.3550
Frequencies --	1497.1067	1505.8261	1510.7563
Frequencies --	1515.4848	1518.7205	1522.4183
Frequencies --	1522.9442	1529.9336	1543.2963
Frequencies --	1605.7003	1741.3477	2857.1428
Frequencies --	2951.7545	2977.2392	3065.8686
Frequencies --	3067.2371	3074.6470	3079.5997
Frequencies --	3099.6891	3104.7843	3107.0412
Frequencies --	3134.4134	3135.8621	3143.9468
Frequencies --	3154.2736	3155.9230	3159.8510
Frequencies --	3171.3548	3172.4806	3177.7650

Structure 15 $(CH_3)_3CO(H)(NO)^+(O_2NC(CH_3)_3)$

1\1\GINC-SFNODE8\FOpt\RB3LYP\6-31+G(d)\C8H19N2O4(1+)\HPC1471\05-Jul-20
05\0\\#B3LYP/6-31+G(D) OPT FREQ GEOM=CHECK GUESS=CHECK\\3nitro-nitrite
step a min. structure\\1,1\C,-2.8591672894,-0.4339528844,-0.343436446
5\O,-1.8155695238,0.6319065308,-0.1509132812\C,-2.5713685341,-1.594908
0866,0.6085382583\C,-4.1915638606,0.252602014,-0.0590273643\C,-2.72564
92573,-0.8396131641,-1.8153599988\N,-1.7274321442,1.4155866185,1.56109
2056\H,-2.6344415603,-1.2842310921,1.6568960011\H,-3.3143768848,-2.384

0962532,0.4537859723\H,-1.5829457676,-2.0294846482,0.4237698538\H,-4.3
308913178,1.1246187332,-0.7056507318\H,-5.0101329488,-0.4477141826,-0.
2523802681\H,-4.2729265688,0.5649205784,0.9885289576\H,-3.4940728686,-
1.5860514681,-2.045595277\H,-2.8726620873,0.0198026666,-2.4759654375\H
,-1.7492014442,-1.2888974828,-2.0252062863\O,0.6860512746,-0.310862464
8,-0.7093043395\N,1.5703547422,0.0673903442,0.0813917403\O,1.315459962
,0.7324001312,1.0770672941\C,3.0395962795,-0.333492815,-0.2438421212\C
,3.3494363714,0.2941704895,-1.6126569087\C,3.9397364938,0.2138944657,0
.8603214638\C,3.0561108558,-1.869148043,-0.3000319849\H,2.6842407534,-
0.0883018387,-2.3905635886\H,3.2759734001,1.3862758114,-1.5784273642\H
,4.3785647157,0.0344759885,-1.8795194242\H,3.8968295304,1.3045791533,0
.921684911\H,3.6865744999,-0.2021174758,1.8392904369\H,4.9694212865,-0
.0731355253,0.6249562148\H,4.0775124293,-2.1891323407,-0.5279091689\H,
2.7733877147,-2.3080187183,0.662707211\H,2.3936972271,-2.2507476481,-1
.0806019191\O,-1.0742540148,2.3106761379,1.4893066249\H,-0.8912962335,
0.2661424666,-0.3234664419\\Version=Sun64-SVR4-Unix-G98RevA.9\HF=-726.
3002566\RMSD=4.860e-09\RMSF=7.754e-06\Dipole=-0.6723116,0.2648509,0.44
18791\PG=C01 [X(C8H19N2O4)]\\@

Zero-point correction= 0.279420

Frequencies --	7.4116	14.7800	33.0068
Frequencies --	44.8511	54.4079	64.4268
Frequencies --	80.2099	111.0092	116.0693
Frequencies --	150.9084	196.7549	203.2513
Frequencies --	235.8248	254.0581	263.2832
Frequencies --	266.0163	272.4510	292.7493
Frequencies --	295.4067	339.2385	349.8744
Frequencies --	358.7783	382.3140	384.3963
Frequencies --	420.0308	452.5767	477.4455
Frequencies --	525.3259	543.8708	585.8683
Frequencies --	726.7188	736.0264	792.1327
Frequencies --	814.1108	854.1614	924.1113
Frequencies --	937.0915	939.9009	942.0107
Frequencies --	946.0358	982.8350	992.4062
Frequencies --	1053.8102	1057.9313	1062.5256
Frequencies --	1064.2042	1188.9924	1197.5858
Frequencies --	1252.5484	1261.1791	1277.4420
Frequencies --	1285.9105	1390.2122	1418.5065
Frequencies --	1424.2648	1427.3863	1434.9328
Frequencies --	1437.7254	1460.8658	1468.0371
Frequencies --	1496.1281	1496.4706	1503.8965
Frequencies --	1504.4652	1504.8472	1509.3809
Frequencies --	1521.3233	1522.1127	1524.8059
Frequencies --	1528.5376	1537.9587	1542.1595
Frequencies --	1585.4469	2140.5966	3057.1825
Frequencies --	3059.5723	3064.4552	3067.7980
Frequencies --	3069.0631	3077.4486	3097.1819
Frequencies --	3126.4107	3128.9834	3131.7680
Frequencies --	3136.8260	3138.1013	3138.7707
Frequencies --	3143.5865	3146.8082	3147.7515
Frequencies --	3155.2623	3157.0533	3161.0578

Structure 16 $((CH_3)_3NO_2)(NO)^+$

1\1\GINC-SFNODE7\FOpt\RB3LYP\6-31+G(d)\C4H9N2O3(1+)\HPC1397\10-Jul-200
5\0\\#B3LYP/6-31+G(D) OPT FREQ SCF=QC\\t-butylNO2-NO (C4H9NO2-NO+, NO
straight on top)\\1,1\C,-0.5482410351,0.2663785324,-1.2869549512\N,0.0
220827659,-0.044269638,0.152255999\C,0.6847992943,0.1840401,-2.2039670
045\C,-1.1321801404,1.6816897235,-1.2111520592\C,-1.5942686931,-0.7971
341249,-1.6048536379\O,0.7419685444,0.7967044008,0.7083306676\O,-0.220
9705023,-1.1214061149,0.7019961307\H,0.3452195245,0.3865804447,-3.2249
342795\H,1.4376694979,0.9308751205,-1.9387380507\H,1.1334162153,-0.814
3502832,-2.1918116552\H,-1.5334160739,1.9242292544,-2.2001950171\H,-1.
9553714353,1.741453841,-0.4920377572\H,-0.3736506396,2.4259929092,-0.9
58204136\H,-1.1691295535,-1.8033355548,-1.6342909176\H,-2.4264763397,-
0.7810496459,-0.895051938\H,-1.9962534054,-0.5707907089,-2.5975920781\
N,1.3898826106,-0.6854110448,2.2394378509\O,1.0031992104,-0.4680090338
,3.2437438012\\Version=Sun64-SVR4-Unix-G98RevA.9\HF=-492.5798319\RMSD=
0.000e+00\RMSF=2.026e-06\Dipole=0.5775879,-0.2416593,1.0877337\PG=C01
[X(C4H9N2O3)]\\@

Zero-point correction=		0.141524	
Frequencies --	20.2396	44.0290	60.5033
Frequencies --	188.9737	204.1951	249.4150
Frequencies --	262.9085	269.4579	285.6453
Frequencies --	294.8733	351.9979	359.0186
Frequencies --	380.7238	440.2103	497.8601
Frequencies --	505.9813	728.4023	771.2141
Frequencies --	870.0879	937.0666	941.4439
Frequencies --	995.0435	1057.5815	1062.4262
Frequencies --	1172.6220	1257.6397	1282.8308
Frequencies --	1371.9459	1425.9433	1432.9606
Frequencies --	1465.3023	1486.8012	1492.2522
Frequencies --	1505.6786	1506.9295	1517.7856
Frequencies --	1520.1184	1540.2454	2230.4955
Frequencies --	3068.6152	3071.9158	3077.8765
Frequencies --	3141.4892	3141.7804	3148.1694
Frequencies --	3158.0988	3160.5192	3164.4472

Structure 17 $(CH_3)_3CNO_2\cdots(CH_3)_3CNO_2H^+$

1\1\GINC-SFNODE9\FOpt\RB3LYP\6-31+G(d)\C8H19N2O4(1+)\HPC1397\20-Apr-20
04\0\\#B3LYP/6-31+G(D) OPT FREQ\\3methylint 1\\1,1\C,0.3486321952,-0.0
14147078,-3.5815324968\N,0.3428098682,-0.0178318643,-2.0246443689\C,1.
7951005777,-0.0735741464,-4.0661724483\C,-0.3462860255,1.2906110837,-4
.0005080614\C,-0.4544291705,-1.2503038435,-4.0130086972\O,-0.754193841
3,0.0058932962,-1.4583510185\O,1.4119204902,-0.0393787829,-1.417943551
4\H,2.300646935,-0.9826676033,-3.7293749895\H,1.7855644535,-0.07360607
65,-5.1611075217\H,2.3745128686,0.7901938883,-3.7296083038\H,-0.372278
2364,1.3333810407,-5.0939907988\H,-1.3728452821,1.3331298882,-3.628072
4623\H,0.2034408711,2.16778922,-3.6422872614\H,-1.4812327501,-1.209640
8299,-3.6414619268\H,-0.4822948205,-1.2797670259,-5.10685374\H,0.01841
76039,-2.1743712944,-3.6630734196\C,-0.3031304705,0.0566085347,2.30590
61315\N,-0.4272983514,0.0836327374,3.8778113206\C,1.2053723197,-0.0786
076053,2.0317817319\C,-1.1061600527,-1.1696709962,1.8441033064\C,-0.88
74288739,1.3751496202,1.8193721174\O,-0.8278795259,0.9886929144,4.5269

988174\O,-0.0152909042,-1.0383873273,4.4779260865\H,1.3191096752,-0.06
28878158,0.941393975\H,1.7689915197,0.7627053491,2.4474041502\H,1.6097
190651,-1.0203844735,2.4102626616\H,-2.1558648948,-1.1056349164,2.1476
350319\H,-1.0674902339,-1.1550682076,0.7498824662\H,-0.6730357401,-2.1
068650038,2.2003626874\H,-0.8284714568,1.3510724448,0.7270556006\H,-1.
9389163836,1.489715339,2.0988975772\H,-0.3210011079,2.2386054142,2.179
3188043\H,-0.1220254503,-0.9072596682,5.452756634\\Version=Sun64-SVR4-
Unix-G98RevA.9\HF=-726.2776351\RMSD=1.843e-09\RMSF=2.207e-06\Dipole=-0
.3793663,-0.3239695,3.4989882\PG=C01 [X(C8H19N2O4)]\\@

Zero-point correction= 0.281531

Frequencies --	19.9790	22.4423	33.7725
Frequencies --	36.2433	41.0354	47.3033
Frequencies --	50.1538	65.7086	201.3867
Frequencies --	220.2202	252.3946	255.4407
Frequencies --	259.9257	263.7448	285.9358
Frequencies --	286.3249	288.9102	302.3294
Frequencies --	316.0144	345.5342	356.9978
Frequencies --	370.6628	371.7510	386.4730
Frequencies --	473.8018	493.1719	522.7416
Frequencies --	549.2523	588.1284	706.0565
Frequencies --	716.6280	738.3354	756.6458
Frequencies --	797.9413	858.7043	936.3024
Frequencies --	943.2767	944.0654	947.3829
Frequencies --	990.9033	1002.6349	1045.9643
Frequencies --	1063.7687	1064.3297	1065.8634
Frequencies --	1108.7105	1166.4074	1205.4570
Frequencies --	1246.5113	1264.3004	1288.8231
Frequencies --	1292.4875	1400.4781	1413.1831
Frequencies --	1423.3095	1425.8526	1433.4886
Frequencies --	1435.5353	1464.1507	1468.0774
Frequencies --	1497.0832	1498.9657	1499.6327
Frequencies --	1502.4722	1505.3366	1512.1801
Frequencies --	1521.1526	1523.1162	1523.6695
Frequencies --	1525.7309	1537.4784	1543.0964
Frequencies --	1595.8846	1749.4320	3059.1985
Frequencies --	3064.1841	3065.7091	3068.7255
Frequencies --	3073.9686	3074.5677	3132.8253
Frequencies --	3133.3933	3135.1327	3141.9556
Frequencies --	3144.1531	3152.7453	3153.4974
Frequencies --	3154.1408	3155.4277	3157.6034
Frequencies --	3161.4669	3167.7092	3523.0409

Structure 18 $(CH_3)_3CNO_2\cdots(CH_3)_3C^+\cdots HONO$

1\1\GINC-SFNODE1\FOpt\RB3LYP\6-31+G(d)\C8H19N2O4(1+)\HPC1397\13-Jan-20
06\0\\#B3LYP/6-31+G(D) OPT FREQ GEOM=CHECK GUESS=CHECK\\3newTSbqst2irc
f TS2 1st bit\\1,1\C,1.6459454566,3.17952561,0.9334592158\C,2.44161282
78,3.1611884083,2.2361089296\C,2.5392297149,3.4591553009,-0.2850753641
\C,0.4517967686,4.1438329856,0.9990062987\H,3.2677473866,2.4460807519,
2.2009890818\H,1.8112905788,2.922345463,3.0968936208\H,2.8618456109,4.
1606890683,2.3879043269\H,3.3552482232,2.7320746854,-0.3572134075\H,2.
9835107805,4.4521179147,-0.1642088828\H,1.964181605,3.4493280777,-1.21

43356135\H,-0.2119738699,3.9007384173,1.8357511992\H,0.8357522565,5.15
62626854,1.1584802774\H,-0.1218730697,4.1347592748,0.069018365\N,1.039
3604182,1.7634545747,0.7005048574\O,1.2623340381,0.8696962936,1.515005
9467\O,0.3482538499,1.5927744285,-0.3104076804\C,-0.8779210446,-1.4856
957063,-0.5594245893\C,-0.2209620004,-1.9583222472,0.6610743457\C,-0.1
199929944,-1.4453595583,-1.8223177206\C,-2.1583194209,-0.7644898372,-0
.4676928097\H,0.3356275579,-1.0606724248,1.0210154619\H,0.5223687285,-
2.7386553047,0.4821295986\H,-0.9185143179,-2.2322383972,1.4557777451\H
,-0.7581444466,-1.3970270387,-2.7075780431\H,0.6235775291,-2.240950961
4,-1.9051926651\H,0.4284233625,-0.4836963988,-1.7710815595\H,-1.857418
6631,0.2888607878,-0.2999042436\H,-2.7706928361,-1.0707959215,0.382862
8248\H,-2.7297028046,-0.7815749289,-1.3989889474\N,-2.0778757249,-3.79
57199672,-1.1009934196\O,-3.234444124,-4.0437815203,-1.2056924645\O,-1
.2247347246,-4.8551310127,-1.2716502188\H,-1.7712546241,-5.6592632506,
-1.4577737042\\Version=Sun64-SVR4-Unix-G98RevA.9\HF=-726.2760822\RMSD=
7.361e-09\RMSF=8.405e-06\Dipole=-0.6006444,-1.2753611,-0.6659496\PG=C0
1 [X(C8H19N2O4)]\\@

Zero-point correction= 0.275386

Frequencies --	10.0331	21.1059	21.9259
Frequencies --	32.0518	38.4575	44.5050
Frequencies --	47.2399	50.9843	69.3772
Frequencies --	92.4707	110.3110	129.9954
Frequencies --	143.7672	198.9023	203.1259
Frequencies --	212.8101	259.2208	263.2736
Frequencies --	282.6428	286.7227	290.7682
Frequencies --	356.6893	371.0798	385.2543
Frequencies --	422.9006	426.2808	437.6298
Frequencies --	521.5132	545.8803	655.2344
Frequencies --	710.8703	737.5940	765.5108
Frequencies --	773.8951	795.9130	802.9109
Frequencies --	857.9749	942.9117	946.2807
Frequencies --	949.2342	989.9761	995.3200
Frequencies --	1040.7114	1048.9995	1062.1094
Frequencies --	1063.7429	1138.0633	1201.6464
Frequencies --	1263.1540	1287.9253	1331.7706
Frequencies --	1332.7846	1355.8253	1378.5300
Frequencies --	1381.6414	1396.0778	1407.7800
Frequencies --	1422.8673	1424.4812	1433.3792
Frequencies --	1466.7014	1467.6035	1468.7630
Frequencies --	1496.7577	1505.0687	1508.6369
Frequencies --	1511.1253	1514.7484	1521.2503
Frequencies --	1522.7845	1542.9571	1545.8737
Frequencies --	1587.3854	1729.6104	2878.4656
Frequencies --	2975.8374	2985.2881	3065.2654
Frequencies --	3066.7630	3075.3767	3112.9645
Frequencies --	3116.6513	3123.0553	3135.2532
Frequencies --	3135.5306	3144.1578	3153.5683
Frequencies --	3155.1342	3157.9682	3177.0366
Frequencies --	3182.9057	3183.1692	3494.6463

Structure 19 $(CH_3)_3CNO_2\cdots(CH_3)_3C^+\cdots O(H)NO$

1\1\GINC-SFNODE8\FOpt\RB3LYP\6-31+G(d)\C8H19N2O4(1+)\HPC1471\01-Dec-20
05\0\\#B3LYP/6-31+G(D) OPT FREQ\\3methyl dimer int----OHNO\\1,1\C,0.36
38544022,-0.0748337417,-3.7407398696\N,0.3803766605,-0.1328315971,-2.1
837923707\C,1.8036157339,-0.1200815453,-4.2458197915\C,-0.334408672,1.
2452951551,-4.1028048746\C,-0.4484128454,-1.2953400693,-4.1997221962\O
,-0.7067539685,-0.1199668907,-1.5949963963\O,1.4577717155,-0.186408654
7,-1.5930467103\H,2.3100271616,-1.0443063115,-3.9547480932\H,1.7779899
685,-0.0750600777,-5.3394197533\H,2.3912703428,0.7276507127,-3.8838463
276\H,-0.3772067451,1.3229508522,-5.1936906569\H,-1.3554750466,1.27874
58711,-3.7146713392\H,0.2242504272,2.108955422,-3.7262760292\H,-1.4707
313672,-1.2648724055,-3.8149507723\H,-0.4905698027,-1.2878527791,-5.29
34213146\H,0.0274336241,-2.2314920555,-3.8883788442\C,-0.4318526369,-0
.233775261,1.6718072395\O,-0.5622683043,-0.2352145798,4.4848778171\C,1
.0264773873,-0.2302185526,1.6541192308\C,-1.1647982489,-1.5023055631,1
.5418260356\C,-1.1692911677,1.0339866552,1.5740095112\N,-0.0350782718,
1.0089113485,4.979098533\H,1.2665501742,-0.2151778814,0.5614550019\H,1
.4684914538,0.6725397404,2.0816262424\H,1.4731391627,-1.1414712354,2.0
579827454\H,-2.1715179103,-1.4568907227,1.9645580103\H,-1.2881802986,-
1.6320142527,0.447869971\H,-0.6084450385,-2.3649422485,1.9136658733\H,
-1.2816360867,1.1906820717,0.4819387102\H,-2.179379424,0.9738941932,1.
9864443406\H,-0.6198133052,1.8876901643,1.9751628415\O,-0.0122846539,1
.0745283118,6.1510126771\H,-0.7961080384,-0.7814552737,5.2727254448\\V
ersion=Sun64-SVR4-Unix-G98RevA.9\HF=-726.2751491\RMSD=6.172e-09\RMSF=3
.316e-05\Dipole=-0.7682394,-0.6645893,0.849562\PG=C01 [X(C8H19N2O4)]\\
@

Zero-point correction= 0.274115

Frequencies --	7.3290	19.4307	24.1102
Frequencies --	36.7573	39.9345	44.1964
Frequencies --	49.9593	56.1009	65.3330
Frequencies --	68.2067	84.6068	90.0410
Frequencies --	99.5070	116.7213	184.9596
Frequencies --	202.1040	261.5785	265.3623
Frequencies --	280.7980	286.4531	294.6502
Frequencies --	356.8978	371.4510	385.0747
Frequencies --	425.1825	432.9405	440.2072
Frequencies --	521.5117	542.5921	545.5510
Frequencies --	650.2830	736.5699	737.3128
Frequencies --	757.5588	794.9744	812.0651
Frequencies --	818.1775	857.7475	943.4369
Frequencies --	946.5011	990.8061	994.0684
Frequencies --	1038.5196	1052.9976	1061.4871
Frequencies --	1064.5069	1147.6241	1201.3976
Frequencies --	1263.0058	1288.0298	1309.9798
Frequencies --	1333.0025	1334.1551	1370.0656
Frequencies --	1375.2152	1392.2621	1403.7202
Frequencies --	1417.1947	1422.4666	1434.1455
Frequencies --	1459.8675	1463.5358	1467.8057
Frequencies --	1497.0020	1505.3055	1509.4445
Frequencies --	1510.6349	1519.2859	1522.1627
Frequencies --	1522.7932	1542.6046	1548.9349

Frequencies -- 1585.8597 1785.1460 2845.4868
Frequencies -- 2971.4971 2982.6862 3065.2747
Frequencies -- 3066.8939 3075.5061 3113.8344
Frequencies -- 3116.0296 3123.5816 3135.0928
Frequencies -- 3135.7240 3144.4806 3153.9517
Frequencies -- 3155.5646 3157.8637 3178.9840
Frequencies -- 3184.9089 3186.4935 3539.5907

Structure 20 $(CH_3)_3CNO_2\cdots(CH_3)_3COH\cdots NO^+$

1\1\GINC-SFNODE5\FOpt\RB3LYP\6-31+G(d)\C8H19N2O4(1+)\HPC1471\30-Nov-20
05\0\\#B3LYP/6-31+G(D) OPT FREQ\\3methyl dimer int OH+NO (nitrite prod
uct from dimer intermediate)\\1,1\C,0.3874002744,-0.1604649723,-3.7056
778212\N,0.3543421224,-0.1559641334,-2.1494522786\C,1.842277247,-0.112
9885741,-4.1661230314\C,-0.3974312297,1.0820400995,-4.151980875\C,-0.3
102383032,-1.4592742378,-4.137993729\O,-0.7530657176,-0.1737604737,-1.
6052010187\O,1.4132100109,-0.1382060052,-1.5255204024\H,2.4087105106,-
0.9806053787,-3.8176112247\H,1.852084308,-0.1145719467,-5.2611076374\H
,2.34919019,0.7923177821,-3.821218311\H,-0.4069660643,1.1117690796,-5.
2462059353\H,-1.4304672135,1.050563862,-3.7971706823\H,0.0770584477,2.
0022107835,-3.7939321444\H,-1.3430320473,-1.4944676003,-3.7824215447\H
,-0.3181467709,-1.5018868614,-5.2318021308\H,0.2262860666,-2.340735716
7,-3.7702396268\C,-0.4455988142,-0.1468075739,2.2153050095\O,-0.700592
1019,-0.1905406302,3.7362051748\C,1.0601156171,-0.1690196611,1.9903538
646\C,-1.1471346836,-1.3995862373,1.6947611683\C,-1.1174439241,1.13539
09828,1.749004143\N,-0.012739545,1.2242328081,4.7931267101\H,1.2587795
445,-0.1673362022,0.912939887\H,1.5449086587,0.7150721367,2.4204261661
\H,1.5196704441,-1.0718901937,2.4111242748\H,-2.2084208225,-1.40374129
25,1.9597119494\H,-1.0637557687,-1.3945336714,0.6018342062\H,-0.674895
832,-2.3180151677,2.0642679238\H,-1.0559271015,1.1721179907,0.65700869
68\H,-2.1745660527,1.1547225973,2.0317834353\H,-0.6190812669,2.0277079
593,2.1427484134\O,-0.1089829865,0.9660622975,5.8682043076\H,-0.368878
0119,-1.0407593447,4.0987464014\\Version=Sun64-SVR4-Unix-G98RevA.9\HF=
-726.2784906\RMSD=5.519e-09\RMSF=1.157e-05\Dipole=-0.128431,0.3081368,
4.4585611\PG=C01 [X(C8H19N2O4)]\\@

Zero-point correction= 0.278534
Frequencies -- 12.6860 18.5465 29.6548
Frequencies -- 32.8859 37.3155 40.6375
Frequencies -- 53.5584 62.4751 81.0762
Frequencies -- 115.6934 197.9744 222.7502
Frequencies -- 231.2597 259.2845 262.6122
Frequencies -- 279.4893 286.5276 291.9202
Frequencies -- 303.1903 327.3174 339.8147
Frequencies -- 357.3607 371.0444 384.4214
Frequencies -- 409.7556 430.1101 449.0527
Frequencies -- 504.1747 523.0327 552.0951
Frequencies -- 568.9588 718.4333 737.7137
Frequencies -- 791.0389 798.7425 858.7461
Frequencies -- 933.2972 941.3672 944.2441
Frequencies -- 947.8428 989.5533 989.9807
Frequencies -- 1040.5137 1057.7895 1062.0766
Frequencies -- 1064.7913 1152.5910 1174.1046

Frequencies --	1207.1076	1264.3274	1283.6242
Frequencies --	1288.8647	1337.3231	1400.4066
Frequencies --	1422.5185	1426.3251	1432.5877
Frequencies --	1437.8526	1460.5084	1467.3800
Frequencies --	1496.5400	1496.8457	1499.3225
Frequencies --	1503.0115	1505.1647	1511.3406
Frequencies --	1522.0569	1522.6669	1527.1728
Frequencies --	1535.3919	1536.8771	1543.1767
Frequencies --	1599.9096	2147.9304	3043.8381
Frequencies --	3050.9077	3063.8340	3064.6045
Frequencies --	3065.4558	3073.7457	3112.7732
Frequencies --	3120.9717	3131.8796	3132.2847
Frequencies --	3133.0883	3136.2153	3141.6700
Frequencies --	3144.0209	3150.0327	3152.9964
Frequencies --	3153.6612	3156.9363	3617.5152

Structure 21 $(CH_3)_3CNO_2C(CH_3)_3^+\cdots HONO$

1\1\GINC-SFNODE1\FOpt\RB3LYP\6-31+G(d)\C8H19N2O4(1+)\HPC1397\30-Apr-20
04\0\\#B3LYP/6-31+G(D) OPT FREQ\\3methyl interm 2\\1,1\C,-1.007693519,
0.2022761895,-1.9025684353\N,-0.9185826326,0.192557114,-0.3314604413\C
,0.1002933335,-0.7017535185,-2.4492957775\C,-2.4162841744,-0.349263586
8,-2.1966648212\C,-0.8506578118,1.659710845,-2.3313320466\O,-1.1361386
335,1.1629744723,0.3298166958\O,-0.6570888174,-0.9708749542,0.18120835
06\H,0.0478393911,-0.6535327738,-3.5415616532\H,1.0896744281,-0.352008
6472,-2.1430647593\H,-0.0283335,-1.7438527656,-2.1501876634\H,-2.54954
67429,-0.3383873957,-3.2831856527\H,-2.5299710165,-1.3803550338,-1.850
6819958\H,-3.197213045,0.277626601,-1.7550846705\H,-0.908790764,1.6853
573827,-3.423792831\H,-1.6448423567,2.2967822321,-1.935259711\H,0.1202
588299,2.0640516135,-2.0322928687\C,-0.6477751941,-1.2253838909,1.7761
182984\C,0.4166016942,-0.3328599948,2.3922508426\C,-2.064836968,-0.983
086854,2.2697167273\C,-0.2598060622,-2.6954792367,1.7613385836\H,1.371
0754052,-0.420011206,1.8663834214\H,0.1205368911,0.7163405591,2.436912
5638\H,0.5698971041,-0.6807535737,3.4208158187\H,-2.7917524561,-1.5885
032457,1.7197168205\H,-2.1015335251,-1.2976363195,3.3194577559\H,-2.35
41346938,0.0692803257,2.2346977141\H,0.7322225174,-2.8456296168,1.3260
057623\H,-0.2323628587,-3.049101556,2.7976770329\H,-0.9902738191,-3.30
14501146,1.2175686618\N,3.2847753546,1.7333949832,-0.228678313\O,3.878
0612794,1.2939453378,0.9534962741\H,4.7463455012,1.7462022299,0.966111
5744\O,2.2087296548,1.2475747575,-0.3628518538\\Version=Sun64-SVR4-Uni
x-G98RevA.9\HF=-726.2879534\RMSD=4.185e-09\RMSF=2.149e-06\Dipole=-0.32
96009,-0.4964687,0.0132459\PG=C01 [X(C8H19N2O4)]\\@

Zero-point correction=	0.279372		
Frequencies --	18.2420	22.4196	24.5042
Frequencies --	38.9015	45.9193	53.7911
Frequencies --	70.4733	84.9928	102.6902
Frequencies --	134.8795	193.4589	201.3472
Frequencies --	214.3081	240.1503	242.5167
Frequencies --	267.6431	269.6499	283.0145
Frequencies --	290.1762	328.7370	348.1601
Frequencies --	364.7247	384.8862	405.4189
Frequencies --	442.3402	445.9255	454.1476

Frequencies -- 511.0211 574.5935 642.2605
Frequencies -- 678.9445 717.8218 773.1166
Frequencies -- 777.2873 880.6787 894.6661
Frequencies -- 930.0482 930.3380 940.6555
Frequencies -- 944.5770 992.6683 997.1566
Frequencies -- 1054.8363 1057.9446 1060.8795
Frequencies -- 1065.5342 1129.7641 1181.1259
Frequencies -- 1232.1271 1262.6759 1290.8546
Frequencies -- 1294.5359 1301.6686 1336.2636
Frequencies -- 1424.7902 1430.7464 1433.4331
Frequencies -- 1435.1073 1458.0989 1460.7928
Frequencies -- 1489.7628 1496.1707 1503.7641
Frequencies -- 1506.6750 1508.6963 1509.1594
Frequencies -- 1518.2567 1519.9037 1521.8188
Frequencies -- 1524.4428 1542.1474 1543.2833
Frequencies -- 1687.3550 1740.3958 3067.1957
Frequencies -- 3068.5134 3069.1522 3075.7945
Frequencies -- 3077.4557 3083.0962 3131.1829
Frequencies -- 3138.0013 3143.3861 3143.8235
Frequencies -- 3148.0923 3153.4245 3154.2097
Frequencies -- 3154.6301 3163.9464 3165.6923
Frequencies -- 3170.8436 3175.8857 3663.6945

TS(1-2)
1\1\GINC-SFNODE4\Freq\RB3LYP\6-31+G(d)\C2H7N2O4(1+)\HPC1471\27-Jul-200
4\1\\#B3LYP/6-31+G(D) OPT=(TS,EF,CALCALL)\\CH3NO2 TSa\\1,1\N\O,1,B1\O,
1,B2,2,A1\H,2,B3,1,A2,3,D1,0\O,1,B4,2,A3,3,D2,0\N,5,B5,1,A4,2,D3,0\O,6
,B6,5,A5,1,D4,0\C,6,B7,5,A6,7,D5,0\H,8,B8,6,A7,5,D6,0\H,8,B9,6,A8,9,D7
,0\H,8,B10,6,A9,9,D8,0\C,1,B11,2,A10,3,D9,0\H,12,B12,1,A11,2,D10,0\H,1
2,B13,1,A12,2,D11,0\H,12,B14,1,A13,2,D12,0\\B1=1.32628035\B2=1.1821249
9\B3=0.99064999\B11=1.477986\B12=1.08925468\B13=1.10369393\B14=1.09044
343\A1=121.86592402\A2=107.5085641\A10=112.86028779\A11=106.91297216\A
12=103.92384804\A13=108.24998922\D1=-6.50851434\D9=177.20681474\D10=-2
02.00684656\D11=-83.70059593\D12=34.5099779\B4=2.90927646\B5=1.2341756
9\B6=1.23028676\B7=1.49560696\B8=1.08833878\B9=1.08893156\B10=1.093534
89\A3=78.23225886\A4=113.73661179\A5=123.71035721\A6=118.05525421\A7=1
07.89097539\A8=107.78591005\A9=106.41568237\D2=75.04723348\D3=117.0412
0093\D4=-4.11116418\D5=181.44056618\D6=204.08190133\D7=122.64765578\D8
=-118.8898534\\Version=Sun64-SVR4-Unix-G98RevA.9\HF=-490.3621883\RMSD=
6.725e-09\RMSF=1.194e-05\Dipole=-0.1418799,1.090552,0.3010794
Zero-point correction= 0.113006
Frequencies -- -39.2865 23.2766 36.0284
Frequencies -- 60.3989 86.2417 103.2025
Frequencies -- 128.3196 205.4656 457.5329
Frequencies -- 482.0764 515.9711 607.0229
Frequencies -- 612.5081 635.8548 660.8976
Frequencies -- 827.5691 924.8960 1064.8474
Frequencies -- 1126.2399 1147.9346 1150.2175
Frequencies -- 1250.8609 1417.2375 1421.3805
Frequencies -- 1444.6742 1459.7089 1471.4122
Frequencies -- 1474.0416 1475.9329 1489.5485

Frequencies -- 1614.8062 1783.6811 2997.7837
Frequencies -- 3099.3453 3161.9936 3195.0227
Frequencies -- 3235.2170 3235.8590 3518.7730

TS(2-3)
1\1\GINC-MS3\Freq\RB3LYP\6-31+G(d)\C2H7N2O4(1+)\POON\21-Mar-2004\1\\#B
3LYP/6-31+G(D) OPT=(TS,EF,CALCALL)\\CH3NO2 TS2\\1,1\C\H,1,B1\H,1,B2,2,
A1\H,1,B3,2,A2,3,D1,0\N,1,B4,2,A3,3,D2,0\O,5,B5,1,A4,2,D3,0\O,5,B6,1,A
5,6,D4,0\C,1,B7,2,A6,3,D5,0\H,8,B8,1,A7,2,D6,0\H,8,B9,1,A8,9,D7,0\H,8,
B10,1,A9,9,D8,0\N,8,B11,7,A10,5,D9,0\O,12,B12,1,A11,2,D10,0\O,12,B13,1
,A12,13,D11,0\H,14,B14,12,A13,1,D12,0\\B1=1.08793129\B2=1.0909741\B3=1
.09280007\A1=112.95003149\A2=112.08469538\D1=-124.97161669\B4=1.496113
2\B5=1.21003725\B6=1.26176328\B7=4.21922056\B8=1.08127572\B9=1.0814729
3\A3=107.26822548\A4=120.71050618\A5=115.59760396\A6=123.46268278\A7=8
4.54340833\A8=84.20166818\D2=118.15578567\D3=7.89238835\D4=-180.600620
95\D5=116.14372227\D6=72.37752753\D7=-120.94915771\B12=1.18232581\B13=
1.34938843\B14=0.99124587\A11=123.89277449\A12=117.09216905\A13=108.35
063073\D10=69.4319192\D11=-172.26137239\D12=172.75064312\B10=1.0816108
5\A9=100.4370177\D8=119.91124405\B11=2.04434847\D9=164.83398214\A10=17
6.11392579\\Version=x86-Linux-G98RevA.7\HF=-490.3309592\RMSD=9.032e-09
\RMSF=5.216e-06\Dipole=0.4702831,0.1748443,-0.3766975
Zero-point correction= 0.110709
Frequencies -- -399.8948 17.8139 35.5046
Frequencies -- 61.4936 72.8817 81.5078
Frequencies -- 126.6173 170.4928 204.2614
Frequencies -- 347.2174 396.3364 491.8735
Frequencies -- 617.9729 659.2504 678.1123
Frequencies -- 702.3503 922.3082 1006.6077
Frequencies -- 1105.1897 1118.4557 1125.3320
Frequencies -- 1148.1044 1243.0785 1377.2347
Frequencies -- 1385.1036 1400.3792 1408.8484
Frequencies -- 1435.1932 1476.0337 1481.1038
Frequencies -- 1648.5259 1757.4035 3099.6023
Frequencies -- 3159.9411 3192.5209 3236.5671
Frequencies -- 3357.9137 3361.8052 3484.7113

TS(2-3)b trans
1\1\GINC-SFNODE8\Freq\RB3LYP\6-31+G(d)\C2H7N2O4(1+)\HPC1471\01-Aug-200
4\1\\#B3LYP/6-31+G(D) OPT=(TS,EF,CALCALL)\\CH3NO2 TS2 twist\\1,1\C\H,1
,B1\H,1,B2,2,A1\H,1,B3,2,A2,3,D1,0\N,1,B4,2,A3,3,D2,0\O,5,B5,1,A4,2,D3
,0\O,5,B6,1,A5,6,D4,0\C,1,B7,2,A6,3,D5,0\H,8,B8,1,A7,2,D6,0\H,8,B9,1,A
8,9,D7,0\H,8,B10,1,A9,9,D8,0\N,8,B11,7,A10,5,D9,0\O,12,B12,1,A11,2,D10
,0\O,12,B13,1,A12,13,D11,0\H,14,B14,12,A13,1,D12,0\\B1=1.08793345\B2=1
.09116381\B3=1.09267877\B4=1.49638501\B5=1.20981327\B8=1.08126732\B9=1
.08193435\B10=1.08186945\B12=1.17501512\B13=1.36589795\B14=0.98110146\
A1=112.89532036\A2=112.18451681\A3=107.22441884\A4=120.71799543\A7=82.
25964561\A8=85.55152061\A9=99.82425624\A11=112.79704961\A12=132.489246
3\A13=107.19662391\D1=-125.00062253\D2=118.04580381\D3=6.46622695\D6=6
3.3001662\D7=-120.63397033\D8=119.38057472\D10=57.1202971\D11=-172.559
52143\D12=-7.63322918\B6=1.26231753\B7=4.23095938\B11=2.04778309\A5=11
5.65882202\A6=123.3583836\A10=176.20911773\D4=179.45883019\D5=117.2988

149\D9=123.81259063\\Version=Sun64-SVR4-Unix-G98RevA.9\HF=-490.3236656
\RMSD=5.541e-09\RMSF=1.389e-05\Dipole=1.4329699,0.8641824,-0.3376091
Zero-point correction= 0.110741
Frequencies -- -391.0396 20.7621 46.0361
Frequencies -- 64.0223 71.2346 96.6845
Frequencies -- 138.0648 169.7001 195.6174
Frequencies -- 356.0785 375.8770 490.8318
Frequencies -- 595.0132 618.2041 658.5553
Frequencies -- 704.2457 920.5182 969.0012
Frequencies -- 1085.9231 1115.0479 1122.9845
Frequencies -- 1147.9894 1236.2159 1340.9286
Frequencies -- 1382.5625 1405.1243 1409.6076
Frequencies -- 1434.7145 1475.9010 1480.6222
Frequencies -- 1648.6095 1799.2751 3099.4857
Frequencies -- 3155.4000 3192.3696 3236.5161
Frequencies -- 3352.2012 3358.1367 3639.4337

TS(8-9)
1\1\GINC-SFNODE7\PTS\RB3LYP\6-31+G(d)\C4H11N2O4(1+)\HPC1471\09-Jun-200
4\1\\#B3LYP/6-31+G(D) OPT=(TS,EF,CALCALL,MAXCYCLES=200)\\CH3CH2NO2 TS2
\\1,1\C\H,1,1.094274\H,1,1.094244,2,A1\N,1,1.51968,2,A2,3,D1,0\O,4,B4,
1,A3,2,D2,0\O,4,B5,1,A4,2,D3,0\C,6,B6,4,A5,1,D4,0\H,7,B7,6,A6,4,D5,0\H
,7,B8,6,A7,4,D6,0\N,7,B9,6,A8,4,D7,0\O,10,B10,7,A9,6,D8,0\O,10,B11,7,A
10,6,D9,0\H,12,B12,10,A11,7,D10,0\C,1,1.51509,2,A12,4,D11,0\H,14,1.094
299,1,A13,2,D12,0\H,14,1.094304,1,A14,2,D13,0\H,14,1.092521,1,A15,2,D1
4,0\C,7,B17,6,A16,4,D15,0\H,18,B18,7,A17,6,D16,0\H,18,B19,7,A18,6,D17,
0\H,18,B20,7,A19,6,D18,0\\B17=1.48535845\B18=1.09361211\B19=1.09804898
\B20=1.09254282\B4=1.21302167\B5=1.2563296\B6=2.17480519\B7=1.08249339
\B8=1.08306022\B9=2.16981168\B10=1.18336174\B11=1.35529351\B12=0.99078
417\A1=107.79863309\A2=103.96353375\A3=120.9377117\A4=115.64884257\A5=
117.6852271\A6=85.15954742\A7=86.00775773\A8=164.76140891\A9=127.56039
028\A10=114.63341683\A11=108.20743792\A12=113.72335918\A13=111.8909325
3\A14=107.59286634\A15=111.88860386\A16=96.22985672\A17=111.31319949\A
18=108.18304869\A19=112.08389675\D1=109.97765073\D2=123.25548971\D3=-5
6.7077519\D4=179.52281875\D5=-60.21198581\D6=57.1821548\D7=-8.65287809
\D8=-55.54086367\D9=122.48755971\D10=-178.35020145\D11=122.97740945\D1
2=-56.65827881\D13=62.06590822\D14=-179.18694166\D15=178.09902325\D16=
-123.8114629\D17=-6.91174472\D18=111.54534092\\Version=Sun64-SVR4-Unix
-G98RevA.9\HF=-568.9771774\RMSD=4.045e-09\RMSF=1.941e-04\Dipole=0.5729
284,-0.6410457,0.0704413\Polar=83.3763732,6.33879,127.4943003,7.706183
,8.5661724,69.8301088\PG=C01 [X(C4H11N2O4)]\\@
Zero-point correction= 0.166624
Frequencies -- -277.2490 14.6153 27.2648
Frequencies -- 39.3415 49.2570 59.9932
Frequencies -- 108.8589 120.8977 124.2067
Frequencies -- 144.8568 240.3254 261.7122
Frequencies -- 293.6545 303.8554 347.4238
Frequencies -- 511.9066 586.9972 627.4700
Frequencies -- 671.4244 701.2179 813.1825
Frequencies -- 827.5855 887.5243 931.8298
Frequencies -- 963.0424 995.2572 1030.9854

Frequencies --	1073.3939	1126.7351	1160.6900
Frequencies --	1194.3067	1212.2633	1307.2030
Frequencies --	1359.6083	1369.7884	1378.5517
Frequencies --	1418.4459	1445.1554	1477.7152
Frequencies --	1482.7926	1488.3256	1508.7321
Frequencies --	1517.0449	1518.8284	1635.7878
Frequencies --	1749.3616	3064.2674	3077.8939
Frequencies --	3097.7573	3126.7369	3141.0077
Frequencies --	3150.0548	3165.9735	3169.0442
Frequencies --	3216.1064	3332.8000	3488.4225

TS(11-12)

1\1\GINC-SFNODE2\Freq\RB3LYP\6-31+G(d)\C6H15N2O4(1+)\HPC1471\14-Sep-20
04\1\\#B3LYP/6-31+G(D) FREQ\\Int 1\\1,1\C\C,1,R2\C,1,R3,2,A3\H,1,R4,2,
A4,3,D4,0\N,1,R5,2,A5,3,D5,0\H,2,R6,1,A6,3,D6,0\H,2,R7,1,A7,6,D7,0\H,2
,R8,1,A8,6,D8,0\H,3,R9,1,A9,2,D9,0\H,3,R10,1,A10,9,D10,0\H,3,R11,1,A11
,9,D11,0\O,5,R12,1,A12,2,D12,0\O,5,R13,1,A13,12,D13,0\C,1,R14,2,A14,3,
D14,0\C,14,R15,1,A15,2,D15,0\C,14,R16,1,A16,15,D16,0\H,14,R17,1,A17,15
,D17,0\H,15,R18,14,A18,1,D18,0\H,15,R19,14,A19,18,D19,0\H,15,R20,14,A2
0,18,D20,0\H,16,R21,14,A21,1,D21,0\H,16,R22,14,A22,21,D22,0\H,16,R23,1
4,A23,21,D23,0\N,1,R24,2,A24,3,D24,0\O,24,R25,1,A25,2,D25,0\O,24,R26,1
,A26,25,D26,0\H,25,R27,24,A27,1,D27,0\\R2=1.52889869\R3=1.52992878\R4=
1.09116141\R5=1.53027232\R6=1.09347442\R7=1.09456021\R8=1.09475813\R9=
1.09367302\R10=1.09479327\R11=1.09454142\R12=1.22197877\R13=1.24554117
\R14=4.72709197\R15=1.47439711\R16=1.47400516\R17=1.08430296\R18=1.090
64441\R19=1.09997158\R20=1.09888994\R21=1.09323993\R22=1.09369342\R23=
1.10305552\R24=6.79118206\R25=1.3588766\R26=1.18589049\R27=0.99075078\
A3=113.95272634\A4=111.42903197\A5=108.37710932\A6=111.1381004\A7=108.
12984155\A8=111.72784844\A9=111.10838488\A10=111.72975357\A11=108.1537
3955\A12=119.22675267\A13=117.6167897\A14=114.20826982\A15=93.87701934
\A16=107.02017595\A17=62.66101052\A18=113.08137282\A19=109.70735879\A2
0=108.71375162\A21=112.46777553\A22=112.82095719\A23=105.75230849\A24=
106.30101582\A25=101.16744464\A26=136.43498947\A27=108.20506265\D4=-12
6.90093433\D5=120.33827851\D6=-55.91230108\D7=119.00333393\D8=-122.343
82567\D9=56.04114106\D10=122.40882027\D11=-118.95886627\D12=-59.776376
75\D13=-179.7781333\D14=132.6939579\D15=-155.7264989\D16=-125.27604921
\D17=120.9500687\D18=59.84948876\D19=122.87938979\D20=-122.66055204\D2
1=-100.23679275\D22=-127.24111634\D23=115.84417232\D24=122.87831004\D2
5=3.96555567\D26=-151.26796841\D27=-158.016317\\Version=Sun64-SVR4-Uni
x-G98RevA.9\HF=-647.6260899\RMSD=3.611e-09\RMSF=7.223e-06\Dipole=-1.04
69635,-0.3361155,-0.4352979

Zero-point correction=		0.221210	
Frequencies --	-132.3683	16.1043	28.1224
Frequencies --	31.9962	35.5803	45.8236
Frequencies --	74.4814	86.3898	100.2733
Frequencies --	126.8403	147.9741	186.1767
Frequencies --	192.8241	214.9175	248.2024
Frequencies --	259.5700	268.7148	301.8719
Frequencies --	331.6930	345.8694	413.5961
Frequencies --	516.3566	626.5506	667.4130
Frequencies --	709.5457	740.7704	818.0447

Frequencies -- 856.3544 861.7744 894.4757
Frequencies -- 923.1406 960.4802 965.5010
Frequencies -- 970.6815 988.2286 1123.6652
Frequencies -- 1128.4780 1149.8004 1159.4070
Frequencies -- 1206.5170 1215.2142 1341.9082
Frequencies -- 1365.3822 1366.2410 1379.7696
Frequencies -- 1393.1216 1399.8539 1423.8391
Frequencies -- 1434.2809 1450.7314 1469.5464
Frequencies -- 1474.1380 1502.9502 1503.3131
Frequencies -- 1508.0550 1518.0159 1521.0675
Frequencies -- 1530.8861 1613.0437 1737.5571
Frequencies -- 3027.4682 3040.8491 3067.4997
Frequencies -- 3070.0318 3085.6388 3111.6262
Frequencies -- 3134.7472 3139.6433 3141.8948
Frequencies -- 3152.4556 3162.4628 3167.1173
Frequencies -- 3180.7862 3258.5859 3486.2469

TS(17-18)
1\1\GINC-SFNODE5\FTS\RB3LYP\6-31+G(d)\C8H19N2O4(1+)\HPC1397\25-Jan-200
5\0\\#B3LYP/6-31+G(D) OPT=QST2 FREQ\\3methyl int\\1,1\C,1.609913502,3.
1197075105,0.9034224366\C,2.3988371768,3.0859879431,2.2099422205\C,2.5
134815471,3.3949510892,-0.3083377448\C,0.4287653964,4.09982429,0.96761
03653\H,3.2146721717,2.3590770782,2.1757444032\H,1.7608359803,2.851679
1881,3.066318576\H,2.8323865405,4.0788440758,2.3684444565\H,3.32095935
59,2.658155261,-0.3789419409\H,2.9689588882,4.3821061107,-0.1814246238
\H,1.9434881848,3.3945879263,-1.240752891\H,-0.2420314819,3.861910975,
1.8002871161\H,0.8244092211,5.107024088,1.1321577853\H,-0.1412533371,4
.1002902036,0.0353239538\N,0.9866377058,1.7132670304,0.660661985\O,1.1
9292419,0.8136396406,1.4724380559\O,0.3003992521,1.5595083023,-0.35543
60799\C,-0.9809461778,-1.7453302405,-0.5760359436\C,-0.2770144422,-2.1
518907556,0.6762582378\C,-0.1463789772,-1.5643022763,-1.8043476901\C,-
2.1878357346,-0.8786352074,-0.4391444447\H,0.255666371,-1.2435216437,1
.0103195432\H,0.4720580001,-2.9297115615,0.510152268\H,-0.9639327429,-
2.4394194398,1.4767335232\H,-0.7435801801,-1.4695737021,-2.715170845\H
,0.6154635601,-2.3384284735,-1.9201112116\H,0.3675221152,-0.6017255437
,-1.6498904681\H,-1.78287128,0.1230051987,-0.2221691887\H,-2.832488000
9,-1.1692429045,0.3937226193\H,-2.7661376015,-0.8011245372,-1.36328244
64\N,-1.9063950269,-3.4770791013,-1.0340027743\O,-3.0709444091,-3.6632
470504,-1.114715366\O,-1.0721825291,-4.5132322674,-1.2525784997\H,-1.6
203302901,-5.3124709219,-1.4579446082\\Version=Sun64-SVR4-Unix-G98RevA
.9\HF=-726.2744091\RMSD=3.269e-09\RMSF=5.892e-06\Dipole=-1.0574866,-2.
4284641,-0.9163976\PG=C01 [X(C8H19N2O4)]\\@
Zero-point correction= 0.278294
Frequencies -- -130.2626 19.7598 22.1694
Frequencies -- 28.9629 36.6975 40.8495
Frequencies -- 43.1415 47.9101 70.3472
Frequencies -- 167.5147 172.4334 201.7139
Frequencies -- 217.4315 256.3345 263.4109
Frequencies -- 275.6442 280.1007 285.5241
Frequencies -- 287.9983 296.7895 356.8003
Frequencies -- 368.5117 370.8894 386.3529

Frequencies --	415.4061	419.7074	447.1603
Frequencies --	522.1185	547.8038	681.3481
Frequencies --	697.7634	738.2854	774.8528
Frequencies --	797.1706	857.9614	870.5973
Frequencies --	883.6830	943.0291	946.8645
Frequencies --	990.7457	998.9649	1028.2384
Frequencies --	1049.4612	1053.5959	1063.3132
Frequencies --	1064.0096	1131.0293	1204.0773
Frequencies --	1264.0897	1288.4920	1314.6622
Frequencies --	1321.5350	1380.5095	1399.6839
Frequencies --	1411.8272	1416.0271	1423.0310
Frequencies --	1433.2670	1439.9272	1466.3611
Frequencies --	1467.4795	1494.4950	1494.9327
Frequencies --	1496.9641	1505.1892	1507.0632
Frequencies --	1509.2222	1511.8423	1521.1400
Frequencies --	1522.9437	1539.9773	1543.0463
Frequencies --	1593.2275	1755.2941	2996.9190
Frequencies --	3030.1105	3037.2063	3064.5257
Frequencies --	3066.0585	3074.5888	3114.2748
Frequencies --	3120.2851	3125.2877	3133.7220
Frequencies --	3134.1953	3142.7752	3153.5371
Frequencies --	3154.6214	3157.6957	3167.0380
Frequencies --	3171.4157	3172.1207	3493.9602

C. OTHER MOLECULES

$CH_3CH_2NO_2$

1\1\GINC-SFNODE3\FOpt\RB3LYP\6-31+G(d)\C2H5N1O2\HPC1418\01-Jun-2004\0\
\#B3LYP/6-31+G(D) OPT FREQ\\ethyl\\0,1\C,0.7218310311,0.6467422911,0.2
436933737\H,0.985360224,0.6282343291,1.3052593119\H,1.6239934853,0.581
8696036,-0.3641904787\N,-0.0236022487,-0.6490199298,0.0040753959\O,-1.
1004542048,-0.7902998736,0.5789603377\O,0.4960325303,-1.476712329,-0.7
409429076\C,-0.1466611412,1.8515720983,-0.0983219252\H,-0.4296444647,1
.8469689903,-1.1561479898\H,-1.0533650996,1.8663144398,0.5114838015\H,
0.4232256528,2.7659634305,0.0986994516\\Version=Sun64-SVR4-Unix-G98Rev
A.9\HF=-284.3433722\RMSD=5.695e-09\RMSF=1.115e-05\Dipole=0.6593017,1.4
188127,0.224885\PG=C01 [X(C2H5N1O2)]\\@

Zero-point correction=		0.078875	
Frequencies --	2.8797	228.1093	282.5281
Frequencies --	476.1818	606.2445	711.1230
Frequencies --	820.0430	880.3987	1004.3011
Frequencies --	1121.2929	1162.5688	1289.4887
Frequencies --	1366.8609	1414.3600	1446.2861
Frequencies --	1501.3352	1512.0632	1526.7333
Frequencies --	1636.8687	3065.9297	3100.6622
Frequencies --	3132.2217	3152.3667	3181.1625

$CH_3CH_2NO_2H^+$

1\1\GINC-SFNODE8\FOpt\RB3LYP\6-31+G(d)\C2H6N1O2(1+)\HPC1471\02-Jun-200
4\0\\#B3LYP/6-31+G(D) OPT FREQ GUESS=CHECK GEOM=CHECK\\ch3ch2no2H+\\1,
1\C,0.8158939658,-0.1611450885,0.6770574816\H,0.9005607696,-1.16291356
15,1.1013130607\N,-0.5745291605,-0.1283465597,0.1044103673\O,-1.059704
739,1.1050498882,-0.017243612\O,-1.1888042913,-1.0738809143,-0.2537311
717\H,-1.9558531159,1.0431532417,-0.4372948182\C,1.8367779554,0.105183
6783,-0.4441407811\H,2.8244496543,0.046063212,0.0249212357\H,1.7794670
145,-0.656593874,-1.2259426767\H,1.7158899391,1.1031798195,-0.87210140
89\H,0.8292305772,0.6119537507,1.4485301029\\Version=Sun64-SVR4-Unix-G
98RevA.9\HF=-284.6361187\RMSD=4.210e-09\RMSF=8.555e-06\Dipole=-0.18380
86,0.3376824,0.1669288\PG=C01 [X(C2H6N1O2)]\\@

Zero-point correction=		0.090665	
Frequencies --	47.1903	229.5527	248.3620
Frequencies --	446.2216	558.1416	619.2805
Frequencies --	717.7023	766.1493	826.3915
Frequencies --	930.9654	1065.2006	1112.0668
Frequencies --	1203.9062	1301.6490	1356.3880
Frequencies --	1422.5199	1441.8568	1487.2269
Frequencies --	1498.5411	1513.8295	1771.3919
Frequencies --	3078.2784	3120.2264	3157.9093
Frequencies --	3172.9635	3201.1644	3502.3783

$(CH_3)_2CHNO_2$

1\1\GINC-SFNODE8\FOpt\RB3LYP\6-31+G(d)\C3H7N1O2\HPC1418\18-Apr-2004\0\
\#B3LYP/6-31+G(D) OPT FREQ\\2methyl 1\\0,1\C,-0.6374669873,-0.00000468
09,0.4125640113\H,-0.6364499977,0.0000022769,1.5039962647\N,0.84825650
39,0.0000444456,0.0578322441\C,-1.2703118909,-1.2790961545,-0.13431420

47\C,-1.2703844911,1.2790481173,-0.1343238012\O,1.6534576289,0.0000927
028,0.9867796998\O,1.1465254987,-0.0000703044,-1.1343189678\H,-1.22394
71008,-1.2996753155,-1.2270281809\H,-0.770799466,-2.1711261758,0.25825
0296\H,-2.3212324159,-1.3137834817,0.1727637351\H,-2.3213052701,1.3136
816823,0.1727592277\H,-0.770918334,2.1711089165,0.2582296382\H,-1.2240
277488,1.2996180997,-1.2270385776\\Version=Sun64-SVR4-Unix-G98RevA.9\H
F=-323.662005\RMSD=1.438e-09\RMSF=2.968e-05\Dipole=-1.6043487,-0.00000
77,0.2530651\PG=C01 [X(C3H7N1O2)]\\@

Zero-point correction= 0.107082

Frequencies --	31.4537	217.4578	251.8465
Frequencies --	264.1671	301.2733	339.3827
Frequencies --	526.9534	634.2478	740.6602
Frequencies --	853.9308	910.2593	957.4727
Frequencies --	968.3723	1131.1324	1153.8607
Frequencies --	1210.3316	1340.0355	1373.0132
Frequencies --	1408.8761	1422.0301	1453.4988
Frequencies --	1505.8052	1511.7780	1519.6992
Frequencies --	1534.6267	1634.9840	3060.1627
Frequencies --	3063.4920	3125.7263	3127.9468
Frequencies --	3129.9038	3144.6410	3154.7096

$(CH_3)_2CHNO_2H^+$

1\1\GINC-SFNODE1\FOpt\RB3LYP\6-31+G(d)\C3H8N1O2(1+)\HPC1418\20-Apr-200
4\0\\#B3LYP/6-31+G(D) OPT FREQ\\2-methylH+ (CH3)2CHNO2H+\\1,1\C,-0.709
9469853,0.0000077338,0.4465563151\H,-0.7096679366,-0.0000660576,1.5388
875585\N,0.7939432107,0.0002388826,0.1621607068\C,-1.307990644,-1.2932
100767,-0.1227501653\C,-1.3082945614,1.2931785399,-0.1225655522\O,1.09
74858601,-0.0002372992,-1.1350394241\O,1.6429210862,0.000118957,0.9869
458354\H,-2.3520627797,-1.3221614895,0.2059114781\H,-1.2888671193,-1.3
018966325,-1.2152725729\H,-0.80795978,-2.1842034058,0.2680749851\H,-2.
3523745487,1.3218304349,0.2060994316\H,-0.8084757038,2.1842303668,0.26
83972471\H,-1.2891693279,1.3020292333,-1.2150859195\H,2.0851122946,-0.
0003450725,-1.214832032\\Version=Sun64-SVR4-Unix-G98RevA.9\HF=-323.959
9288\RMSD=5.254e-09\RMSF=1.196e-04\Dipole=0.3096368,-0.0001368,-0.2752
557\PG=C01 [X(C3H8N1O2)]\\@

Zero-point correction= 0.118562

Frequencies --	33.4366	209.0126	244.4096
Frequencies --	249.1985	277.7891	332.7720
Frequencies --	485.4193	575.7375	605.8009
Frequencies --	727.4950	731.6446	847.1466
Frequencies --	953.1617	969.4373	1054.7151
Frequencies --	1131.3049	1139.3862	1209.8039
Frequencies --	1341.4719	1389.3681	1422.9874
Frequencies --	1426.6113	1454.9940	1494.5998
Frequencies --	1500.2128	1509.7340	1525.2122
Frequencies --	1757.6131	3074.4812	3075.6881
Frequencies --	3139.5021	3149.2104	3150.7483
Frequencies --	3168.2683	3173.6810	3510.4341

$CH_3NO_2CH_3^+$

1\1\GINC-SFNODE4\FOpt\RB3LYP\6-31+G(d)\C2H6N1O2(1+)\HPC1471\11-Mar-200

4\0\\#B3LYP/6-31+G(D) OPT FREQ\\CH3NO2CH3\\1,1\C,0.6847199545,1.541768
7701,0.7861657564\H,0.4547188255,1.6985211934,1.8384083841\H,1.7561173
541,1.4278529061,0.5988311273\H,0.2700667982,2.3212592733,0.1408734489
\N,0.0333050859,0.2588161213,0.3973453844\O,0.2327338003,-0.0555024247
,-0.8655066912\O,-0.6027184141,-0.4229251502,1.1336849881\C,-0.3884799
783,-1.3220697214,-1.3201075491\H,-0.0904681859,-1.3612023949,-2.36565
63452\H,0.029320792,-2.1450289197,-0.7372153675\H,-1.4704541316,-1.243
8886004,-1.1984345578\\Version=Sun64-SVR4-Unix-G98RevA.9\HF=-284.63805
72\RMSD=1.504e-09\RMSF=2.968e-06\Dipole=0.3123867,0.402745,-0.2286183\
PG=C01 [X(C2H6N1O2)]\\@

Zero-point correction=	0.090057		
Frequencies --	25.2298	171.9357	194.5211
Frequencies --	292.0182	439.0962	607.2075
Frequencies --	620.4131	862.9334	879.9380
Frequencies --	1090.3393	1142.0193	1155.8186
Frequencies --	1207.5921	1269.8552	1422.0544
Frequencies --	1465.8578	1465.8864	1474.4101
Frequencies --	1479.6408	1485.5319	1737.2897
Frequencies --	3087.7063	3097.0336	3178.4133
Frequencies --	3201.7240	3235.9263	3240.1923

$CH_3CH_2NO_2CH_2CH_3^+$

1\1\GINC-SFNODE5\FOpt\RB3LYP\6-31+G(d)\C4H10N1O2(1+)\HPC1471\03-Jun-20
04\0\\#B3LYP/6-31+G(D) OPT FREQ GEOM=CHECK
GUESS=CHECK\\ethylprod\\1,1\C,1.7334172253,0.0535792559,0.7294114244\H,2.0115573403
,1.0176692237,1.1595563242\N,0.3 954614046,0.3126172113,0.0860883828\C,2.7300040979,-
0.4236700654,-0.3359708016\O,-0.409558894,- 0.7231929944,0.1192033048\O
,0.1082849201,1.3394148793,-0.4452529419\H,2.421544585,-1.3746709192,-
0.7780401032\H,2.8707715025,0.3281119044,-1.117142092\H,3.6875069023,-
0.5750701253,0.1725304355\C,-1.7639506776,-0.5696069252,-0.542636642\H
,-1.5941021298,-0.0372576583,-1.4801919995\C,-2.7435445684,0.109447919
6,0.391708308\H,-3.7237694982,0.0919121016,-0.0995106011\H,-2.83246683
26,-0.4315101306,1.3379068075\H,-2.4876826782,1.1551692135,0.581847290
2\H,-1.9957942354,-1.6181656112,-0.7291057556\H,1.5488405397,-0.692784
6668,1.5028543787\\Version=Sun64-SVR4-Unix-G98RevA.9\HF=-363.2864347\R
MSD=4.126e-09\RMSF=4.340e-06\Dipole=0.2697603,-0.3574433,0.1888301\PG=
C01 [X(C4H10N1O2)]\\@

Zero-point correction=	0.147358		
Frequencies --	25.2247	78.1415	106.2490
Frequencies --	203.0557	223.2463	249.1121
Frequencies --	319.3771	384.4809	468.7094
Frequencies --	571.1334	710.2836	755.6842
Frequencies --	793.9772	827.8045	878.7107
Frequencies --	950.5769	960.2923	1096.7486
Frequencies --	1109.3564	1128.8985	1195.2629
Frequencies --	1215.9746	1312.7378	1318.8745
Frequencies --	1358.2168	1396.6751	1433.8568
Frequencies --	1436.4426	1490.3874	1496.8605
Frequencies --	1502.6429	1503.9126	1516.8087
Frequencies --	1518.8847	1717.6348	3070.5380
Frequencies --	3077.0534	3124.5955	3127.0531

Frequencies -- 3141.6205 3156.0736 3160.1827
Frequencies -- 3165.6561 3201.5067 3202.0596

$(CH_3)_2CHNO_2CH(CH_3)_2^+$
1\1\GINC-SFNODE10\FOpt\RB3LYP\6-31+G(d)\C6H14N1O2(1+)\HPC1418\18-Apr-2
004\0\\#B3LYP/6-31+G(D) OPT=(MAXCYCLES=100) FREQ\\2methylprod\\1,1\C,-
1.6355019318,-0.0867134786,1.1140276222\H,-1.6269303607,-0.0578040173,
2.2056791019\N,-0.1305365758,-0.0842594095,0.8130254844\C,-2.234363029
,-1.3965129529,0.5939889099\C,-2.2570596234,1.1812385059,0.5238775337\
O,0.1631966442,-0.0993844188,-0.4588912799\O,0.7014814483,-0.077512401
5,1.6694023689\H,-2.2227906246,-1.4394907065,-0.4981789238\H,-1.722627
6829,-2.272165311,1.0048458142\H,-3.2759544379,-1.4298546169,0.9294237
886\H,-1.761008325,2.086937545,0.8857985385\H,-2.2459999372,1.16508694
62,-0.5689472522\H,-3.2991529017,1.2142494805,0.8576084495\C,1.6621989
553,-0.105882105,-0.8624295996\H,2.1354634701,-0.7540506378,-0.1215103
174\C,1.6412192011,-0.728206985,-2.2421117147\C,2.1681059048,1.3224773
341,-0.7868038225\H,1.2096744864,-1.7330236123,-2.228837074\H,1.095633
1673,-0.1054240485,-2.9575058342\H,2.6778910005,-0.8123415084,-2.58712
14214\H,3.2204945723,1.318964628,-1.0932103101\H,1.6184812951,1.973946
1403,-1.4729687648\H,2.1255607071,1.7315582372,0.2263635285\\Version=S
un64-SVR4-Unix-G98RevA.9\HF=-441.9321889\RMSD=4.578e-09\RMSF=1.721e-06
\Dipole=-0.3148745,-0.0626619,-0.0395317\PG=C01 [X(C6H14N1O2)]\\@
Zero-point correction= 0.203041
Frequencies -- 27.3439 73.7640 85.2013
Frequencies -- 143.9328 208.9021 216.3261
Frequencies -- 230.7074 243.6007 255.5437
Frequencies -- 275.7362 330.4894 361.6781
Frequencies -- 410.5199 452.2526 502.7327
Frequencies -- 537.0161 681.8807 722.8517
Frequencies -- 861.8724 869.5290 887.2062
Frequencies -- 946.1794 958.0122 960.2550
Frequencies -- 968.0279 1077.6874 1112.1485
Frequencies -- 1143.2665 1168.1840 1179.5734
Frequencies -- 1214.1902 1223.2687 1353.0634
Frequencies -- 1355.3546 1372.9534 1404.0377
Frequencies -- 1426.6215 1432.3974 1448.1632
Frequencies -- 1451.9146 1497.8121 1500.3242
Frequencies -- 1502.4887 1504.5632 1515.1293
Frequencies -- 1515.6759 1526.8627 1527.9937
Frequencies -- 1692.3883 3067.7158 3071.1919
Frequencies -- 3072.6473 3074.2972 3128.3209
Frequencies -- 3136.6265 3136.7055 3142.5556
Frequencies -- 3146.0023 3147.7591 3154.5741
Frequencies -- 3159.5769 3161.1626 3167.9618

$(CH_3)_3CNO_2C(CH_3)_3^+$
1\1\GINC-SFNODE10\FOpt\RB3LYP\6-31+G(d)\C8H18N1O2(1+)\HPC1397\18-Apr-2
004\0\\#B3LYP/6-31+G(D) OPT=(MAXCYCLES=100) FREQ\\3methylprod (CH3)3CN
O2C(CH3)3\\1,1\C,-0.2913031737,-0.5021218123,-1.8677726086\N,-0.290519 8376,-
0.501218546,-0.2921727349\C,1.1863226706,-0.5036690681,-2.289079
5602\C,-1.0251199205,0.7805253257,-2.2887217038\C,-1.0265426418,-1.768

1257497,-2.2960090553\O,0.3044021782,0.5248586281,0.2348538092\O,-0.79
38550842,-1.3691220084,0.3566129866\H,1.7066227702,0.4006235839,-1.965
3474469\H,1.7133586419,-1.3857976854,-1.9114617307\H,1.2144890217,-0.5
407332352,-3.3826894387\H,-2.0524328497,0.800957347,-1.9109332721\H,-0
.4975696165,1.6805799806,-1.9649188139\H,-1.0714490401,0.7868048286,-3
.3823229431\H,-0.5239884629,-2.675206253,-1.9495376721\H,-2.063369448,
-1.7812805005,-1.9492878347\H,-1.0359648498,-1.7840482135,-3.390115344
3\C,0.4211566248,0.7260715475,1.8383525679\C,1.1835505122,2.0409168091
,1.8420078519\C,-0.9923065125,0.8491911084,2.3824966971\C,1.2302157253
,-0.4395039316,2.3824020042\H,2.1595932258,1.9448998618,1.3578132124\H
,0.6153417577,2.8403111225,1.3578271159\H,1.3513005446,2.3302080241,2.
8852515079\H,-0.9093375848,1.1648430376,3.4292976801\H,-1.560582076,1.
619965509,1.8529832978\H,-1.540601049,-0.0945224517,2.3664687039\H,2.1
813899693,-0.5498278739,1.8527691441\H,1.4630860279,-0.2106914764,3.42
91725231\H,0.6835354221,-1.3841541146,2.3664489299\\Version=Sun64-SVR4
-Unix-G98RevA.9\HF=-520.5695399\RMSD=3.484e-09\RMSF=5.378e-05\Dipole=0
.1485133,0.2559972,-0.1441758\PG=C01 [X(C8H18N1O2)]\\@

Zero-point correction= 0.257832

Frequencies --	18.4245	60.9067	93.3458
Frequencies --	130.8826	193.7741	194.3682
Frequencies --	201.1258	236.6709	243.8885
Frequencies --	258.2873	259.0862	281.1637
Frequencies --	286.2299	325.5360	344.5045
Frequencies --	360.2659	382.0464	400.6625
Frequencies --	436.9082	442.4196	446.3942
Frequencies --	506.5382	570.0315	717.6542
Frequencies --	771.4676	775.8004	878.2819
Frequencies --	928.8383	931.5672	938.8236
Frequencies --	941.1844	990.9955	992.9577
Frequencies --	1052.7263	1055.9482	1058.9701
Frequencies --	1061.5084	1127.5385	1177.8171
Frequencies --	1231.6445	1258.4035	1290.9725
Frequencies --	1297.2940	1301.4363	1424.6162
Frequencies --	1429.9566	1431.1146	1432.8282
Frequencies --	1455.5611	1459.0351	1487.2607
Frequencies --	1493.7423	1502.4996	1503.7833
Frequencies --	1506.1219	1508.4257	1516.3691
Frequencies --	1518.3974	1519.0536	1519.5161
Frequencies --	1538.8533	1541.8971	1684.2043
Frequencies --	3067.5430	3067.7203	3070.3161
Frequencies --	3071.1463	3074.6931	3078.7511
Frequencies --	3131.6244	3132.1673	3142.1204
Frequencies --	3142.3401	3142.5323	3151.8068
Frequencies --	3153.9680	3158.6961	3160.6378
Frequencies --	3164.0484	3166.9456	3169.3869

$(CH_3)_3COH$

1\1\GINC-MS10\FOpt\RB3LYP\6-31+G(d)\C4H10O1\POON\30-May-2005\0\\#B3LYP
/6-31+G(D) OPT FREQ\\t-butanol\\0,1\C,-0.0059548224,-0.0000041498,0.01
10089182\O,-0.0692546826,-0.0494739649,1.4535605311\H,0.833609703,-0.1
342347865,1.800691557\C,0.6316077241,-1.2931688584,-0.5190397122\H,1.6

688452465,-1.3907142044,-0.1702227276\H,0.0698512826,-2.1659980244,-0.
1687414329\H,0.6488110707,-1.3073385099,-1.6156465445\C,-1.4643715304,
0.117250943,-0.4384688401\H,-2.0384937512,-0.7527209809,-0.1015236471\
H,-1.9224987031,1.0154843618,-0.0102806776\H,-1.5307088454,0.177848662
5,-1.5305835249\C,0.8037698357,1.2303634154,-0.4252442547\H,1.84005240
27,1.1656371701,-0.0664228753\H,0.8364256281,1.3171799947,-1.518205444
3\H,0.357836185,2.1439999348,-0.0170855992\\Version=x86-Linux-G98RevA.
7\HF=-233.6839036\RMSD=1.869e-09\RMSF=3.135e-05\Dipole=0.5279687,-0.02
58957,-0.4442901\PG=C01 [X(C4H10O1)]\\@

Zero-point correction= 0.135752

Frequencies --	201.0157	255.3837	272.6259
Frequencies --	292.7494	339.9445	341.3288
Frequencies --	417.9863	461.5226	465.4177
Frequencies --	748.2477	916.4258	924.0854
Frequencies --	932.6746	969.8982	1036.8466
Frequencies --	1053.6034	1162.8250	1240.9847
Frequencies --	1266.6764	1369.3810	1418.9649
Frequencies --	1424.2549	1447.6073	1496.8294
Frequencies --	1504.9022	1508.8251	1520.2442
Frequencies --	1527.2345	1538.2078	3031.0415
Frequencies --	3037.0829	3054.2212	3091.0761
Frequencies --	3098.5914	3117.7004	3117.9753
Frequencies --	3125.7426	3126.0677	3732.0667

HONO (trans)

1\1\GINC-MS3\FOpt\RB3LYP\6-31+G(d)\H1N1O2\POON\15-Jan-2004\0\\#B3LYP/6
-31+G(D) OPT FREQ=NORAMAN\\NO2H\\0,1\N,-0.4962410204,0.,-0.1542065245\
O,-0.4793574755,0.,1.0224865037\O,0.8284923709,0.,-0.6816432403\H,0.68
06079798,0.,-1.6473004355\\Version=x86-Linux-G98RevA.7\State=1-A'\HF=-
205.7096587\RMSD=9.520e-09\RMSF=6.607e-05\Dipole=-0.0089965,0.,-0.8888
442\PG=CS [SG(H1N1O2)]\\@

Zero-point correction= 0.020141

Frequencies --	592.5535	627.4068	833.1358
Frequencies --	1314.5914	1785.0996	3687.9948

HONO (cis)

1\1\GINC-MS3\FOpt\RB3LYP\6-31+G(d)\H1N1O2\POON\21-Mar-2005\0\\#B3LYP/6
-31+G(D) OPT FREQ\\CH3NO2 TS2\\0,1\N,-0.5174881725,0.0003286543,-0.185
8463054\O,-0.4374156557,-0.0000472086,1.0014595587\O,0.7150396168,-0.0
001443949,-0.8245790083\H,1.4014255184,-0.0007677528,-0.1141202653\\Ve
rsion=x86-Linux-G98RevA.7\HF=-205.7090923\RMSD=9.884e-09\RMSF=2.291e-0
5\Dipole=0.6190478,-0.0004248,0.1956389\PG=C01 [X(H1N1O2)]\\@

Zero-point correction= 0.020088

Frequencies --	639.4030	705.9481	894.1951
Frequencies --	1352.6263	1717.4986	3507.8135

HNO_2

1\1\GINC-MS3\FOpt\RB3LYP\6-31+G(d)\H1N1O2\POON\15-Jan-2004\0\\#B3LYP/6
-31+G(D) OPT FREQ\\HNO2 (MP2)\\0,1\N,0.,0.,0.3114634291\H,0.,0.,1.3540
197522\O,1.101135312,0.,-0.2208914847\O,-1.101135312,0.,-0.2208914847\
\Version=x86-Linux-G98RevA.7\State=1-A1\HF=-205.7024352\RMSD=1.575e-09

\RMSF=1.305e-04\Dipole=0.,0.,1.0894445\PG=C02V [C2(N1H1),SGV(O2)]\\@
Zero-point correction= 0.021991
Frequencies -- 778.8429 1044.3396 1411.4105
Frequencies -- 1536.2532 1673.2493 3208.6704

NO
1\1\GINC-SFNODE10\FOpt\UB3LYP\6-31+G(d)\N1O1(2)\HPC1396\16-Aug-2005\0\
\#B3LYP/6-31+G(D) OPT FREQ\\NO\\0,2\N,0.,0.,-0.6174270846\O,0.,0.,0.54
02486991\\Version=Sun64-SVR4-Unix-G98RevA.9\HF=-129.8954773\S2=0.75301
6\S2-1=0.\S2A=0.750006\RMSD=5.751e-09\RMSF=5.894e-06\Dipole=0.,0.,0.03
44458\PG=C*V [C*(N1O1)]\\@
Zero-point correction= 0.004511
Frequencies -- 1980.2666

NO^+
1\1\GINC-SFNODE3\FOpt\RB3LYP\6-31+G(d)\N1O1(1+)\HPC1396\15-Aug-2005\0\
\#B3LYP/6-31+G(D) OPT FREQ\\NO+\\1,1\N,0.,0.,-0.5720937699\O,0.,0.,0.5
005820486\\Version=Sun64-SVR4-Unix-G98RevA.9\State=1-SG\HF=-129.532154
\RMSD=3.805e-09\RMSF=4.859e-10\Dipole=0.,0.,-0.1697374\PG=C*V [C*(N1O1
)]\\@
Zero-point correction= 0.005650
Frequencies -- 2480.2292

NO_2
1\1\GINC-SFNODE4\FOpt\UB3LYP\6-31+G(d)\N1O2(2)\HPC1418\13-Dec-2005\0\\
#B3LYP/6-31+G(D) OPT FREQ\\NO2\\0,2\N,-0.2835181249,0.,-0.1618578972\O
,-0.4241511086,0.,1.0316463881\O,0.6722294679,0.,-0.8900207281\\Versio
n=Sun64-SVR4-Unix-G98RevA.9\State=2-A'\HF=-205.0838872\S2=0.753562\S2-
1=0.\S2A=0.750009\RMSD=4.498e-09\RMSF=1.186e-04\Dipole=-0.1212537,0.,-
0.0697321\PG=CS [SG(N1O2)]\\@
Zero-point correction= 0.008786
Frequencies -- 749.1053 1396.6712 1710.6151

NO_2^+
1\1\GINC-SFNODE2\FOpt\RB3LYP\6-31+G(d)\N1O2(1+)\HPC1418\12-Jan-2006\0\
\#B3LYP/6-31+G(D) OPT FREQ\\NO2+\\1,1\N,0.0002615183,0.,0.0001095475\O
,-0.4410520763,0.,1.0394263021\O,0.4408232478,0.,-1.0395221561\\Versio
n=Sun64-SVR4-Unix-G98RevA.9\State=1-A'\HF=-204.7154624\RMSD=2.324e-09\
RMSF=1.101e-04\Dipole=0.0002097,0.,0.000082\PG=CS [SG(N1O2)]\\@
Zero-point correction= 0.010298
Frequencies -- 630.1164 1446.2833 2443.7676

N_2O_3
1\1\GINC-SFNODE9\FOpt\RB3LYP\6-31+G(d)\N2O3\HPC1418\13-Dec-2005\0\\#B3
LYP/6-31+G(D) OPT FREQ\\N2O3\\0,1\N,0.3825071333,0.011988314,0.5104536
955\O,0.2817088803,0.0383869198,1.7146442093\O,1.3551164956,-0.0020814
916,-0.2069110014\N,-1.2101486602,-0.0121046317,-0.4529685964\O,-0.912
6390398,-0.0362036502,-1.5580326696\\Version=Sun64-SVR4-Unix-G98RevA.9
\HF=-334.9938035\RMSD=6.739e-09\RMSF=1.379e-05\Dipole=-0.7234236,-0.01
44478,-0.5945024\PG=C01 [X(N2O3)]\\@
Zero-point correction= 0.017332

Frequencies -- 136.5514 212.9141 284.6105
Frequencies -- 460.0544 657.4501 806.3349
Frequencies -- 1382.8250 1725.9556 1941.2726

$N_2O_3^+$

1\1\GINC-SFNODE10\FOpt\UB3LYP\6-31+G(d)\N2O3(1+,2)\HPC1418\11-Jan-2006
\0\\#B3LYP/6-31+G(D) OPT FREQ\\N2O3+\\1,2\N,0.7196355554,-0.0000004344
,0.6413375532\O,0.4734650011,-0.0000498915,1.7831322064\O,1.5343539522
,0.0000003448,-0.2010238731\N,-1.4537005147,-0.0001225524,-0.554756452
4\O,-1.3655121138,0.0001571602,-1.6578667966\\Version=Sun64-SVR4-Unix-
G98RevA.9\HF=-334.6434354\S2=0.75201\S2-1=0.\S2A=0.750003\RMSD=4.089e-
09\RMSF=5.235e-05\Dipole=-0.7501138,0.000008,-0.4923989\PG=C01 [X(N2O3
)]\\@
Zero-point correction= 0.016055
Frequencies -- 72.9016 75.2505 136.6481
Frequencies -- 298.3232 369.1196 609.8445
Frequencies -- 1305.2884 2009.0669 2170.8728

$(CH_3)_2CH^+$

1\1\GINC-SFNODE3\FOpt\RB3LYP\6-31+G(d)\C3H7(1+)\HPC1471\13-Dec-2005\0\
\#B3LYP/6-31+G(D) OPT FREQ\\isopropyl ion\\1,1\C,-0.3837988803,0.10985
36609,-0.2186834766\C,-0.4841246717,-0.1198549059,1.2021006877\C,0.818
4707076,0.024101014,-1.0115709773\H,0.4105312218,-0.5298265666,1.67377
85394\H,-1.4059064959,-0.6589208893,1.4694138355\H,-0.675140014,0.8983
64908,1.621808252\H,0.6632246893,-0.894554126,-1.6291115859\H,1.744824
937,-0.087814619,-0.4456253755\H,0.8658754373,0.8140336761,-1.77676297
55\H,-1.3066927088,0.3741190028,-0.7445780926\\Version=Sun64-SVR4-Unix
-G98RevA.9\HF=-118.2127046\RMSD=3.868e-09\RMSF=3.114e-06\Dipole=-0.303
5281,0.0870747,-0.1730176\PG=C01 [X(C3H7)]\\@
Zero-point correction= 0.088594
Frequencies -- 120.7594 135.7076 420.6986
Frequencies -- 645.5826 738.1620 906.4529
Frequencies -- 972.7047 1114.6283 1224.1387
Frequencies -- 1246.4719 1311.2108 1336.9068
Frequencies -- 1384.3517 1392.4246 1452.2443
Frequencies -- 1499.3214 1555.7209 2894.7326
Frequencies -- 2906.9130 3051.3962 3053.6833
Frequencies -- 3154.8650 3182.0040 3187.1419

$(CH_3)_3C^+$

1\1\GINC-SFNODE4\FOpt\RB3LYP\6-31+G(d)\C4H9(1+)\HPC1471\13-Dec-2005\0\
\#B3LYP/6-31+G(D) OPT FREQ\\t-butyl ion\\1,1\C,-0.0021134745,-0.004462
4951,-0.0013408194\C,0.0201332434,0.0095243476,1.4640644491\C,1.259294
7449,-0.0183328711,-0.7501492829\C,-1.281938202,0.0056345261,-0.714791
2412\H,-0.2999824048,-1.0045177381,1.7792533863\H,-0.7529806385,0.6747
660125,1.8729530306\H,1.0006457631,0.2122429898,1.898224996\H,1.144594
634,-0.1386063979,-1.8282371315\H,1.9333400624,-0.7864891207,-0.337621
7953\H,1.786367327,0.930175109,-0.5353576861\H,-2.1568598509,-0.117793
7538,-0.0741930496\H,-1.2792181948,-0.7158289293,-1.5438011097\H,-1.34
81645683,0.9918707839,-1.2179192742\\Version=Sun64-SVR4-Unix-G98RevA.9
\HF=-157.5556472\RMSD=5.117e-09\RMSF=1.253e-04\Dipole=0.0097684,0.0186

378,0.0081301\PG=C01 [X(C4H9)]\\@

Zero-point correction= 0.117041

Frequencies --	60.2734	61.7591	180.5496
Frequencies --	404.0833	406.6294	451.8055
Frequencies --	770.9980	798.3821	829.1096
Frequencies --	986.5904	998.8287	1003.5214
Frequencies --	1129.3905	1311.6661	1317.3361
Frequencies --	1363.3316	1370.0332	1376.0178
Frequencies --	1435.3556	1442.6095	1459.6938
Frequencies --	1511.9603	1513.8254	1517.5801
Frequencies --	2971.3967	2976.9660	2999.1321
Frequencies --	3047.5222	3071.1347	3073.2983
Frequencies --	3176.7817	3177.0081	3180.5065